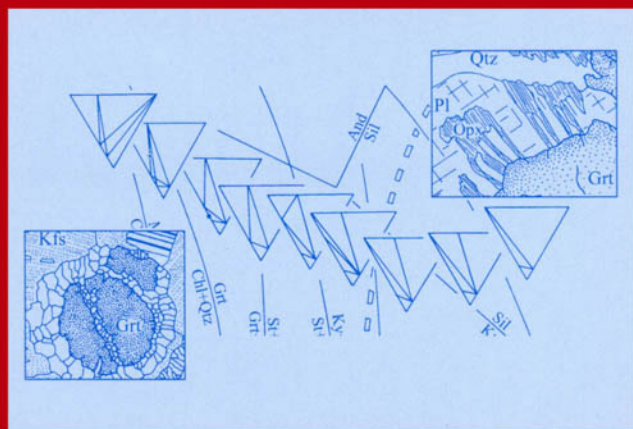


PETROLOGY AND STRUCTURAL GEOLOGY

JACQUES KORNPÖBST

Metamorphic Rocks and Their Geodynamic Significance

A Petrological Handbook



KLUWER ACADEMIC PUBLISHERS

METAMORPHIC ROCKS AND THEIR GEODYNAMIC SIGNIFICANCE

Petrology and Structural Geology

VOLUME 12

Series Editor:

ADOLPHE NICOLAS

*Department of Earth and Space Sciences,
University of Montpellier, France*

Metamorphic Rocks and Their Geodynamic Significance

A Petrological Handbook

by

JACQUES KORNPORST

*Professor Emeritus,
Magmas and Volcanoes Laboratory,
Blaise Pascal University,
Clermont-Ferrand, France*

KLUWER ACADEMIC PUBLISHERS

NEW YORK, BOSTON, DORDRECHT, LONDON, MOSCOW

eBook ISBN: 0-306-48097-2
Print ISBN: 1-4020-0893-7

©2003 Kluwer Academic Publishers
New York, Boston, Dordrecht, London, Moscow

Print ©2002 Kluwer Academic Publishers
Dordrecht

All rights reserved

No part of this eBook may be reproduced or transmitted in any form or by any means, electronic, mechanical, recording, or otherwise, without written consent from the Publisher

Created in the United States of America

Visit Kluwer Online at: <http://kluweronline.com>
and Kluwer's eBookstore at: <http://ebooks.kluweronline.com>

ACKNOWLEDGEMENTS

To Michel Durand-Delga who inculcated me in the rudiments of geology.

To Bruce Velde also who showed me that a good triangle is better than a long discourse.

Consciously or unwittingly the following persons collaborated in the elaboration of this text: Francis Albarède, Pascal Andrieux, Bernard Azambre, Gilbert Boillot, Pierre Boivin, Alain Bonneville, Fernand Conquéré, Jacques Fabriès, Michel Fontelles, Claude Gagny, Claude Herzberg, Albert Jambon, Jean Jung, Thierry Juteau, Jean-Robert Kienast, Jean-Marc Lardeaux, Christine Laverne, Philippe Leloup, Christian Marignac, Hans Massonne, Adolphe Nicolas, Christian Nicollet, Mireille Nicollet, Michael John O'Hara, Ariel Provost, Jean-François Raoult, Jean Ravier, Danielle Velde, Philippe Vidal, Daniel Vielzeuf, Jean-Claude Vilminot, Alain Weisbrod, and Alan Woodland. Also the students of C1 at Paris-Sorbonne and Paris Jussieu from 1967 to 1972; the petrology students at Blaise-Pascal University of Clermont-Ferrand from 1973 to 1993; and the students Magistère "Sciences de la Terre" of the ENS, Lyon since 1986.

To the memory of Jacques de Lapparent.

This page intentionally left blank

PREFACE

From metamorphism to metamorphosis, there is only a shade of a nuance. Because metamorphic rocks are not only what they are, but also what they were, and they tell of what happened in between. What must be discovered: how to recognize in the butterfly, the caterpillar that was, or in the caterpillar the butterfly that will be? And how to describe the metamorphosis, excuse me, metamorphism which leads from one to the other?

It is to this engaging history, this marvelous tale, written progressively over time, which Jacques Kornprobst leads us.

If the sedimentary and magmatic rocks have been the object of reflection for a long time, for which a contradiction was established in the XVIIIth century in the confrontation between the Neptunism of Werner for whom everything came from the sea, and the Plutonism of Hutton who derived all rocks from the interior of the earth, the “crystalline schists” as they were called, and as we call them today for simplicity, appear most ambiguous: they had the crystals of rocks of endogenous origin and appeared to have the stratification of exogenous rocks with which one confused the schistosity. These crystalline schists are in some ways the bats of the rock kingdom.

One understood, from this ambiguity, that they were transformed, metamorphosed, recrystallized. Long condemned to the depths of the crust, that justified imprecision, metamorphism has known a rejuvenation in the last decades, with its studies participating in the general renewal of the Earth Sciences. Today, metamorphism is for rocks, what evolution is for living things, an every-day process which puts the present in the temporary, which separates the past from the future. In truth, it is the life of rocks.

Jacques Kornprobst guides the reader with a steady hand through the forests of this knowledge, describing the objects and the framework of the transformation, the actors in this tale, their significance for the history of the earth, for which they are the archives of its geodynamic evolution.

On finishing this book, the reader, over and above the instruction received, can but reflect on the lesson given by metamorphism on the mobile world which is ours. All is but an eternal riddle, even the crystalline schists, which one can but believe in as symbols of eternity...

Jacques Kornprobst’s book reads as a saga of rocks, transparent parables of destiny.

Jean Aubouin
Member of the Institute

This page intentionally left blank

FOREWORD

In the neighbourhood of high temperature intrusions (granite massifs, for example) sedimentary series present very different characteristics from those observed far from the intrusions. The average grain size is greater and the mineral assemblages include *endogenous* minerals (micas, amphiboles, pyroxenes, etc.) which are normally absent. It is clear that these sedimentary rocks in this environment underwent mineralogical and textural transformations linked to the addition of heat. These transformations commonly leave untouched the characteristic structures of the original series (stratification, sedimentary structures, etc.) and even fossils are still identifiable. The process responsible for this transformation, or recrystallization, is called *contact metamorphism* because its effects appear and increase in the vicinity of intrusions.

In certain regions, the rocks occurring over vast areas (several hundreds or thousands of km²) have mineralogical and textural characteristics similar to those observed in contact metamorphic series, but lack a visible link to intrusions. These materials have generally undergone significant plastic deformation which results in the development of planar and linear structures: *schistosity* and *lineations*. The process responsible for the transformation of these rocks is called *regional* (or *general*) *metamorphism* in order to stress the fact that an individual heat source is not identified, but rather that it results from a thermal anomaly of vast proportions.

In the one case, as in the other, contact or regional metamorphism, the materials initially characterized by low temperature and pressure mineral assemblages (assemblages of biologic, skeletal and diagenetic origin of the sediments or sedimentary rocks), underwent changes at relatively elevated temperatures and under varying load pressures. This *thermobaric* evolution is directly linked to the dynamics of the earth, and in this way, the study of metamorphism is essential for the understanding of the mechanisms which control the internal geodynamics of the earth.

The objective of this text is to allow the reader to have a clear vision of the nature of metamorphic rocks, as well as the mechanisms which formed them. The understanding of these mechanisms brings a critical approach to diverse geodynamic processes which are intimately associated with the development of metamorphism. The author has not endeavoured to develop the theoretical aspects exhaustively, in particular the thermal, thermodynamic and mechanical aspects. To develop his analysis further, the reader should consult various more specialized works referred to at the end of the book.

This page intentionally left blank

TABLE OF CONTENTS

ACKNOWLEDGEMENTS	v
PREFACE	vii
FOREWORD	ix
FIRST PART	1
METAMORPHISM AND METAMORPHIC ROCKS	1
CHAPTER 1	
METAMORPHISM: FACTORS AND MECHANISMS	3
DEFINITION OF METAMORPHISM.....	3
1.1 Metamorphism, diagenesis and anchimetamorphism	3
1.2 Metamorphism and migmatization	3
PRESSURE AND TEMPERATURE IN THE EARTH	4
1.3 Pressure	4
1.3.1 <i>Definition of lithostatic pressure</i>	4
1.3.2 <i>Stress anisotropy and tectonic overpressure</i>	5
1.4 Temperature	6
1.4.1 <i>Geothermal degree</i>	6
1.4.2 <i>Heat flow and heat production</i>	7
1.5 Conduction and geothermal gradient	8
1.5.1 <i>Conductive geotherm</i>	8
1.5.2 <i>Perturbations of the conductive geothermal gradient</i>	9
1.6 Geothermal gradient in dynamic context	11
METAMORPHIC TRANSFORMATIONS	13
1.7 Mineral reactions	13
1.8 Polymorphic changes	14
1.8.1 <i>Example of the aluminosilicates</i>	14
1.8.2 <i>Summary thermodynamic interpretation</i>	14
1.8.3 <i>Slope of the equilibrium curves in P-T space</i>	16
1.9 Reactions between the phases of a system	18
1.9.1 <i>Binary systems</i>	18
1.9.2 <i>Ternary Systems</i>	20
1.10 The role of the fluid phase	22
1.10.1 <i>Location of fluid in a rock</i>	22
1.10.2 <i>Fluid pressure</i>	25
1.10.3 <i>Fluid partial pressure and fugacity</i>	25
1.10.4 <i>Variation of molar volume in the fluid phase</i>	26
1.10.5 <i>Fluid liberation and entropy difference</i>	27
1.10.6 <i>Fluid partial pressure and the stability fields of hydrated and carbonate phases</i>	28
1.11 Metasomatic reactions	29
RESUME: THE FACTORS OF METAMORPHISM	30

CHAPTER 2

METAMORPHIC ROCKS	33
TEXTURES STRUCTURES AND NOMENCLATURE	33
STRESSES AND TEXTURES	33
2.1 Syntectonic recrystallization	33
2.2 Annealing	33
STRESSES AND STRUCTURES	34
2.3 Development of planar and linear structures: schistositities, foliations and lineations	34
2.3.1 <i>Discontinuous and continuous deformation</i>	34
2.3.2 <i>Strain ellipsoid</i>	36
2.3.3 <i>Slaty and fracture cleavage</i>	36
2.3.4 <i>Schistositities and lineations</i>	37
2.4 Schistosity, recrystallization and relative chronology	37
2.4.1 <i>Pre- syn- and post-kinematic phases</i>	38
2.4.2 <i>Temporal evolution of metamorphic conditions; P-T-t paths</i>	40
2.4.3 <i>Polyphase metamorphism or polymetamorphism</i>	40
2.4.4 <i>“Clockwise” and “anti-clockwise” P-T-t paths: a question of choice</i>	42
2.5 Texture and nomenclature of metamorphic rocks	42
2.5.1 <i>Principal textures of metamorphic rocks</i>	42
2.5.2 <i>Nomenclature of metamorphic rocks</i>	44

CHAPTER 3

EVALUATION OF METAMORPHIC CONDITIONS	47
INDEX MINERALS AND METAMORPHIC ISOGRADS	47
METAMORPHIC FACIES	48
3.1 Use of metamorphic facies	48
3.1.1 <i>Choice of typomorphic mineral assemblages</i>	49
3.1.2 <i>Choice of a projection system</i>	49
3.1.3 <i>Use of triangular projections; interest and limits</i>	52
3.2 Metamorphic facies and subfacies	54
3.3 Grades or degrees of metamorphism, another way of presenting facies and subfacies.	56
GEOMETRICAL ANALYSIS	56
3.4 Definitions and reminders	57
3.5 Variance of a system: the phase rule	57
3.5.1 <i>The idea of variance or degrees of freedom of a system</i>	57
3.5.2 <i>Number of assemblages possible in a system as a function of the variance</i> ...	58
3.6 Applications to simple systems	59
3.6.1 <i>Systems with one independent constituent</i>	59
3.6.2 <i>Construction of phase diagrams</i>	61
3.6.3 <i>Systems with two independent constituents</i>	61
3.6.4 <i>Systems with three independent constituents</i>	64
3.6.5 <i>The case where $f > n + 2$: petrogenetic grids</i>	69
3.6.6 <i>Systems with more than three independent constituents</i>	71

DIVARIANT REACTIONS GEOLOGIC THERMOMETRY AND BAROMETRY ...	72
3.7 An example of a divariant reaction: $bt + sil = grt + Kfs + H_2O$	72
3.8 Partition of iron and magnesium between biotite and garnet: An independent geothermometer	74
3.8.1 Principles of thermometry based on Fe-Mg exchange	74
3.8.2 Experimental calibration of the reaction	78
3.9 Example of a geothermobarometer: The reaction cordierite = garnet + sillimanite + quartz + H_2O	78
3.9.1 The cordierite-garnet barometer	79
3.9.2 The independent geothermometer <i>crd-grt</i>	79
3.10 “Automatic” geothermobarometry	80
GEO THERMOBAROMETRY OF FLUID INCLUSIONS	80
3.11 Composition of fluid inclusions	81
3.12 Characterization of isochores	82
PART 2	
METAMORPHISM AND GEODYNAMICS	85
Introduction	87
CHAPTER 4	
CONTACT METAMORPHISM	89
EMPLACEMENT OF AN INTRUSION IN A LOW TEMPERATURE HOST ROCK DYNAMIC ASPECTS	89
4.1 In brittle domains	89
4.2 In ductile host rocks	89
HEAT DIFFUSION IN THE HOST ROCKS	90
4.3 Static model	90
4.3.1 Critical parameters	90
4.3.2 The intrusion-wallrock system	92
4.3.3 Temperature at the intrusion contact and the width of the aureole	94
4.3.4 Evolution of temperature conditions in the aureole with time	94
4.3.5 High grade contact metamorphism	95
4.4 Dynamic emplacement	95
METASOMATIC REACTION AT THE CONTACT OF AN INTRUSION: SKARN GENESIS	96
4.5 Short range reactions (several cm to several m) or diffusion metasomatism	97
4.6 Ionic transport in solution, or percolation metasomatism	100
CHAPTER 5	
REGIONAL METAMORPHISM	101
THE CONCEPT OF A METAMORPHIC GRADIENT	101
5.1 P-T evolution in a metamorphic series: prograde gradients	101
5.2 Polyphase evolution of metamorphic rocks: retrograde gradients	102
DIFFERENT TYPES OF PROGRADE GRADIENTS	103

5.3 The Franciscan gradient	103
5.4 The Dalradian gradient	103
5.5 The Ryoke-Abukuma gradient	104
PROGRADE GRADIENTS, PARTIAL FUSION AND MIGMATIZATION	106
5.6 Partial fusion of metapelites	106
5.6.1 <i>Granitic liquid by partial fusion</i>	106
5.6.2 <i>Refractory solid residue</i>	106
5.7 Extraction of leucosome: different types of migmatites	107
5.7.1 <i>Nebulitic migmatite</i>	107
5.7.2 <i>Stromatite</i>	108
5.7.3 <i>Diktyonite</i>	108
5.7.4 <i>Agmatite or agmatitic migmatite</i>	109
5.8 Migmatites and the granulite facies	109
GEODYNAMIC INTERPRETATION OF METAMORPHIC GRADIENTS	110
5.9 Retrograde evolution and exhumation	110
5.9.1 <i>Erosion and isostatic re-equilibration</i>	112
5.9.2 <i>Tectonic exhumation</i>	112
5.10 Prograde thermal evolution and burial	113
5.10.1 <i>Subduction of oceanic crust: diversity of metamorphic facies</i>	113
5.10.2 <i>Underthrusting of crustal units: plunge versus isostatic re-equilibration</i> ..	113
5.11 Preferred sites for metamorphism	115
5.11.1 <i>Extension domains</i>	115
5.11.2 <i>Subduction zones</i>	115
5.11.3 <i>“Behind” subduction zones</i>	115
HP-LT METAMORPHISM OR THE “FRANCISCAN” GRADIENT	115
5.12 Prograde HP-LT gradients and subduction: example of the Western Alps ..	116
5.13 Retrograde gradients and exhumation of HP-LT units	118
5.13.1 <i>Diversity of the retrograde evolution of HP-LT series</i>	118
5.13.2 <i>Retrograde evolution and tectonic exhumation</i>	120
5.14 HP-LT metamorphism and obduction	121
INTERMEDIATE PRESSURE METAMORPHISM: THE “DALRADIAN”	
GRADIENT	122
5.15 The prograde Dalradian gradient: burial slowdown	124
5.16 Underthrusting of continental units: migmatization and retrograde gradients .	124
.....	124
5.17 Retrograde evolution of eclogitic metabasites: the initial HP-LT gradient ...	124
5.18 Retrograde and prograde units	126
5.19 Underthrusting and inverse metamorphism	128
LOW PRESSURE METAMORPHISM OR THE “ABUKUMA” GRADIENT	129
5.20 Behind subduction zones and paired metamorphic belts	130
5.20.1 <i>Subduction and high temperature</i>	131
5.20.2 <i>A problem of chronology</i>	132
5.21 Collision, crustal thickening and metamorphic core complexes	133
5.21.1 <i>The Hercynian Chain of Western Europe</i>	133

5.21.2 <i>Retrograde migmatitic domes and prograde metapelites: Example of the Agly and Montagne Noire Massifs</i>	133
5.21.3 <i>Migmatitic metamorphic cores and post-collisional extension</i>	138
5.22 Metamorphism in extension zones: Recrystallization of the oceanic crust near oceanic ridges	141
5.23 Sea water convection and low pressure recrystallization near ocean ridges .	141
5.23.1 <i>The recharge zone</i>	143
5.23.2 <i>The reaction zone</i>	143
5.23.3 <i>The discharge zone</i>	145
5.23.4 <i>Sea floor metamorphism in the Atlantic: Goringe Bank and the Mid-Cayman Rise</i>	145
5.23.5 <i>An example of sea floor metamorphism in the Alpine Chain: the Chenaillet Massif</i>	147
5.24 Metamorphism in extension zones: rifts	148
5.24.1 <i>Continental rifts: zones of high heat flow</i>	148
5.24.2 <i>Metamorphism and crustal thinning: Example of the Madagascar granulites.</i>	150
5.24.3 <i>Active metamorphism in the Salton Trough: lithospheric thinning in a transform zone</i>	152
5.24.4 <i>Lithospheric thinning and crustal shearing: Metamorphism of the North Pyrenean Zone</i>	155
5.25 The role of friction:	162
HT-LP gradients and continental shear zones	162
5.25.1 <i>High temperature gneiss</i>	162
5.25.2 <i>Shearing and high temperature</i>	163
5.25.3 <i>Frictional heat and vertical transfer</i>	165
METAMORPHISM UNDER EXTREME CONDITIONS	165
5.26 Coesite-bearing crustal units: example of the Dora Maira massif	165
5.26.1 <i>Dora Maira Massif: European continental margin</i>	165
5.26.2 <i>The coesite-bearing unit: VHP prograde gradient</i>	166
5.26.3 <i>Dora Maira: a continental margin subducted to great depth</i>	168
5.27 Diamond-bearing crustal units	168
5.28 Mantle eclogites: recycled oceanic lithosphere?	170
5.28.1 <i>Mafic enclaves in kimberlites and alkali basalts: evidence of ocean engulfed in the mantle?</i>	171
5.28.2 <i>Convective circulation of the oceanic lithosphere</i>	173
5.28.3 <i>The upper mantle: marble cake or plum pudding?</i>	176
APPENDIX 1	
CHARACTERISTIC MINERAL ASSEMBLAGES OF THE PRINCIPAL METAMORPHIC FACIES	179
APPENDIX 2	
GRAPHICAL REPRESENTATION OF ROCK AND MINERAL COMPOSITIONS ON TRIANGULAR DIAGRAMS	183

ACF - A'KF diagrams	183
AFM Diagrams	185
 APPENDIX 3	
EXAMPLES OF GEOTHERMOMETERS AND GEOBAROMETERS	187
The orthopyroxene-clinopyroxene thermometer	187
The clinopyroxene - garnet thermometer	188
The Si 4+ in phengite barometer	189
 APPENDIX 4	
STRUCTURAL FORMULAE OF MINERALS CITED IN THIS TEXT	191
 APPENDIX 5	
MINERAL ABBREVIATIONS	195
 BIBLIOGRAPHY	 197
REFERENCES CITED	199
INDEX	205

FIRST PART

METAMORPHISM AND METAMORPHIC ROCKS

This page intentionally left blank

METAMORPHISM: FACTORS AND MECHANISMS

DEFINITION OF METAMORPHISM

Metamorphism is the sum of all transformations which cause a rearrangement of the elements of a rock at the atomic scale, leading to a recrystallization in the *solid state* (with or without a fluid phase), as a result of variations in temperature, pressure or of composition.

1.1 Metamorphism, diagenesis and anchimetamorphism

This definition of metamorphism excludes the processes of surface alteration, which, functioning both at the atomic and ionic scale, lead chiefly to the destruction of rocks by leaching and mechanical disaggregation, and not to their transformation. The above definition does include diagenesis, the process which changes unconsolidated sediments into sedimentary rocks. Diagenesis consists in large part in a reduction of the sediment porosity by compaction; but it also implies recrystallization. Metamorphism generally takes place at higher temperature and pressure conditions than diagenesis, but the intrinsic nature of the physico-chemical mechanisms is the same for both processes. Metamorphism is generally related to orogenic or pre-orogenic phenomena, whereas diagenesis is related to the dynamics of sedimentary basins. This distinction is extremely subtle because sedimentary basins precede, follow or accompany orogenesis and their dynamics are therefore related. There is, incontestably, a problem in defining the limit between metamorphism and diagenesis which may not always be clearly resolved.

One criterion, based on *illite crystallinity*, is often used to limit the respective fields of metamorphism and diagenesis. This criterion (Fig. 1) measures the crystallographic evolution of phyllosilicates from argillaceous phases (typical of the diagenetic domain) up to micaceous phases (typical of metamorphism). The evolution passes through an intermediate domain, that of *anchimetamorphism*, which is considered either to be the final stage of deep diagenesis or the result of the first effects of metamorphism.

1.2 Metamorphism and migmatization

As a process of recrystallization in the *solid state*, metamorphism is, in principle, distinct from magmatic phenomena, implying the participation of a silicate liquid. However, in certain domains of high grade metamorphism, the temperature is sufficiently high to allow partial fusion of the material and the production of liquids, generally of granitic composition. If these liquids remain enclosed and crystallize within the rock bodies from which they were derived, they result in a mixed formation or *migmatites* which belong in the metamorphic domain. Migmatites and migmatization will therefore be studied in the context of this text.

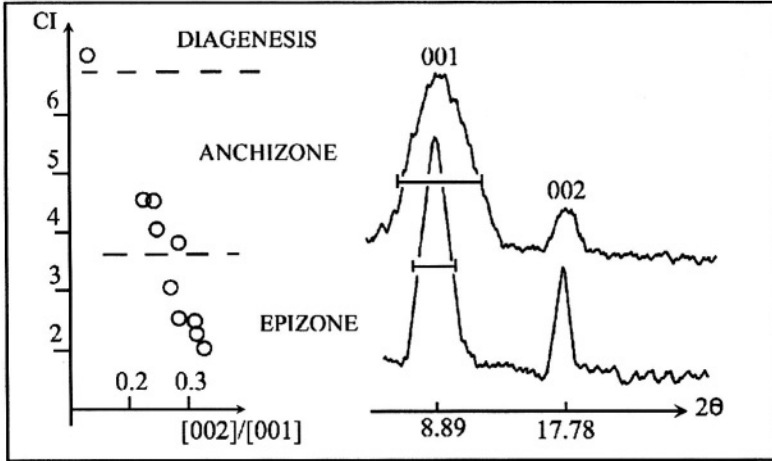


FIG. 1. — Domains of diagenesis, anchizone and epizone characterized by the crystallographic properties of illite.

The right part of the figure is a portion of an X-ray diffractogram showing the [001] and [002] reflection of illite (θ = of refraction). The sharpness of the peak measures the degree of crystallinity of the crystal lattice, the height of the [002] peak represents the quantity of Al which enters the crystal lattice, a function of T. The left part of the figure (Esquevin diagram, in Frizon de la Motte, 1985) shows the variation of the ratio [002]/[001] with respect to the crystallinity index CI, width of the [001] peak at a third of its height under standardized experimental conditions (Kübler, 1984).

PRESSURE AND TEMPERATURE IN THE EARTH

The nature of the minerals of metamorphic rocks as well as the array of textures which they display, demonstrate that recrystallization is produced at a certain depth below the earth's surface and therefore under relatively elevated temperatures and pressures. The following paragraphs examine the evolution of the P and T parameters within the earth.

1.3 Pressure

1.3.1 Definition of lithostatic pressure

Pressure is the force per unit surface area. It is expressed as Pascals in the IS ($1\text{Pa} = 1\text{Newton.m}^{-2}$); geologists still commonly use the bar, a multiple of the barye in the CGS system, ($1\text{bar} = 10^6\text{ dynes.cm}^{-2} = 10^5\text{Pa}$). In this text pressures will be expressed variously in MPa (10^6 Pa), GPa (10^9 Pa), or kb (10^8 Pa).

The *atmospheric pressure* is the force exerted per unit area by the mass of the atmosphere under the gravitational pull of the earth at the earth's surface. At sea level this pressure is about 10^3 hPa or 1 bar. The effect of atmospheric pressure is nil on metamorphic systems.

In phreatic systems (subterranean water table) and at the ocean floor, the *hydrostatic pressure* at a point represents the force $\rho g z$ exerted per surface unit, by the overlying mass of the water (ρ = specific gravity of water, about 1000 kg per m^3 ; g = gravitational constant = 9.81 m s^{-2} ; z = height of the water column in metres; fig. 2). The hydrostatic pressure

plays an important role in the alteration and metamorphism of oceanic basalts, for example. It reaches values of 25 to 30 MPa (250 to 300 bars) in the high temperature zones close to mid-ocean ridges and 70 to 100 MPa in the ocean trenches.

The *lithostatic pressure* or *solid pressure* (P_s) at a point represents the force ρgz applied to a surface area by the overlying rocks (Fig. 2). The value ρ depends on the nature of the material. In the continental crust ρ is close to 2600 kg.m^{-3} and $P_s = 260 \text{ MPa}$ at about 10 km depth. In the ultramafic upper mantle ρ is on the order of 3300 kg.m^{-3} , pressures of the order of 3 GPa (about 30kb) are achieved at about 100 km depth near the low velocity zone (LVZ).

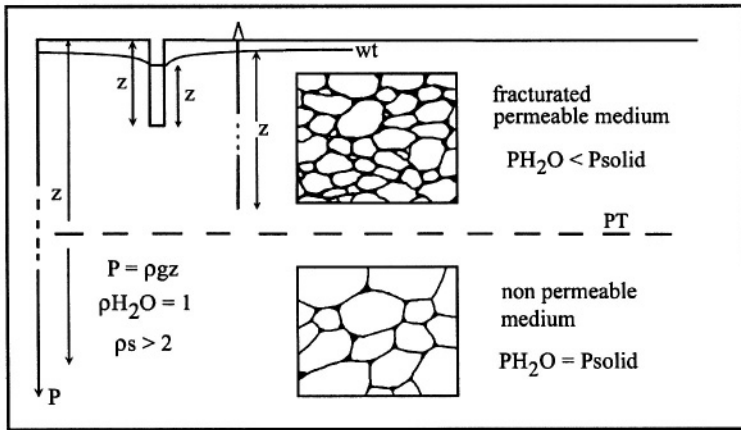


FIG. 2. — *Hydrostatic pressure P_h and solid pressure P_s .*

Both are expressed as the product ρgz where ρ is the density of the medium (1000 kg.m^{-3} for water; $2000 - 2800 \text{ kg.m}^{-3}$ for rocks of the continental crust); g is the gravitational force (9.81 m. s^{-2}) and z the depth in metres. At equal depths the water pressure is lower than the solid pressure in a fractured medium open to surface (because $\rho_{water} < \rho_{rock}$); it is equal to P_s at depth if there is no other fluid present in regions with little or no permeability. PT = piezometric threshold; $P = \text{depth}$, wt = water table. The two drawings at the centimetric scale show the relation between water (in black) in relation to the mineral grains. The limit between the permeable environment (open porosity) and the impermeable or weakly permeable environment (closed porosity) occurs around 15 km depth. (cf. Fig. 14)

1.3.2 Stress anisotropy and tectonic overpressure

When a system is only under lithostatic pressure, it undergoes, if it is sufficiently ductile (from about 3-4000 metres in depth), equal forces in all directions. The system is in dynamic equilibrium. The stress is said to be isotropic, and it is represented by a sphere in which the system occupies the centre (Fig. 3). When tectonic forces come into play, the stress is no longer isotropic. This is represented by a triaxial ellipsoid with a maximum stress σ_1 , and a minimum stress σ_3 (Fig. 3). In this case there is a stress anisotropy ($\sigma_1 - \sigma_3$); the pressure which is exerted on the system in the direction σ_1 , if it is different from the vertical, is greater than the lithostatic pressure P_s inducing the effect of a *tectonic overpressure*. In reality the stress anisotropy develops into a shear stress τ whose intensity is the same order of magnitude as the overpressure applied to the system (Fig. 3). It is at a maximum on planes situated at 45° to the principal stresses σ_1 and σ_3 ; consequently:

$$\tau = \left(\frac{\sigma_1 - \sigma_3}{2} \right) \sin 2\alpha$$

The interplay between shear stresses results in the deformation of rocks, which in turn results in a more or less rapid return to stress equilibrium. In the plastic domain, deformation is efficient for values of τ of several tens to several hundred bars (Fig. 4). The effect of tectonic overpressure is significant in relative value, only in near-surface domains. It becomes negligible at depth, for values of P_s of several kb. Its effects are therefore neglected in the following treatment. This position is not accepted by all authors, of which certain consider tectonic overpressure a determinant factor, notably in the genesis of eclogites.

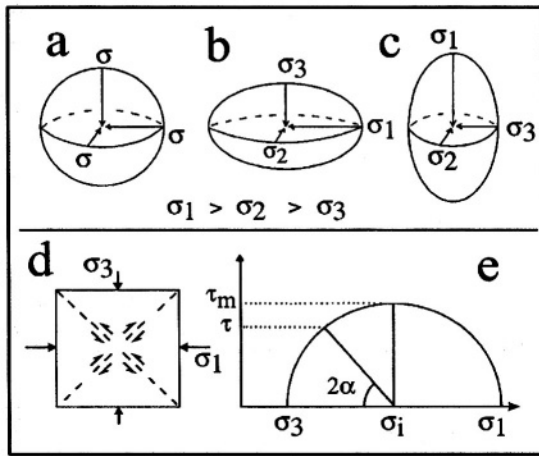


FIG. 3. — *Representation of a stress system.* (after Mattauer, 1973, Nicolas, 1988)

- Isotropic stress: forces applied to the system are equal in all directions; no deformation.
- Anisotropic stress: σ_3 parallel to the vertical $P_s = \sigma_3$ and $\sigma_1 > P_s$.
- Anisotropic stress: σ_1 parallel to the vertical $P_s = \sigma_1$ and $\sigma_3 < P_s$.
- Development of shear stress τ resulting from stress anisotropy. Maximum value τ_m occurs at planes 45° to the principal stresses.
- Representation of the stresses in a Mohr circle diagram. σ_3 is the load pressure, σ_1 tectonic stress; shear stress achieves a maximum τ_m value for $\alpha = 45^\circ$. The tectonic stress (or deviator) is equal to $(\sigma_1 - \sigma_3)/2 = \tau_m$. As a result, for relatively high values of σ_3 (several kb) in ductile domains, tectonic overpressure is negligible (*cf.* Fig. 4)

1.4 Temperature

1.4.1 Geothermal degree

Temperature increases with depth; this fact is verified by direct measurement in mine workings and in geothermal and oil wells. (*cf.* Fig 105). It is therefore possible to define local geothermal degrees; the vertical thickness of terrain corresponding to an increase in temperature of 1°C . In stable continental zones the value of the geothermal degree is of the order of 30 metres, but it may vary widely between 10 and 50 metres.

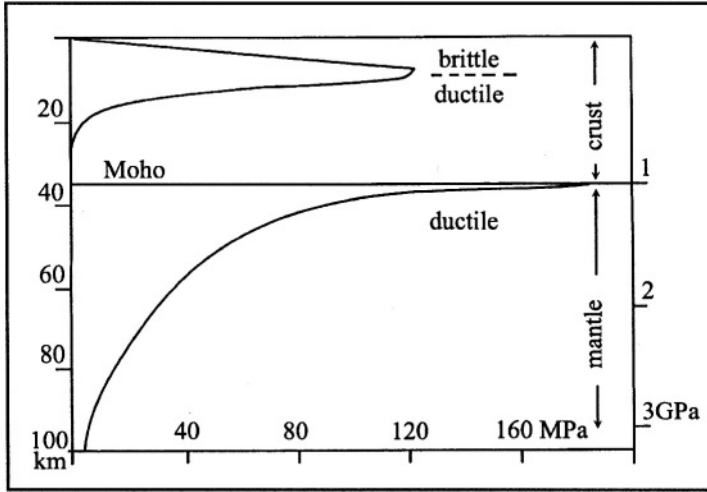


FIG. 4. — Evaluation of the intensity of shear stress as a function of depth in a strike-slip zone (numerical modeling after Leloup and Kienast 1993)

The shear stress τ (abscissa) attains a maximum value at 120 MPa (1.2 kb) at around 8 km depth and a temperature of 200 °C (the model takes into account the addition of mechanical heat τV). Below this depth the value decreases rapidly as an inverse function of the temperature. It becomes negligible in a ductile continental crust. At the top of the brittle lithospheric upper mantle the shear stress is again high (2 kb) but drops to zero around 100 km depth at the low velocity zone.

1.4.2 Heat flow and heat production

The thermal gradient is the expression of a $\partial T/\partial z$ gdegree where z is the depth. This gradient results from the heat transfer toward the surface of the earth, fed by regional heat flow (heat coming from the mantle) and by local heat production derived from the radioactive breakdown of certain elements (^{238}U ; ^{235}U ; ^{232}Th ; and ^{40}K). In a strict conductive model:

$$K = \frac{\partial T}{\partial z} q_m + A_0 H$$

Where K is the thermal conductivity of the material ($\text{watt.m}^{-1}.\text{K}^{-1}$), q_m the heat flow (watt.m^{-2}) derived from the mantle, A_0 the heat production (watt.m^{-3}) and H the thickness of the productive level. The flow q_m - the quantity of heat crossing a given surface per time unit, is generally very small: on the order of 0.2 watt per m^2 except around ocean ridges and areas characterized by important lithospheric thinning (Fig.6). Heat production is demonstrated by the empirical relation:

$$A_0 = \rho 10^{-5} (9.7[\text{U}] + 2.7[\text{Th}] + 3.6[\text{K}]) \text{ W.m}^{-3}$$

Where ρ is the specific gravity, $[\text{U}]$ and $[\text{Th}]$ the concentration in ppm of these elements and $[\text{K}]$ the concentration of potassium in weight percent. Thus the heat production of a granitic basement is of the order of 2.6 mW per m^3 , 40 times that of tholeiitic basalts and

200 times that of peridotites which have a low radioactive element content. The heat production is therefore significant in units of continental crust, but negligible in oceanic crust and even more so in the upper mantle.

1.5 Conduction and geothermal gradient

1.5.1 Conductive geotherm

Knowing the heat flow and local heat production, and based on a certain number of approximations, it is possible to calculate the shape of the geothermal gradient $\partial T/\partial z$, that is to say the shape of the geothermal gradient down to depths which exceed possible direct measurement. The general equation of conductive heat transfer may be used:

$$\rho c \frac{\partial T}{\partial t} = \frac{\partial}{\partial x} \left(K \frac{\partial T}{\partial x} \right) + \frac{\partial}{\partial y} \left(K \frac{\partial T}{\partial y} \right) + \frac{\partial}{\partial z} \left(K \frac{\partial T}{\partial z} \right) + A_{(x,y,z)}$$

Where ρ is the density, c the specific heat of the material. The expression describes the evolution of the temperature T during time t for a point with Cartesian coordinates x , y , and z , under the influence of a temperature gradient varying in three directions. If the thermal conductivity K and the heat production A , are considered constant in all directions:

$$\rho c \frac{\partial T}{\partial t} = K \left(\frac{\partial^2 T}{\partial x^2} + \frac{\partial^2 T}{\partial y^2} + \frac{\partial^2 T}{\partial z^2} \right) + A_0$$

or else

$$\frac{\partial T}{\partial t} = \kappa \left(\frac{\partial^2 T}{\partial x^2} + \frac{\partial^2 T}{\partial y^2} + \frac{\partial^2 T}{\partial z^2} \right) + \frac{A_0}{\rho c}$$

where κ ($s^{-1}.m^2$) or thermal diffusion, is equal to $K/\rho c$.
Using the Laplace operator

$$\nabla^2 = \frac{\partial}{\partial x^2} + \frac{\partial}{\partial y^2} + \frac{\partial}{\partial z^2}$$

$$\text{it becomes: } \frac{\partial T}{\partial t} = K \nabla^2 T + \frac{A_0}{\rho c}$$

In a steady state, the temperature no longer depends on time: $\frac{\partial T}{\partial t} = 0$

The heat equation may be simplified to: $\nabla^2 T = -\frac{A_0}{K}$

T_0 , q_0 and A_0 being the temperature, the heat flow and the heat production at surface ($z = 0$) the solution of the equation becomes:

$$T = T_0 + \left(\frac{q_0}{K}\right)z - \left(\frac{A_0}{2K}\right)z^2$$

This is the equation of a parabola which gives the temperature as a function of the depth z . It is therefore possible to construct different geothermal gradients (Fig. 5) for which the shape depends on the value of the different initial parameters (Q_0 , K , etc.) and which give the temperature in relation to pressure: the “continental gradient” corresponds to older, thick, stable shield areas characterized by relatively low temperatures compared to those of the “oceanic gradient” for areas of recent expansion.

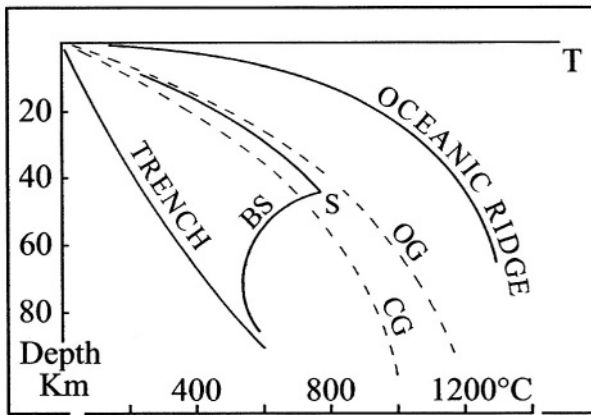


FIG. 5. — Representation of the different types of geothermal gradient in a temperature-depth diagram.

Dashed lines: conductive models of Clark and Ringwood (1964) based on heat diffusion in terrestrial materials. OG and CG oceanic and continental geothermal gradients. Solid lines: different geothermal gradients based on convective models (see Fig. 6). BS: possible shape of gradient located behind subduction zones. An inversion of the gradient appears at S, at the level where the temperature-depth profile cuts the subduction plane.

1.5.2 Perturbations of the conductive geothermal gradient

The rocks of the crust and mantle are very poor heat conductors, their thermal conductivity, K , is of the order of $2.5 \text{ watts} \cdot \text{m}^{-1} \cdot ^\circ\text{K}^{-1}$ for granite, $4 \text{ watts} \cdot \text{m}^{-1} \cdot ^\circ\text{K}^{-1}$ for peridotites. The conductivity of iron is 30 times greater and silver 175 times. As a result of the insulating character of lithic material, heat diffusion is an inefficient mechanism to dissipate thermal energy within the earth. In consequence local heat additions by diverse mechanisms induce long-lived perturbations in conductive thermal gradients, requiring hundreds, thousands or even millions of years to straighten out by conduction.

Water convection in a porous medium. This heat transfer mechanism applies only to the upper part of the crust characterized by sufficient porosity and permeability to allow water circulation (or in a more general way, a fluid phase). Water, cold at surface, equilibrates its

temperature with the surrounding rocks at depth and its density diminishes. If it is a free fluid the system begins to convect when its Rayleigh number exceeds the critical value of 10^3 .

$$\mathbf{Ra} = \frac{\mathbf{g}\rho d^3 \alpha \Delta \mathbf{T}}{\kappa \eta} > 10^3$$

where \mathbf{g} is the gravity constant, ρ the density, d the vertical dimension of the system, $\alpha \Delta \mathbf{T}$ the variation of the density induced by the temperature variation, κ the coefficient of thermal diffusion and η the fluid viscosity. In reality, in the particular case of convection in a porous medium, the expression is more complex because surface tension related to fluid circulation in small diameter conduits comes into play. Whatever the case, once convection starts, a heat transfer takes place towards the surface, which depends on the flow and the temperature attained by the fluid phase at depth. In the upper part of the system the fluid loses a determined quantity of heat to the enclosing rocks, for which the temperature varies as a function of time according to the expression:

$$\rho_r c_r \frac{\partial \mathbf{T}}{\partial t} = \mathbf{K} \nabla^2 \mathbf{T} + \rho_f c_f v_f \frac{\partial \mathbf{T}}{\partial z}$$

where $\rho_r c_r$ and $\rho_f c_f$ are densities and specific heats of the encasing rocks and the fluids respectively and v_f is the vertical speed of the flow.

The development of a hydrothermal convective system may result in a mushroom-shaped thermal plume at surface (Fig. 61). The isotherms corresponding to the conductive gradient are strongly perturbed by the fluid circulation. Some examples of this mechanism will be given in the second part of the text.

Magmatic injections. Magmas from the upper mantle (basalts) or the deep continental crust (granites) are powerful agents of heat transfer, which, in the same fashion as hydrothermal systems, result in a rise of the isotherms related to a conductive gradient. An analogous reasoning to the preceding may be applied to this case, with the caveat that magmas do not represent a true convective system because they inevitably freeze after having undergone a certain amount of cooling; however, numerous authors use the expression “convective transfer” (or advective) to designate this method of heat transfer. Magmas circulating in fissures in the enclosing rocks (which they may therefore induce by hydraulic fracture) transfer a significant part of the heat they carry to the host rocks. In the case of an intrusion localized within a host considered “infinite”, this transfer obeys the laws of heat diffusion, as presented in the second part of the text under contact metamorphism. In the case of intrusion in a closely-spaced network, such as repeated intrusions, they make an important contribution to the heat budget in the form of a local geothermal gradient:

$$\mathbf{K} \frac{\partial \mathbf{T}}{\partial z} = \mathbf{q}_m + v_i \rho_i c_i (\mathbf{T}_i - \mathbf{T})$$

where v_i , ρ_i , and c_i are the vertical speed, density and specific heat of the intrusive magma. The production of radioactive heat is not taken into consideration here. The “advection vector” has the same significance as v_f in the preceding equation, \mathbf{T}_i is the temperature of the intrusion and \mathbf{T} that of the host rocks.

The stepwise transfer of magmas by “underplating” and by injection across the continental crust is a significant mechanism for the understanding of certain high temperature gradients characterizing certain metamorphic series, examples will be given later on.

Vertical transfer of lithosphere units. Large fragments (several thousand km^3) of the oceanic or continental lithosphere, initially in thermal equilibrium on a conductive gradient may be displaced by tectonic or gravity mechanisms. If the displacement includes a vertical component, all areas of the unit undergo a conductive thermal re-equilibrium of the form:

$$\frac{\partial T}{\partial t} = \kappa \nabla^2 T + \frac{A_0}{\rho c} - \mathbf{v} \frac{\partial T}{\partial z}$$

Both the conductive transfer term and the radioactive heat production may be seen in this expression to which a term for vertical mass transfer is added algebraically. If the size of the mass transfer vector \mathbf{v} is large with respect to that of thermal diffusion κ , the unit remains in thermal disequilibrium with respect to the conductive gradient; this results in deformation of the isotherm, all the more prominent if \mathbf{v} is large (Fig. 71). This deformation results in a plunge (or invagination) of the isotherms if the unit goes into the earth (the case of subduction, for example), and the geothermal gradient $\partial T/\partial z$ has a local steep slope (Fig. 5). If, on the contrary, a unit rises to the surface, the isotherms become more closely spaced, and a gentle slope results (Fig. 5, 6). Different possibilities are characteristic of different geodynamic settings, which are analyzed in the second part of the text (*cf.* Fig. 71). In this case, as in magmatic injection, the expression “convective transfer” is also used; it takes on its real sense when applied to movements in the asthenosphere (or of the whole mantle), which represents a convection *sensu strictu*.

Mechanical heat production along tectonic breaks. Rock deformation, as a result of tectonic stress, supplies work, which is in large part transformed into heat. The quantity of heat produced is dependent on the intensity of the shear stress τ (in Pa) and the speed v (in m.s^{-1}) of movement of the rock walls along the break. The reality of this mechanism is attested to by the sporadic occurrence of very high temperature, partly glassy, rocks (pseudotachylites) along certain major tectonic breaks. The conductive dissipation of the heat could have the effect of somewhat perturbing the thermal regime along large tectonic breaks. Examples based on subduction and on a shear zone across the Asiatic continent are presented in the second part of the text.

The importance of the role of this heat source is, however, controversial. In reality the increase in temperature from a mechanical source has the immediate effect of lowering the viscosity of the rocks, and, in consequence, the value of τ (Fig.4). Thus, according to numerous authors, the mechanical heat cannot add a significant, maintainable perturbation in the geothermal gradient.

1.6 Geothermal gradient in dynamic context

The earth is not a thermal system in conductive equilibrium because “convective” heat transfer is associated with the dynamics of mantle and continental units. The movement of

terrestrial materials, poor heat conductors, as a result of lithospheric plate dynamics (expansion, subduction and collision) or magmatism, operate at faster rates than that of heat diffusion in rocks. Gradients calculated from conductive models are, in reality, strongly perturbed outside of the stable continental zones (cratons). Figure 6 represents the distribution of isotherms in the first thousand kilometres of depth calculated on the basis of material displacements at speeds on the order of several cm per year in the framework of mantle convection. These isotherms are closely spaced in zones of high heat flow which correlate to the rise of hot material (around oceanic ridges, for example): they are widely spaced, in contrast, in domains of low heat flow related to the descending slabs of lithosphere (subduction). The different shapes of gradients deduced from this thermal configuration are seen in Figure 5.

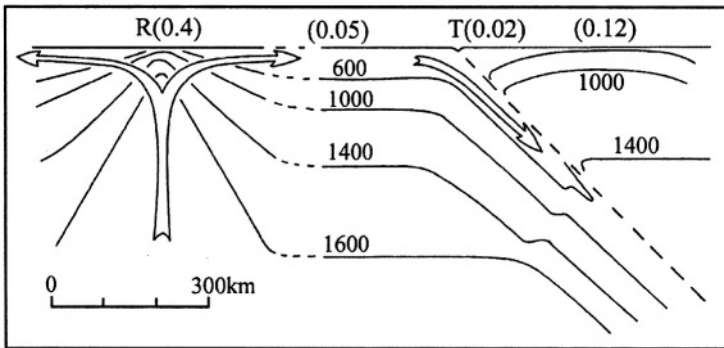


FIG. 6 — *Distribution of isotherms in the upper mantle - "convective" model (after Oxburg, 1980 and Turcotte and Schubert, 1982)*

Temperature of isotherms in °C. R: ocean ridge; T: ocean trench; Heat transfer related to ascending and descending material in the mantle are much more efficient than conductive thermal transfer. This explains the closing up of isotherms around ridges and their invagination around subduction zones. Arrows indicate the sense of displacement of material at rates on the order of several centimetres per year. Numbers in brackets indicate heat flow in watts per m².

The geothermal gradient is a result of the evolution of the temperature with respect to depth: it represents, as well, *ipso facto* the evolution of the temperature with respect to pressure. In this perspective, the P-T conditions to which displaced geological units are exposed fall into several simple cases (Fig. 6).

- 1) Units rising to the surface in a high heat flow region (oceanic ridges, rising mountain chains): these undergo a rapid decompression at high temperature, this evolution is, in certain cases, quasi-adiabatic (without heat exchange with the enclosing formations) as a result of the poor thermal conductivity of rocks.
- 2) Units associated with descending oceanic slabs along subduction zones: these undergo increasing pressure while maintaining low to moderate temperatures.
- 3) Units which have been subducted, but which remain blocked at a certain depth during collision: these undergo a thermal re-equilibration by diffusion and local heat production which induces a quasi-isobaric temperature rise (at constant pressure).

These examples show that it is not enough to consider just the dynamic geothermal gradients as presented (Figs. 5, 6) in the study of metamorphic processes. It is also necessary to envisage their temporal evolution, in a given place or other, for an individual geological unit in a context of extension, convergence or collision. This evolution results, in

fact, in the development over time of pressure and temperature parameters, which control recrystallization in rocks. The temporal aspect of metamorphic conditions (P-T-t paths, where t = time) will be especially developed in the second part of the text.

METAMORPHIC TRANSFORMATIONS

Rearrangements of the constituents of a rock at the atomic or ionic scale in the course of metamorphism respond to a thermodynamic requirement - the minimization of the total energy stored in the system. This energy is stored in rocks in three principal forms:

- 1) surface energy on intergranular surfaces
- 2) dislocation energy related to deformation, and
- 3) electrostatic bonding energy between atoms (or *free energy*, also called *free enthalpy*)

The minimization of surface and dislocation energy leads to a textural evolution in the rocks (modification of grain geometry, annealing and syntectonic recrystallization, respectively). These mechanisms are described further on in the chapter on structures and textures of metamorphic rocks. The minimization of free energy is the principal cause of mineralogical reactions, that is to say, the instability of minerals and mineral assemblages under certain P-T conditions, and their replacement by other species. These reaction processes are naturally very important in the course of metamorphism and are described briefly below.

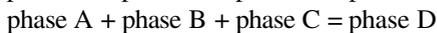
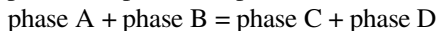
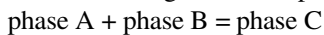
1.7 Mineral reactions

These take three principal forms:

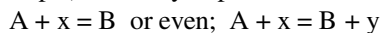
- a) Change in the structure of a mineral (solid phase) without change in chemical composition. This is a *polymorphic change* which is expressed in the following fashion:



- b) Instability between two or more mineral phases of the rock (or the system) leading to *mineral reactions* between the phases. The reactions are expressed in the following fashion, according to the complexity of the mineral system:



- c) Changes in the composition of the system: an addition or loss of fluids for example (H_2O , CO_2 etc.) or addition, loss or exchange of cations in solution ($\text{Na}^+ \leftrightarrow \text{K}^+$, for example) are likely to provoke mineral reactions of the form:



x and y are cations in solution in the fluid phase.

The polymorphic changes and mineral reactions without change in the composition of the system are described as *topochemical* changes. Reactions requiring a modification of the composition of the system are described as *metasomatic* changes. In the first case the system is *closed*, and the ionic transport which results in metamorphic changes are on the same order of magnitude as the grain size of the system. Metasomatism implies, in contrast, an *open* system, and the transport of material takes place at a scale beyond the dimensions of the system.

1.8 Polymorphic changes

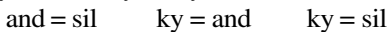
There are several such changes in natural systems. Moreover six different minerals with six different crystal structures have exactly the same chemical composition, SiO_2 . These are α quartz, β quartz, tridymite, cristobalite, coesite, and stishovite; each of these species is stable in a particular P-T domain. Two carbonates, calcite and aragonite have the same composition, CaCO_3 . Aragonite is, in principal, the high pressure polymorph. Three aluminosilicates also have the same chemical formula. This last family of polymorphs is of particular interest in metamorphic petrology.

1.8.1 Example of the aluminosilicates

The three known aluminosilicates are andalusite, sillimanite and kyanite. These minerals have a chemical composition expressed by the formula Al_2SiO_5 . As all are silicates, they are composed of more or less regular compact stacks of oxygen anions O^{2-} (ionic radius $r = 1.4 \text{ \AA}$) which define tetrahedral holes filled with small cations Si^{4+} ($r = 0.42 \text{ \AA}$) and octahedral holes which contain Al^{3+} cations ($r = 0.51 \text{ \AA}$) slightly larger than Si. The exact form of the stacking (or crystal lattice) differs from one mineral to another, which explains why the three polymorphs (minerals of the same composition but with different structure) have different crystal lattice dimensions, for example, or optical properties and densities. The highest density (that of kyanite) corresponds to the most compact crystal packing. The passage from one structure to another requires relatively small modifications of the shape of the crystal lattice and ionic displacements on the order of the dimensions of the crystal lattice (several \AA).

Each of these aluminosilicates corresponds to well-defined stability conditions in P-T space (Fig. 7a). One important fact may be drawn from this diagram: continued variation in P, T intensity results in discontinuous variations in crystal structure for the simple reason that the possible mutual arrangement of ions from a geometric, electrostatic and an energetic point of view are limited in number. Also it may be noted that, at a given temperature, it is the high pressure phase that has the highest density.

In Figure 7 the lines which limit the stability fields of the three polymorphs represent mineralogical equilibrium, which, in the sense of a temperature rise (a convention which will be used systematically), may be written in the following way:



Two polymorphs are stable at the same time (coexistent) along each of the equilibrium boundaries. The three polymorphs are stable at a single point in the diagram, at the convergence of the three equilibrium boundaries.

1.8.2 Summary thermodynamic interpretation

A crystal structure represents the mobilization of a certain amount of energy. At 0°K this internal energy U is strictly electrostatic in origin and represents the sum of all bond energies between the atoms which comprise the structure and depends on the respective position of the different ions in the crystal. If T and P increase, the internal energy U increases as well, because the crystal stores a certain amount of heat dq which results in the ions becoming agitated about their theoretical equilibrium position, and a certain amount of work dw results in an elastic crowding of the structure. It becomes, therefore;

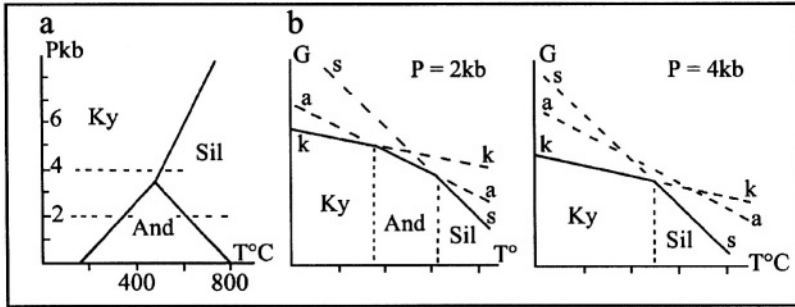


FIG. 7.— *Polymorphic changes in the aluminosilicates.*

a) Phase diagram after Holdaway (1971). b) Position of the free energy surfaces in a G-T diagram at 2 and 4 kb. At 2 kb each of the polymorphs is characterized by a temperature domain in which it represents the most stable phase (a configuration which represents the lowest free energy). At 4 kb the free energy of andalusite is always higher than the two other polymorphs; this mineral is not stable under these pressure conditions. Ky = kyanite ($\rho = 3.6$); Sil = sillimanite ($\rho = 3.25$); And = andalusite ($\rho = 3.15$); kk, aa, ss free energy surfaces for kyanite, andalusite and sillimanite.

$$dU = dq + dw$$

$$\text{where } dq = TdS \text{ and } dw = -PdV$$

S is the entropy, which measures the disorder of the crystal structure, V is the volume, which is an inverse function of pressure. These theoretical values are generally reduced to a finite quantity of crystalline matter and both the molar volume \bar{V} and the molar entropy \bar{S} of a certain number of useful phases used in the following expression are given in Table 2.

In a closed system (at constant composition) equilibrium is established at a given P and T when the free energy G (or Gibbs free energy) is a minimum, with

$$G = U - TS + PV$$

G, a value which may be summed, is proportional to the number of molecules of constituents in the system and can be expressed by a finite quantity \bar{G} .

When P and T are varied, if equilibrium is maintained, the change in free energy is written:

$$dG = -SdT + VdP$$

Furthermore, in PTG space (Fig. 8) all mineral species are characterized by a free energy surface which shows that the change in G is a function of P and T. The free energy surfaces of two mineral species having the same composition generally cut one another in P-T space. In the case of the two polymorphs kyanite and andalusite, for example, the line of intersection between the two surfaces corresponds to the equation:

$$G_{\text{kyanite}} = G_{\text{andalusite}}$$

which may be written

$$\Delta G = G_{\text{and}} - G_{\text{ky}} = 0$$

The two polymorphs are both stable under these conditions. If P and T vary independently, the equilibrium conditions no longer lie on the intersection of the two free energy

surfaces and $\Delta G \neq 0$. The stable phase is that with the lowest free energy. If:

$$G_{\text{ky}} - G_{\text{and}} = \Delta G > 0$$

equilibrium is displaced to the left and kyanite is the stable phase; if P and T vary so that:

$$G_{\text{ky}} - G_{\text{and}} = \Delta G < 0$$

the equilibrium is displaced to the right and any kyanite present changes to andalusite.

Furthermore the curves separating the stability fields of the three aluminosilicate polymorphs (andalusite, sillimanite and kyanite, Fig. 7) represent the projections of the intersection of the free energy surfaces of each of these minerals on the P-T plane. The convergent point of the three curves is the projection of the unique point common to all three surfaces.

1.8.3 Slope of the equilibrium curves in P-T space

Equilibrium conditions between two polymorphs, phases of the same composition, correspond to $\Delta G = 0$. It is possible to show that the equation for the equilibrium in P-T space may be written:

$$d(\Delta G) = (\Delta V)dP - (\Delta S)dT = 0 \quad \text{or} \quad \frac{dP}{dT} = \frac{\Delta S}{\Delta V}$$

The shape of the equilibrium curve in the P-T diagram is equal, according to the Clapeyron equation, to the quotient of the entropy difference divided by the volume difference of the reaction.

Entropy difference. The difference in entropy for the reaction is:

$$\Delta S = S_{\text{product}} - S_{\text{reactant}}$$

it is always positive if the reaction proceeds in the sense of a temperature rise. In effect the increase in entropy corresponds to an increase in the disorder of the mineral structure, which may be, in certain cases, a slight modification of the shape of the crystal sites which contain the cations. In other cases an entropy difference results in more radical changes of the crystallographic sites of certain cations ($\text{Al}^6 \rightarrow \text{Al}^4$, for example, in other words the introduction of a larger cation in a small crystallographic site), or perhaps destabilization of hydrated phases, the OH^- going from a solid phase into the vapour phase (see below).

Volume difference. The volume difference for the reaction is:

$$\Delta V = V_{\text{product}} - V_{\text{reactant}}$$

If this difference is examined in the light of a temperature increase ($\Delta S > 0$), it is either positive ($\Delta V > 0$) or negative ($\Delta V < 0$). Thus, in the aluminosilicate diagram (Fig. 7) the reaction kyanite \rightleftharpoons sillimanite has a positive ΔV because the product (sillimanite) has a lower density than the reactant (kyanite). The slope of the reaction curve is therefore positive because the $\Delta S/\Delta V$ is positive. In contrast, the change andalusite \rightleftharpoons sillimanite has a negative ΔV because the product has a higher density than the reactant; the slope of the reaction is therefore negative.

Solid phases are characterized by a small variation of \bar{V} as a function of P and T because their coefficient of compressibility and their thermal expansion is small. The molar entropy of a particular phase varies greatly as a function of temperature, but the difference ΔS between product and reactant of a polymorphic change does not vary significantly with

respect to ΔS° (where S° represents the entropy of the product and the reactant in the “standard state”, conditions under which they can be measured, (in general 298 °K and 1 bar). In consequence, for an equilibrium curve which only concerns solid phases which do not change composition as a function of P and T, the ratio $\Delta S / \Delta V$ remains practically constant, close to $\Delta S^\circ / \Delta V^\circ$. The equilibrium curve, therefore, maintains a constant slope in P-T space — a reaction line.

Calculation of equilibrium curve slopes. The molar volume of a phase is equal to the quotient of its molecular mass divided by its specific gravity or density. It is expressed in m^3 per mol in the international system (IS) or in cm^3 per mol in the cgs system: V° is easily calculated for minerals of simple composition such as the case of the aluminosilicates; tables supply values for more complex species (Table 2). The molar entropy S° is a more difficult parameter to obtain because it requires delicate calorimetric measures. More or less precise values are also available in the literature (Table 2); the molar entropy is expressed in Joules per °K or in calories per °K in the cgs system. The slope of an equilibrium curve is therefore calculated directly in $\text{Pa } ^\circ\text{K}^{-1}$ or in $\text{bar } ^\circ\text{K}^{-1}$.

$$\frac{dP}{dT} = \frac{\Delta S^\circ}{\Delta V^\circ} = \frac{\text{J} \cdot \text{mole}^{-1} \cdot ^\circ\text{K}^{-1}}{\text{m}^3 \cdot \text{mol}^{-1}} = \text{Pa } ^\circ\text{K}^{-1}$$

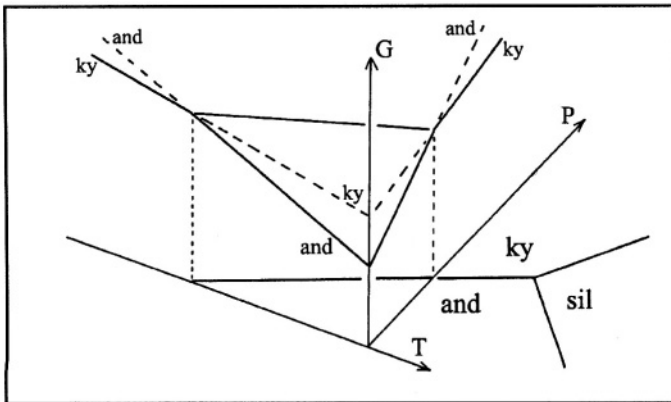


FIG. 8. — Evolution of G as a function of P and T : The free energy surfaces of kyanite and andalusite.

The intersection of the two surfaces corresponds to the equilibrium boundary kyanite = andalusite, that is to say the condition $\Delta G = G_{\text{and}} - G_{\text{ky}} = 0$. At lower temperature $\Delta G > 0$; kyanite is the stable polymorph, and should crystallize under these conditions; at higher temperature it is the inverse $\Delta G < 0$, and andalusite is the stable phase. Equilibrium in the P-T diagram is the projection of the intersection between the free energy surfaces onto the P-T plane. The free energy surface of sillimanite is not shown in order not to overload the diagram. Legend the same as Fig. 7.

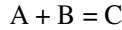
In effect the product $J.m^3$ is the definition of Pa (1 Newton per m^3).

The calculation of slopes for reactions between the three aluminosilicates is illustrated in Figure 7. Examples of calculations of the slopes of other mineral reactions are given in Chapter III as well as the method of determining coordinates for the origin of the curve.

1.9 Reactions between the phases of a system

1.9.1 Binary systems

Two phases A and B may react together to produce a third phase C.



The reactants A and B are shown in an xy or binary system along which all the intermediate compositions between A and B are represented (Fig. 9); x and y are the constituents of the system. Each composition of the system is characterized by a concentration X :

$$X_y = y/(x + y) \qquad X_x = x/(x + y)$$

(x and y are generally expressed in mols). In the particular case where A and B represent the two extremities of the system, the compositions are defined by the concentration $X_A = A/(A + B)$ or $X_B = B/(A + B)$. In a closed system the composition of phase C is obligatorily located on the segment AB between A and B. Figure 9 is therefore a TX diagram which represents the mineralogical evolution of the system as a function of temperature at constant pressure, TX(P). It is also possible to construct PX(T) or GX(T,P) diagrams.

At low temperature (below the temperature of reaction T_r), the association, or mineral assemblage, A + B is the most stable of the possible assemblages. Above T_r , phase C is more stable than the association A + B, it therefore should crystallize at the expense of A +

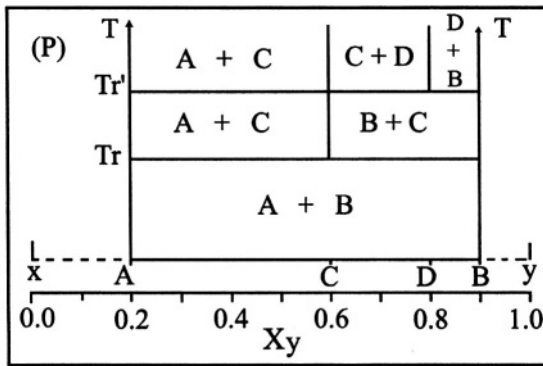


FIG. 9. — T-X plot (concentration versus temperature) of a binary system x, y.

The pressure (P) is fixed, composition of phases A, B, C and D are defined by the concentration X_y or X_x ($y/(x+y)$ or $x/(x+y)$). At temperature T_r , phase C is more stable than the assemblage A + B. At pressure (P), therefore T_r corresponds to the equilibrium curve: $A + B = C$ with the equation $\Delta G = G_c - (G_A + G_B) = 0$ (taking into account the stoichiometric coefficients of the phases in the reaction). From the compositions considered for the segment xy, a new assemblage A + C or B + C appears, depending on whether A or B is the excess phase. At temperature T_r , phase D is more stable than the assemblage B + C etc.

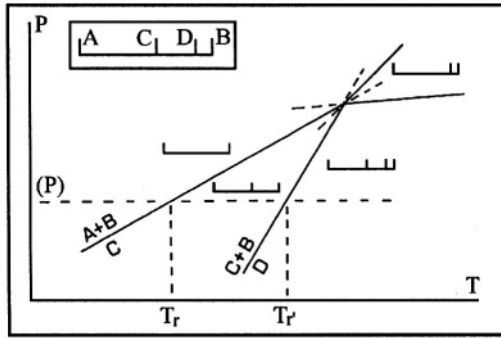


FIG 10. — *P-T diagram showing the mineral reactions in a binary system.*

The segments shown in the different fields of the diagram describe the mineral assemblages in each field, as a function of the composition of the system. A key is provided in the inset. The *P-T* conditions expressed in the *T-X* diagram (Fig. 9) are shown here: (*P*), *T_r*, *T_r*. Besides the equilibria *A + B = C* or *B + C = D*, two other reactions appear in the diagram; these are necessary for the geometrical logic of the scheme (*cf.* Chapter III).

Exercise:

Write the two unknown reactions.

B. The exact nature of the mineral assemblage depends on the initial composition of the system on the *AB* segment; the critical composition is that of phase *C* (*X_y* = 0.6); for *X_y* < 0.6 the stable assemblage above *T_r* is *A + C*, in effect, for at that composition all of phase *B* is consumed by the reaction and phase *A* remains “in excess”; for *X_y* > 0.6 the stable assemblage is *B + C* where *B* is the excess phase; for *X_y* = 0.6 only phase *C* is present. At temperature *T_r* the stable assemblage is *A + B + C* for all values of *X_y* different from 0.2 (composition of *A*) and 0.9 (composition of *B*).

This reaction is represented on a *P-T* diagram (Fig. 10) analogous to that of Figure 7. The nature of the mineral assemblages in relation to the reactions is clarified using segment *AB* which defines the composition of the system. As in the case of the polymorphic changes the reaction curve is the projection on the *P-T* plane, of the intersection of the free energy surfaces. The difference in free energy of the reaction is:

$$\Delta G = G_C - (G_A + G_B)$$

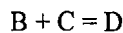
in taking into account the stoichiometric coefficients of the phases participating in the reaction.

The graphical representation of free energy of a mixture of two phases is shown in Figure 11.

The slope of the equilibrium curve is given by:

$$\frac{dP}{dT} = \frac{\Delta S^\circ}{\Delta V^\circ} = \frac{S_C^\circ - (S_A^\circ + S_B^\circ)}{V_C^\circ - (V_A^\circ + V_B^\circ)}$$

The diagram *TX* (Fig. 9) shows that at temperature *T_r*, an instability develops between *B* and *C*:



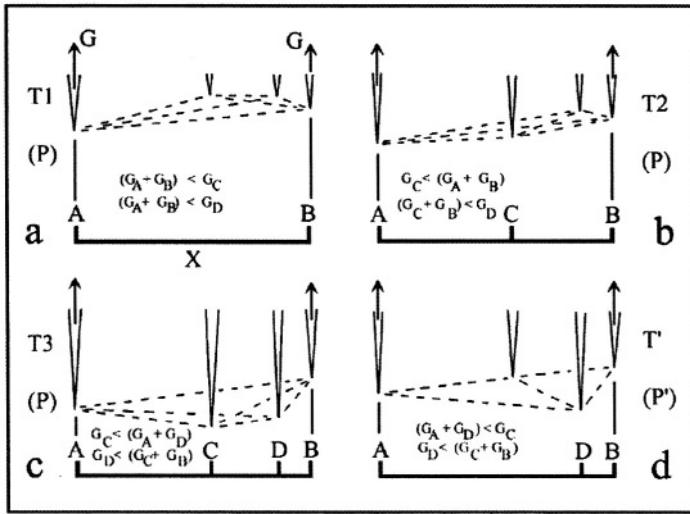


FIG. 11. — Interpretation of the reaction in a binary system in a G - X diagram.

The relative values of G are shown schematically for the four phases A, B, C and D involved in the reactions. The very acute shape of the free energy curves (which depend, nevertheless on a continuous function) signify that phases have closely defined compositions on the A-B segment (compare with solid solutions, Fig. 47). For each of the phases G decreases in relation to T (Fig. 8). For a given composition X , the stable assemblage is that which has the lowest total free energy. Diagram (a), (b) and (c) at constant pressure (P), diagram (d) at pressure $P' > (P)$; $T_1 < T_r$; $T_r < T_2 < T_r$; $T_r < T_3$; $T' \geq T_3$.

Exercise:

Compare with figures 9 and 10.

This reaction, naturally, only applies to those compositions of the system falling between $X_y = 0.6$ and $X_y = 0.9$ and the assemblage A + C does not react above T_r under the pressure conditions considered (P).

Reactions in a binary system of the type $A + B = C$ involve more important ionic displacements than those which result from polymorphic changes. The recombination of elements between different phases involves, in effect, migrations which are on the order of magnitude of the size of the crystals in the mineral assemblage (several mm to several cm). The time parameters which control the diffusion rate of atoms within the assemblage must therefore be taken into account to determine the kinetics of the reaction, the time required to achieve equilibrium. These kinetics are slower at lower temperature, so that equilibrium is never attained under conditions of low grade metamorphism. It is thanks to these extremely low reaction kinetics at low temperatures that high grade metamorphic assemblages are observed at all, and may be studied at the low temperature and pressure conditions of present-day outcrops.

1.9.2 Ternary Systems

The composition of the system is defined by three chemical components (or ingredients) x , y and z , which form the three points of a triangular diagram. Each point located within the triangle represents a particular composition of the system characterized by a concentration

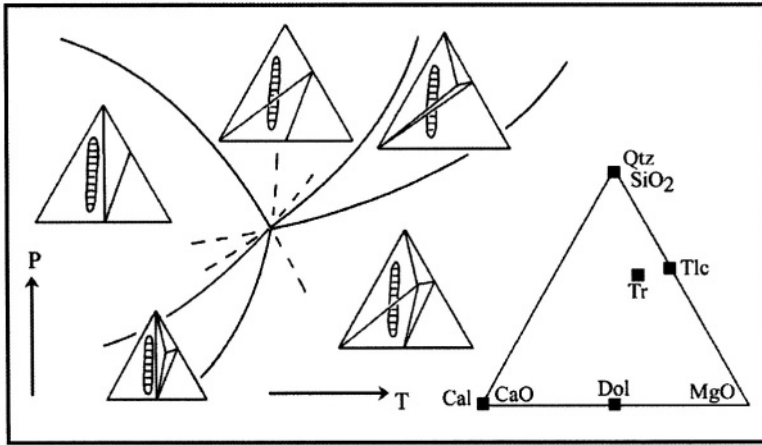


FIG. 12. — P - T plot of compatibility diagrams in a ternary system SiO_2 - CaO - MgO (+ H_2O + CO_2).

At the right of the figure, legend indicating the composition of the different phases appearing in the compatibility triangles. (qtz = quartz; tlc = talc; trm = tremolite; dol = dolomite; cal = calcite). H_2O and CO_2 are in excess. This triangle appears in different sections of the P - T diagram on the left of the figure and characterizes the different stable assemblages and mineral reactions. The reaction quartz + dolomite + H_2O = calcite + talc + CO_2 occurs at low temperature (<380 °C) and relatively high pressure. The different reactions which appear in the diagrams are geometrically necessary for the coherence of the system, as in the previous diagram (cf. Chapter III).

Exercise:

Write the reactions and characterize the different resultant mineral assemblages. Select those which are to be expected if natural compositions are taken into account.

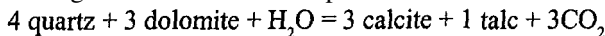
composition, and it is not possible to use T - X or P - X projections as before. It is possible, however, to show the mineral reactions and resultant stable assemblages in a simple fashion in P - T space (Fig. 12).

Consider a system which is widespread in nature, that of the quartz-bearing carbonate rocks. This system is represented by the triangle SiO_2 - CaO - MgO on the understanding that sufficient water and carbon dioxide are always present in order for a reaction to proceed (it is said that H_2O and CO_2 are "in excess"). The compositions of such carbonate rocks are shown in the diagram (hatched field). Under low temperature and pressure conditions (diagenesis) all of these rocks display the same mineral assemblage.

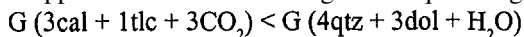
calcite + dolomite + quartz (+ H_2O + CO_2)

The right part of the diagram is unoccupied; the mineral assemblages which are theoretically possible under these conditions are unrealistic, lacking material of a suitable composition.

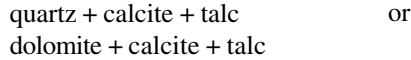
At moderate P and T (about 380 °C) quartz and dolomite become unstable together. The following mineral reaction takes place:



The appearance of the assemblage talc + quartz signifies that



The reaction curve (Fig. 12) represents, as in the previous cases, the projection of the intersection of the free energy surfaces of the two associations onto the P-T plane. The carbonate rocks display two different mineral assemblages depending on their initial composition:



A part of the calcite and talc are reaction products, quartz or dolomite are “excess” phases which can no longer coexist.

Different possible mineral reactions in this system are also shown in Figure 12. The following points should be noted:

- 1) certain theoretically possible reactions (for example $\text{qtz} + \text{dol} + \text{talc} \Rightarrow \text{tremolite}$) do not concern the composition under consideration; they do not take place, therefore, in the topochemical system under scrutiny, lacking the presence of an appropriate composition.
- 2) certain mineral assemblages are never practical for the composition under scrutiny (for example $\text{qtz} + \text{talc} + \text{tr}$; also $\text{talc} + \text{tr} + \text{dol}$).
- 3) all the postulated reactions must be geometrically feasible; the tie line between the products must necessarily cut the tie line between the reactants ($\text{qtz} + \text{dol} = \text{cal} + \text{talc}$ is a possible reaction; $\text{cal} + \text{dol} = \text{talc} + \text{qtz}$ is incorrect). Or else the triangle defined by the reactants contains the product of the reaction ($\text{cal} + \text{talc} + \text{qtz} = \text{tr}$ is a possible reaction; $\text{dol} + \text{talc} + \text{cal} = \text{tr}$ is incorrect). If these conditions are not respected, it is not possible to balance the reaction.

The arrangement of the reactions and mineral assemblages as shown in Figure 12 obeys the phase rule and the strict geometrical constraints which are outlined in Chapter 3.

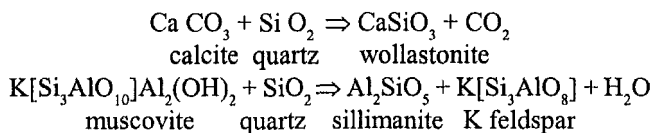
1.10 The role of the fluid phase

In the preceding paragraphs it is clear that fluids, such as water (H_2O) or carbon dioxide (CO_2) are produced or consumed by mineral reactions. These fluids have an important influence on the shape of the reaction curve and the stability fields of mineral assemblages. It is necessary to clarify their behaviour in rocks.

1.10.1 Location of fluid in a rock

Molecules of water and carbon dioxide (the principal fluids of geologic interest) occur in four different situations within rocks. They are *bonded*, *adsorbed*, *dissolved*, or *free*. (Fig. 13).

Bonded fluids. Molecules of the fluid phase make up a part of the crystal structure of hydrous or carbonate minerals in the form of $(\text{OH})^-$ and $(\text{CO})^{2-}$ radicals. These are not proper fluids. These molecules may be liberated into the fluid phase by dehydration and decarbonation reactions which break up the crystal structure of the hydrated or carbonated phases.



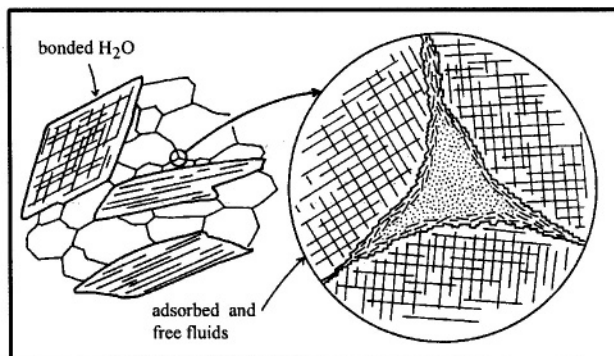


FIG. 13. — *Schematic sketch of fluid occurrence in mineral assemblages.*

The “bonded” fluids are part of silicate and carbonate structure (here H₂O is present as a hydroxyl radical (OH) in the amphibole structure). The “adsorbed” fluid (dashed lines) constitute a thin film (several Å thick) of molecules arrayed in some semblance of order along crystal surfaces. The “free” fluids appear in vapour form (dotted) separated in intergranular pores and in fluid inclusions in minerals. The porosity (size of the intergranular pores) and permeability are very low from 15 km downwards.

Adsorbed fluids on crystal surfaces. Molecules of H₂O and CO₂ are arrayed in approximate order along the crystal surfaces of the rock to the thickness of several Å. These molecules constitute, therefore, an immobile or partly mobile fluid phase of variable volume:

a) on one hand, as a function of the minerals and their grain morphology (as a consequence of the surface tension and the electrostatic effects of the surface).

b) on the other hand, as a function of the ambient P and T.

The extreme case is montmorillonite, a clay mineral, whose fine flakes are capable of adsorbing twice their volume of water. Under metamorphic conditions the quantity of adsorbed fluid is small. Even though it is immobile, this supply of water and carbon dioxide plays an important role in the evolution of mineral reactions, it constitutes a medium for intergranular diffusion which allows rapid dispersion of ions, and favours deformation and recrystallization as well.

Dissolved fluids in silicate liquids. This is a particular case which ought not, in the strictest sense, be considered in the framework of metamorphic petrology. It does concern, however, the high temperature domain of migmatites. The water liberated by partial fusion of the hydrated minerals goes into solution in the silicate liquid (up to 10 weight %) as long as it is not saturated. The liquid intergranular film, rich in dissolved water, also constitutes a diffusion medium which is very favourable for ionic exchanges and reaction mechanisms. It is interesting to note that partial fusion of metamorphic rocks is an efficient means of extracting water, which is easily dissolved in the silicate liquid in increasing quantities under elevated pressures. The solid residue of the partial fusion is therefore generally water deficient, which explains why they generally have granulite facies assemblages (*cf.* Chapter III).

Free fluids. The fluid phase is said to be “free” or “mobile” when it is identified as such (in the supercritical state under metamorphic conditions) in the pores of the mineral assem-

blage or in inclusions in the minerals. The rock is, therefore, “saturated” in fluid. Actually there is no clear limit between the mobile and the adsorbed fluid, the relative quantities of fluid in both situations vary as a function of P-T conditions.

The presence of a free fluid phase allows the definition of a *fluid pressure*, an important parameter for the extent of stability fields of the hydrated phases (micas, amphiboles) as well as the carbonate phases (calcite, dolomite). The displacement of fluid phases across the system (as a function of permeability, and in response to a pressure gradient) naturally influences the transport of ions in solution in the fluid, which represents the principal vector of *metasomatism*, or large-scale ionic transport (m to km) in metamorphic rocks.

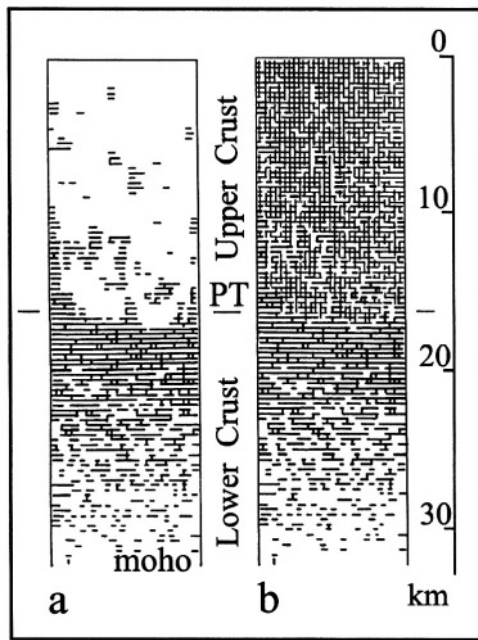


FIG. 14. — *Percolation in the continental crust. Modeling based on a probability calculation (after Gavrilenko and Gueguen, 1994)*

a) Percolation in the lower crust: this is essentially controlled by a network of horizontal fractures unconnected to surface. The fluid pressure in the network is therefore equal to the lithostatic pressure ($P_f = P_s$). This arrangement accounts for the horizontal seismic reflectors which characterize the lower crust, as well as the high electric conductivity of the unit, according to the authors.

b) Percolation throughout the continental crust: The upper crust is characterized by a high density of vertical fractures connected to surface: the fluid pressure (P_{H_2O} essentially) is therefore less than lithostatic pressure ($P_f < P_s$).

In this model the limit between the upper and lower crust corresponds to the “percolation threshold” (PT) from which point the rocks no longer have significant permeability. moho = Mohorovicic discontinuity.

1.10.2 Fluid pressure

The pressure of the fluid phase of a rock is expressed in relation to the ambient solid pressure. Two distinct cases occur:

Surface fractured domain. This case concerns water pressure P_{H_2O} in particular. Interstitial water exchanges with phreatic water by the intermediary of more or less vertical fractures; its pressure is given by the expression $P_f = \rho_f g z$ where ρ_f is the density of the fluid ($= 1000 \text{ kg.m}^{-3}$ for surface water), g the gravity constant, and z the height of the water column (Fig. 2 and 14). The water pressure is, in this case, much less than the lithostatic pressure of the environment $P_s = \rho_s g z$ where ρ_s is the mean density of surface rocks ($> 2000 \text{ kg.m}^{-3}$). This fractured domain of high permeability occurs in the upper part of the crust from 6-15 km depth (Fig. 2 and 14). The difference between P_{H_2O} and P_s is the reason why wells drilled to great depth (several thousand metres) have a tendency to block rapidly unless they are cased.

Deep domain, separate from the surface. In this domain the permeability is very low and the interstitial fluid phase is not connected to surface. However the pores which contain the water-rich fluid phase are apparently interconnected in the horizontal plane, which may explain certain geophysical characteristics of the deep continental crust: notably the electric conductivity and the seismic reflectors. A simple reasoning shows that in this domain the fluid pressure P_f equals the lithostatic pressure. In effect, a situation in which $P_f < P_s$ implies the existence of a pressure gradient at the microscopic structural scale. This gradient must equilibrate rapidly by reduction of the pore volume until $P_f = P_s$. Inversely, if $P_f > P_s$ (a possible case, notably in certain volcanic processes), the pore volume must increase or else the overpressured fluid must move to a site where the pressure is lower, until $P_f = P_s$. Therefore at equilibrium the fluid pressure may be considered as equal to the solid pressure, except in particular cases.

1.10.3 Fluid partial pressure and fugacity

The interstitial fluid phase is composed of water (H_2O) or carbon dioxide (CO_2) or of other fluids of geologic interest (CH_4 , SH_2 , Cl , F , O_2 , N_2 , etc.). Commonly, under metamorphic conditions the fluid is *mixed*, constituting a mixture of two or more fluid phases. In this case the pressure of an individual species or fluid partial pressure (P_{pf}) may be expressed approximately as a function of the total pressure P_s and of the molar fraction of the specific species in the fluid phase; for example:

$$P_{H_2O} = P_s \left(\frac{H_2O}{H_2O + CO_2 + CH_4 \dots} \right) = P_s X_{H_2O}$$

The partial pressure of one species in a mixed fluid is always less than the total pressure because:

$$P_s \text{ or } P_{total} = \sum P_{pf} = P_{H_2O} + P_{CO_2} + P_{CH_4} \dots$$

Therefore, for a system with an interstitial fluid half composed of water and half of carbon dioxide (in mols) the partial pressure of water may be considered as close to $0.5 P_s$.

In reality, this expression of the partial pressure of a fluid as a function of the concentration in the fluid phase is only rigorous if the fluid is an ideal mixture of perfect gases. This is not the case for water and carbon dioxide mixtures. The pertinent thermodynamic parameter to describe the partial pressure of a fluid in a mixture is the *fugacity* or *effective partial pressure* f which is an expression of the chemical potential μ_i of the species i in the fluid phase. Thus for the chemical potential of carbon dioxide at temperature T , pressure $P = 1$ bar, and for a molar concentration $X_{\text{CO}_2} = 1$ (the fluid phase contains only carbon dioxide).

$\mu^{\circ}_{\text{CO}_2} = \mu_{\text{CO}_2(T, 1, 1)}$
 The fugacity of carbon dioxide f_{CO_2} is defined so that:

$$\mu_{\text{CO}_2(T, P, X)} = \mu^{\circ}_{\text{CO}_2} + RT \ln f_{\text{CO}_2}$$

For perfect gases:

$$f_{\text{CO}_2} = XP = p$$

Where P is the total pressure of the fluid and p the partial pressure of the fluid under consideration.

For gaseous phases which are not perfect gases:

$$f = XP\gamma$$

where γ is the fugacity coefficient.

It is important to know the fugacity of minor species in the fluid phase. The fugacity of oxygen f_{O_2} for example, which corresponds to an extremely small partial pressure (on the order of 10^{-10} to 10^{-20} bar) is nevertheless an important parameter in the study of systems which contain iron, because it controls the degree of oxidation $\text{Fe}^{2+}/\text{Fe}^{3+}$ of this element.

1.10.4 Variation of molar volume in the fluid phase

The molar volume or the specific volume of the fluid phase varies greatly and continuously as a function of P and T following a relation similar to that for ideal gases.

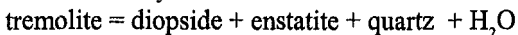
$$PV = nRT$$

Where R is the ideal gas constant and n the number of mols of fluid. Figure 15 shows the variation of the specific volume of water in the form of an *isochore* curve: along which the specific volume is kept constant. For an increase in pressure of 2000 bars (= 0.2 GPa) at 600°C, it is easy to see that the specific volume of water decreases by half.

This continuous variation of specific volume of the fluid phase contrasts with the discontinuous variation of the molar volume of the solid phases: in reality, for a specific solid state assemblage, V varies almost negligibly as a function of P and T ; in contrast, V varies radically when the assemblage becomes unstable in favour of another more stable assemblage during metamorphic reactions. This difference in behaviour between solid and fluid phases explains the particular shape of mineral reactions involving a vapour phase.

Thus, in contrast to what is observed for the reaction between solid phases of constant composition, for which $\Delta S/\Delta V$ remains almost invariable for all values of P and T , this ratio is variable along equilibrium curves which involve a fluid phase because ΔV varies continuously with P and T .

Take the case of a dehydration reaction:



$$\Delta V = (V_{\text{di}} + V_{\text{en}} + V_{\text{qtz}} + V_{\text{H}_2\text{O}}) - (V_{\text{tr}})$$

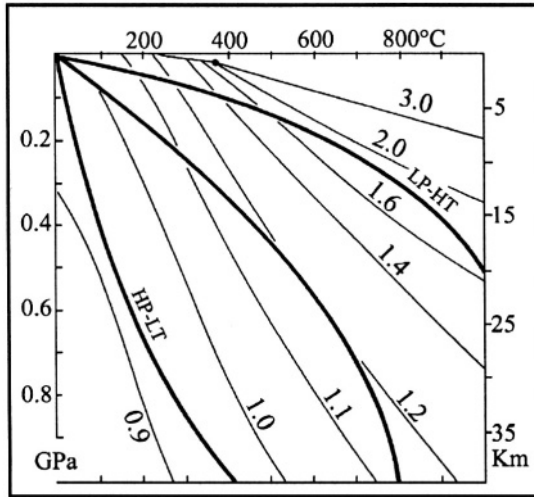


FIG 15. — Variation of the specific volume of water as a function of P and T (after Burnham, Holloway and Davis, 1969)

“Isochore” curves (at constant volume) in cm^3 per gram of water. For most cases, metamorphic conditions fall in the supercritical domain. At the critical point (black spot) the liquid and vapour phase have the same specific volume (*i.e.* the same specific gravity or density). The fluid maintains a specific volume of $1 \text{ cm}^3 \cdot \text{g}^{-1}$ for a geothermal gradient of 13°C per km. These conditions are realized in the case of low temperature - high pressure metamorphism (*cf.* second part of the text). In the more common case, the specific volume of the water vapour phase is greater than this value. Three examples of geothermal gradients taken from figure 5 are added to the diagram (heavy lines). LP-HT : low pressure - high temperature; HP=LT : high pressure - low temperature

This reaction displays a low positive slope at low pressure in the P - T diagram; under these conditions $V_{\text{H}_2\text{O}}$ is high and consequently ΔV is high. As pressure increases $V_{\text{H}_2\text{O}}$ decreases and $dP/dT = \Delta S / \Delta V$ increases, the slope is infinite when $\Delta V = 0$, and becomes negative in the area of P - T space where $V_{\text{H}_2\text{O}}$ is low enough that $\Delta V < 0$. Such slope inversion is characteristic of dehydration reactions of the amphiboles (Fig. 16).

1.10.5 Fluid liberation and entropy difference

The dehydration and decarbonation reactions result in the liberation of water and carbon dioxide molecules formerly locked into crystal lattices in hydrated or carbonate mineral. These reactions involve, therefore, an increase in structural disorder, or, in other words an increase in the entropy of the system. As entropy increase is always linked to a temperature increase, the assemblage which contains a free fluid phase is generally the high temperature assemblage. The high ΔS values which characterize the dehydration and decarbonation reactions explain the steep slopes ($\Delta S / \Delta V$) of the reactions, nearly parallel to the pressure axis under normal metamorphic conditions. These reactions are generally good thermometers if it is possible to evaluate the partial pressures of CO_2 and H_2O .

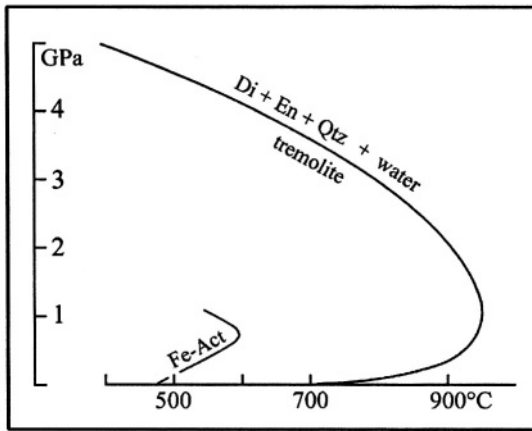


FIG. 16. — Evolution of the slope of the tremolite dehydration reaction for $P_{H_2O} = P_{total}$ (according to Fry and Fyfe, 1969).

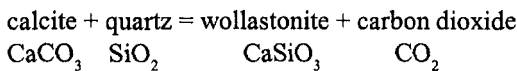
The slope is infinite ($\Delta V = 0$) for P_{H_2O} close to 12 kb at around 950 °C. These conditions are not commonly realized in metamorphic conditions, but may be encountered in the upper mantle. The dehydration reaction Fe actinolite = fayalite + hedenbergite + quartz + water shows a slope inversion around 8 kb and 600 °C (Vielzeuf, 1982), conditions obtainable along certain metamorphic gradients.

Exercise:

Describe the two reactions shown in the figure, in the system CaO - SiO₂ - MgO (H₂O + CO₂) and CaO - SiO₂ - FeO (H₂O + CO₂) (cf. Fig.12). What assemblages result? Are these assemblages found in the carbonate rock series?

1.10.6 Fluid partial pressure and the stability fields of hydrated and carbonate phases

As a rule, the stability of solid phases which accept the (OH)⁻ and (CO₃)²⁻ radicals in their crystal lattice is favoured by high partial pressures of water and carbon dioxide. Take the common reaction in carbonate rocks:



In a closed system where the fluid phase contains only CO₂ ($X_{CO_2} = 1$) the reaction takes place at higher temperatures when the total pressure ($P_s = P_{CO_2}$) is high. The reaction line is a curve because ΔV decreases as function of the pressure. For $X_{CO_2} = 0$ the stability field of the cal + qtz assemblage is considerably reduced because the reaction curve moves to the right at low temperature. But this reaction produces free CO₂ and in a closed system the condition $X_{CO_2} = 0$ cannot be maintained; in the absence of another fluid the assemblage cal + qtz remains stable under the conditions defined by $P_{CO_2} = P_s$. The slope of the reaction for $X_{CO_2} = 0$ (Fig. 17) was established for an open system which allows the CO₂ produced to escape; equilibrium was not attained, and the curve has no geological significance.

Intermediate compositions of the fluid phase ($0 < X_{CO_2} < 1$) are attained when the system contains another fluid phase as well, water, for example. Start from an initial situation in which $X_{CO_2} = 0$ and $X_{H_2O} = 1$. The reaction takes place at low temperature and

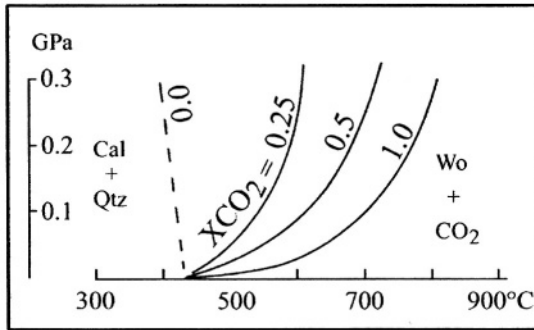


FIG. 17. — Conditions for the reaction $\text{CaCO}_3 + \text{SiO}_2 = \text{CaSiO}_3 + \text{CO}_2$ as a function of partial pressure of CO_2 .

The partial pressure of CO_2 is expressed by the molar concentration of CO_2 in the fluid phase H_2O and CO_2 . The dashed line ($X_{\text{CO}_2} = 0.0$) has no geologic or thermodynamic significance; it was calculated from experiments at atmospheric pressure (1 bar) in an open system. Its negative slope signifies that the CO_2 liberated by the reaction was not taken into consideration in calculating ΔV . Figure after Winkler, 1967 and Vernon, 1976.

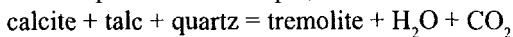
produces CO_2 ; an increase in X_{CO_2} in the fluid phase and in the partial pressure of CO_2 in the system results. The equilibrium moves to higher temperature to a point where the chemical potentials are in equilibrium:

$$\mu_{\text{CaCO}_3} + \mu_{\text{SiO}_2} = \mu_{\text{CaSiO}_3} + \mu_{\text{CO}_2}$$

where

$$\mu_{\text{CO}_2} = \mu_{\text{CO}_2}^{\circ} + RT \ln f_{\text{CO}_2}$$

Figure 17 shows the variation of the reaction for $X_{\text{CO}_2} = 0.25$ and 0.5 . Displacement of this reaction curve produces a vapour phase of pure CO_2 . But other reactions may liberate a mixed fluid phase. For example, the reaction :



liberates a fluid phase characterized by $X_{\text{CO}_2} = 0.6$.

1.11 Metasomatic reactions

In the preceding case only reactions in systems of constant composition (topochemical) were considered. Now consider examples of reactions in an open system. In this case the composition is a *variable* the same as pressure and temperature. In metamorphic systems compositional variations are generally related to movements of the interstitial pore fluid carrying an ionic charge in solution. Short range diffusion (on the order of a metre) also occurs through the interstitial fluid. Solid diffusion through the crystal lattices is generally so slow that it cannot be important in metasomatic processes.

Consider an Al_2SiO_5 system with a fluid phase composed of water with SiO_2 in solution. Note the behaviour of the system under the influence of increasing concentration of K^+ in solution in the fluid phase (Fig. 18).

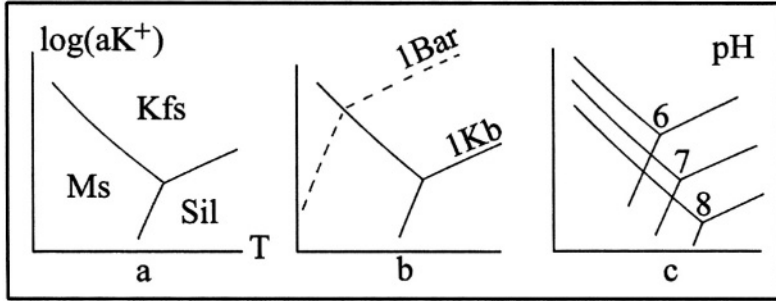


FIG. 18. — *Metasomatic reactions in the $Al_2SiO_5 + SiO_2 + H_2O + K^+$ system.*

The two variables shown on the figure are the temperature and the activity of K^+ in the solution (logarithmic scale). Sil = sillimanite; Ms = muscovite; Kfs = potassium feldspar. Figures 18b and 18c show the respective effect of the water pressure (1 bar and 1 kb) and the pH of the solution (pH 6, 7, 8) on the position of the reactions. After Eugster (1970) in Vernon (1976).

Three reactions may be envisaged:

- (1) $3 \text{ sil} + 3 \text{ SiO}_2 + 2 \text{ K}^+ + 3 \text{ H}_2\text{O} = 2 \text{ ms} + 2 \text{ H}^+$
- (2) $\text{sil} + 5 \text{ SiO}_2 + 2 \text{ K}^+ + \text{H}_2\text{O} = 2 \text{ Kfs} + 2 \text{ H}^+$
- (3) $\text{ms} + 6 \text{ SiO}_2 + 2 \text{ K}^+ = 3 \text{ Kfs} + 2 \text{ H}^+$

These reactions are controlled by the activity of K^+ ($= [a K^+]$) and silica ($= [a SiO_2]$) in solution in the fluid phase. They are also controlled by pH_2O which plays a role in reaction (1) and (2), but not in reaction (3) because H_2O is not involved in this reaction. fH^+ plays a part in all three reactions. This last parameter is the hydrogen fugacity expressed as the pH of the solution (antilogarithm of the H^+ concentration of the solution). A low pH (high H^+ concentration in the solution) widens the stability field of sillimanite and muscovite at the expense of potassium feldspar, because movement of the reaction to the right produces free H^+ . The phase relations in the system depend, in consequence, on the intensity of these two parameters as shown in Figure 18. Reaction (3) is not displaced in the diagram by the variation of pH_2O , and the stability field of muscovite is greatly enlarged under high pH_2O conditions.

RESUME: THE FACTORS OF METAMORPHISM

The nature of the mineral assemblages and the textures of metamorphic rocks depend on different factors:

The *pressure* P is expressed as lithostatic pressure P_s and as fluid pressure P_f when a free fluid phase is present. The partial pressure of a postulated fluid depends on the concentration of that phase in the fluid, or more precisely on its fugacity. The effect of tectonic overpressure is negligible under metamorphic conditions, but stress anisotropy becomes shear stress τ which controls the deformation; the development of textures in metamorphic rocks depends largely on this parameter (see Chapter II). At a given pressure, or depth, the temperature T depends on the shape of the geothermal gradient, which, in turn, reflects the lithosphere dynamics of the particular region. The free energy G of mineral assemblages varies as a function of P and T. Under given conditions, the most stable assemblage is that with the lowest free energy. The nature of the mineral assemblages is, therefore, the direct

result of the P-T conditions applied to a given system at a given moment.

The *composition of a system* is expressed as masses or concentrations of its constituents. The reaction curves which separate a system depend, naturally, on its composition. Systems are commonly considered *closed* and do not change composition in the course of metamorphism. They should sometimes be considered as *open*, especially to the circulation of fluids which transport ions in solution, in this case the evolution of the system is *metasomatic*.

The *time*: the intensity of the P and T variables evolve through time in relation to the deformation of geothermal gradient, a consequence of the global dynamics of lithospheric plates and the convective mantle. This results in a temporal evolution of P-T conditions in metamorphic systems which reflect global evolution and internal geodynamics. Mineral reaction kinetics are generally less rapid than the variation of crystallization conditions which results in the superposition of disequilibrium assemblages in metamorphic rocks. Interpreting the evolution of mineral assemblages in a metamorphic rock or in a metamorphic series, therefore, contributes to the understanding of the internal dynamics of the earth.

This page intentionally left blank

METAMORPHIC ROCKS

TEXTURES STRUCTURES AND NOMENCLATURE

In contrast to eruptive rocks which are classified in different logical ways on the basis of their mineralogical and chemical composition, metamorphic rocks do not yet have a clear, universally accepted nomenclature. An international commission is at work, but its recommendations are not yet available.

Metamorphic rock nomenclature uses structural or textural criteria, the nature of the rock's *protolith* (original rock from which the rock was derived) or the observed mineral assemblages. It is not totally rational and depends on local or regional usages. For this reason it is useful in all cases to describe the rock briefly, underlining its textural and mineralogical characteristics in precise terms.

STRESSES AND TEXTURES

Texture describes the different types of arrangements between the minerals of a rock. They are the result of a competition between different processes of crystallization. These recrystallizations are in part related to the reactional mechanism, in other words the minimization of the Gibbs free energy (*cf.* preceding chapter), but they result also from simple textural rearrangements without modification of the mineral assemblage. These rearrangements also correspond to the minimization of potential energy. Detailed descriptions of textures, and the mechanisms that produce them, are given in the works cited at the end of this volume.

2.1 Syntectonic recrystallization

This type of recrystallization occurs in material which has undergone anisotropic stress; it is the consequence of tectonic deformation and, in general, it results in a diminution of the average grain size. Deformation effectively strains the crystal lattices of the grains, which acquire an elastic deformation energy by the increase in lattice defects in the crystals. In order to minimize this deformation energy, these dislocations must be eliminated. This results first in the formation of *subgrains* then by *neoblasts* at the expense of the deformed crystals. These latter commonly occur only sporadically; they consist of clasts, or porphyroclasts when their size remains significantly greater than that of the neoblasts (Fig. 19a).

2.2 Annealing

This is principally a post-dynamic process. It consists in part of the final dissipation of deformational energy in its waning stages, but its most important aspect is that it is controlled by a very important process for textural rearrangement, the *minimization of inter-*

granular surface energy. The grain contacts (or interfaces) correspond effectively to disoriented structural domains in which atoms are not as regularly arranged as they are in the core of the crystals. The grain boundaries possess a disorder energy which is proportional to the surface area, to which the surface tension energy must be added. The minimization of this energy requires a reduction in intergranular surface, in other words an increase in grain size by migration of the grain borders (Fig. 19b). In a monomineralic system under isotropic stress at an appropriate temperature, the minimum intergranular surface results in the development of equidimensional grains with faces making an angle of 120° . This ideal case is almost attained in rocks exclusively composed of calcite (marble), quartz (quartzite), plagioclase (anorthosite) or olivine (dunite).

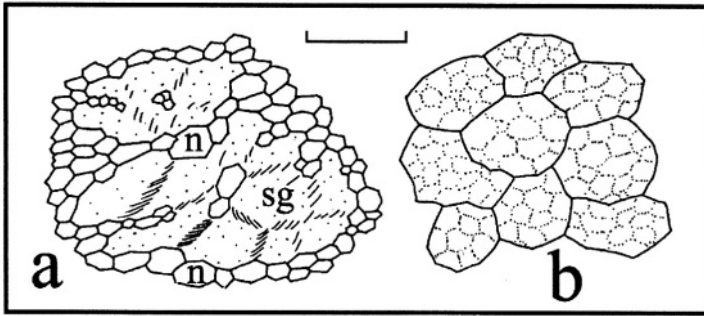


FIG. 19. — *Recrystallization in the solid state.*

a) Synkinematic recrystallization: deformed grains divide into subgrains (sg) and recrystallize as neoblasts (n). This results in a minimization of the dislocation energy. The deformed relics of the original grains form porphyroclasts. b) Annealed; late to post-kinematic. The original grains (outlined in dotted lines) reorganize, reorient and grow in size by the migration of grain boundaries. This results in a minimization of crystal surface energy. For more details consult Nicolas, 1988. Scale of figure about 2 mm.

STRESSES AND STRUCTURES

Certain structures in metamorphic rocks are inherited from their protolith. This is often the case in contact metamorphic rocks which commonly preserve the trace of sedimentary stratification. Inherited igneous structures are also observed, former veins and xenoliths, for example. The most common and most characteristic structures are the planar and linear structures acquired during the deformation and recrystallization which accompany regional metamorphism.

2.3 Development of planar and linear structures: schistosity, foliations and lineations

2.3.1 Discontinuous and continuous deformation

As a result of anisotropic stress, rocks deform in two different ways depending on their ductility.

Brittle mode. This affects competent rocks. The shear stress τ is at a maximum in planes

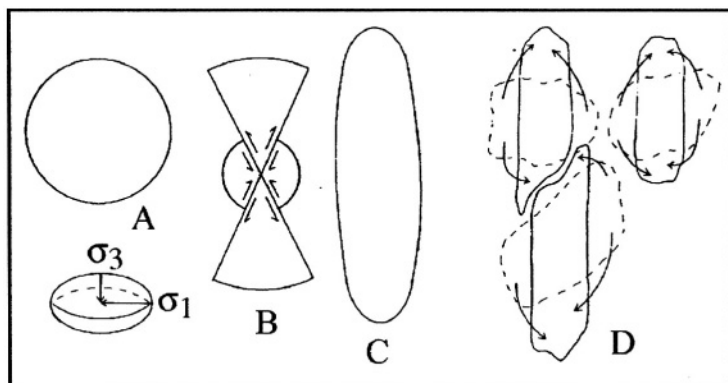


FIG. 20. — *Continuous and discontinuous deformation.*

Competent materials deform in a brittle mode when anisotropic stress is applied (B). The elongation (parallel to σ_2) and shortening (parallel to σ_1) are accommodated by shear planes located at 45° to the principal stresses. These fault planes rotate into the axial plane of the deformation as the flattening becomes marked. Incompetent materials (C) flow in the elongation or transport direction parallel to σ_3 . This flow is the result of a rearrangement of particles (D) which leave high energy sites (in the σ_1 direction) to go to low energy sites (in the σ_3 direction). A initial solid system. B discontinuous deformation. C continuous deformation. D sketch of the flow mechanism: particles diffuse along intergranular boundaries if an interstitial or adsorbed fluid phase is present. For more details consult Mattauer (1973), Bard (1980) Nicolas 1989) and Gratier (1993).

containing σ_2 and at 45° to the principal stresses σ_1 and σ_3 (Fig. 3). The elongation and shortening of the system is assured by slip along discrete faults near these planes (Fig. 20).

Ductile mode

This affects incompetent materials. It results in solid flow controlled by a solution-recrystallization mechanism which contributes to the minimization of deformation energy. Crystals in the presence of an intergranular fluid phase are dissolved at *high energy* sites (perpendicular to σ_1) and develop in *low energy* sites (in the transport direction σ_3). This results in a flattening of the system perpendicular to σ_1 and an elongation parallel to σ_3 . If, for the sake of argument, the initial rock was composed of spherical particles, each of the spheres is transformed into a flattened ellipsoid in the σ_2 - σ_3 plane. This results in a planar structure perpendicular to σ_1 (Fig. 20). The solution-recrystallization mechanism is controlled by the development of a chemical potential difference $\Delta\mu$ between the solution zone and the recrystallization zone such that:

$$\Delta\mu = \Delta\sigma_n V + \Delta V\sigma_n + \Delta W_E + \Delta W_P + \Delta W_S$$

In the expression $\Delta\sigma_n = \sigma_1 - \sigma_3$; ΔV = the difference in molar volume of the solid, ΔW_E , ΔW_P and ΔW_S the difference in elastic, plastic and surface energy between the solution and crystallization zones. This excess potential in the solution zones adds its effect to an ultimate excess in free energy ($\Delta G > 0$) with respect to the crystallization zones, which accounts for the fact that mineral reactions are favoured by deformation. When the temperature is high, continued deformation is controlled by the plasticity *sensu stricto* character-

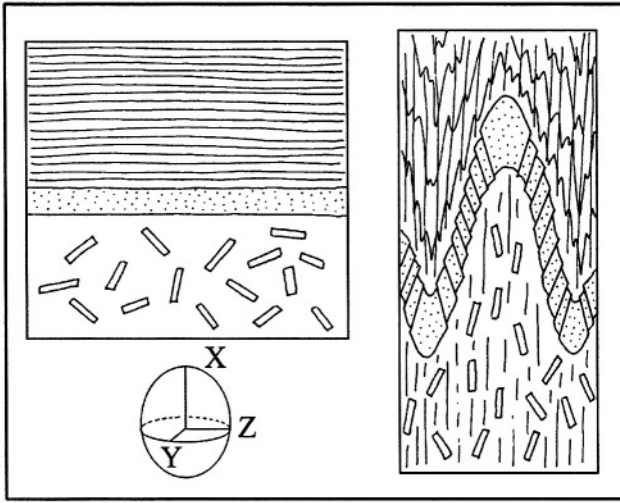


FIG. 21. — *Development of a planar structure (schistosity and foliation) in metamorphic rocks in a pure shear regime*

Orientation of passive markers (rectangles) during flattening; development of slaty cleavage parallel to the axial planes of folds (and perpendicular to σ_1) by flow of ductile material (lines). Development of fracture cleavage in the more competent rocks (dotted). Fracture cleavage is oblique to the axial plane of folds, but approaches it with increasing flattening. Furthermore, the materials become incompetent with increasing temperature; as a result fracture cleavage is only present in zones of relatively low grade metamorphism. X, Y and Z axes of the strain ellipsoid.

2.3.2 Strain ellipsoid

In reality the spatial relationship between the stress axes and structure is not directly apparent from the study of rock deformation. In fact, cleavage and foliation often develop in a “simple shear” regime and the deformation is not coaxial (*cf.* the work of Nicolas, 1988). It is, therefore, more realistic to consider the “finite deformation” of a sample represented by the “strain ellipsoid”. The X and Z axes of this ellipsoid (Fig. 21, 22) represent respectively the maximum shortening and elongation registered by the sample, or by the geologic unit.

2.3.3 Slaty and fracture cleavage

Metamorphism takes place at relatively high temperatures ($> 300^\circ\text{C}$). Under these conditions most materials are likely to flow under the influence of anisotropic stress, all the more easily if metamorphic reactions take place involving a rearrangement at the crystalline scale (minimization of G). Planar anisotropies develop in metamorphic rocks, therefore, called slaty cleavage, schistosity or foliation. In pure shear regimes these surfaces are parallel to the axial planes of folds contemporaneous with the deformation (Fig. 21).

In heterogeneous series, contrasting competencies are often associated. Under low grade, low temperature conditions, deformation is therefore heterogeneous, and a slaty cleavage develops in ductile (incompetent) materials whereas the more competent horizons are still affected by a brittle deformation, which leads to the development of a non-penetrative fracture cleavage, oblique to the axial planes of folds (Fig. 21). The overall flattening

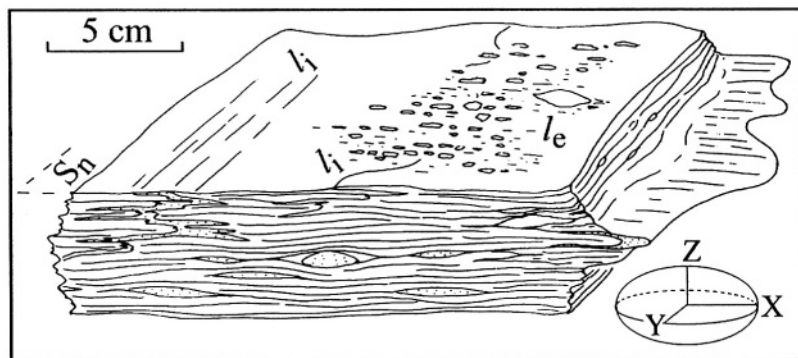


FIG. 22. — *Structural characterization of a deformed metamorphic rock (gneiss or schist)*
 The left part of the figure shows a moderate deformation (flattening domain), the right part shows a more intense deformation (flow domain). S_n = schistosity or principal surface. Elements of a folded earlier surface ($S_{(n-1)}$) are seen on the figure as well as prekinematic objects stretched into almonds and displaying pressure shadows (porphyroclasts). The intersection between S_n and $S_{(n-1)}$ defines the lineation li , parallel to the Y axis of the strain ellipsoid, in the flattening zone, but more or less stretched in the elongation direction in the flow domain. The hinge of an intrafolial fold, which is shown on the right, is also stretched in the elongation direction and becomes a sheath fold. The principal surface S_n contains synkinematic mineral assemblages which describe an elongation lineation L_e parallel to X. For more detail, consult Mattauer (1973) and Nicolas (1988). X, Y and Z : axes of the strain ellipsoid.

tive fracture cleavage, oblique to the axial planes of folds (Fig. 21). The overall flattening of the heterogeneous series accentuates the development of a planar structure. Effectively, the greater the shortening, the more the fracture cleavage planes approach the axial planes of the folds. In particular, *passive* markers (unrecrystallized by the deformation) which are tabular (feldspars, micas, etc.) and originally randomly distributed, assume a clearer orientation when the flattening is greater (Fig. 21).

2.3.4. Schistositities and lineations

Lineations are linear structures within the schistosity planes, and there are two principal types; intersection and stretching lineations.

Intersection lineations. These are formed by the trace of an earlier surface, such as a stratification or an earlier schistosity on the plane of schistosity

Stretching lineations. These are formed by oriented crystal growth during schistosity development induced by solution-recrystallization and flow mechanisms as well as by the deformation of passive markers in the elongation direction.

Based on the preceding elements, figure 22 shows schematically the principal structures observed in metamorphic rocks.

2.4 Schistosity, recrystallization and relative chronology

The sequential development of schistositities in metamorphic rocks allows elaboration of a relative chronology of deformation. Rarely is the principal surface observed in a metamorphic rock the stratification (S_0); in most cases it is a schistosity (S_n) which may commonly

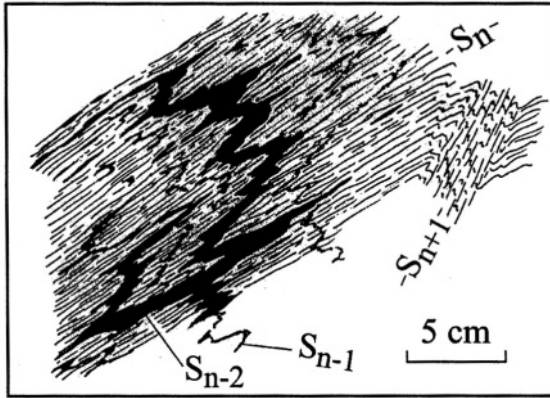


FIG. 23. — *Superposed deformations in a metamorphic rock*

The principal surface S_n is superposed on an earlier surface $S_{(n-1)}$, which is itself a schistosity affecting a surface $S_{(n-2)}$ drawn in black. This $S_{(n-2)}$ surface is possibly the original stratification S_0 . An early fold hinge $F_{(n-1)}$ may be seen refolded by F_n . The S_n surface is itself refolded by a crenulation $S_{(n+1)}$ associated with a crude schistosity. An average observer is capable of deciphering such superposed surfaces in certain outcrops of metamorphic rocks found in the French Massif Central and elsewhere in the world.

Exercise:

Identify the different fold generations.

be demonstrated to result from deformation affecting an earlier schistosity (S_{n-1}). The principal surface (S_n) is itself often deformed and affected by a crenulation, accompanied by a crude schistosity (S_{n+1}). Figure 23 shows the overprinting of deformations schematically.

2.4.1 Pre- syn- and post-kinematic phases

Three generations of crystals or parageneses may be distinguished with reference to the principal schistosity. The pre-schistosity (or prekinematic) domain is characterized by a mineral assemblage which antedates the development of the reference schistosity. The syn-schistosity minerals developed at the same time as the schistosity, and the post-schistosity phase postdates that surface (Fig. 24).

Detailed descriptions of different criteria used to distinguish these three generations of minerals are given in reference volumes. Only the most evident characteristics are summarized here.

Pre-schistosity phases. These are affected by the deformation which accompanied schistosity development. They show a weak to marked distortion (undulose extinction, development of subgrains, mechanical twins, flexures, folds, etc.: Fig. 24a). They have generally undergone a partial recrystallization which is more or less accentuated, depending on the intensity of the deformation. They also define the extent of sheltered zones which have not undergone the general flattening of the rocks; these *pressure shadow* zones are the site of unoriented syn-schistosity recrystallization. Where pre-schistosity phases occur as relatively big crystals, these phases are called clasts or porphyroclasts.

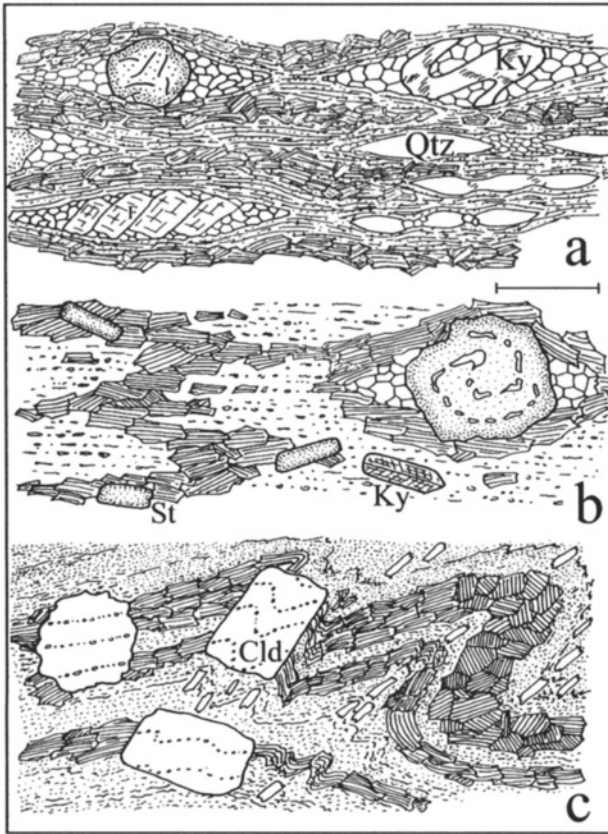


FIG. 24. — *Differing types of parageneses with respect to schistosity development.*

a) Pre-tectonic paragenesis: note the deformation in the crystals of kyanite (Ky) and feldspar (F), the boudinage of the quartz almonds (Qtz) and the pressure shadow zone controlled by the pre-tectonic minerals which resisted the flattening of the rock.

b) Syntectonic paragenesis: note that the biotite orientation is independent of the fold drawn on the left hand side of the figure; the orientation of the staurolite (St) and kyanite (Ky) controlled by the schistosity without pressure shadows, and the train of helicitic inclusions in the garnet.

c) Post-tectonic paragenesis: note the crystals superimposed on earlier structures, one of the chloritoid porphyroblasts (Cld) and the flakes of white mica are developed on the axial plane of the crenulation; their crystallization is controlled by this deformation; note that the early biotite is recrystallized in a post-dynamic manner in the fold hinge to the right of the drawing. This is a phenomenon known as "polygonal recovery". Scale 0.5 mm to 1 cm. For more details consult Bard (1980) and Nicolas (1988).

Syn-schistosity phases. Their growth is controlled by schistosity development. These phases are generally oriented parallel to the schistosity plane (particularly planar minerals such as the micas), and sometimes parallel to the elongation direction defining a lineation. The syntectonic minerals are not deformed by the syndeformational folds and they often give the impression of “cutting across” fold hinges. Garnets have a spectacular growth habit, commonly having helicitic inclusion trains (Fig 24b) which result from a rotation of the crystals during their development, caused by shearing induced by the deformation. This interpretation is controversial.

Post-tectonic phases. These develop independent of the stresses causing the schistosity. They commonly have a porphyroblastic growth typical of the annealing phase, which leads to crystals with a large grain size in relation to other elements of the rock (porphyroblasts). Their forms are superimposed on earlier structures (schistositities, folds, crenulation) which are observed as “palimpsest” texture within the crystals (Fig. 24c). Birefringent minerals are characterized by a sharp extinction as opposed to the undulose extinction of porphyroclasts.

2.4.2 Temporal evolution of metamorphic conditions; P-T-t paths

In certain ideal cases the P-T stability conditions of successive, pre- syn- and post-tectonic parageneses can be evaluated for a rock or a suite of metamorphic rocks (*cf.* Chapter 3). The resulting variation in conditions, in relation to schistosity development, or their temporal development, are shown in P-T diagrams which interpret, more or less faithfully, the play of geodynamics accompanying (or responsible for) the metamorphic recrystallization. This schematic representation of the pressure and temperature evolution over time is called the “P-T-t path” followed by the sample or the entire metamorphic rock series.

2.4.3 Polyphase metamorphism or polymetamorphism

An important point is to determine if the apparently oldest paragenesis of a metamorphic rock (pre-tectonic paragenesis) was developed during the same geological event as the later parageneses (syn- or post-tectonic) or if it relates to an earlier tectonometamorphic episode. These two opposite cases are polyphase metamorphism and polymetamorphism.

Polymetamorphism. The development of new mineral assemblages and schistositities in a metamorphic rock sometimes leaves deformed relics of an earlier paragenesis. In this case there is a superposed effect of two events, distinct in time, that is to say, polymetamorphism. A clear example of polymetamorphism is observed in certain rock units in the Internal Zone of the Alps (Sesia Lanzo: Fig.25a) where Eoalpine (120 Ma) recrystallization is superimposed on Hercynian (280 Ma) assemblages. The coexisting older and younger parageneses result from very different crystallization conditions. The first are still preserved in the least deformed rocks (low dislocation energy) because the Alpine recrystallization occurred at low temperature where the reaction kinetics were very slow.

Polyphase metamorphism. In this case the succession of recrystallizations is the result of a single tectonometamorphic event. The example depicted (Fig. 25b) is also from the Sesia Lanzo zone (Internal Zone of the Alps). The relative succession of the different paragen-

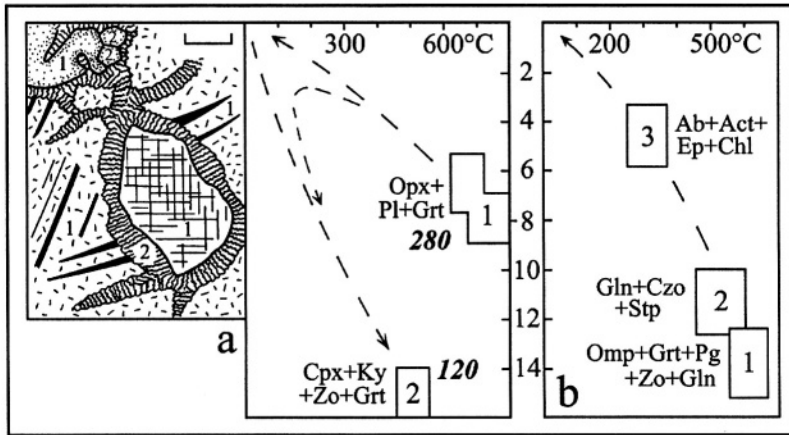


FIG. 25. — *Polymetamorphism and polyphase metamorphism*

a) Example of polymetamorphism; a Hercynian granulite (280 Ma) from the Sesia Lanzo zone (Internal Zone of the Alps) displays an initial assemblage (1) of orthopyroxene (cross-hatched), plagioclase (twinned), and garnet (dotted). This assemblage recrystallized during an Eoalpine phase (120 Ma) and fine crystals of kyanite and zoisite developed (dashed lines) within the plagioclase (1); the original garnet (1) is partly recrystallized in garnet (2) with an enrichment in Ca and Mn; symplectite (wavy lines) develops between the crystals of the first paragenesis (1); it is composed of clinopyroxene, kyanite and zoisite (scale 0.2mm). This evolution results from very contrasting crystallization conditions caused by the involvement of crustal units belonging to the Austro-Alpine margin in the Eoalpine subduction (*cf.* second part of text). After Lardeaux and Spalla (1991).

b) Polyphase evolution of an eclogite schist in the Sesia Lanzo zone. The primary paragenesis of omphacite and garnet (rectangle 1) represents the peak of metamorphism and was recrystallized at lower pressure conditions (rectangle 2) before being partly transformed into a low pressure assemblage (rectangle 3). This evolution results from rapid subduction of oceanic crustal units, followed by their rapid rise to the surface during collision (*cf.* second part of text). After Pognante 1991. opx = orthopyroxene; pl = plagioclase; grt = garnet; cpx = clinopyroxene; ky = kyanite; zo = zoisite; omp = omphacite (jadeite-rich clinopyroxene); pg = paragonite (Na analogue of muscovite); gln = glaucophane (Na amphibole); czo = clinozoisite; stp = stilpnomelane; ab = albite; act = actinolite; ep = epidote; chl = chlorite. Temperature in °C.

eses may be observed in relation to the development of one or several schistositities, or by the almost continuous zoning of the crystals characterizing the evolving P-T conditions during metamorphism. They follow in a continuous variation which results from a succession of convective and conductive thermal mechanisms related to the metamorphism (*cf.* second part of this book). As a result, the rocks pass through several metamorphic facies (*cf.* Chapter III) during their evolution. The *polyphase* metamorphism which results, may also be called *multifacies* metamorphism. It is sometimes possible to date each of the separate parageneses by detailed geochronological methods. The evolution of the mineral assemblages of multifacies metamorphism is therefore placed in a precise chronological framework (Fig. 26).

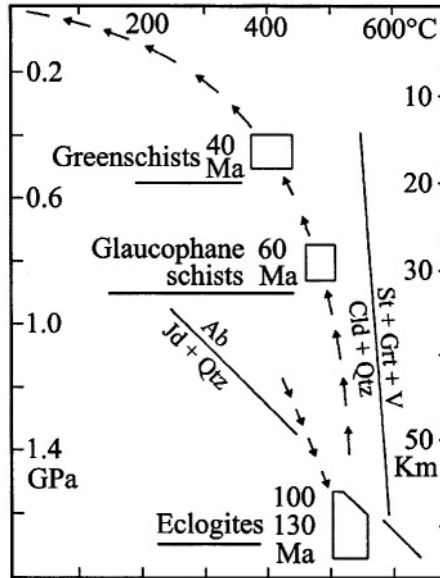


FIG. 26. — Age of recrystallization in the Sesia Lanzo zone (after Rubie, 1984). The high pressure stage (eclogites; clinopyroxene + garnet) was dated as Lower Cretaceous by the Rb-Sr method. The glaucophane schist and greenschist were dated as Paleocene and Eocene by the K/Ar method. Jd = jadeite; Qtz = quartz; Ab = albite; Cld = chloritoid; St = staurolite; Grt = garnet; V = vapour. Arrows follow path of Alpine polyphase metamorphism.

2.4.4 “Clockwise” and “anti-clockwise” *P-T-t* paths: a question of choice

The evolution of metamorphic conditions over time, for a sample or for a metamorphic series, generally develops a curve in *P-T* space whose shape may have an interesting geodynamic significance. As a result, numerous authors distinguish “clockwise” and “anti-clockwise” behaviour. This distinction is only significant if the ordinal axes of the diagram are always shown in the same way, increasing pressure values toward the top of the figure. In this text they may be presented differently in a certain number of diagrams with pressure rising with depth, or toward the bottom of the figure. The significance of the clockwise and anti-clockwise terms may then be inverted. To avoid confusion, these terms will not be used in the following treatment.

2.5 Texture and nomenclature of metamorphic rocks

The preceding data provide a basis for a systematic classification of metamorphic rocks.

2.5.1 Principal textures of metamorphic rocks

The development of textures (Fig. 27) is controlled by the stress regime and by the nature of the minerals of the rocks or their chemical composition. *Granoblastic* texture characterizes rocks composed essentially of minerals with relatively regular shapes (quartz, feldspar, garnet, cordierite, pyroxenes, olivine, carbonates etc.). When the stresses are isotropic or weakly anisotropic during recrystallization, the textures produced are close to the ideal

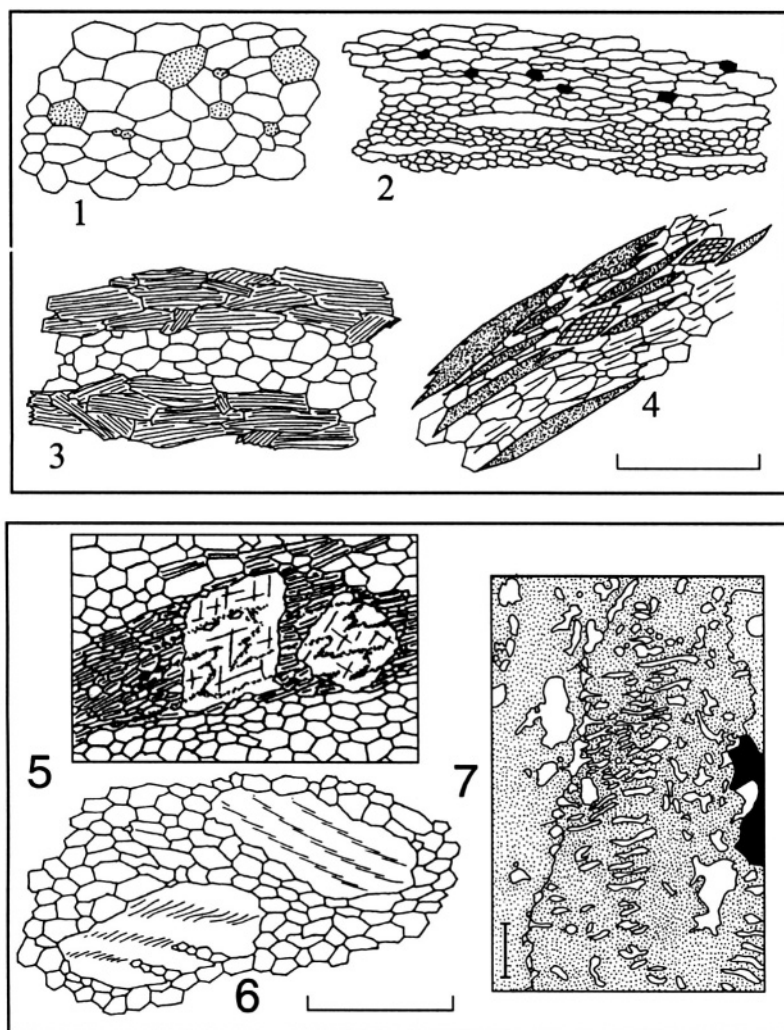


FIG. 27. — *Principal textures of metamorphic rocks.*

Scale: 1 to 6, 1 cm to 1 mm; 7, 0.1 mm. 1) Granoblastic texture, hornfels, granofels or marble. 2) Oriented granoblastic and blastomylonitic texture, gneiss, leptynite. 3) Granolepidoblastic texture, gneiss, schist. 4) Granonematoblastic texture, amphibolite. 5) Porphyroblastic texture. 6) Porphyroclastic texture. 7) Symplectitic texture, reactional intergrowth of clinopyroxene and plagioclase in an eclogite (in Joanny, 1991).

arrangement resulting from the minimization of surface energy, with grain boundaries at 120° . More sharply anisotropic stresses lead to a preferential growth of grains parallel to the foliation, and the texture becomes *oriented granoblastic*, the orientation being determined by the trace of the foliation on the observation plane. A strongly accentuated deformation (strong stress anisotropy) leads to *blastomylonitic* texture characterized by very fine-grained neoblasts amongst which porphyroclasts are dispersed.

The *lepidoblastic* textures (from *lepidos* = scale) are characteristic of rocks rich in phyllosilicates (chlorite and micas of platy *habit*) disposed parallel to the schistosity. The *nematoblastic* texture (from *nematos* = needle) is characteristic of rocks rich in acicular minerals (amphibole, sillimanite) whose orientation commonly defines an elongation lineation.

The association of centimetric bands rich in platy or acicular minerals alternating with bands rich in quartz and feldspar in the same rock, results in mixed textural terms (*granolepidoblastic* and *granonematoblastic*) which are extremely widespread in metamorphic series formed by the recrystallization of pelites and greywackes.

The term *porphyroblastic* denotes all textures characterized by the development of large crystals (*porphyroblasts*) generally post-kinematic. The term *porphyroclastic* is used to describe the presence of deformed pre-kinematic crystals of large size (*porphyroclasts*).

Finally the texture *symplectitic* (or *symplectic*) is characterized by the abundant reactional intergrowths in which newly formed crystals remain in a very fine-grained vermicular form imbricated on one another (*symplectite*). This type of texture results from the development of *coronas* around reactional minerals, or their partial transformation into a corona resulting from a chemical instability. The symplectite evolution or coronization characterizes rapid thermobaric evolution in which assemblages do not reach equilibrium. The temperature is too low at the end of the evolution to allow the minimization of surface energy and the annealing of the symplectites.

2.5.2 Nomenclature of metamorphic rocks

As mentioned at the start of this chapter, there is no classification to speak of. The nomenclature of metamorphic rocks is essentially descriptive and falls in a framework of more or less widely used terms. There are also a certain number of synonyms and one or other may be used according to the particular character of the rock which appears desirable for emphasis. It is possible to present three different points of view; the nature of the protolith, the structure and the mineral composition of the rocks.

2.5.2.1 Nature of the protolith. If the original rock (protolith) is still clearly recognizable it is useful to attach the prefix *meta* to the rock name. *Metabasalt*, *metagranite*, *metapelite* and *metachert* are some examples of names widely used. When the protolith is not clearly identified, but if its origin—igneous or sedimentary—is identified, the prefixes *ortho* and *para* are often used. Thus an *orthogneiss* may be a metamorphosed granite whereas a *paragneiss* may be a *metapelite* or a *metagreywacke*.

2.5.2.2 Structure of the rocks. Here the nomenclature is largely founded on the presence or absence of a schistosity.

Non-schistose rocks. These are generally characterized by an isotropic granoblastic texture. These are the *hornfels* or *granofels*, depending on the mean grain size (less than or greater than 0.1 mm respectively). These terms are not applied to carbonate rocks.

Schistose rocks. These are called *schist* when the schistosity planes are closely spaced

(thickness of the laminae between the schistosity on the order of mm). They become *gneiss* when the spacing is of the order of cm. The current usage among French speaking geologists is to reserve the term *gneiss* to granolepidoblastic rocks which show an alternance of quartzofeldspathic and micaceous layers at the cm scale. Micaceous layers are relatively scarce or absent in orthogneisses. The term *schist* designates either biotite or muscovite rich micaceous schists. Contrary to certain abuses in the past, there is no reason to suppose *a priori* that a *gneiss* is necessarily the result of a higher degree of metamorphism than a *schist*, and only the descriptive character of these terms must be retained.

A relatively common category of schists is the *spotted schist*, for those rocks generally associated with contact metamorphism (*cf.* second part of the text) which are characterized by porphyroblasts of cordierite and/or andalusite altered to phyllosilicates (white mica and chlorite) disposed in a fine-grained, unoriented, granoblastic matrix.

The nomenclature based on structure is applied essentially to metapelites, metagreywackes and metagranitoids. However the term *schist* may also be applied to certain metabasites: *greenschist* (epidote, chlorite and albite schist); *glaucophane schist*, etc.

Certain textural elements drawing attention to specific characteristics of rocks may be used to complete this nomenclature. One of these typical cases is *augen gneiss* (*augen* = eyes in German). These rocks contain large feldspathic or quartzofeldspathic masses dispersed in an oriented granulepidoblastic matrix, whose grain size is significantly finer. In a large number of cases the eyes of the *augen gneiss* are composed of a pre-metamorphic element (Fig. 28). The *augen* are:

- a) either porphyroclasts of potassium feldspar or plagioclase derived from former granitoid phenocrysts. In this case the *augen* structure proves the *ortho-derived* nature of the *gneiss*, or
- b) quartzofeldspathic almonds, more or less drawn out, formed by synkinematic boudinage of granitic veinlets formerly included in a migmatized metapelite; in this case the *augen gneiss* is *para-derived*.

2.5.2.3 Mineral composition of the rock. The nature of the mineral assemblage allows an *ad libitum* qualification to the description of metamorphic rocks (epidote hornfels; staurolite-kyanite schist; sillimanite-garnet *gneiss*; etc.). It is also the basis of the common nomenclature of the metabasites, and in a more general fashion, the metamorphic rocks rich in Ca.

The terms amphibolite and pyroxenite define themselves as well as their more precise equivalents (glaucophanite, diopsidite, etc.). Biotitite, albitite, epidotite are also used more or less systematically. Each of these terms is commonly modified by the additional notation of another significant mineral in the paragenesis (epidote amphibolite, garnet pyroxenite, etc.).

Eclogites are garnet pyroxenites, by definition devoid of plagioclase; a negative approach, but essential for the definition of these rocks. Experience shows that the clinopyroxene of eclogites (omphacite) is relatively rich in *jadeite* ($\text{NaAlSi}_2\text{O}_6$) but this is not always respected.

The metamorphosed carbonate rocks (calcite and dolomite) are *marbles* where the

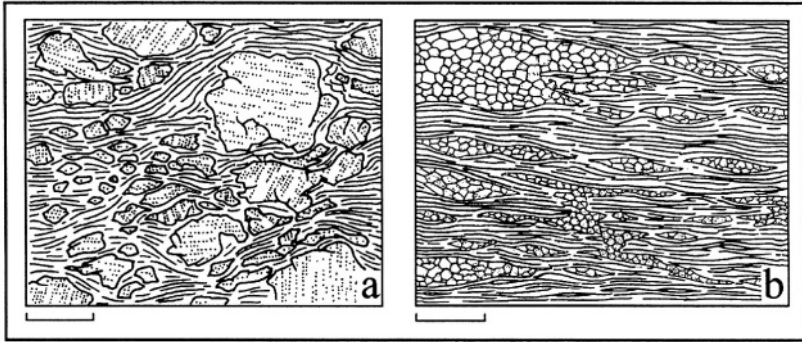


FIG. 28. — *Texture of augen gneisses*

- a) The “eyes” are composed of single prekinematic crystals of potassium feldspar and plagioclase, which are more or less deformed and fragmented. Scale = 3 cm. This porphyroclastic texture is the result of deformation and metamorphism of a porphyritic granite. The rock is an ortho-augen gneiss. Canigou gneiss, Eastern Pyrenees, after Guitard, 1970.
- b) The “eyes” are composed of a granoblastic quartzofeldspathic assemblage including a bit of biotite. Scale = 5 cm. The eyes are formed by synkinematic boudinage (syn- or late migmatite) of granitic veinlets injected in a metapelite during a phase of migmatization. This is a para-augen gneiss. Port-Navalo gneiss, Loire Atlantique, after Johannes, 1988.

schistosity is poorly or not developed, in the other case the term *calc-schist* is used. Marbles and calc-schists are nearly always *metalmstones*, the probability of the existence of *metacarbonatites* is extremely small. Note that the term marble has a wider and more general application in the dimension stone industry where it denotes any rock capable of taking sufficient polish to be used for ornamental purposes. Many of the marbles of this industry may actually be granitoids, anorthosites and serpentinites.

Among the different terms presented in this section, certain are used not only to give a petrographic characteristic for this type of rock (greenschist, amphibolite, eclogite) but also to define metamorphic conditions (*cf.* Chapter 3). The ambiguities which result from this double usage will be underlined further on.

EVALUATION OF METAMORPHIC CONDITIONS

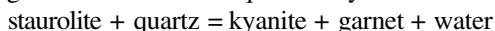
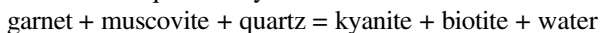
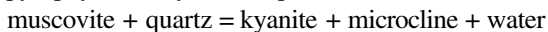
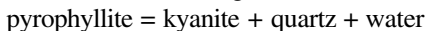
The nature of the most stable mineral assemblage in a rock of a given composition is a consequence of the minimization of the free energy G of the system. As G is a function of P and T , there is, therefore, a direct liaison between a paragenesis and its crystallization conditions. The evaluation of these conditions is a difficult exercise which has aroused the interest of petrologists for decades. The results which can presently be obtained are not completely satisfactory; however, without being able to determine the absolute values of P and T with great precision, it is still possible to characterize metamorphic gradients as well as their evolution in time conveniently from the data provided by the metamorphic parageneses. These parameters are the basis for thermal models which themselves reflect the geodynamic mechanisms responsible for the formation of mountain chains.

INDEX MINERALS AND METAMORPHIC ISOGRADS

An elementary method, which can be used in the field with the aid of a simple hand lens, allows (in principle) mapping of surfaces of equal metamorphic intensity, or *isograds*. These isograds are based on the appearance, or eventually the disappearance, in the series, of characteristic minerals or *index minerals*. These observations have demonstrated, since the initial work of Tilley in 1925, that successive zones are the result of conditions of increasing metamorphic grade. The chlorite, biotite, garnet, staurolite, kyanite, sillimanite zones, for example, appear in the metapelites of the Scottish Highlands or of the Lower Limousin (Fig. 29).

Mapping isograds is the fundamental field technique for the study of a metamorphic series, but this method is too crude to allow a detailed interpretation. Three factors, in particular, result in the index minerals becoming unreliable;

- 1) the appearance or disappearance of a mineral phase does not depend uniquely on metamorphic conditions, but also on the composition of the rock. In heterogeneous series the distribution of index minerals is of no use in mapping an isograd surface, especially if the metamorphic zones are oblique to the lithology.
- 2) The appearance or disappearance of a phase is the result of mineral reactions. The different reactions involved in the crystallization of an index mineral do not necessarily take place under the same conditions. The appearance of kyanite (**isograd ky^+**) could result from the following reactions:



Therefore, to map the appearance of kyanite without paying attention to the nature of the reactions which are responsible for the crystallization of the mineral provides little reliable information on the real distribution of metamorphic isograds.

- 3) The spatial distribution of index minerals depends on the deformation which affected

the series after crystallization. Isograds or pseudo-isograds which can be proven to have been considerably deformed offer, as a result, no direct significance to the interpretation of metamorphism. Figure 30 shows the structural complexity of the Lower Limousin, which, after a second look, does not lend itself to a clear study of metamorphic isograds, using only index minerals.

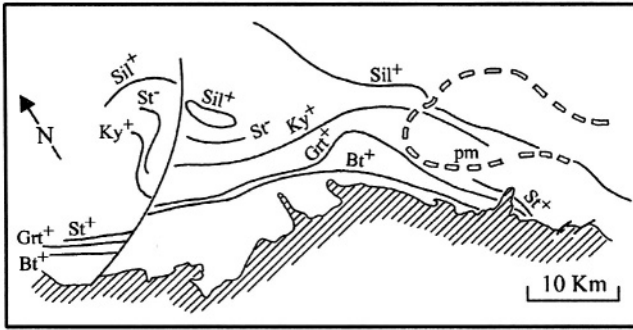


FIG. 29. — Example of mappable isograds based on the appearance and disappearance of index minerals: Lower Limousin (after Floc'h *et al.*, 1978)

Distribution of isograds. The + sign indicates the appearance of an index mineral, the - sign its disappearance. Bt = biotite; Grt = garnet (almandine-rich); St = staurolite; Ky = kyanite; Sil = sillimanite; pm = partial melting (anatexis isograd). Note that:

- 1) metamorphic intensity increases globally to the NE;
- 2) the fact that the sil⁺ isograd is locally closed signifies that the series was strongly refolded by late to post-metamorphic deformation (*cf.* Fig. 30);
- 3) to characterize an isograd by the absence of a phase (st, for example) is neither sure, nor very satisfactory.

METAMORPHIC FACIES

Methods of evaluation of metamorphic intensity based on the study of *metamorphic facies* or *mineral facies* were introduced by Eskola in 1915. They were further developed by Turner and Verhoogen in 1960 and popularized by Winkler from 1965 on.

3.1 Use of metamorphic facies

Mineral assemblages of rocks are identified by the polarizing microscope. They may be compared to lists of characteristic minerals, or, better, to diagrams prepared and refined through usage. Lists of type minerals characterizing the different facies are furnished in the appendix.

Diagrams allow qualitative evaluation of metamorphic conditions. P-T space is divided into a certain number of areas (Fig. 31), each representing a *metamorphic facies*; each facies includes all metamorphic rocks; or, more precisely, all mineral assemblages which result from approximately the same P-T conditions, whatever their chemical composition. Each metamorphic facies, therefore, contains all the possible mineral assemblages stable under the conditions considered. The metamorphic facies carry conventional names which should not be taken in the literal sense; the *greenschist facies*, for example corre-

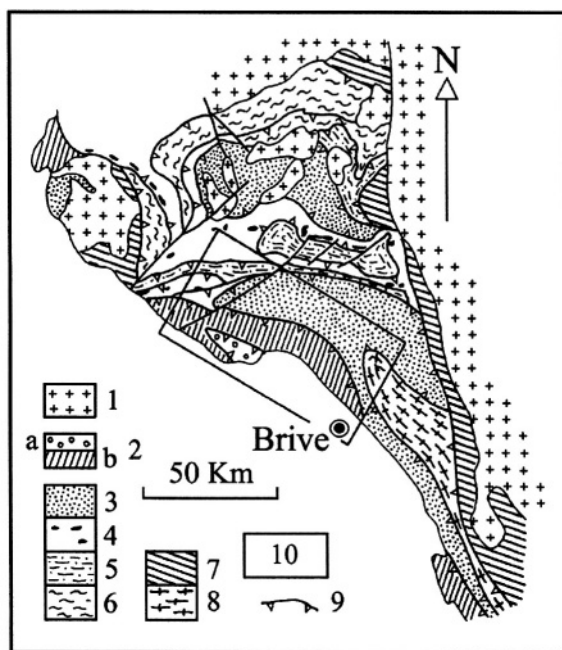


FIG. 30. — *Structural map of Limousin* (simplified after Floc'h, 1983 and Dubuisson *et al.*, 1988).

The metamorphic domain of Limousin is composed of stacked tectonic units separated by abnormal syn- or post-metamorphic overthrusts (*cf.* Figs. 84 and 85). The isograd map (Fig. 29) does not show the structural complexity, which involves six different units! In particular note that the “anatexis isograd” corresponds closely to the tectonic contact between the parautochthon and the upper allochthonous units. 1) granitoids; 2) Genis (a) and Thiviers (b) allochthonous units ; 3) upper unit; 4) intermediate unit with ophiolite remnants; 5) lower unit; 6) basal unit; parautochthonous units: 7) schists; 8) gneiss and migmatites; 9) thrusts; 10) location of figure 29.

sponds to the P-T conditions under which rocks of a certain composition (metabasites) crystallized as a greenschist (epidote + actinolite \pm chlorite + albite \pm quartz assemblage).

The same diagrams allow an approximation of the overall chemical composition of the rocks. From this estimate, hypotheses as to the nature of the protolith may be advanced.

3.1.1 Choice of *typomorphic mineral assemblages*

It is critical to take into consideration those equilibrium assemblages resulting from the same recrystallization period. Depending on the case, these *typomorphic* mineral assemblages (so-called because they characterize a metamorphic facies) are syn- or post-kinematic according to the importance of their development in the rocks under consideration. It is essential to compare any assemblage with one chronologically comparable within the same metamorphic series.

3.1.2 Choice of a *projection system*

In order to describe a metamorphic series in all its diversity better, and in order to make

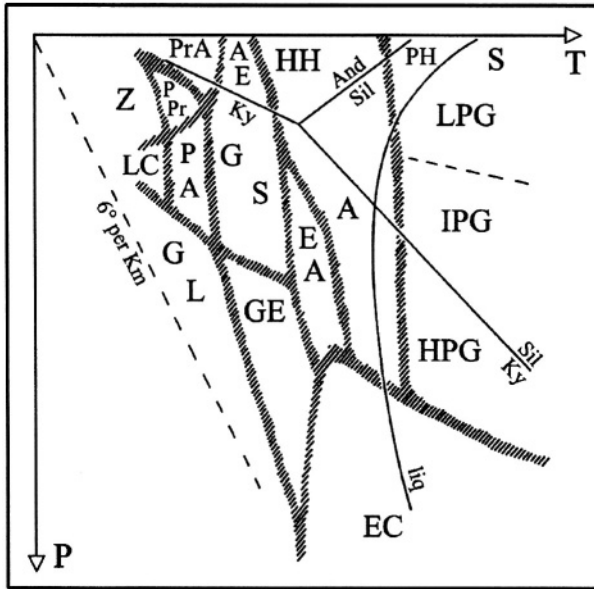


FIG. 31. — *The metamorphic facies*

P-T space is divided into areas which group the mineral assemblages of varying composition which crystallized under the same conditions. These areas were defined over time, on the basis of the presence of certain minerals (*cf.* appendix 1). The names of the facies were also established over time, even though they lead to certain ambiguities. As theoretical and experimental studies advanced, the facies have become more or less fixed, with absolute values of temperature and pressure. The stability fields of the aluminosilicates are presented on the figure (and = andalusite; sil = sillimanite; ky = kyanite) as well as the solidus for hydrous granites (liq). Z = zeolite facies; PrA = prehnite-actinolite facies; LC = lawsonite-chlorite facies; PPr = prehnite pumpellyite facies; PA = pumpellyite-actinolite facies; GL = glaucophane-lawsonite facies; GE = glaucophane-epidote facies; EC = eclogite facies; AE = albite-epidote hornfels facies; CH = hornblende hornfels facies; CP = pyroxene hornfels facies; S = sanidinite facies; GS = greenschist facies; EA = epidote amphibolite facies; A = amphibolite facies; LPG = low pressure granulite facies; IPG = intermediate pressure granulite facies; HPG = high pressure granulite facies.

comparisons between different series, it is useful, even essential, to use a tool which can present a large variety of chemical compositions. A well-developed system for presenting the principal metamorphic facies is the combination of two diagrams, the ACF and the A'KF (Fig. 32; simplified construction described in the appendix) which allows characterization of the majority of usual mineral assemblages. This system, popularized by H.G.F. Winkler, does, however, have several disadvantages:

- 1) by its construction, it is impossible to show sodic phases; this is a major disadvantage in the study of high pressure-low temperature metamorphism, in whose parageneses albite (sodic plagioclase), glaucophane (sodic amphibole) and jadeite (sodic pyroxene) are critical minerals.
- 2) it combines iron (Fe) and magnesium (Mg). These two cations have an ionic radius similar to one another (0.74 and 0.66 Å, respectively) and often play comparable roles in the occupation of structural sites in minerals. In practice Fe and Mg are not distributed in the same way between two or more ferromagnesian phases in equilibrium (gar-

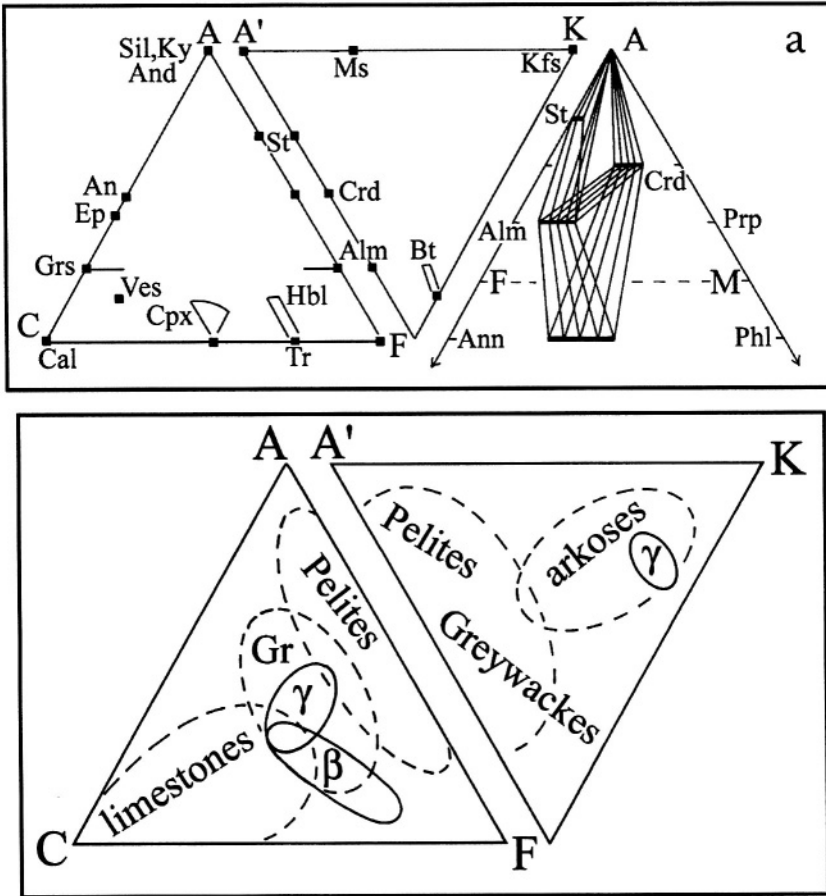


FIG. 32. — Example of graphical presentation of metamorphic assemblages

a) ACF-A'KF diagrams and the AFM triangle (*cf.* appendix 2). The F pole of the ACF and A'KF combine Fe and Mg whereas the AFM distinguishes these two elements. The assemblages aluminosilicate + staurolite + garnet and aluminosilicate + cordierite + garnet appear on the AFM (they describe a paragenetic triangle) whereas they are collinear (arrayed on the same segment) in the ACF-A'KF. In practice, staurolite is generally iron-rich whereas cordierite is always more magnesian than coexisting garnet and biotite. In the ACF and A'KF diagrams, many minerals are shown as compositional fields: clinopyroxene (cpx); hornblende (hb); grossularite (grs); almandine (alm); biotite (bt). The other minerals have compositions which are considered fixed. Variations in composition of plagioclase (an = anorthite) cannot be shown because sodium does not appear on the diagram. sil: sillimanite; ky: kyanite; and: andalusite; ep: epidote; ves: vesuvianite; cal: calcite; tr: tremolite; crd: cordierite; st: staurolite; ms: muscovite; bt: biotite; Kfs: K feldspar (microcline); prp: pyrope; ann: annite (= Fe biotite); phl: phlogopite (= Mg biotite).

b) Plot of the compositional fields of the principal sedimentary and igneous rocks on the ACF-A'KF diagrams. γ: granitoids; A: arkoses; P: pelites; Gr: greywackes; β: basalts and andesites.

net-biotite, for example or even orthopyroxene-clinopyroxene). It is therefore often necessary to use a projection which distinguishes between Fe and Mg, such as the

projection point. No calcic minerals occur in the paragenesis, and there is not even a point representing this rock in the ACF diagram.

Assemblage (2) is more difficult to treat:

it contains a calcic mineral (plagioclase) and a potassic mineral (muscovite); it should be projected simultaneously in the ACF and **A'KF** diagrams,

in each diagram it corresponds to two representative points;

2a muscovite + staurolite + cordierite + plagioclase + quartz

2b muscovite + staurolite + sillimanite + plagioclase + quartz

In reality, these two points are only the same because this represents an equilibrium paragenesis. Therefore it is the projection system which is not entirely satisfactory. This may be verified in the AFM diagram where a paragenetic triangle (sil + st + crd) results from the fact that staurolite and cordierite in equilibrium do not have the same Fe/Mg ratio. The combination of these two elements makes the presentation of this triangle impossible in the **ACF-A'KF** diagrams.

Therefore, the imperfect nature of these triangular projections must be accepted in order that, in simplifying the composition of the system into three constituents, only a restricted number of phases may be considered, three only, when it is often necessary to consider four or five. This aspect is approached in a more theoretical manner in the second part of this chapter. Despite these imperfections, the triangular projections allow simultaneous:

- a) evaluation of the chemical components of a metamorphic rock on the basis of its mineral assemblage, or the approximation of its protolith.
- b) evaluation of the metamorphic conditions.

3.1.3.1 Evaluation of the chemical composition of a rock. The compositional domain of different sedimentary and igneous rocks are shown in the diagram; the position of the point representing a rock with respect to these fields serves as a guide for the definition of the protolith (Fig 32b). Certain domains are, however, ambiguous because they characterize both the field of basalts (for example) as well as that of carbonate-rich pelites (marls). Supplementary observations are necessary to resolve these ambiguities; such as the abundance of Ti-rich phases (sphene, rutile) which characterize an igneous protolith.

3.1 3.2 Evaluation of metamorphic conditions. Metamorphic rocks are classified, as a function of the nature of the mineral assemblage, into conventional pigeonholes which represent the mineral facies in a P-T diagram (Fig. 31) elaborated from field observations as well as theoretical and experimental data. A rapid microscope study allows immediate classification of one assemblage in relation to another in the same metamorphic series; or between different metamorphic series. This handy, simple and rapid method has, nevertheless, two serious flaws.

Semantic ambiguity in the naming of facies. The amphibolite facies groups all the assemblages which crystallized at P-T conditions under which green hornblende and plagioclase are produced in rocks of appropriate composition; however, rocks which do not contain any hornblende also belong to the amphibolite facies (sil + bt + Kfs + qtz or crd + grt + bt + qtz; etc.). Furthermore, certain amphibole-bearing assemblages do not belong to the

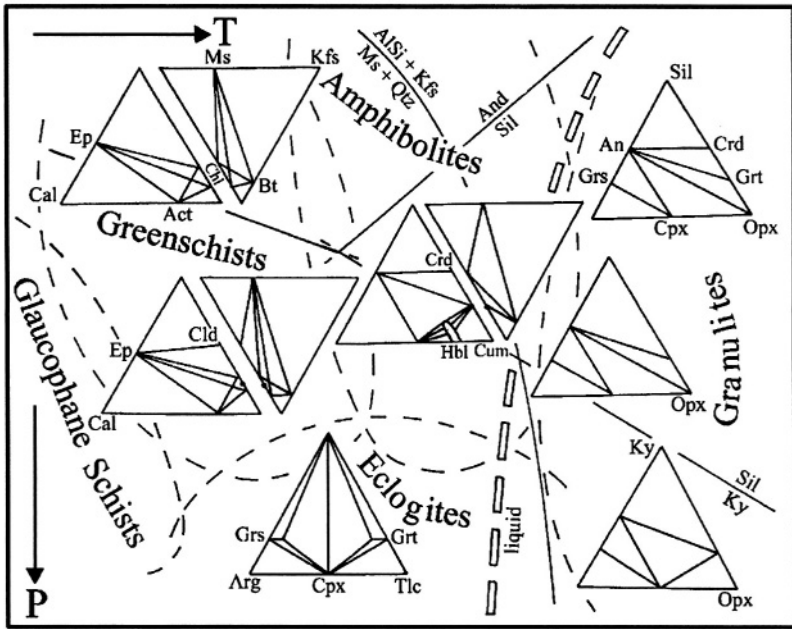


FIG. 34. — *Metamorphic facies and mineral reactions*

Example of the characterization of the principal facies based on several critical mineral reactions; facies limits in dashed lines.

ep = epidote; cal = calcite; chl = chlorite; act = actinolite; bt = biotite; ms = muscovite; Kfs = K feldspar (microcline to orthoclase according to P-T conditions); cld = chloritoid; grt = garnet (almandine-pyrope-spessartine); grs = grossularite garnet; arg = aragonite; cpx = clinopyroxene; tlc = talc; crd = cordierite; hbl = hornblende; cum = cummingtonite; an = anorthite; opx = orthopyroxene; alsi = aluminosilicates; qtz = quartz; liquid = partial fusion of metapelites.

Exercise:

Identify the reactions which mark the transition from one facies to another.

amphibolite facies (actinolite + epidote + albite; glaucophane + lawsonite + albite; etc.) but to the greenschist or glaucophane schist facies respectively.

An approximate localization of mineral assemblages in the P-T diagram. The fields of certain metamorphic facies are extremely large (greenschist, amphibolite, granulite). So much so, that metamorphic rocks which crystallize under very different P-T conditions from one another, are likely to be classified within the same metamorphic facies.

The first fault is rapidly overcome by learning the real significance of the terms. The second is lessened by the introduction of *subfacies* which allow location of the assemblages in P-T space with a greater precision.

3.2 Metamorphic facies and subfacies

The utility of metamorphic facies rests in the possibility of immediate characterization, in thin section, of the metamorphic conditions for a large range of composition, with respect

to a standard diagram (Fig. 34). It is for this reason that the conditions are poorly defined, or rather defined in a general fashion. In fact a facies takes into consideration a large number of mineral assemblages governed by a number of mineral reactions dispersed in P-T space. A more precise localization of an assemblage is possible by taking into account only narrow compositional domains, thus limiting the number of mineral reactions. This more precise, but less general, localization, brings up the definition of metamorphic subsfacies. In this perspective, the petrologist's ideal metamorphic series is one which presents a large variety of rocks of different composition, closely associated to one another (an initial marl-pelite sequence, for example). The diversity of mineral assemblages will allow subdividing the facies into a large number of subsfacies, thanks to different mineral reactions which behave in a different fashion for rocks of differing composition.

Examples of subdivision into subsfacies are given in Figure 35. In practice, once the technique of division into subsfacies is applied, there is no longer a rigorously defined scheme, and everyone is able to suggest subsfacies which are best adapted to the study of a particular series.

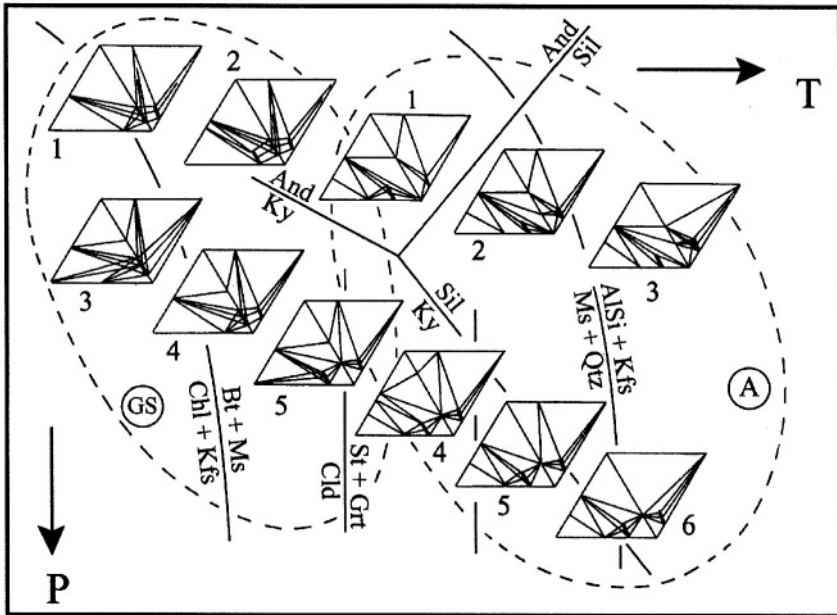


FIG. 35. — *Facies and subsfacies*

Blow-up of the greenschist (SV) and amphibolite (A) facies in eleven subsfacies (classic subsfacies of Winkler, 1967). The distinction between the various subsfacies is made by the interplay between one or more mineral reactions operating in a relatively restricted compositional domain.

Exercise:

Identify the reactions which limit the subsfacies.

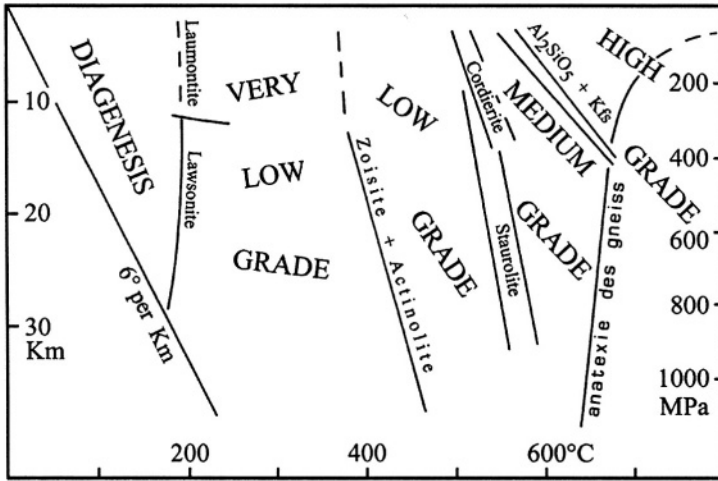


FIG. 36. — *Plan showing the degrees or grades of metamorphism* (after Winkler, 1970)
Each of the degrees is subdivided into narrower domains in the style of subfacies.

3.3 Grades or degrees of metamorphism, another way of presenting facies and subfacies.

The evaluation of the intensity of metamorphism is based on certain key reactions which segment the field of increasing metamorphic intensity; very low grade, low grade, moderate grade and high grade (Fig. 36). These reactions apply to rocks of different composition: pelitic and granitic; basaltic and andesitic; carbonate; etc. The method is similar to that of mineral facies, but the limits of the fields are defined more rigorously, in close relation to mineral reactions. It has the advantage of setting aside the facies nomenclature which is too closely associated with particular rock compositions, for a more objective nomenclature. However this cannot bring the same precision as that which may be drawn from a study of subfacies.

GEOMETRICAL ANALYSIS

Mineral reactions are the definitive elements in the petrologic analysis of metamorphic series. They correspond to a particular case of minimization of the free energy of a system, in which the assemblage which has the lowest G value develops preferentially under the conditions considered. The slopes of these reactions are controlled by the difference in volume and entropy between the reactants and the products. In a particular system the reactions are not independent of one another. Their arrangement in P - T space is closely controlled by the phase rule and geometrical constraints which follow from the principle of minimization of free energy. The geometrical analysis (the rules for which were introduced by Schreinemakers, and developed by Zen) of a system allows elaboration of petrogenetic grids, which are extremely valuable tools for the study of metamorphic series and constitute the basis for all experimental investigations. The concerted use of geometrical analysis

and thermodynamic data results in a more precise petrologic analysis of metamorphic conditions, even if the absolute values of P and T are not always known precisely.

3.4 Definitions and reminders

A rock is a complex *system* either open or closed. It consists of a certain number of *phases*, either solid (minerals), liquids (glasses) or fluids. In metamorphic rocks there is no liquid phase, except in the particular case of *migmatites*. In what follows in this chapter, only closed systems are considered. In these *topochemical* systems the mass of chemical constituents does not change during reactions; both terms of an equilibrium equation are constituted of the same number of molecules of the same *independent constituents*.

The *independent constituents* are the chemical constituents necessary and sufficient to describe all the phases of the system. This is a fundamental notion which depends on the reactions studied in the system. Thus, for the reaction:

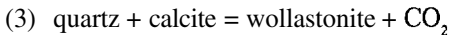


Only one independent constituent Al_2SiO_5 is necessary and sufficient to define the two phases, andalusite and sillimanite which have the same composition. But the reaction:

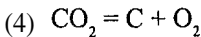


is described by two independent constituents SiO_2 and Al_2O_3 . The system is seemingly chemically analogous to that established for reaction (1).

The reaction:



is described by three independent constituents; SiO_2 , CaO and CO_2 but a fourth constituent must be taken into account in the case where a low oxygen fugacity results in the reaction:



In practice what may be defined as an independent constituent of a system is all the chemical elements present in sufficient quantity to control the stability of a specific phase. For example Ti or TiO_2 is not considered as an independent constituent when it is disseminated in the crystal structure of biotite, amphibole or pyroxene. It becomes an independent constituent if it is in sufficient quantity to allow the formation of a titaniferous phase such as rutile or sphene.

3.5 Variance of a system: the phase rule

The phase rule which establishes a relation between the variance ω of a system and the number of independent constituents n , the number of intensive variables v , and the number of phases ϕ is written:

$$\omega = n + v - \phi$$

3.5.1 The idea of variance or degrees of freedom of a system

Divariant equilibria. Their stability fields in the diagram are the surfaces limited by two reactions. These surfaces represent two degrees of freedom: in effect P and T may vary independently, one from the other, within defined limits, without changing the nature of the assemblage. These surfaces are surfaces of divariant equilibrium for which $\omega = 2$.

Univariant equilibria. These are the lines or curves of the reactions themselves. These reactions have only one degree of freedom. They represent the many variations of an intensive parameter as a function of the other to maintain equilibrium. These equilibria are univariant $\omega = 1$.

Invariant equilibrium. Such an equilibrium is shown in the figure by the point of convergence of the three univariant curves. It is defined by one value for each of the intensive parameters, and has no degree of freedom. It is an *invariant* point for which $\omega = 0$.

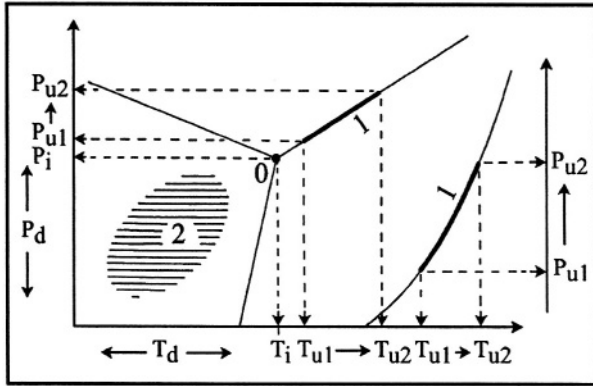


FIG. 37. — *Variance of mineral equilibria in a system*
Two intensive variables are taken into consideration (P, T). Three types of equilibrium are defined.

- 1) The divariant equilibrium assemblages are limited by two reactions; the P_d and T_d parameters may vary independently of one another within certain limits (marked by the reactions) without the nature of the equilibrium being changed; there are, therefore, two degrees of freedom, the variance $\omega = 2$ and n phases are in equilibrium.
- 2) The univariant equilibrium corresponds to a reaction line or curve; in order to preserve the equilibrium conditions, any pressure variation $P_{u1} \Rightarrow P_{u2}$ must be accompanied by a defined temperature variation $T_{u1} \Rightarrow T_{u2}$ which depends on the slope and the shape of the equilibrium curve. There is only one degree of freedom $\omega = 1$ and $n + 1$ phases are in equilibrium.
- 3) Invariant equilibrium is defined by a single temperature T_i and a single pressure P_i . There are no degrees of freedom $\omega = 0$, and $n + 2$ phases are in equilibrium. In the figure, the number of univariant equilibrium curves with the invariant is incorrect for all values of n save 1 (cf. below). 0 = invariant point; 1 = univariant equilibrium curve; 2 = divariant equilibrium field.

In a system influenced by three intensive variables (P, T, P_f for example), an assemblage with three dimensions has three possible degrees of freedom, it is trivariant ($\omega = 3$). As indicated by the phase rule, the number of phases in equilibrium in a system depends on the variance:

for	$\omega = 2$	$\phi = n + v - 2$
	$\omega = 1$	$\phi = n + v - 1$
	$\omega = 0$	$\phi = n + v$

3.5.2 Number of assemblages possible in a system as a function of the variance

Suppose a system has n independent constituents. The total number of phases in equilib-

rium for the conditions of an invariant point $\omega = 0$, is equal to $n + v$. How many possibilities C , are there to distribute these phases at:

- invariant equilibrium for $(n + v)$ phases ($\omega = 0$)?
- univariant equilibrium for $(n + v - 1)$ phases ($\omega = 1$)?
- divariant equilibrium for $(n + v - 2)$ phases ($\omega = 2$)?

The reply is given by the combining formula which indicates the number of possibilities C to combine K objects taken m by m .

$$C_{k,m} = \frac{k!}{m!(k-m)!}$$

k is the total number of phases available $k = n + v$; m is the number of phases in equilibrium for each value of the variance: $m = \phi$. In consequence:

$$C_{((n+v),\phi)} = \frac{(n+v)!}{\phi!(n+v-\phi)!} = \frac{(n+v)!}{\phi!\omega!}$$

because $\omega = n + v - \phi$

Suppose a system under two intensive variables (P and T): $n + 2$ phases can only be combined at one invariant point, n . However, the calculation shows there are $(n + 2)$ univariant equilibria. The number of possible divariant equilibria increases rapidly as a function of n (Table 2).

TABLE 1. — *Number of invariant, univariant and divariant equilibria as a function of the number of independent constituents for two intensive variables (P and T).*

$\omega \backslash n$	1	2	3	4	5
0	1	1	1	1	1
1	3	4	5	6	7
2	3	6	10	15	21

3.6 Applications to simple systems

3.6.1 Systems with one independent constituent

Consider the Al_2SiO_5 system already examined (Fig. 38a). The phase rule and the combining formula show that three phases are in equilibrium at one invariant point when two intensive variables are imposed on the system. The invariant point is defined by three two-phase univariant equilibria. There are three divariant fields where one phase is stable. Despite its simplicity, this figure brings insights into the general behaviour.

Designation of univariant equilibria (or univariant reactions). By convention an equilibrium curve carries the name of the phase which is not involved. Thus the equilibrium curve kyanite = sillimanite is named andalusite. It is written:

ky (and) sil

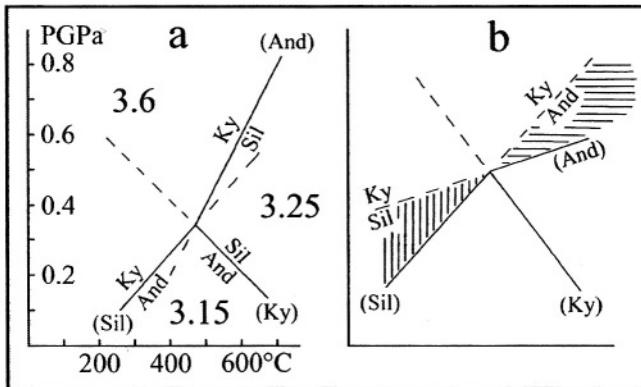


FIG. 38. — System with one independent constituent

a) Example of the aluminosilicates Al_2SiO_5 ; the three phases, andalusite, sillimanite and kyanite are in stable coexistence at one invariant point. Three univariant equilibrium curves (And), (Sil), and (Ky) allow stable coexistence of two phases, and three divariant fields have one stable phase. A univariant equilibrium curve is named for the phase which does not participate. The equilibrium curve and its metastable extension (dashed line) which represents the projection of the intersection of the free energy surfaces onto the P-T plane, divide the field into two domains. The phases (reactants or products) which are involved on one side of the reaction are found in one of these fields, as the equilibrium curves which bear their names are in the field on the other side of the reaction. The phase with the highest density is always the high pressure assemblage (*cf.* the specific gravity values are noted on the diagram).

b) The univariant equilibrium curves cut P-T space into angular sections $< 180^\circ$; if this was not the case, other more stable phases would be present (in the hachured zones, sillimanite or andalusite in the case presented here) rather than the phase (kyanite) which is supposed to be the most stable.

Metastable extensions of univariant equilibria. A univariant equilibrium curve is the projection of the intersection onto the P-T plane, of the free energy surfaces of the two assemblages (here with only one phase) involved in the equilibrium. There is no reason that the intersection of the two planes (or surfaces) should stop at an invariant point; but beyond this, another assemblage occurs which is more stable than the preceding ones. The univariant equilibrium curves are therefore extended beyond the invariant point in a dashed line called the *metastable extension*.

Extent of the divariant fields. It is a demonstration *ad absurdum* to show that the divariant fields are limited by the univariant equilibrium curves which define sectors of arc less than 180° . If this was not so, the stability fields of divariant assemblages would contain the metastable extension of the univariant curves which bound the fields (Fig 38b). The divariant fields would therefore contain two domains in which the most stable assemblage would be different from the stable assemblage for the sector. This situation is unacceptable.

Distribution of univariant equilibrium curves in P-T space. A univariant equilibrium curve and its metastable extension divide the P-T plane in two domains. A stable divariant assemblage is necessarily found on one side of that line, the univariant equilibrium curves which have the names of the phases of that assemblage are found necessarily on the other side. In

reality, the univariant equilibria are designated by the name of the phases which do not participate in the reaction, it is obligatory that they are found in a domain in P-T-G space in which the eponymous phase is not part of the stable assemblage for the system under consideration. This *rule of metastable extension* is particularly easy to understand and to apply in a system with a single independent constituent such as has just been examined (Fig. 38a). It is so axiomatic, it performs a valuable service in constructing diagrams where n is greater than one.

3.6.2 Construction of phase diagrams

Starting with the geometrical constraints which have been detailed, and the thermodynamic characteristics of the three aluminosilicates, it is easy to construct the phase diagram shown in Figure 38a, without, however, being able to fix the absolute temperature and pressure conditions. The high pressure phases are those with the greatest density (smallest V); the high temperature phases are those which have the highest disorder in their structure (highest S). Commonly V and S of the usual phases are available in the literature. The slopes of the equilibrium curves are calculated directly from the ratio $\Delta S/\Delta V$. Thus, for the reaction:

andalusite = sillimanite

$$\frac{dP}{dT} = \frac{\Delta S}{\Delta V} = \frac{(S_{\text{sill}} - S_{\text{and}})}{(V_{\text{sill}} - V_{\text{and}})} = \frac{2.89}{-1.63 \cdot 10^{-6}} = -1.77 \cdot 10^6 \text{ Pa} \cdot \text{K}^{-1}$$

or $-17.7 \text{ bar deg}^{-1}$

The reader has the data necessary (Table 2) to construct the rest of the diagram for himself. At this point the reactions are not calibrated in absolute values of temperature and pressure. These calibrations are effected using experimental data, principally the determination of the enthalpy difference ΔH of the reaction by calorimetry:

$$\Delta G = \Delta H_{\text{1bar, T}} - T\Delta S + (P-1)\Delta V$$

At equilibrium ($\Delta G = 0$) and atmospheric pressure (normal conditions for calorimetric measurements):

$$\Delta H - T\Delta S = 0 \quad \text{or} \quad T = \frac{\Delta H}{\Delta S}$$

The enthalpy differences at 1 bar for the reaction kyanite = sillimanite and kyanite = andalusite are respectively 7406 and 4351 J.mol⁻¹. The equilibrium temperatures at atmospheric pressure are 599 °K and 460 °K. From these values and the slopes of the reactions it is easy to locate the invariant point in the P-T diagram (Fig. 38a). However, in spite of this apparent ease there is no general agreement on the position of the triple point of the aluminosilicates in a P-T diagram.

3.6.3 Systems with two independent constituents

Consider the system $\text{SiO}_2\text{-Al}_2\text{O}_3$. Four phases are in equilibrium at the invariant point. The composition of these phases must be plotted within the system, in other words on the segment $\text{SiO}_2\text{-Al}_2\text{O}_3$. Also the choice of phases must be realistic, and guided by observations; it is possible to control, geometrically, any sort of diagram associating any sort of

TABLE 2. — *Thermodynamic data for some common phases taken from Rubie et al. (1978) and Helgeson et al. (1978).*

Phase	Structural formula	\bar{S}° J/mol $^{\circ}$ K	\bar{V}° cm 3 /mol
Andalusite	Al ₂ SiO ₅	93.22	51.530
Mg-biotite	K[Si ₃ AlO ₁₀]Mg ₃ (OH) ₂	319.66	144.910
Fe-biotite	K[Si ₃ AlO ₁₀]Fe ₃ (OH) ₂	398.30	154.320
Calcite	CaCO ₃	91.71	36.934
Corundum	Al ₂ O ₃	50.92	25.575
Coesite	SiO ₂	40.38	20.641
Fe-cordierite	Fe ₂ Al ₃ AlSi ₅ O ₁₈	537.95	237.070
Mg-cordierite	Mg ₂ Al ₃ AlSi ₅ O ₁₈	466.22	233.220
Dolomite	CaMg(CO ₃) ₂	155.18	64.340
K Feldspar	KAlSi ₃ O ₈	213.93	108.870
Fe-garnet	Fe ₃ Al ₂ Si ₃ O ₁₂	316.31	115.280
Mg-garnet	Mg ₃ Al ₂ Si ₃ O ₁₂	222.00	113.270
Kaolinite	Al ₂ Si ₂ O ₅ (OH) ₄	203.05	99.520
Kyanite	Al ₂ SiO ₅	83.76	44.090
Mullite	Si ₂ Al ₆ O ₁₃	269.57	134.550
Muscovite	K[Si ₃ AlO ₁₀]Al ₂ (OH) ₂	287.90	140.700
Pyrophyllite	Al ₂ Si ₄ O ₁₀ (OH) ₂	239.40	127.820
Quartz	SiO ₂	41.46	22.688
Sillimanite	Al ₂ SiO ₅	96.11	49.900
Stishovite	SiO ₂	27.78	14.014
Wollastonite	CaSiO ₃	82.01	39.930
Water	H ₂ O at 25 °C	188.70	(a)
Water	H ₂ O at 800 °C	235.80	(a)

(a) $\bar{V}_{\text{H}_2\text{O}}$ is equal to the molecular weight of H₂O (=18) multiplied by the specific gravity of the H₂O phase; this can be evaluated at P and T from Figure 15.

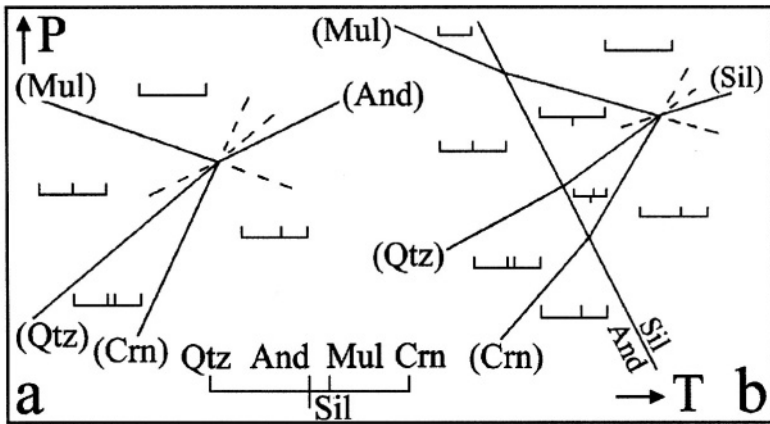


FIG. 39. — A system with two independent constituents
 Example of $\text{SiO}_2\text{-Al}_2\text{O}_3$. Two different configurations are given.

- a) The invariant point is stable in the andalusite field.
- b) It is stable in the sillimanite field.

Qtz = quartz; And = andalusite; Sil = sillimanite; Mul = mullite; Crn = corundum.

Exercise:

Write all the reactions: verify that the rule of metastable extension was not violated, verify the slopes of the reactions are correct.

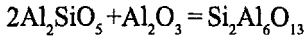
phases, but the diagram in this case may have no petrogenetic significance. As well, in the case presented (Fig. 39) all the phases (quartz, andalusite, sillimanite, mullite and corundum) are stable under relatively low pressure and high temperature conditions, it is unrealistic to take kyanite into consideration in place of andalusite because kyanite has never been observed in association with mullite. In contrast, it is possible to hesitate between andalusite and sillimanite to construct the invariant point (considering the uncertainty in the position of the corresponding invariant point for kyanite-sillimanite-andalusite) and Figure 39 gives two possible versions.

Four univariant equilibrium curves with three phases converge toward the invariant point:

and + crn	(qtz)	mul
qtz + crn	(and)	mul
and	(mul)	qtz + crn
and	(crn)	qtz + mul

By convention these equilibrium curves are written in the sense of rising temperature. The necessary indications are furnished by observation of natural assemblages in the contact aureoles of intrusions; at low pressure andalusite-bearing assemblages pass into mullite-bearing assemblages with a temperature increase. Also the corundum-quartz association has a low molar volume with respect to the other assemblages; it is from a theoretical viewpoint the high pressure assemblage. These observations are confirmed by the values of molar entropies (Table 2) which allow calculation of positive ΔS values for all these reactions. The entropy difference ΔS is therefore positive from the left going to the right. The molar volumes are calculated from the molecular and specific masses of the reactants and products or taken directly from Table 2. ΔV , as well as ΔS , is calculated taking into

account the stoichiometric coefficients of the products and reactants. The reaction (qtz) for example, must be written:



All the reactions under consideration have positive slopes: $\Delta S/\Delta V > 0$. Finally, the rule of metastable extension will make it possible to arrange the univariant curves with respect to one another around an invariant point (Fig. 39). The diagram outlined graphically is completed giving each of the equilibrium curves its actual slope using thermodynamic data (Table 2). If andalusite is replaced by sillimanite, (this means that the invariant point is located in the stability field of sillimanite and not that of andalusite) the figure stays the same with a change in the slope of the univariant lines in crossing the reaction: and (ky) sil. This change is linked to the molar volume and entropy differences between the sillimanite and andalusite bearing assemblages.

In both cases the six divariant assemblages predicted by the phase rule are separated among four divariant spaces limited by four univariant equilibrium curves. Each of the four divariant spaces has one single specific assemblage, respectively $\text{cm} + \text{qtz}$; and (or sil) + qtz ; and (or sil) + mul ; $\text{mul} + \text{qtz}$.

This diagram, apparently correct from the geometric and thermodynamic point of view, presents, nevertheless, a particular problem; the rarity, read absence, in nature of the corundum-quartz association, and the omnipresence of the association aluminosilicate (andalusite, sillimanite or kyanite) and quartz.

3.6.4 Systems with three independent constituents

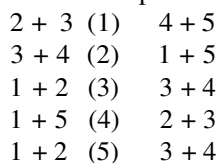
For two intensive variables (P,T) five phases are in equilibrium at the invariant point (Table 1). Five univariant equilibria of four phases define five divariant spaces in which ten different divariant assemblages are distributed, each composed of three phases. The graphical representation of a system with three constituents is triangular. Presenting five phases in a triangle leads to three different figures (Fig. 40):

- 1) The five phases define a pentagon
- 2) Four phases define a quadrilateral with the fifth phase located inside
- 3) Three of the phases define a triangle within which the other two are located.

The three constituent system leads to cases of *collinearity* when three phases are aligned on the same segment; the system is considered *degenerate*, and no longer has the predicted number of univariant and divariant equilibria.

These different configurations are examined below.

3.6.4.1 Pentagonal distribution: the general case. This configuration leads to the construction of a nearly symmetrical form, for, by definition there are always two reactions around a univariant equilibrium and its metastable extension (Fig. 41). In fact all the equilibria have two reactants and two products:



The distribution of the univariant equilibria around an invariant point obeys the rule of

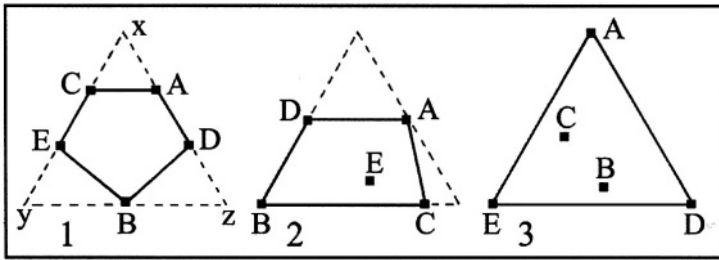


FIG. 40. — The three possible configurations of the arrangement of five phases in a three independent constituent system xyz .

1: pentagon; 2: quadrilateral; 3: triangle. Five phases A, B, C, D and E are disposed in an order based on the rule of diagonals defined later (Fig. 41).

metastable extension. This is automatically applied if the five phases are numbered according to the rule of diagonals (Fig. 41). The five corresponding equilibria follow one another around the invariant point in numerical order; or, in the absence of geologic or thermodynamic constraints it is not possible to orient the diagram in P-T space; and the numeric succession can be established just as well in the clockwise or counterclockwise sense. The construction brings out the predicted ten divariant assemblages. Each of the five divariant fields delimited by the univariant equilibria contains one unique specific assemblage (1 + 4 + 3; 1 + 4 + 5; 1 + 2 + 5; 1 + 2 + 3; 2 + 3 + 4). This characteristic is most interesting for the distinction between subsacies, as a specific assemblage essentially characterizes a sector of P-T space around the invariant point, but for diverse compositions in a three component system (Fig. 41).

3.6.4.2 Cases of degeneration of the system. Different cases of degeneration may be identified according to the number of collinear phases.

Simple degeneration. Three phases are collinear. Consider the A'KF system and the five phases sillimanite, muscovite, K feldspar, biotite and garnet (Fig 42a). The three first phases lie on the A'K segment and are therefore *collinear*. The rule of diagonals applied in this situation expunges the median phase in the collinear segment (here muscovite) from the triangle, without crossing any tie lines. The possible (probable?) succession of univariant equilibria around the invariant point is therefore the following:

grt + ms	(Kfs)	sil + bt
ms + bt	(sil)	grt + Kfs
ms	(bt)	sil + Kfs
bt + sil	(ms)	grt + Kfs
ms	(grt)	sil + Kfs

With the exception of Kfs all the equilibria are written at the onset in the direction of a temperature increase. In fact the liberation of a vapour phase (H_2O) by the dehydration reactions translates to an entropy increase (*cf.* the stoichiometric expression of these equilibria in Table 3). The ΔS 's are therefore positive. The ΔV 's are also positive and these reactions have a positive slope in the P-T diagram. There is no vapour phase in the (Kfs) equilibrium, and the balance of the Al coordination ($Al^6 \Rightarrow Al^4$) is zero. It is impossible to appreciate the difference in entropy ΔS of the Kfs equilibrium in a simple way. This entropy

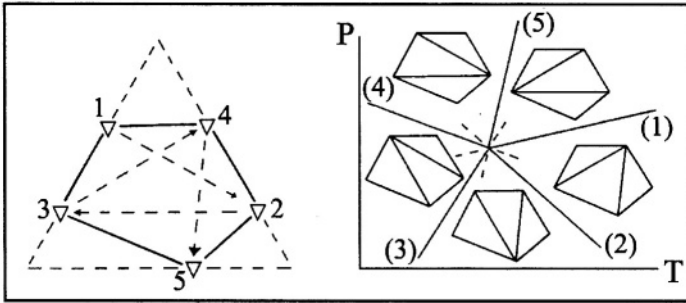


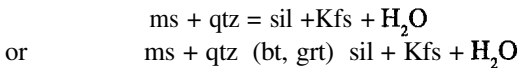
FIG. 41. — System with three independent constituents: pentagonal configuration. On the left of the figure: numbering the phases according to the rule of diagonals. On the right: distribution of the univariant equilibrium curves and divariant fields.

Exercise:

Write the reactions; verify the number of divariant equilibrium assemblages; verify the presence of a specific assemblage for each of the divariant fields.

difference is taken from the literature (Table 2); the highest entropy, high temperature assemblage is sil + bt. The grt + ms assemblage has a lower molar volume than the sil + bt assemblage. It is therefore the high pressure assemblage, and the $\Delta S/\Delta V$ slope of the equilibrium is therefore positive.

The remarkable aspect is the two univariant equilibria (bt) and (grt) correspond to the same reaction:



In this particular case this reaction crosses the invariant point, it is called (grt) on one side of the point and (bt) on the other; each of the two reactions is mixed up with the metastable extension of the other.

The consequence of the degeneration of the system is the disappearance of one divariant assemblage; nine only may be seen. But each of the divariant fields contains a specific divariant assemblage (ms + grt + bt; sil + bt + ms; sil + bt + Kfs; sil + grt + Kfs; ms + grt + Kfs).

As in the preceding cases (one or two independent constituents) the data from the literature (S and V) covering the phases, as well as the stoichiometric formulation of these reactions (Table 3) make it possible to calculate the slopes of the reaction approximately. For this specific case the exercise becomes more difficult:

- 1) The dehydration reactions (there are four to consider) have a variable slope because of the continuous variation of \bar{S} and \bar{V} in the fluid phase. Knowing (?) approximately the P-T conditions of the invariant point (say 500MPa or 5 kb and 650°C) it is possible to fix a corresponding value at these conditions for each of the two parameters (Table 2). From these average values the slopes of the reactions are considered to be straight lines.
- 2) The ferromagnesian phases, biotite and garnet, which are involved in the reaction have different values for \bar{S} and \bar{V} as a function of their actual composition, that is their Fe/(Fe+Mg) ratios. If the composition of the phases is known, S and V can be evaluated using an adjustment between the values for the iron-rich and magnesium-rich end mem-

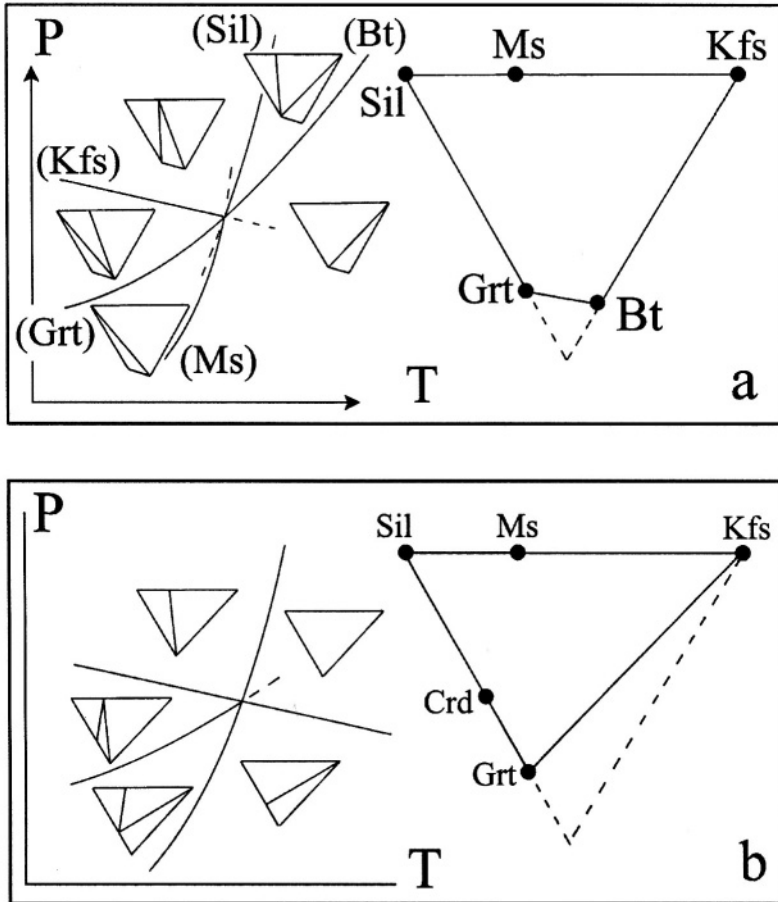


FIG. 42. — *Examples of degeneration of a three independent constituent system (quartz plus H₂O in excess)*

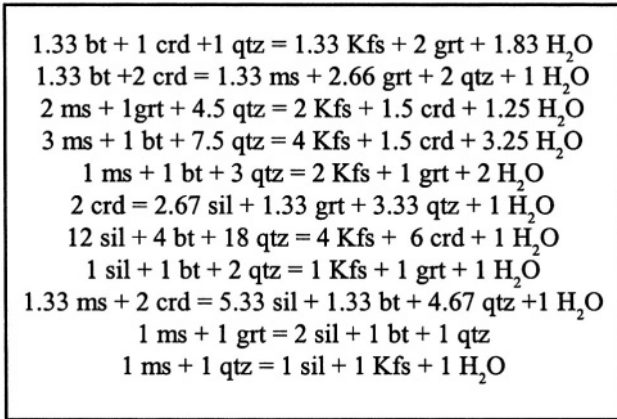
- a) Simple degeneration: Sil, Ms, and Kfs are collinear: each of the reactions (Bt) and (Grt) is confused with the metastable extension of the other. There are only nine divariant assemblages.
 b) Double degeneration: Sil, ms and Kfs on one hand and Sil, Crd and Grt on the other are collinear. There are only eight divariant equilibrium assemblages.

Exercise:

Write all the reactions; identify the divariant equilibrium assemblages; verify that the metastable extension rule is respected. Calculate the slopes of the different reactions using the data in Table 2 and the following values for H₂O: $S = 225 \text{ J} \cdot \text{mol}^{-1} \cdot \text{K}^{-1}$; $V = 22 \text{ cm}^3$. Report the results on a drawing with a convenient scale; compare all the diagrams made for a pure magnesian system with those for a pure iron system.

bers. This presupposes an ideal solid solution between Fe and Mg biotite on the one hand and Fe and Mg garnet on the other (that the physical properties of these mineral species vary linearly between the end members). Even if this hypothesis is incorrect, it produces acceptable results at this stage of analysis.

TABLE 3. — *Equilibrated reactions in the system* (K₂O - (MgO, FeO) - Al₂O₃ - SiO₂ - H₂O) (KMASH) (in Vielzeuf and Boivin, 1984)



Double degeneration. Five phases are collinear, three and three (with one phase common to both segments). This is the case for the A'KF system when sillimanite, muscovite, potassium feldspar, cordierite and garnet are considered. The two segments A'K and A'F each have three phases. Application of the rule of the diagonals dictates the following succession around the invariant point (Fig. 42b).

crd	(ms)	grt + sil
ms	(crd)	sil + Kfs
crd	(Kfs)	grt + sil
ms + grt	(sil)	crd + Kfs
ms	(grt)	sil + Kfs

As in the preceding case, the univariant equilibrium reactions (crd) and (grt) result from the same muscovite breakdown reaction and the (ms) and (Kfs) equilibria result from the same reaction $\text{crd} = \text{grt} + \text{sil}$. These two reactions cross the invariant point. They have both been studied experimentally, which constrains the diagram (Fig 42b). Eight divariant assemblages instead of ten appear in the five divariant spaces. Each of these is characterized by a specific assemblage (sil + grt + Kfs; sil + ms + grt; crd + ms + grt; ms + crd + Kfs; sil + crd + Kfs). A new ferromagnesian phase appears in this system: cordierite. Knowledge of its actual composition, as in the case of biotite and garnet, allows evaluation of the pertinent values S and V from data for pure end members (Table 2)

Regarding these latest applications, if the system is degenerate or not, it must be noted that assemblages which contain two ferromagnesian phases (grt + bt and grt + crd) pose a particular problem in the unequal distribution of iron and magnesium between the phases. This important aspect introduces the idea of *divariant reactions* which will be discussed later on.

3.6.4.3 Other phase distribution modes; quadrilateral and triangle. The same procedure as above is applied in the two cases; geometric analysis seconded by geological observa-

tions and thermodynamic and experimental data. The numbering of the phases following the rule of diagonals in expelling (at the numbering time) the phase or phases contained within the figure, on the side where there are the least lines to cross. Respect for the rule of metastable extensions requires attention as the quadrilateral involves two asymmetric equilibrium reactions (one phase on one side, three on the other) and the triangle involves four such reactions. An example of quadrilateral construction has already been given for the system $\text{SiO}_2\text{-MgO-CaO (CO}_2\text{-H}_2\text{O)}$ (Fig. 12). An example of triangular distribution in the $\text{SiO}_2\text{-Al}_2\text{O}_3\text{-H}_2\text{O}$ system is given in Figure 43.

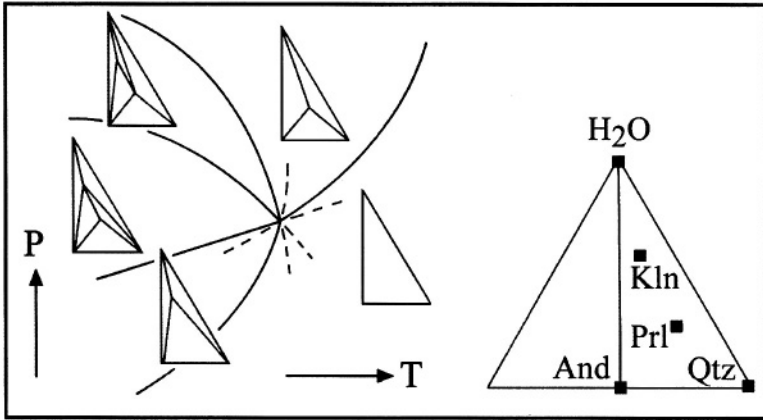


FIG. 43. — System with three independent constituents: triangular configuration $\text{SiO}_2\text{-Al}_2\text{O}_3\text{-H}_2\text{O}$

Prl = pyrophyllite; Kln = kaolinite.

Exercise:

Write all the reactions; identify the divariant assemblages. Calculate the slopes of the reactions from the data presented in Table 2 and the following values for H_2O : $S = 198 \text{ J}\cdot\text{mol}^{-1}\cdot\text{K}^{-1}$; $V = 18 \text{ cm}^3$. Examine the evolution of the reactions which extend at high pressure into the kyanite stability field.

3.6.5 The case where $\phi > n + 2$: petrogenetic grids

Consider the $A'KF$ system and the six phases already used in this system: potassium feldspar, muscovite, sillimanite, cordierite, garnet and biotite. In a three independent constituent system, five phases are in equilibrium at one invariant point when two intensive variables are considered. With six phases available, the following obtains:

$$C_{k.m} = \frac{6!}{5!(6-5)!} = 6$$

six possibilities of five phase invariant assemblages. The univariant and divariant equilibria number respectively:

$$C = \frac{6!}{4!(6-4)!} = 15 \quad \text{and} \quad C = \frac{6!}{3!(6-3)!} = 20$$

Therefore an invariant point must be constructed for each of the phases under consideration. However, the total number of univariant and divariant assemblages is restricted (15 instead of 30; 20 instead of 60) because the six invariant points are not independent of one another, but interconnected by the same univariant equilibria. This connection into a network constitutes a petrogenetic grid (Fig. 44) which allows detailed examination of the evolution of the mineral assemblages as a function of P and T. Note that:

- 1) As each of the invariant points is characterized by the mutual stability of five phases, one of the six phases under consideration plays no role. This phase gives its name to the invariant point considered.
- 2) All the invariant points are not stable; certain, in fact, are defined by the convergence of metastable extensions of univariant equilibrium curves (Fig. 44). This signifies that these points have geometric reality, but that their assemblages have no reason to exist. They are metastable from a thermodynamic point of view because there are one or several mineral assemblages composed of the same number of molecules of the same independent constituents which are more stable than these metastable assemblages because they result in a lower free energy G.

An example of the geologic usage of a part of this petrogenetic grid is given in Figure 45.

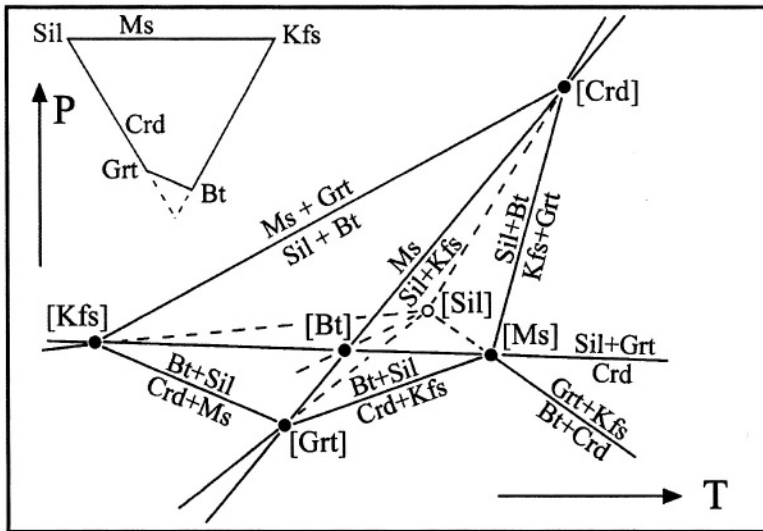


FIG. 44. — *Example of a petrogenetic grid* (Vielzeuf and Boivin, 1984).

Each of the six phases correspond to an invariant point at which it is absent. One of the six points (Sil) is metastable (it represents the convergence of the metastable extensions of five univariant equilibria) in the choice made by the authors. This type of grid makes it possible to trace the evolution of P-T conditions during metamorphism (Fig. 45). The univariant equilibrium curves are here shown as straight lines. As they are nearly all dehydration reactions, they should be presented as curves in a rigorous treatment.

Exercise:

Construct each of the six invariant points involved in the figure separately. Compare the constructions for a pure magnesium and a pure iron system.

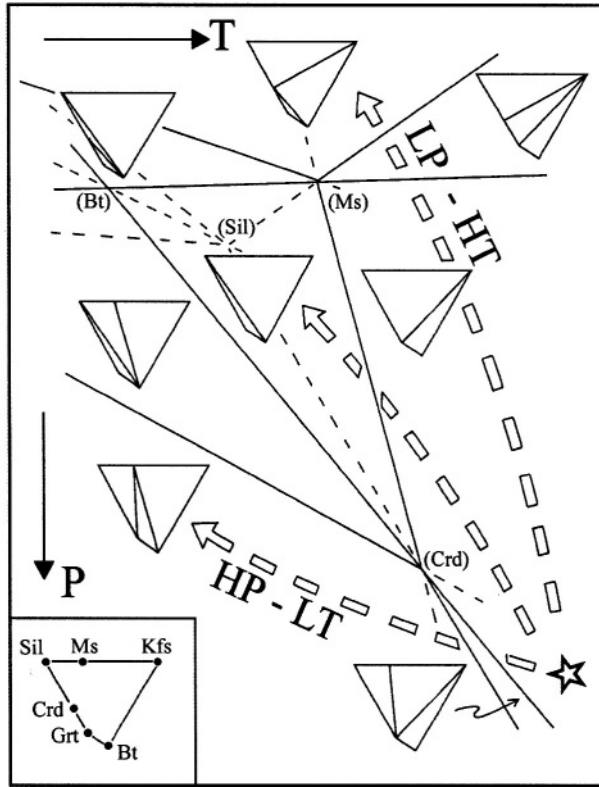


FIG. 45. — Use of a petrogenetic grid (Fig. 44) to characterize the breakdown conditions of the HP-HT assemblage garnet + *K* feldspar + water (after Vielzeuf, 1984).

Following the succession of reactions observed over time, three different types of retrograde gradients or “retrotypes” are likely to appear: a HP-LT gradient which crosses the muscovite stability field; an intermediate gradient characterized by the stability of the assemblage Sil + Bt + Kfs and a HT-LP gradient which enters the stability field of Crd + Kfs.

3.6.6 Systems with more than three independent constituents

The systems with more than three constituents have invariant points with $(n + 2)$ phases in equilibrium (for two intensive variables). From these $(n + 2)$ univariant equilibrium curves, with $(n + 1)$ phases, are arrayed. The number of divariant assemblages with n phases grows rapidly as a function of n (Table 1). It presents a thorny problem for graphical representation of all these assemblages in multidimensional space. Tetrahedral presentations ($n = 4$) are still usable even though they create problems of perspective, but over three dimensions the projections do not allow direct reading. Amongst other problems, supplementary cases of system degeneration appear, not only by collinearity (three phases on the same segment) and by coplanar array (four phases on the same plane) but also by occurring in space with more than three dimensions which is impossible to control graphically. The present tendency is to explore these systems of $(3 + x)$ constituents by matrix calculations and by development of algorithms which then construct the diagram automatically for the critical domain of multidimensional space.

DIVARIANT REACTIONS GEOLOGIC THERMOMETRY AND BAROMETRY

For the preceding analyses, the phases involved in the reactions were always considered to be of constant composition. However it is commonly noted:

- 1) Ca enters the plagioclase lattice progressively (from albite, purely sodic, towards a more calcic composition, as a function of the activity of Ca in the system).
- 2) Al enters the amphibole lattice progressively (from tremolite and actinolite up to aluminous hornblende).

This evolution of plagioclase and amphibole characterizes the transition between the greenschist and the amphibolite facies on the one hand and between the albite-epidote and hornblende hornfels on the other, in relation to an increase in temperature. Further changes take place in the concentration of Al⁶ in biotite, also as a function of rising temperature. It was noted above that coexistence of ferromagnesian phases (grt - bt; grt - crd; opx - bt; opx - grt; etc.) two by two, or in a larger number, is generally characterized by an unequal distribution of iron and magnesium between different phases. The iron and magnesium have comparable dimensions and fit generally in the same structural sites in ferromagnesian minerals, but their ionic radii are, however, different from one another (0.74 and 0.66 Å, respectively), so that variations in the concentration X_{Fe} and X_{Mg} in the ferromagnesian minerals generally engender significant variations in thermodynamic properties, S and V for example (*cf.* Table 2). The minimization of free energy G of an assemblage containing two or more ferromagnesian minerals implies, as a result, a generally unequal distribution of iron and magnesium between these phases. This behaviour results in divariant or continuous reactions which are the basis for numerous methods of calculating the temperature and pressure of crystallization.

3.7 An example of a divariant reaction: $bt + sil = grt + Kfs + H_2O$

Consider the reaction:

- (1) biotite + sillimanite + quartz = garnet + K feldspar + water

This reaction appears as a univariant reaction in the A'KF diagram (reaction (ms) in Figure 42a). Knowing that bt and grt in equilibrium and do not have the same Fe/Mg ratio, this reaction should be looked at in an AFM projection (Fig. 46): the garnet, one of the reaction products, is characterized by a lower X_{Mg} concentration than that of the biotite with which it is in equilibrium. Its composition is, therefore, not situated on the tie line between the starting biotite and sillimanite. From the standpoint of balance, the biotite in equilibrium with the garnet is characterized by a higher X_{Mg} concentration than that of the initial biotite. Examine the evolution of the reaction in a T-X diagram (Fig. 46). Once conditions are attained for the reaction (T_1 for chemical composition X_s) an infinitesimal quantity of garnet appears, characterized by an X_{Mg} concentration clearly lower than that of the biotite of the starting assemblage. This garnet and the new biotite (+ sil + Kfs + water) are in equilibrium for the conditions under consideration. If the temperature rises, the composition of the garnet and biotite in equilibrium move along the *solvus* of these two minerals. The amount of garnet increases and the amount of biotite decreases. At the temperature at the end of the reaction (T_2) biotite has completely disappeared from the assemblage, and the garnet is

characterized by a X_{Mg} concentration X_s equal to that of the initial biotite.

In fact, Figure 46 makes two univariant reactions appear, one for each “end member”.

- (2) annite + sillimanite + quartz = almandine + K feldspar + water
 (3) phlogopite + sillimanite + quartz = pyrope + K feldspar + water

Annite and phlogopite are the ferrous and magnesian end members, respectively, of biotite, almandine and pyrope are the ferrous and magnesian end member garnets. All the intermediate compositions between these end members constitute a “solid solution”. These solid solutions are said to be “ideal” if the physical properties vary in a linear fashion between the end members; in the opposite case they are said to be “non ideal”, which is the more frequent situation. It is worthwhile examining the variation of Gibbs free energy of a solid solution, for example:

$$G_{\text{biotite}} = \sum \mu_i \eta_i = \left(\mu_{\text{ann}}^{\text{bi}} \eta_{\text{ann}}^{\text{bi}} \right) + \left(\mu_{\text{phl}}^{\text{bt}} \eta_{\text{phl}}^{\text{bt}} \right)$$

and

$$G_{\text{garnet}} = \left(\mu_{\text{alm}}^{\text{grt}} \eta_{\text{alm}}^{\text{grt}} \right) + \left(\mu_{\text{prp}}^{\text{grt}} \eta_{\text{prp}}^{\text{grt}} \right)$$

where μ_i is the chemical potential and η_i the number of mols of constituent i in the phase under consideration.

Thus, at constant P and T , the free energy of the solid-solution varies as a function of its composition. The lowest value of G generally corresponds to an intermediate composition between the end members (Fig. 47). As a result, the intersection between the two free energy curves in the G - X diagram does not generally occur at the lowest value of G , but rather on a tangent to the two curves. The minimization of G is therefore realized by the equilibrium between the two phases, one relatively iron-rich and the other relatively magnesium-rich. The free energy of the biotite and garnet mixture is equal to the sum of free energies of the parts of the mixture. Figure 47 describes the different steps of the divariant reaction (1) in a G - X diagram.

Reaction (2) takes place at relatively low temperatures and reaction (3) at more elevated temperatures. These two reactions allow construction of two petrogenetic grids, one for Fe and another for Mg (Fig. 48). All intermediate compositions on the X_{Mg} segment correspond to a reaction involving a relatively iron-rich garnet and a magnesium-rich biotite, the Fe/Mg ratio of these minerals being a function of temperature. From experimental and/or thermodynamic data, lines of equal X_{Mg} value (X_{Mg} isopleths) for biotite and garnet are traced on the P - T diagram (Fig. 48). This figure shows that the equilibrium resulting from reaction (1) is maintained over a range of nearly 250°C, in other words, over a vast divariant field. The AS of the equilibrium is high whereas the ΔV is low (*cf.* data from Table 2). The shape of reaction (2) and (3) and that of the isopleths is practically independent of pressure and this divariant equilibrium is usable as a geothermometer.

As all the components of an equilibrium reaction, reactants and products, are stable along a surface in the P - T diagram, this reaction is considered *divariant*. In fact the composition of two of these phases (garnet and biotite) varies in a continual fashion as a function of temperature. The isopleths demonstrate the advancement of the continuous reaction as a function of temperature (more and more garnet and less and less biotite) and provides a frame for evaluating the temperature of the studied assemblages and provides a

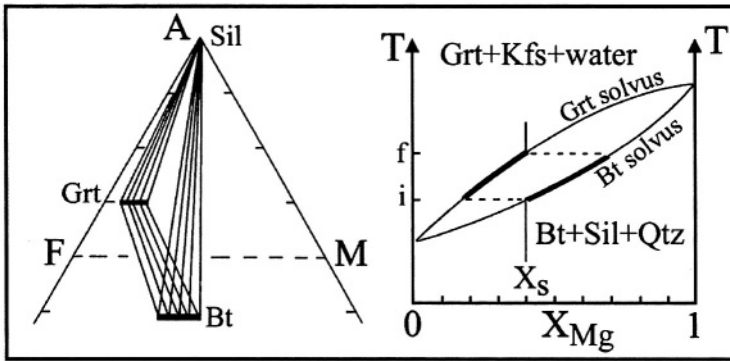


FIG. 46. — *The divariant reaction $Bt + Sil + Qtz = Grt + Kfs + water$*

The divariant assemblage $Grt + Bt + Sil (+ Kfs + Qtz + water)$ is shown on the left in an AFM diagram. The T-X diagram (on the right) shows the progression of the divariant reaction as the temperature increases. i : start of the reaction; an amount ϵ of iron-rich garnet appears; f : end of reaction; biotite disappears completely from the assemblage. Between i and f the amount of biotite diminishes and the amount of garnet increases. X_s : X_{Mg} concentration of the initial biotite at $T < i$. Between i and f , all phases involved in the reaction coexist in the divariant field between the two solvi. The (X_{Mg}) composition of the biotite and garnet each move along their respective solvus up to the disappearance of the biotite. The garnet composition become X_s' .

method of evaluating the temperature of the studied assemblages. These temperatures are usable if the garnet and the biotite are in equilibrium with sillimanite, potassium feldspar, quartz and water vapour, and if the concentration of water in the fluid phase is known with a reasonable precision.

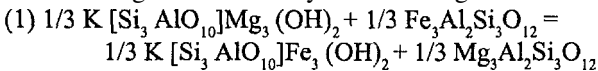
3.8 Partition of iron and magnesium between biotite and garnet: An independent geothermometer

3.8.1 Principles of thermometry based on Fe-Mg exchange

A popular method of thermometry is based on the partition of Fe and Mg between coexisting biotite and garnet in a mineral assemblage. These two minerals effectively exchange the two elements when they are contiguous phases, and the exchange balance is a function of temperature. The exchange is measured by the distribution coefficient K_D :

$$K_{D_{Fe-Mg}} = \frac{(Mg/Fe)_{grt}}{(Mg/Fe)_{bt}} = f(T) \quad \text{Kretz, 1961}$$

This exchange is described by the following reaction:



In other words: $\frac{1}{3}$ phlogopite + $\frac{1}{3}$ almandine = $\frac{1}{3}$ annite + $\frac{1}{3}$ pyrope

Phlogopite and annite are the magnesian and ferrous end members of biotite and almandine and pyrope are the ferrous and magnesian garnet end members. If only pure phases are considered at equilibrium, the chemical potentials of the two members of the reaction are equal:

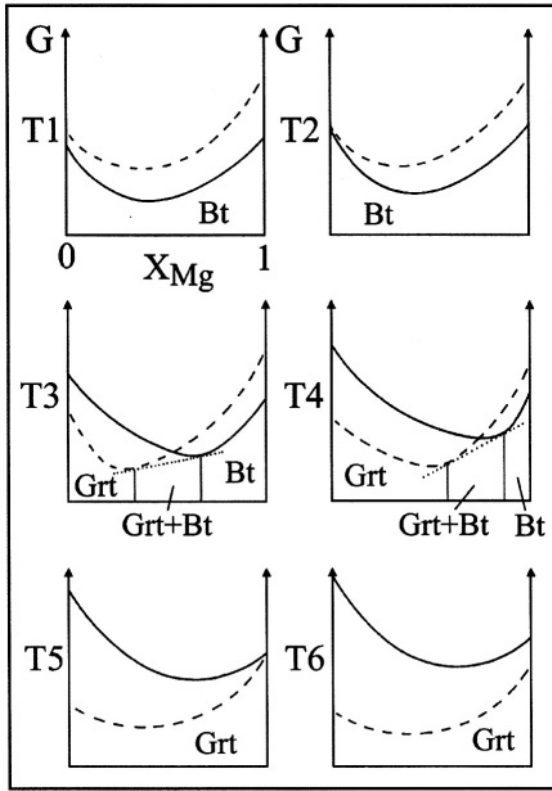


FIG. 47. — *The divariant reaction $Bt + Sil + Qtz = Grt + Kfs + water$ in a $G-X$ diagram*
 In the presence of Sil, Qtz, Kfs and water vapour, at constant P and T, the free energies of biotite and garnet vary as a function of the composition (X_{Mg}) of the two phases. G_{min} corresponds to intermediate Fe/(Fe+Mg) ratios between the pure magnesian and ferrous end members. The relative position of the free energy curves for biotite and garnet evolve as a function of temperature. At T1 the free energy curve of the biotite (solid line) shows lower G values than that of the garnet free energy curve (dashed line); Bt + Sil + Qtz is therefore the stable assemblage for all values of X_{Mg} . At T2, $G_{annite} = G_{almandine}$, equilibrium conditions are achieved for $X_{Mg} = 0$ (reaction of the ferrous end members). In T3 and T4 the free energy curves cut one another and the intersection corresponds to a G value above the G_{min} for biotite and garnet. The minimization of G is therefore not realized for equilibrium between a garnet and a biotite having the same X_{Mg} , but for the association of an iron-rich garnet and a magnesium-rich biotite, defined by the tangent to the two free energy curves (dotted line). At T5 $G_{phlogopite} = G_{pyrope}$; at T6, Grt + Kfs + water is the stable assemblage for all values of X_{Mg} .

$$(2) \quad \frac{1}{3} \mu_{phl}^{bt} + \frac{1}{3} \mu_{alm}^{grt} = \frac{1}{3} \mu_{ann}^{bt} + \frac{1}{3} \mu_{prp}^{grt}$$

But because these are solid solutions the activities (apparent concentrations) of the constituents must be considered:

$$(3) \quad \mu_{i,T} = \mu_i^0 + RT \ln a_i$$

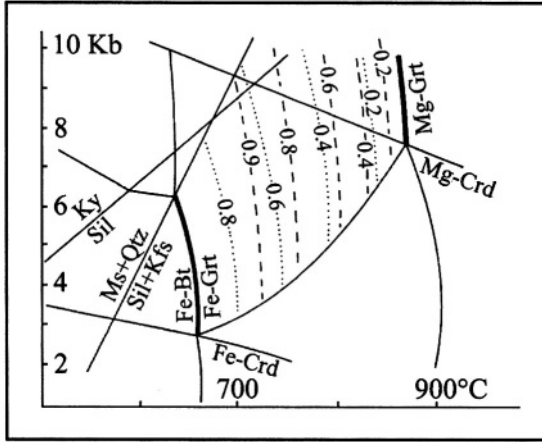


FIG. 48. — Divariant field for the reaction $Bt + Sil + Qtz = Grt + Kfs + water$ for $X_{H_2O} = 0.4$ (after Vielzeuf, 1984)

The field is limited by the two end member reactions. Fe at low temperatures, Mg at high temperature. The respective compositions of garnet (dashed) and biotite (dotted) are given in X_{Fe} .

Exercise:

Determine the temperatures T_1 and T_2 appearing in the diagram of Figure 46.

Where μ_i^0 is the chemical potential of a constituent i in a solid solution at the standard state (298°K and 1 bar) and a_i the activity of the constituent i . The activity of this constituent i in the solid solution is the product of the concentration of that element and the activity coefficient γ :

$$(4) \quad a_i = (X_i \gamma_i)^\alpha$$

Where α is the stoichiometric coefficient of constituent i in the solid solution. Reaction (2) is therefore expressed as follows:

$$(5) \quad \left(a_{phl}^{bt} \right)^{\frac{1}{3}} \cdot \left(a_{alm}^{grt} \right)^{\frac{1}{3}} = K \left(a_{ann}^{bt} \right)^{\frac{1}{3}} \cdot \left(a_{prp}^{grt} \right)^{\frac{1}{3}}$$

Where K is the equilibrium constant which may be written:

$$K = \frac{\left(a_{phl}^{bt} \right)^{\frac{1}{3}} \cdot \left(a_{alm}^{grt} \right)^{\frac{1}{3}}}{\left(a_{ann}^{bt} \right)^{\frac{1}{3}} \cdot \left(a_{prp}^{grt} \right)^{\frac{1}{3}}}$$

Combining (4) and (6)

$$K = \left[\frac{X_{Fe}^{bt} \cdot X_{Mg}^{grt}}{X_{Mg}^{bt} \cdot X_{Fe}^{grt}} \right] \cdot \left[\frac{\gamma_{Fe}^{bt} \cdot \gamma_{Mg}^{grt}}{\gamma_{Mg}^{bt} \cdot \gamma_{Fe}^{grt}} \right] = K_D \left[\frac{\gamma_{Fe}^{bt} \cdot \gamma_{Mg}^{grt}}{\gamma_{Mg}^{bt} \cdot \gamma_{Fe}^{grt}} \right]$$

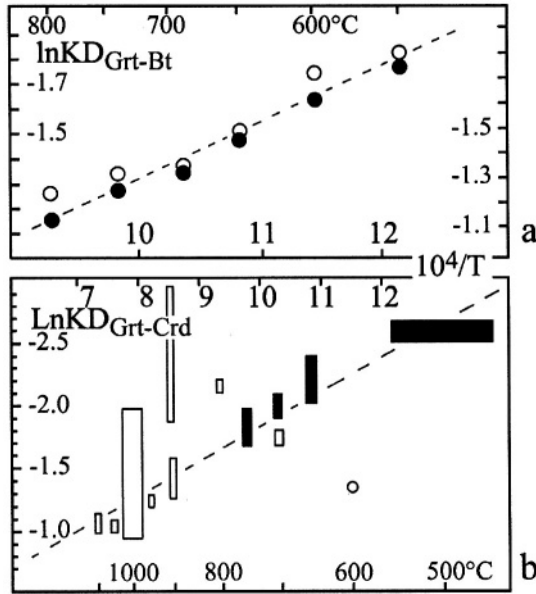


FIG. 49. — Correlation between $\ln K$ and $1/TK$.

a) For the reaction phlogopite + almandine = annite + pyrope (experimental data of Ferry and Spear, 1978).

b) For the reaction Fe cordierite + pyrope = Mg cordierite + almandine: white symbols; experimental data of various authors; black symbols; data calculated from natural assemblages (after Thompson, 1984).

The correlation is excellent for the biotite-garnet equilibrium; it is poor for cordierite-garnet, which limits the application of this geothermometer.

At equilibrium, at constant pressure, and taking into account (3), it becomes:

$$\Delta G = \Delta G^\circ + RT \ln K = 0 \qquad \text{or } \ln K = -\frac{\Delta G^\circ}{RT}$$

take

$$\Delta G^\circ = -RT \ln K = \Delta H^\circ - T \Delta S^\circ = 0 \quad \text{from which}$$

$$\ln K = -\frac{\Delta H^\circ}{RT} + \frac{\Delta S^\circ}{R}$$

Therefore at constant pressure, or for small variations of molar volume, $\ln K$ varies linearly as an inverse function of T . If the minerals involved in the reaction are ideal solid solutions (a risky approximation which is often used) the activity coefficients γ are equal units, and in consequence:

$$K = K_p$$

under these conditions K_p whose value can be measured directly by chemical analysis using the electron microprobe, is an inverse linear function of the temperature.

3.8.2 Experimental calibration of the reaction

The relation between $\ln K_{D(\text{bt-grt})}$ and $1/T$ has been calibrated first by experimental results at pressures of 2.07 kb between 550 and 800°C (Fig 49a). The concentration of iron and magnesium of the phases produced experimentally was determined by electron microprobe. The experimental points define a good linear relation in the diagram $\ln K_D$ versus $10^4/T$. The equation of this line was established empirically:

$$(1) \quad \ln K_{D(\text{bt-grt})} = -\frac{2109}{T^\circ \text{K}} + 0.782$$

The temperatures calculated using this equation, on the basis of the iron and magnesium concentration in biotite and garnet in equilibrium in rocks, are, rigorously speaking, only valid for the experimental pressures (2.07 kb). In reality, the minor difference in volume involved in the reaction, in other words the small pressure influence, allows a generalization of this expression over the whole stability range of the biotite-garnet association. The more general expression, proposed by Vielzeuf (1984), may also be used:

$$T^\circ \text{K} = \frac{4151 + (P - 1) \cdot 0.019}{1.554 - R \ln K_D}$$

Where P is the pressure in bars and R the ideal gas constant (= 1.98726). This expression takes into account the effect of pressure on the variation of free energy:

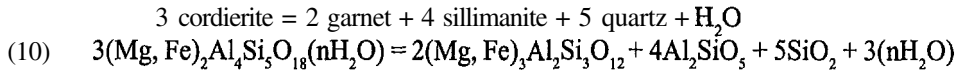
$$\Delta G = \Delta H^\circ - T\Delta S^\circ + (P - 1) \Delta V^\circ + RT \ln K = 0$$

Other calibrations of this reaction have been recently proposed which are based on the same principle, but which take into account the Ca concentration of the system as expressed by the grossularite content in the garnet solid solution.

3.9 Example of a geothermobarometer:

The reaction cordierite = garnet + sillimanite + quartz + H₂O

Rocks with the stable assemblage cordierite + garnet + sillimanite + quartz (\pm biotite) are very widespread in metamorphic series belonging to the granulite or amphibolite facies. These constitute the *kinzigitic* series which sometimes crop out over several kilometres of thickness. This mineral assemblage, therefore, remains stable over a wide range of pressure and temperature, and as such fulfills the definition of a divariant equilibrium. The reaction is written:



This reaction only takes into consideration the ferromagnesian garnets (almandine and pyrope) to the exclusion of the calcic molecule, grossularite. The value of n which measures the quantity of water involved in the reaction is open to discussion. This reaction theoretically extends into the kyanite stability field, but kyanite-cordierite stable assemblages are unknown in nature. The density of cordierite (2.6 to 2.7) is low compared to that of the products of the reaction, and if water is not taken into consideration, the reaction results in a difference in molar volume on the order of -20% (*cf.* data in Table 2). This characteristic indicates the great barometric potential of the reaction which has been the subject of numerous theoretical and experimental investigations. The behaviour of water

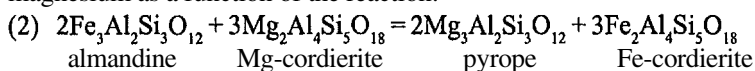
in cordierite is not quite clear, water quantities are variable, and its exact structural location in the crystal lattice is disputed. There are, therefore, some difficulties in the thermodynamic interpretation of reaction (1), which limits its use somewhat.

3.9.1 The cordierite-garnet barometer

The cordierite and garnet which coexist in reaction (1) do not have the same Mg/Fe ratio, at equilibrium cordierite always has a greater XMg than that of garnet. Reaction (1) is therefore a divariant reaction and can be treated in exactly the same way as the biotite-garnet reaction examined above. But here, because of the low entropy and high volume difference, pressure is the most significant parameter, and not temperature. The equilibrium is therefore examined in a PX diagram at constant temperature (Fig. 50). In this diagram there is a vast divariant field extending over nearly 9 kb, over which the cordierite and garnet compositions measure the advancement of the reaction as a function of pressure. A series of G-X diagrams analogous to those of Figure 47 (but at constant T and increasing P) would account for the evolution of the reaction (1) in the same way. Starting from the values of $(XMg)_{grt}$ and $(XMg)_{crd}$ calculated from experimental and thermodynamic data, the pressure of a crd-grt assemblage in equilibrium with sillimanite and quartz may be evaluated between 4 and 8 kb, if the crystallization temperature is known (Fig. 50).

3.9.2 The independent geothermometer crd-grt

As in the case of the association biotite-garnet, cordierite and garnet exchange iron and magnesium as a function of the reaction:



An analogous procedure to that which was developed for garnet-biotite equilibrium leads to a linear relation between $\ln K_{D_{Fe-Mg}}$ and the temperature (Fig 49b). The experimental curve is much less well constrained than the preceding case, and values obtained from this relation should be viewed with caution. Several thermodynamic equations have nevertheless been proposed:

$$T^{\circ} K_{crd-grt} = \frac{5415 + (P - 1) \cdot 0.031}{1.781 - R \ln K_D} \quad \text{or else} \quad = \frac{6150 + (P - 1) \cdot 0.030}{2.69 - R \ln K_D}$$

$$\text{where } K_D = \frac{(Fe/Mg)_{crd}}{(Fe/Mg)_{grt}} \quad \text{and} \quad R = 1.98726$$

The equations for the thermodynamic curves were established from a clearly defined expression of K_D , and naturally care must be taken not to introduce parameters into the calculation of K_D that do not correspond to those that were used to define the equation.

The value $\ln K_D$ may be used directly to complete the grid of Figure 50, which gives, with some errors (these may be important) the position of the assemblage crd + grt + sil + qtz in the P-T diagram, using the composition of garnet and cordierite in equilibrium.

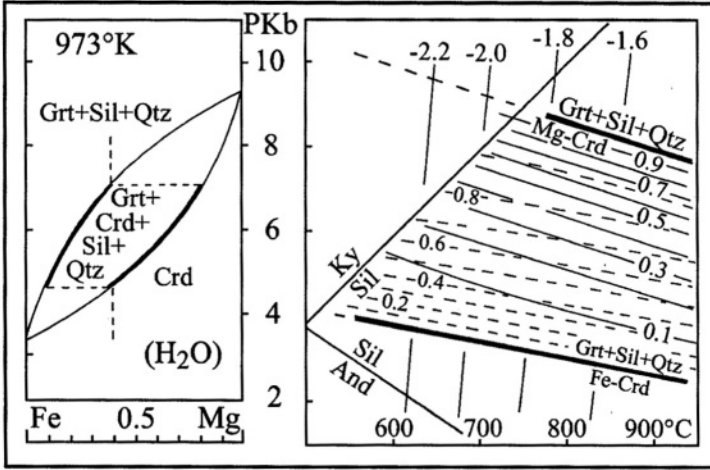


FIG. 50. — The divariant reaction cordierite = garnet + sillimanite + quartz + water (after Vielzeuf, 1984).

The figure on the left is a P-X section at 973°K; the two solvi develop over a large pressure interval which confers a potential as a barometer to the reaction (ΔV is large). The figure on the right shows the development of the divariant field between the Fe and the Mg reactions. The cordierite composition (dashed lines) and garnet (full lines) are given in X_{Mg} . The values for the $\ln K_{D_{\text{crd-grt}}}$ (Fe and Mg exchange between cordierite and garnet) are also shown on the figure; these are capable of giving barometric information as well as temperature data, but the crd-grt thermometer is scarcely reliable (cf. Fig. 49b).

Exercise:

- 1) Verify that the two figures are coherent
- 2) Construct a P-X diagram for $T^{\circ}\text{K} = 1073$.

3.10 “Automatic” geothermobarometry

A large number of reactions with a geothermometric and geobarometric potential have been studied theoretically and experimentally. Some, among the most utilized, are presented briefly in the appendix, either in the form of thermobarometric equations, or in graphical form. It becomes difficult to manipulate all these reactions at the same time, and a computer programme becomes important in handling all the data. Several programmes have been developed, which reproduce all the reactions observed within the same metamorphic series graphically, as a function of the composition of the phases. The crystallization conditions are supposed to correspond to the best intersection of different reaction curves. Figure 51 gives an example of this type of automatic treatment.

GEO-THERMOBAROMETRY OF FLUID INCLUSIONS

The minerals of a metamorphic rock often contain fluid inclusions, microscopic cavities (sometimes in negative crystal form) filled with a mixture of liquid, gas and even solid phases (Fig. 52a). With certain restrictions, the content of the inclusion is considered as representative of the interstitial fluid phase which was present in the system at the time of metamorphic recrystallization, and which was trapped by the crystals during their growth. This hypothesis is only acceptable if the trapping occurred in a reservoir (mineral cavity)

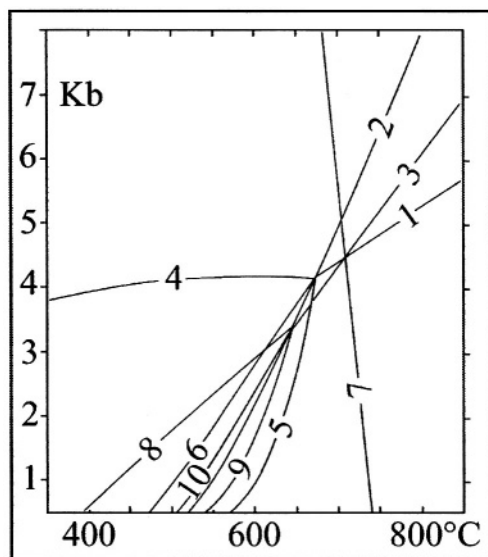


FIG. 51.— Example of automatic calculation using the programme *GeO-Calc* (Berman 1988). The conditions calculated are those for the crystallization of a sample from the aureole of the Ballachulish granite (Scotland) (Fig. 54). They represent the assemblage $Ms + Qtz + And + Sil + Kfs + Crd + Bt$. The best estimate is 3.8 kb at 660°C. 1: $Ann + And + Qtz = FeCrd + Kfs + H_2O$; 2: $Ms + Qtz = And + Kfs + H_2O$; 3: $Phl + And + Qtz = MgCrd + Kfs + H_2O$; 4: $Ms + FeCrd = And + Ann + Qtz$; 5: $Ms + FeCrd = And + Ann + Kfs + H_2O$; 6: $Ms + Ann + Qtz = FeCrd + Kfs + H_2O$; 7: $FeCrd + Phl = MgCrd + Ann$; 8: $Ms + MgCrd = And + Phl + Qtz$; 9: $Ms + MgCrd = And + Phl + Kfs + H_2O$; 10: $Ms + Phl + Qtz = MgCrd + Kfs + H_2O$. After Pattison and Tracy, 1991.

both impermeable and inert, not having reacted subsequently with the imprisoned fluid. Specialists claim that quartz crystals have these qualities and their inclusions allow an effective determination of the composition of the interstitial fluid present during recrystallization.

3.11 Composition of fluid inclusions

The composition of the trapped fluid phase in these fluid inclusions is obtainable by different techniques. The fluid can be extracted by crushing the samples, or by heating and analyzing by conventional or mass spectrometry. But the techniques most commonly used at present are microthermometry and Raman spectroscopy. In the first case, the evaluation of the inclusion's composition is obtained by determining the freezing and melting points (appearance and disappearance of solid phases such as clathrates, the carbon dioxide eutectic, ice, NaCl for example) and the homogenization points (disappearance of gas phases). These data are obtained by the microscopic study of inclusions using a heating-freezing stage (-180 to 600°C) which allows direct observation of the appearance and disappearance of phases at measured temperatures. Raman spectroscopy furnishes an approximate chemical analysis of the inclusions (Fig 52b). These are generally composed of mixed fluids, principally composed of C - O - H - N. These fluids can be treated in a relatively simple system $H_2O + CO_2 \pm CH_4 \pm N_2$ containing variable quantities of NaCl in solutions

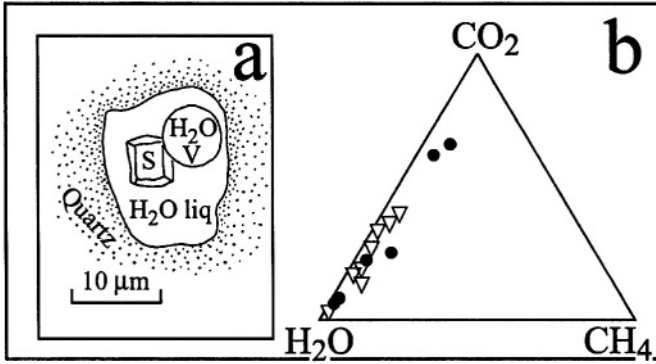


FIG. 52. — *Fluid inclusions in minerals* (after Cathelineau, 1993)

- a) Example of a fluid inclusion in a quartz vein of the Monteverdi granite (Lardarello geothermal field, Italy): s is an unidentified solid phase, possibly sodium chloride.
 b) Ternary composition of a homogenized fluid phase (Montagne Noire gold district : black circles : Cabrespine ; triangles : Malabau) after Raman spectroscopy data.

and subordinate amounts of CaCl_2 and KCl . Inclusions in a metamorphic series belonging to the greenschist and amphibolite facies are particularly water-rich, those of rocks recrystallized under granulite facies conditions, on the other hand, are water-poor and carbon dioxide-rich; which explains the absence or rarity of hydrous phases in these units.

3.12 Characterization of isochores

During metamorphism the fluid phase was homogeneous at the time of trapping (or is supposed to have been homogeneous except for a few particular cases); and was *monophase*. During subsequent evolution toward lower temperature and pressure, the volume of the inclusion remains constant, if the effects of the compressibility of quartz are neglected, and the overall composition does not change. The fluid evolution is, therefore, controlled by a univariant path in P-T space, or an isochore path (volume and density constant). The inclusion remains monophase while the P-T conditions along the isochore remain in the one fluid phase domain (Fig. 53). It begins to unmix starting at the temperature T_h - homogenization-unmixing temperature. When the isochore crosses or follows the univariant equilibrium curve of the phase diagram for the appropriate composition, different gas, liquid and solid phases appear by boiling, immiscibility and precipitation.

During this evolution the pressure in the inclusion is totally controlled by the temperature, which is the only independent variable because the volume is constant (by virtue of a relationship close to that of ideal gases: $PV = nRT$). This evolution is therefore reversible by simple heating of the inclusion, for example using the heating stage, and the solid and gaseous phases disappear progressively and starting at temperature T_h the inclusion is rehomogenized and consists of a single fluid phase which has the density (or specific gravity) and composition of the interstitial fluid phase present at the time of metamorphism. Starting with T_h and a series of models of varying precision, it is possible to calculate the density of the fluid phase, and, as a consequence, the position in P-T space of the univariant curve, and the corresponding isochore. If all these basic assumptions are verified, the

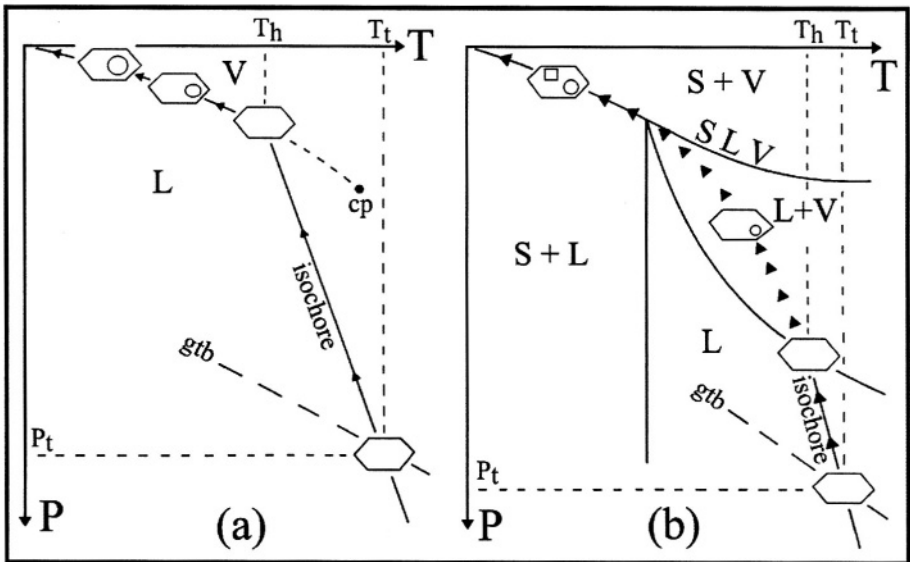


FIG 53. — Use of fluid inclusions in geothermobarometry

a) Biphasic inclusion (liquid and vapour). During trapping (at P_t and T_t) the inclusion consisted of a homogeneous fluid phase (monophase), representative of the interstitial fluid. When T decreases the inclusion remains monophase along the isochore path (at constant volume) whose slope in P - T space is controlled by the specific gravity, in other words by the composition of the fluid. Starting at temperature T_h (homogenization temperature) a vapour phase appears, whose volume increases as the P - T conditions change along the $L + V$ (liquid + vapour) equilibrium curve. The microthermometry consists of reversing the path of the fluid inclusions; starting from ambient conditions, the inclusion is heated at constant volume (that of the cavity which contains it): at T_h it becomes monophase. Knowing the composition of the homogeneous fluid, it is possible to calculate the slope of the isochore. Used in conjunction with a mineral geothermobarometer (gtb), this isochore can then define the trapping conditions if the inclusion has not undergone modification during its history. pc = critical point (after Pécher, 1984)

b) Evolution of a triphase inclusion in the H_2O - $NaCl$ system (after Weisbrod, 1984). S = solid ; L = liquid ; V = vapour.

monophase interstitial phase was necessarily on that isochore during metamorphism (Fig. 53). Fluid inclusions allow the determination of thermobarometric data independent of those furnished by solid assemblages. They add very important information relative to the P - T conditions at the time of metamorphism and trapping.

The experimental heating of the inclusion can be raised above T_h to no particular purpose, the P - T conditions in the inclusion follow the isochore without any other phenomena being observed in the inclusion, which remains monophase. At temperature T_d the decrepitation temperature, the inclusion explodes because the internal pressure exceeds the mechanical resistance of the inclusion walls. Effectively the microthermometric heating is applied at atmospheric pressure, and the internal pressure of the inclusion is not compensated by a confining pressure P_s as it was during metamorphism. When fluid inclusions are trapped at high pressure the internal pressure may exceed its confining pressure during the P - T evolution of the sample; a natural decrepitation then occurs which destroys the fluid inclusion.

This page intentionally left blank

SECOND PART

METAMORPHISM AND GEODYNAMICS

This page intentionally left blank

INTRODUCTION

In the preceding chapters it was apparent that the principle factors which control metamorphic recrystallization are temperature and pressure. The evolution of these parameters over time, within the same lithologic units, is directly related to global dynamics. Therefore the study of the mineral assemblages of metamorphic rocks and their evolution with time, fixes a certain number of constraints on geodynamic models. The dual processes, contact and regional metamorphism, emphasized in the first part, make it possible to examine the recrystallization process from two different angles, thermal and dynamothermal. In the first case, that of contact metamorphism, heat diffusion plays an essential role; in the case of regional metamorphism, heat transfer related to tectonic displacement of units (convective transfer in the broad sense) plays a much more important role and the effects of thermal diffusion are, by comparison, limited.

In the pages which follow, contact and regional metamorphism will be examined successively and separately. It will become clear that the action of these two processes is most often closely associated throughout the evolution of orogens.

This page intentionally left blank

CONTACT METAMORPHISM

The recrystallization produced during contact metamorphism has a directly observable cause: the immediate proximity of a high temperature magmatic intrusion. The intrusion carries a certain quantity of heat, which diffuses into the colder wall rocks and controls the formation of a contact metamorphic aureole (Fig. 54). This aureole is generally narrow with respect to the size of the intrusion, because rocks are a poor conducting medium. Thermal diffusion is, therefore, an inefficient method of heat transfer.

EMPLACEMENT OF AN INTRUSION IN A LOW TEMPERATURE HOST ROCK DYNAMIC ASPECTS.

The emplacement of an intrusion requires the introduction of a finite volume of rock material into the host rocks. This volume is emplaced under one of two regimes which depend on the mechanical properties of the host rocks (Fig. 56).

4.1 In brittle domains

The host rocks are “permissive”; magmatic injections follow pre-existent fractures, or those generated by the intrusion itself. These take the form of veins or dykes where they cross the structure of the host rocks, and they become sills or laccoliths where they are parallel. Conical fractures often develop in the roof of intrusions, and occasionally the emplacement takes the shape of circular dykes (“ring dykes”).

4.2 In ductile host rocks

The intrusion forces its way in, pushing aside the rocks it penetrates. These domains are therefore subjected to a more or less prominent flattening, accompanied by the development of a schistosity, and eventually by synkinematic isoclinal folds. This deformation is geometrically controlled by the pluton; schistositities, in particular, envelope the intrusion. In a situation where several intrusions are injected in the same district, “triple points” in the schistosity traces correspond to the intersection of these different surfaces (Fig. 56). These structures are, however, commonly blurred or erased by the intense general annealing which follows the emplacement of the intrusions (see following).

It must be noted that the rheological behaviour of the host rocks of the same pluton may vary with depth: brittle at the roof, near the surface, and more ductile at depth, notably on account of the addition of heat from the intrusion (Fig. 55).

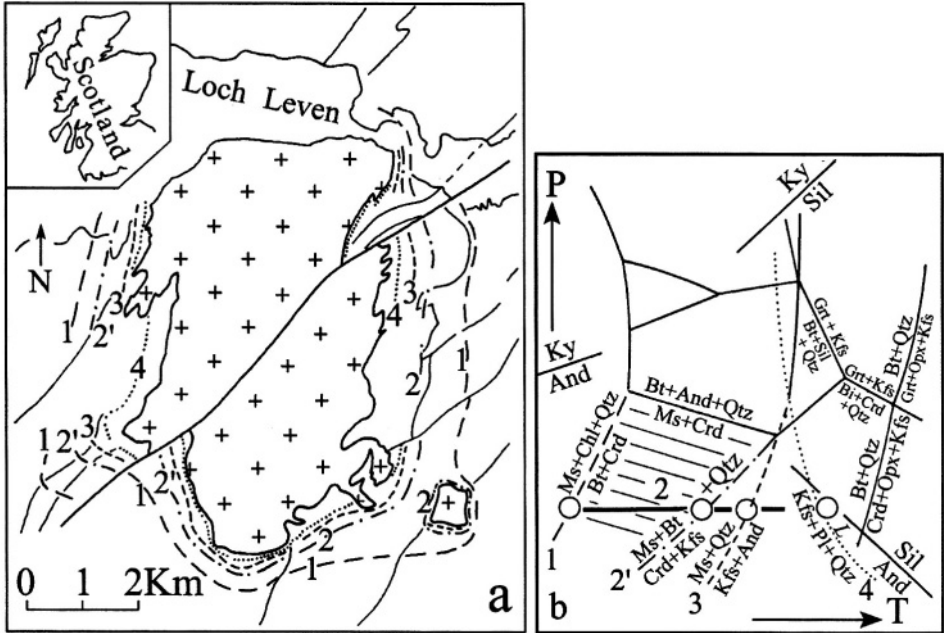


FIG. 54—Example of contact metamorphism: the thermal aureole of the Ballachulish (Scotland) granodioritic batholith.

a) Map of the intrusion and its aureole, simplified from Pattison and Harte (1988). The granitoids (cross pattern) were injected in the Devonian into a quartzo-pelitic sedimentary series. Four principal isograds were noted, based on the following reactions:

- 1) $Ms + Chl + Qtz = Bt + Crd$
- 2) $Ms + Crd = Bt + And + Qtz$
- 2') $Ms + Bt + Qtz = Crd + Kfs$
- 3) $Ms + Qtz = Kfs + And + vapour$
- 4) $Kfs + Qtz (\pm Bt) = liquid + aluminosilicate$

Reactions 2 and 2' operated in two different formations (Leven schists and Ballachulish pelites, respectively), which do not have the same composition (*cf.* Fig. 54b).

b) Diagram showing the crystallization conditions in the aureole in the KFMASH system ($K_2O - MgO - Al_2O_3 - SiO_2 - H_2O$). The disappearance of muscovite and the appearance of melt in the andalusite stability field indicates low pressure emplacement conditions (< 3 kbar or less than 10 km depth).

The succession of reactions 1 - 2 - 3 - 4 or 1 - 2' - 3 - 4 occurred under the same pressure conditions, the difference being a higher iron concentration (X_{Fe}) in the schists than in the pelites. The hachured domain represents the divariant slip of reaction 2 toward lower pressure as a function of an increase in X_{Fe} .

HEAT DIFFUSION IN THE HOST ROCKS

4.3 Static model

4.3.1 Critical parameters

The most simple, but approximate, way to envisage heat diffusion in the host rocks consists of taking into consideration a body at elevated temperature emplaced instantaneously into an environment at a lower temperature. Under these conditions the temperatures

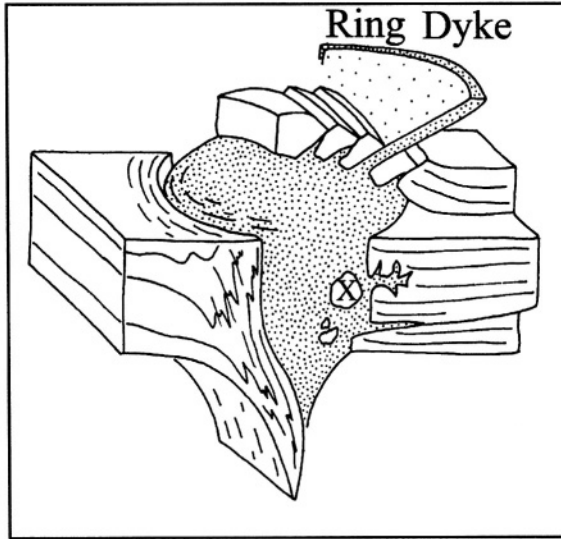


FIG. 55 — *Emplacement of an intrusion* (after Paterson *et al.*, 1991).

The emplacement is “permissive” into a brittle host rock (near-surface and relatively cold; to the right at the top of the figure) which deforms by fracturing; the intrusive material injects along the fractures as sills and dykes. Xenoliths (x) from the walls and the roof may be isolated within the intrusion. The pluton develops a regime of extension stress at its top, resulting in the emplacement of a series of circular dykes (“ring dykes”). In the ductile host rocks (deep and hot) the emplacement results in the development of isoclinal folds, schistosity and stretching lineations whose spatial distribution is controlled by the form of the pluton (*cf.* Fig. 56). These structures are commonly blurred or erased by post-emplacement annealing. The intrusion itself is the site of planar and linear deformation near its contact, both in the viscous (liquid present) and solid state.

which obtain at any point in the intrusion-host rock ensemble depends on the following parameters:

Size and initial temperature of the intrusion. These two parameters represent the quantity of heat Q brought by the intrusion; the first depends particularly on the shape (tabular or spherical, for example) of the intrusive body.

Initial temperature of the host rocks. This depends on the local geothermal gradient (before being perturbed by the intrusion) and therefore on the depth, which also fixes the pressure of crystallization ($P = \rho gz$).

Distance from the centre of the intrusion. Any point under consideration can be situated either in the host rocks themselves or within the intrusion; in essence, if the host rock temperature rises near the intrusion, the latter cools at the same time because it gives its heat to its environment. The contact surface between the intrusion and the wall rocks, therefore, plays a critical role in modeling the heat transfer process.

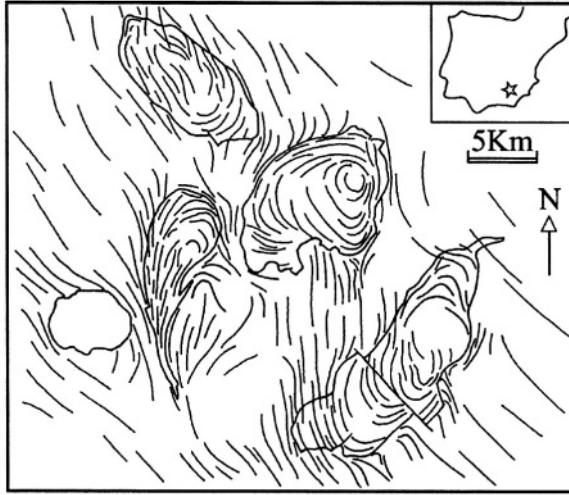


FIG. 56 — *Development of planar structures (schistosity) in granitoid intrusions and their host rocks (after Brun and Pons, 1981).*
 Example of the Burgillos region (Spain). Note the presence of “triple points” in the schistosity.

Thermal conductivity of rocks. The quantity of heat which crosses a unit of surface area during a unit of time (“**density of thermal flux ϕ** ”) depends on the potential gradient and the thermal conductivity K of the material;

$$\phi = - K \text{ grad } T$$

Elapsed time after the emplacement of the intrusive body.

Heat diffusion in contact metamorphism is a flow which decreases as a function of time while the intrusion cools. Therefore an evolution of the temperature in time may be expected at all points in the intrusion -wallrock system.

4.3.2 *The intrusion-wallrock system*

The simple model given below makes it possible to represent the diffusive heat transfer between an intrusion and its wallrock as long as one closes one’s eyes to two important approximations.

1) This is an entirely static model in that the intrusion is considered fixed in time $t=0$; in particular it is not the site of any convection which would have the effect of renewing the hot material at the contact with the wallrock. This condition is possibly acceptable for granitoids of relatively high viscosity, but it is certainly not applicable for mafic intrusions.

2) Only heat conduction in solids is taken into consideration, to the exclusion of the endothermic and exothermic processes related to mineral reactions

If the intrusion is a sheet with thickness $2a$ injected in wall rocks whose lateral extension is considered infinite, the temperature T at time t , at a distance x from the centre of the intrusion, is given by the general formula of Carslaw and Jaeger:

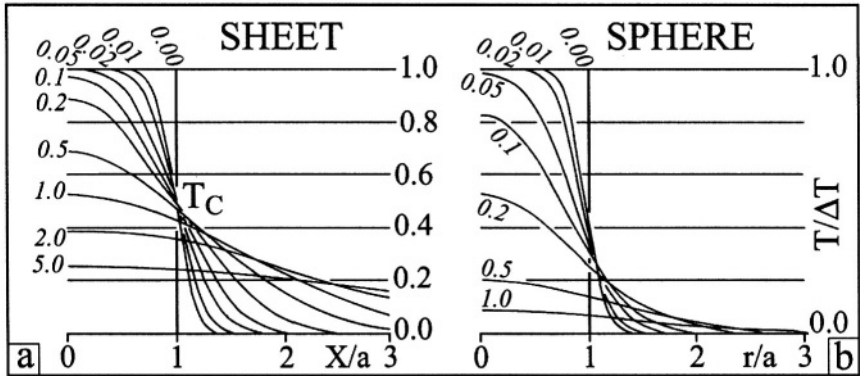


FIG. 57 — Graphic modeling of heat diffusion in the wall rock of an intrusion (after Jaeger, 1964, and Furlong *et al.*, 1991).

The intrusion consists of a rectangular sheet (a) or a sphere (b). The wall rocks are considered infinite relative to the volume of the intrusion.

Abscissa : distance from the centre of the intrusion 0; (a) is equal to the half thickness of the sheet, or the radius of the sphere; the contact corresponding to x/a or $r/a = 1$. The ordinate is $T/\Delta T$; temperature ($T_x - \tau$) measured against $\Delta T_0 (= T_0 - \tau)$ where T_x is the temperature at point x , T_0 the initial temperature of the intrusion and τ the initial temperature of the wall rocks. For each of the cases considered the curves give the temperature at all points in the system (intrusion and wall rocks) for time intervals ($t = 0.00$ to $t = 5.00$) without dimension. These diagrams demonstrate that the temperature at the contact of the intrusions is much lower than the initial temperature of the intrusion, especially in the case of the sphere. The contact temperature (T_c) decreases when the core of the intrusion cools down, whereas the temperature continues to rise in the wall rocks away from the contact.

Exercise:

What is the temperature at 1 km from the contact of a gabbro sheet 2 km thick, 20,000 years after emplacement in host rocks at 100C, knowing that the temperature in the core of the intrusion goes from 1000 °C to 800 °C in 5000 years?

$$T(x, t) = \tau + \left(\frac{(T_0 - \tau)}{2} \operatorname{erf} \frac{a - x}{(4\kappa t)^{1/2}} + \operatorname{erf} \frac{a + x}{(4\kappa t)^{1/2}} \right)$$

Where τ is the initial temperature of the wall rocks, T_0 the initial temperature of the intrusion and κ the thermal diffusivity of the rocks. It is more convenient to represent this expression by graphs which describe the evolution of temperature conditions across the intrusion/host rock ensemble as a function of time (Fig. 57). Two cases may be envisaged, depending on the shape of the intrusion within the infinite host rocks. A limited-sized sheet (parallelepiped; Fig. 57a) and a sphere (Fig. 57b). The spherical form most closely approximates a diapiric intrusion (Fig. 55). These diagrams are only as good as the data put into them, however, they make certain interesting observations possible.

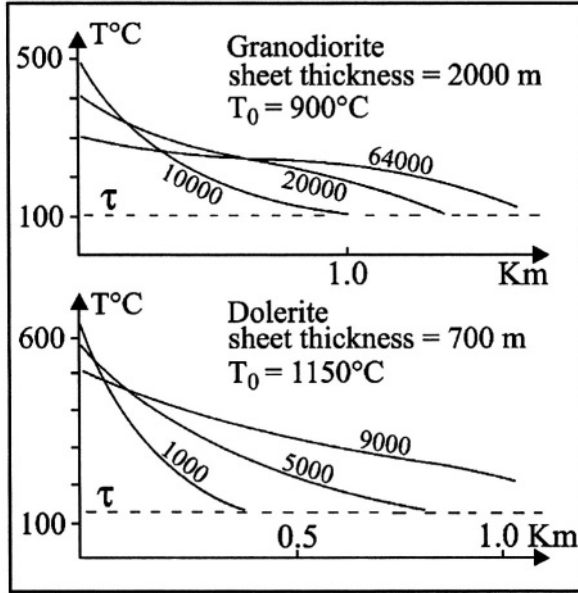


FIG. 58 — Temperature evolution as a function of time in the aureole of an intrusion (after Jaeger, 1964).

Each of the curves represents the temperature profile in the wall rocks away from the contact at a particular time (in years), for two types of intrusion.

4.3.3 Temperature at the intrusion contact and the width of the aureole

At the contact of an intrusion in an infinite host rock sequence, the temperature cannot exceed the value $T_c = \tau + (T_0 - \tau)/2$. This temperature is maintained at the contact while the core of the intrusion remains at T_0 . It decreases when the centre of the intrusion cools down from the initial temperature (Fig. 57). Thus, a near-surface granitic intrusion ($T_0 = 700^\circ\text{C}$; $\tau = 100^\circ\text{C}$, for example) can only induce recrystallization at a relatively low temperature at its contact ($T_0 \leq 400^\circ\text{C}$). Granodioritic or gabbroic intrusions ($T_0 > 1000^\circ\text{C}$) in a deep environment ($\tau = 300^\circ\text{C}$) must be considered in order to achieve contact temperatures of the pyroxene hornfels facies (and a limited partial fusion in a pelitic host rock). In all cases the maximum temperature achieved in the aureole decreases rapidly as a function of distance from the contact (Fig. 57). This accounts for the habitual structure of contact aureoles consisting of a very thin high-temperature envelope which surrounds the intrusion itself, surrounded in turn by a wider envelope of progressively lower temperature conditions which merge eventually with the value τ (Fig. 58).

4.3.4 Evolution of temperature conditions in the aureole with time

Even at the contact, the temperature $T_c = \tau + (T_0 - \tau)/2$ is only maintained while the core of the intrusion remains at T_0 . This induces an annealing which blurs and wipes out structures acquired at the contact during emplacement. Over time the temperature decreases slowly at the contact (Fig. 57), whereas it rises, in contrast, farther from the intrusion. This often results in a partial or complete retrograde change of high grade assemblages to lower grade

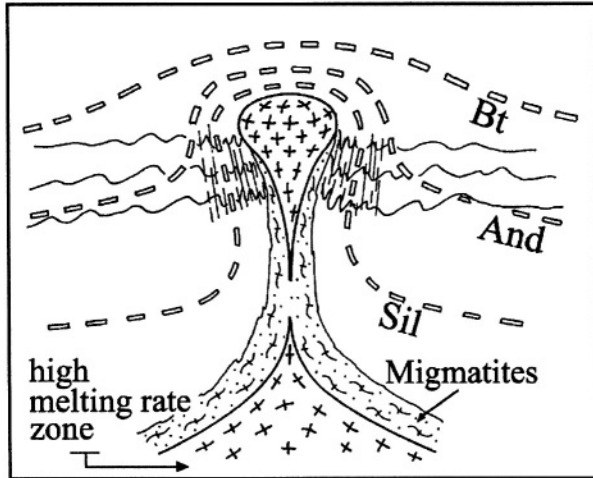


FIG. 59 — Schematic diagram of the dynamic emplacement of a pluton (*diapiric emplacement hypothesis*) in the upper levels of the continental crust (after Flood and Vernon, 1978). The pluton propagates toward the surface from a largely melted lower crustal zone, driven by the Archimedes effect, based on the relatively low density of granitic magma relative to the wall rocks. This rise is facilitated by the high temperature of the material situated at the immediate contact of the intrusion at depth, which accompany it in its movement. In this perspective, the migmatites which appear in the internal zone of contact aureoles cannot be considered autochthonous. The general thermal configuration around the intrusion results in a progressive deformation of the regional isotherms, and not to a simple diffusion model such as seen in Figure 57 (*cf.* first part: perturbation of geothermal gradients by an intrusion).

ones, especially if the contact zone was affected by a fluid phase. Figure 58 shows this evolution of temperature in the aureole over time.

4.3.5 High grade contact metamorphism

In the static model envisaged, conditions suitable for the pyroxene hornfels facies ($T > 650^{\circ}\text{C}$) are only attained in contact metamorphic aureoles around high-temperature intrusions emplaced in relatively deep domains. Conditions for the sanidinite facies ($T > 800^{\circ}\text{C}$) are never realized. The assemblages corresponding to these conditions do not occur in aureoles, but in enclaves torn from the walls of intrusions and surrounded by the magma (Fig. 55). The conditions previously envisaged to apply the formula of Carslaw and Jaeger; “infinite wall rocks with respect to the intrusion” cannot be applied in this case. It is actually the contrary, the volume of the intrusion is almost infinite with respect to the volume of the enclaves, and the temperature attained can approach T_0 . A variety of high temperature assemblages result from this, corresponding to the highest grade facies of contact metamorphism. These enclaves may melt partially and become “buchites” with assemblages which are restitic; they are occasionally partly or totally dissolved in the intrusive magma, which is contaminated by its wall rock as a result.

4.4 Dynamic emplacement

The development of a contact aureole is in reality much more complex than described

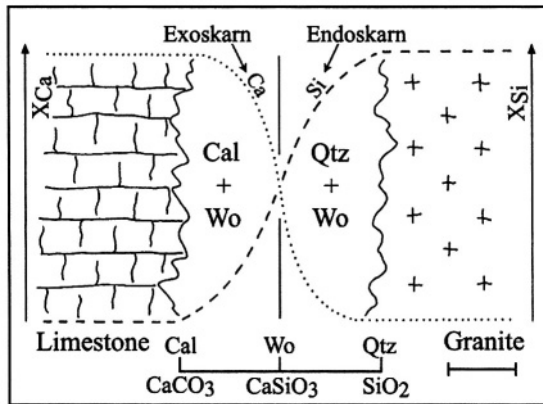


FIG. 60 — *Metasomatic reactions between a granite intrusion (crosses) and limestone wall rocks (brick pattern).*

At time t_0 of the emplacement, strong chemical potential gradients are established between the two milieus, particularly for Si and Ca. The tendency for these potentials to equilibrate results in the diffusion of Si toward the limestone, and Ca into the granite. These elements diffuse along grain boundaries and not in the solid milieu. The granite is changed into quartz + wollastonite endoskarn and limestone into a calcite-wollastonite exoskarn. Scale: several cm to several m.

above. The diffusion of heat into the wall rock and the cooling of the intrusion occur while the magmatic body progresses toward the surface. The distribution of isograds over time is therefore more complicated than the Jaeger model, but must be modeled taking into consideration the differential equation of heat transfer used in Chapter 1 for the case of the vertical transfer of magmas. The resulting graphs are too complicated to be presented here. Nevertheless the dynamic evolution of the intrusion-wall rock ensemble has two consequences:

- 1) at the immediate contact of the intrusion, the wall rock is likely to have a temperature greater than the value $\tau + (T_0 - \tau)/2$; the emplacement of the pluton is therefore facilitated by a ductile interface which plays the role of a lubricant, especially if the wall rock has ambient conditions close to those for partial fusion (Fig. 59);
- 2) the intrusion, cooled along its borders, has an increasing rate of crystallization and as its viscosity becomes greater and greater, its emplacement is accompanied by the development of oriented fabrics, first magmatic, then in the solid state, up to the complete arrest of its progress towards the surface.

METASOMATIC REACTION AT THE CONTACT OF AN INTRUSION: SKARN GENESIS

The emplacement of an intrusion in sedimentary wall rocks often results in the juxtaposition of materials of contrasting composition. The contact at the theoretical instant t_0 is characterized not only by a strong thermal gradient but also by abrupt chemical potential gradients. Moreover, a contact zone is generally the site of high fluid mobility (CO_2 , H_2O , etc.); both fluids associated with the intrusion and those resulting from the dehydration and decarbonation of the wall rocks. These high temperature fluids migrate toward zones of

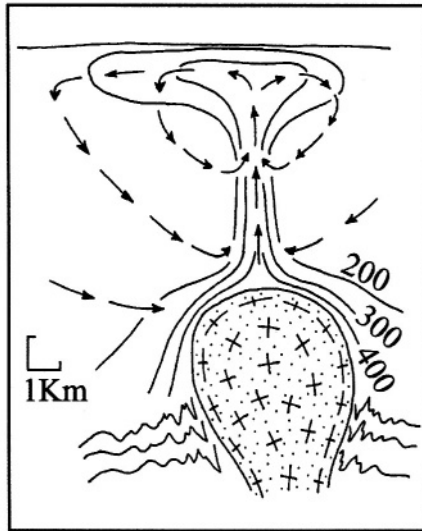


FIG. 61 — Schematic diagram of a convective hydrothermal system developed in the roof of an intrusion (crosses) (after Fyfe and Henley, 1973).

The fluid phase (water vapour and hydrocarbonic fluid) has a high fugacity around the intrusion and reaches the low energy (low pressure and temperature) near-surface domain. Cooled and condensed near the surface, the fluid phase sinks to depth following the convection circuit shown by the arrows. This circulation is accompanied by a convective heat transfer toward the surface, forming a hydrothermal plume over the intrusion (isotherms in degrees C). Silicates are dissolved by the high temperature fluids and the cations in solution precipitate at low temperature along the hydrothermal veins (*cf.* Fig. 63) which characterize former convective systems (see also Fig. 98).

lower energy, transporting elements in solution which then precipitate a certain distance from the contact. These aureoles are therefore the site of reaction in an open system or metasomatic reactions of which certain result in exploitable mineral deposits.

4.5 Short range reactions (several cm to several m) or diffusion metasomatism

Chemical potential gradients μ , just as in thermal gradients, have a tendency to equilibrate on one side or other of the interface between environments of differing composition. This “interdiffusion” of elements follows laws analogous to those for heat diffusion. To apply them, it only requires a substitution of concentrations for temperature in the Carslaw-Jaeger equation, as well as the diffusion coefficient D of the elements to be considered for the thermal diffusion coefficient, for the environment and P-T conditions under consideration. D is expressed in the same manner as K

$$\phi = - D \text{ grad } C$$

where ϕ is the flow of material and $\text{grad } C$ the concentration gradient.

It becomes then:

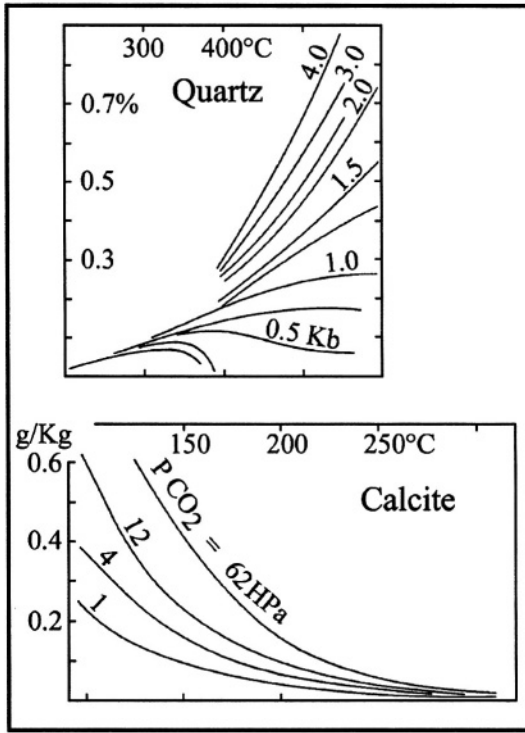


FIG. 62—Solubility of quartz and calcite in water as a function of temperature and pressure (after Fyfe *et al.*, 1978).

For quartz : solubility in weight percent and pressure in kb; for calcite : solubility in g. kg⁻¹ and partial pressure of CO₂ in hPa.

Note the inverse behaviour of the two phases, quartz solubility increases as a function of temperature and pressure, that of calcite increases as a function of partial pressure of CO₂, but varies inversely with temperature.

$$X_{i(x,t)}^i = X_i^e \left(\frac{X_i^i - X_i^e}{2} \operatorname{erf} \frac{a-x}{(4Dt)^{1/2}} + \operatorname{erf} \frac{a+x}{(4Dt)^{1/2}} \right)$$

X_i^i and X_i^e represent the concentrations of the element in the intrusion and the wall rocks.

D varies considerably as a function of temperature. For temperatures below 1000 °C the diffusion coefficient for elements in solids is very low (on the order of 10⁻²⁰ m² s⁻¹). Solid state diffusion is, as a result, an extremely inefficient mechanism to re-equilibrate chemical potentials, even at a geological time scale. In metasomatism, element or ionic diffusion takes place along intergranular boundaries; it is particularly rapid and efficient when the boundaries are bathed in an interstitial fluid (H₂O or CO₂) which is an excellent environment for diffusion.

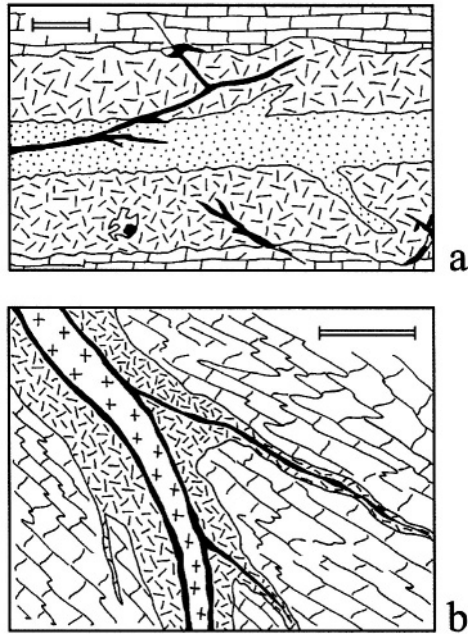


FIG. 63 — Development of metasomatic skarn veins around the Salau intrusion (Eastern Pyrenees) (after Fonteilles *et al.*, 1989).

a) Exoskarn : the limestone wall rocks (brick pattern) are recrystallized (isochemically) and become marbles; the metasomatic changes are developed along hydrothermal veins; in the first phase epidote (dotted) and hedenbergite (dashed) skarn zones develop at the marble contact. A second hydrothermal phase deposited grossularite veins (black) which cut the preceding ones.

b) Geometric relations between endoskarn and exoskarn : epidote + amphibole + sphene endoskarn (crosses) results from the metasomatic transformation of a granite dyke injected into the limestone; exoskarn consists of an internal grossularite zone (black) and an external zone of hedenbergite and scheelite (dashed). The scheelite is not exploitable in this context; leached, concentrated and redeposited, it resulted in the formation of economic deposits during a second hydrothermal phase. Scale bars = 20cm.

At the time t_0 of emplacement, a strong concentration gradient is developed for Si and Ca, at the contact between granite and limestone (Fig. 60). These gradients evolve as a function of time, in the same manner as thermal gradients, by the intergranular transfer of Ca towards the granite and Si towards the limestone. Seen in a simplified fashion this interdiffusion translates into the development of wollastonite + quartz and wollastonite + calcite parageneses in a domain of composition intermediate between granite and limestone. This is generally a very thin domain (several m at a maximum) which is called “skarn”. This skarn consists of two zones (Fig. 60):

- 1) an internal zone resulting from the metasomatic transformation of the intrusion, or “endoskarn”, and
- 2) an external zone resulting from the metasomatic transformation of the wall rock, or “exoskarn”.

In reality, the reactions between granite and carbonate rocks are generally much more complex. The granite contains significant or notable proportions of Al, Fe, Mg, K and Na.

These elements have different diffusion coefficients, which depend on their ionic radii. As a result, varied mineral assemblages appear at the contact, commonly mono- or bimineralic, composed of different calcic minerals such as hedenbergite, grossularite, epidote, vesuvianite, etc., as well as quartz and wollastonite.

4.6 Ionic transport in solution, or percolation metasomatism

Skarn zones are commonly the site of economically important mineral assemblages, notably tungsten. Metallic concentrations there are hundreds or thousands of times superior to the concentrations observed in the intrusion or in the wall rock, which is not compatible with a model of re-equilibration of concentrations by diffusion. Detailed studies show that these deposits are not formed in the simple manner described above, but result from complex metasomatic processes related to the mobility of fluids.

The emplacement of an intrusion is usually accompanied by the release and circulation of a significant quantity of fluid. A water-rich fluid phase initially dissolved in the silicate liquid is released by crystallization of the magma. Hydrous or carbonate fluids are produced by dehydration and decarbonation reactions in the sedimentary wall rocks. This fluid phase, at high temperature and relatively high pressure (0.4 to 0.2 GPa, 700 to 300°C) tends to migrate to the surface towards low pressure and temperature zones. An intrusion is therefore accompanied by a convective hydrothermal or hydrocarbonic system (Fig. 61) which extends the thermal effects in the wall rocks beyond that possible by simple heat diffusion mechanisms.

Depending on the composition, temperature and pressure, the fluid phase is capable of dissolving solids selectively in the percolation network in which it circulates. Quartz (Fig. 62a) and in a general manner, all silicate minerals, are more soluble when the temperature is higher, in contrast to the carbonate minerals, whose solubility decreases with increasing temperature (Fig. 62b). As a result, in a carbonate wall rock, calcic silicates (hedenbergite, grossularite, wollastonite, epidote and vesuvianite) precipitate in veins (exoskarns) resulting from the interaction between the limestone and a fluid supersaturated in silica (Fig. 63a). The intrusion itself, or its apophyses, (Fig. 63b) are also transformed into calcic assemblages (endoskarns) by the action of fluids rich in carbonic ion coming from the wall rocks.

The cyclic character of the convective circulation of fluids (Fig. 61) results in the exceptionally high concentration of certain elements encountered as a result of successive episodes of solution and precipitation. This is how tungsten, in the form of scheelite (CaWO_4) associated with the exoskarns of the Salau (Ariège) intrusion was concentrated during at least two successive stages:

- 1) circulation of magmatic fluids (540-450 °C) producing non-exploitable pre-concentration of W in hedenbergite skarns and
- 2) a leaching of the skarns by fluids (450-350 °C) partly coming from the wall rocks is the source of a second generation of epidote and garnet skarns carrying the exploitable mineralization (Fig. 63).

The modeling of percolation metasomatism, in other words, recrystallization in an open system, depends of the “theory of perfectly mobile constituents” of Korjinskii. This theory is too complex to be developed, even summarily, in this text.

REGIONAL METAMORPHISM

In contrast to contact metamorphism which is directly related to the emplacement of intrusions, regional metamorphism does not have a directly observable cause. It is developed over vast area (several hundred to several thousand km^2) and is accompanied, in the majority of cases, by the development of several schistositys and stretching lineations. Regional metamorphism, therefore, results in general in dynamic recrystallization (sometimes blurred by a late annealing) under anisotropic stresses. It is generally polyphase, resulting from an evolution of the recrystallization conditions over time. All of these characteristics underline the close liaison between regional metamorphism and orogenic evolution.

THE CONCEPT OF A METAMORPHIC GRADIENT

The geologic units affected by a regional metamorphism generally show a spatial variation of metamorphic facies corresponding to an evolution of the P-T conditions of recrystallization. This characterization results in metamorphic isograds on maps (Fig 29), or, strictly speaking, the distribution of metamorphic facies at the regional scale. The linked variation of pressure and temperature expressed in this evolution, results from a variation of temperature as a function of depth, or in other words, the shape of the geothermal gradient (Fig. 5) at the time of metamorphism of the region under consideration. In addition, the mineral assemblages observed in different samples of a metamorphic series often show the effects of a partial re-equilibration (heterogeneous recrystallization) which result in the crystallization of secondary assemblages. These result from an evolution of the recrystallization conditions over time, and, in consequence, an evolution of the shape of the local geothermal gradient over time.

5.1 P-T evolution in a metamorphic series: prograde gradients

The succession of mineralogical reactions observed (or more or less deduced from the assemblages) along a metamorphic gradient in a lithologically homogeneous series (Fig 64) results in successive steps in the recrystallization. The assemblages, which really correspond to the most intense metamorphic conditions, are supposed to have passed through all the different stages represented by the lower grade assemblages, which reproduces, as a result, the path of the unit through P-T space. This path, corresponding to an increase in metamorphic conditions, is called a prograde gradient. Pressure conditions appearing to increase in the majority of cases, this prograde gradient results from a deep burial of the unit.

Attention must be paid to the coherence of the data chosen for the construction of a proposed gradient in a P-T diagram. The mineral assemblages of each of the samples supposed to be on the gradient must correspond to the same chronological situation, with relation, for example, to the succession of deformations; these are the *type assemblages*. Note that prograde reactions are generally very difficult to identify directly, as they formed in a milieu of homogeneous penetrative deformation at a rising temperature; dislocation

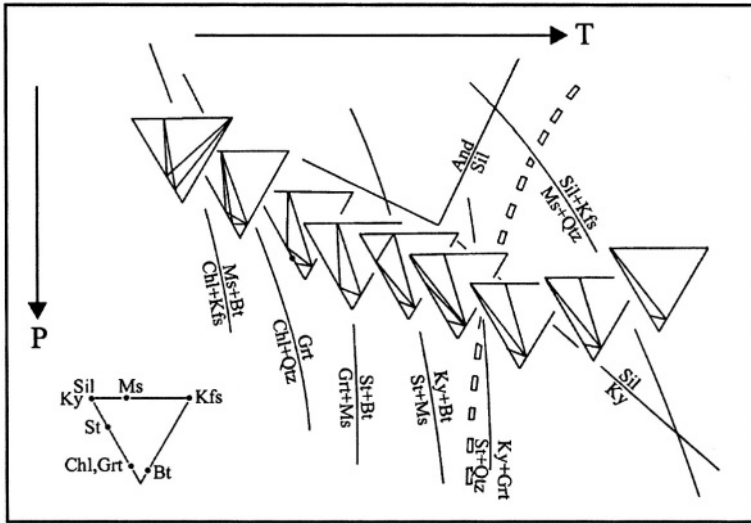
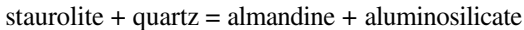


FIG. 64 — Characterization of an intermediate pressure prograde gradient (“Dalradian”): example of Bas Limousin (after the data of Floc’h *et al.*, 1978, Floc’h, 1983).

The prograde reactions are not directly observed, but deduced by the succession of synkinematic type assemblages in the field. Thick dashed line : metapelite fusion for $P_{H_2O} = P_{total}$. The inflection in the gradient toward lower pressure in the sillimanite field foreshadows the shape of the retrograde gradient.

energy supported rapid recrystallization of the assemblages and low temperature relics are not generally preserved. A classic step at relatively low temperature is marked, in metapelites, by the presence of staurolite relics “armoured” by garnet crystals. These inclusions bear witness to the operation of the prograde reaction:



This reaction is interrupted when the staurolite and quartz are no longer in mutual contact. Other types of armoured relics (lawsonite in garnet, for example) sometimes allow precise verification of the coherence or incoherence of gradients drawn from the observation of type assemblages. The sporadic character of these relics does not allow their systematic use to prove prograde reactions.

5.2 Polyphase evolution of metamorphic rocks: retrograde gradients

Most metamorphic series are polyphase. The type assemblages developed under peak P-T conditions are variously replaced by reactional parageneses resulting from the instability of the primary phases (Fig. 65). These reactions generally take place in a static milieu (local isotropic stress) or under moderate and heterogeneous deformation; the recrystallization is often incomplete, and undeformed zones are almost free of recrystallization. The type synkinematic, and the other tardi- and post-kinematic assemblages may all coexist. The succession of these assemblages, over time, makes it possible to follow the temporal P-T

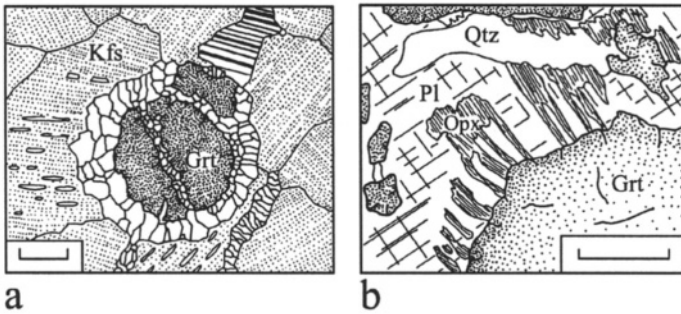


FIG. 65 — Examples of heterogeneous recrystallization characterizing retrograde gradients.

a) Development of a fine granoblastic cordierite-biotite-quartz assemblage at the expense of garnet (Grt : dark stipple) and potassium feldspar (Kfs : light stipple). This local recrystallization (note in particular the role of a fracture allowing circulation of a water-rich fluid) results from retrograde action (in the sense of diminishing P and T) of the reaction : $Bt + Crd + Qtz = Grt + Kfs + \text{water}$, Scale = 0.25 mm. Metapelitic granulite of the North Pyrenean Zone (after Vielzeuf, 1984).

b) Crystallization of orthopyroxene (Opx) and plagioclase (Pl) at the expense of the HP-HT association garnet (Grt) + quartz (Qtz). Scale = 0.1 mm. Granulitic metapelite of the Rif (after Kornprobst, 1974).

evolution registered by the sample (*cf.* Fig. 77). In the majority of cases this evolution is characterized by a drop in pressure, commonly accompanied by a drop in temperature which is usually defined as a *retrograde gradient*. It makes it possible to detail the processes of cooling and exhumation (rise to the surface) of metamorphic units.

DIFFERENT TYPES OF PROGRADE GRADIENTS

Three principal types of prograde gradient were noted by Miyashiro in 1961 (Fig. 66).

5.3 The Franciscan gradient

This is the high pressure and low temperature gradient which is represented in particular by units composed of glaucophane and lawsonite schists and eclogite. The aluminosilicate, when it is present, is always kyanite, the highest density polymorph. This gradient, defined in the San Francisco (California) region on the shore of the Pacific Ocean, is widely represented in the metamorphic series of the Alpine chain, in particular in the Liguro-Piemontais zones of the Franco-Italian Alps (Fig. 67). The common metabasaltic character of the protolith, the frequency of serpentines and peridotites associated with the blue schists and eclogites show that the Franciscan units are generally derived from the recrystallization of ophiolitic series or other elements of the oceanic crust.

5.4 The Dalradian gradient

This is an intermediate pressure gradient which was described from the Eocaledonian series of Scotland. It is a synonym for the "Barrovian gradient". It is essentially based on

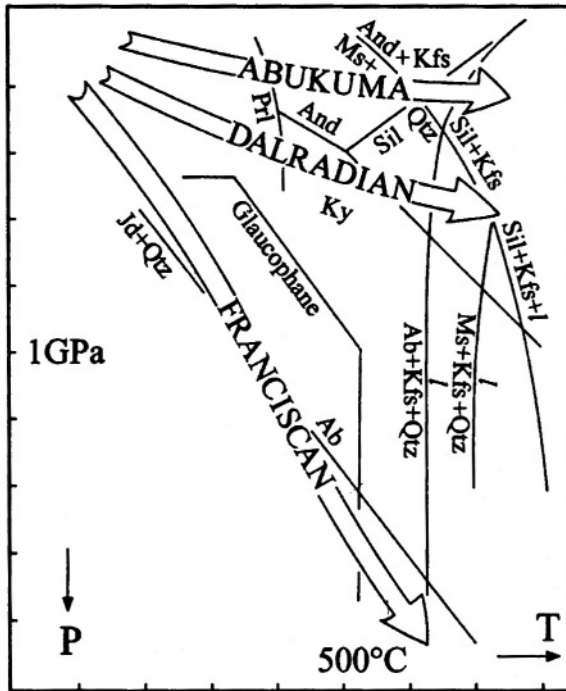


FIG. 66 — The three principal types of prograde gradients of regional metamorphism (according to Miyashiro, 1961).

The Franciscan gradient (HP-LT) is characterized by the assemblages of the glaucophane schist and eclogite facies; barring exceptions, it does not cross the wet granite fusion curve, and the Franciscan series generally has no migmatites. The Dalradian gradient (intermediate pressure) is characterized by the prograde transition kyanite \Rightarrow sillimanite. The Abukuma gradient (HT-LP) is characterized by the transition andalusite \Rightarrow sillimanite, and the reaction muscovite + quartz \Rightarrow aluminosilicate + K feldspar commonly occurs in the andalusite stability field. These characteristics are close to those observed in the aureoles of contact metamorphism. The higher degrees of Dalradian and Abukuma gradients involve the partial fusion of metapelites. Migmatites play an important role in these metamorphic series; at low pressure the partial fusion can take place in the andalusite stability field.

metapelitic assemblages which have a clear affinity with the continental crust and are characterized by the kyanite-sillimanite transition (Fig. 66). Dalradian metamorphism comprises vast domains in older rock belts, in particular the Hercynian belt. In France (Fig. 67) it is particularly well represented in the Western Massif Central.

5.5 The Ryoike-Abukuma gradient

This is a low pressure-high temperature gradient close to the contact metamorphic thermal gradient. Defined in Japan, in the mafic and metapelite protoliths of the Abukuma and Ryoike belts, it is characterized by the andalusite-sillimanite transition, kyanite, in principle, is never observed (Fig. 66), although this is not precisely the case in the Abukuma belt. These type localities are in recent belts (Upper Cretaceous) but low pressure gradients are equally well represented in the Hercynian chain, especially in the later stages of orogeny

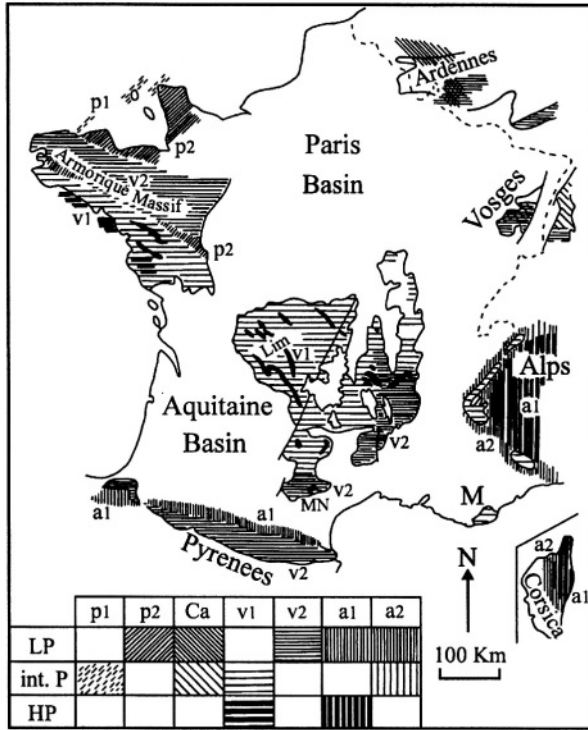


FIG. 67 — Distribution of metamorphic series in France as a function of their age and type of prograde gradient (after Kornprobst *et al.*, 1981).

LP : Abukuma gradient; int P : Dalradian gradient; HP : Franciscan gradient; p₁ : Archean (Icartian); p₂ : Upper Proterozoic (Cadomian); Ca : Caledonian; v₁ : Variscan; v₂ : Hercynian; a₁ : Eoalpine; a₂ : Lepontine; M : Maures Massif; MN : Montagne Noire; Lim : Limousin. The black sausages represent the principal swarms of high pressure rock (eclogite and granulite, which appear as relics in the Dalradian Series.

(around 300 Ma). In France, the Montagne Noire, the Northern Pyrenean Agly massif, and the Canigou and Roc de France massifs in the axial core of the Pyrenees, are characterized by this type of gradient (Fig. 67). Metamorphism in the North Pyrenean Zone of Upper Cretaceous age (98-81 Ma) also corresponds to these low pressure conditions.

The Franciscan and Abukuma gradients both have trajectories in P-T space which differ considerably from that of geothermal gradients measured in stable zones (Fig. 66). Development of such metamorphic gradients results from significant dynamothermal perturbation of the lithosphere. In contrast, the intermediate pressure gradients are not far from unperturbed geothermal gradients. This does not signify, naturally, that this type of metamorphism was developed in stable zones, as the associated intense deformation demonstrates effectively the opposite, but during recrystallization of the Dalradian units, the competition between convective and diffusive heat transfer was indecisive (*cf.* below).

In fact, in a general way, as can be seen clearly in Figure 67, different types of prograde gradient are generally closely implicated in the same region, and even in the same

unit. As well, significant eclogite relics (typical Franciscan elements) are known in Dalradian domains of the Caledonian and Hercynian chains. The Dalradian gradients often evolve regionally toward lower pressures and high temperatures. The different prograde metamorphic gradients appear, therefore, much as successive steps in the same orogenic evolution at the scale of a mountain chain.

PROGRADE GRADIENTS, PARTIAL FUSION AND MIGMATIZATION

The Abukuma and Dalradian gradients generally cross the fusion curve for hydrous granites (Fig. 66). Under these high temperature conditions ($T > 650$ °C) liquids of granitic composition are produced by partial fusion of metapelites. This process leads to the formation of migmatites, composite rocks consisting of intimate mixtures of the products and residues of fusion. Rigorously, it is a magmatic process because it involves the appearance of a liquid phase, but its close liaison with high grade metamorphism requires that it must be described in this manual. Note that, as a result of their very steep gradient, the Franciscan series are generally not affected by migmatization (Fig. 66) except in certain, particular, cases.

5.6 Partial fusion of metapelites

Figure 68 shows the phase relations at the liquidus in the A' KF system, which gives a reasonable representation of the metapelite, and to a lesser extent the calcium-rich metagreywacke composition. The composition of the first liquids of partial fusion remains pretty well constant over a large pressure range (0.2 to 2 GPa): these are liquids of granite composition in equilibrium with mineral assemblages whose nature depends on the P-T conditions, the fusion rate, and the composition of the original rock. With a higher fusion rate, potassium feldspar and biotite disappear, and the solid assemblages consist essentially of plagioclase, sillimanite, cordierite and/or garnet. Limited partial fusion of metapelite and metagreywacke leads to a more or less close association between the different materials resulting from the same "protolith".

5.6.1 Granitic liquid by partial fusion

It is called "leucosome" to characterize its light colour.

5.6.2 Refractory solid residue

This is the "melanosome", with darker colours than the leucosome. Leucosome and melanosome constitute the "neosome" which results from a redistribution of the elements of the rock by partial fusion. Fragments of these, little or unaffected by partial fusion, occur sometimes in migmatites: they are composed of "mesosome" (intermediate colour between leuco- and melanosome) or even "paleosome" if it can be demonstrated that it is really the original material. The process of migmatization is summarized in the following scheme:

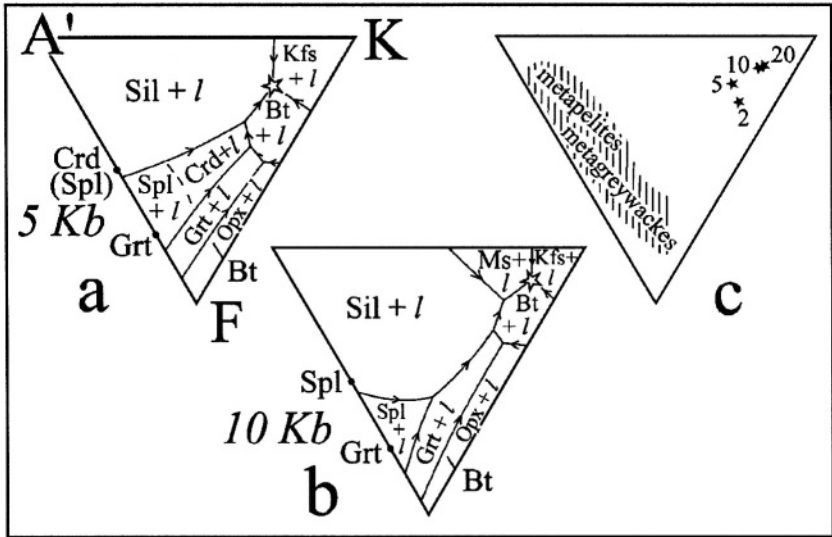


FIG 68 — Phase relations at the liquidus in the $A'KF$ system (after Vielzeuf and Holloway, 1988).

This system is convenient to represent the metapelites and metagreywackes of the continental crust (c) in neglecting the Ca concentration *i.e.* plagioclase. This system contains no free water; water liberated by the dehydration reactions is dissolved in the liquid. Diagram (a) and (b) show the composition of the anatectic liquid produced at 5 and 10 kb for all compositions of the system (white stars). Triangle (c) shows the composition of the eutectic liquids at 2, 5, 10 and 20 kb (black stars). Partial fusion for all metapelite and metagreywacke compositions leads to the appearance of a leucosome of granitic composition, and an anhydrous or water-poor melanosome enriched in refractory minerals: sillimanite (Sil), cordierite (Crd), garnet (Grt), spinel (Spl), and orthopyroxene (Opx). l = liquid; Bt = biotite; Kfs = potassium feldspar; Ms = muscovite.

protolith or
paleosome or ⇒ neosome ⇒ leucosome (partial fusion liquid)
mesosome +
melanosome (solid residue)

5.7 Extraction of leucosome: different types of migmatites

A complex nomenclature fed by an abundant literature describes the geometric relations between leucosome, melanosome and neosome. The four most common structures are the following: “nebulitic migmatite”, “stromatite”, “diktyonite” and “agmatite” (Fig. 69).

5.7.1 Nebulitic migmatite

This contains irregular islets of neosome dispersed in the paleosome, the limits between the two are blurred and irregular. They represent the most elementary stage of migmatization. The very viscous liquid was produced by *in situ* partial fusion, (zones of particularly favourable composition most probably determining the location of the spots) in small quantities under conditions of isotropic or weakly anisotropic stress. This not very mobile liquid is collected in pockets of such small size that they cannot generate significant buoyancy (Archimedes Principle) relative to the melanosome.

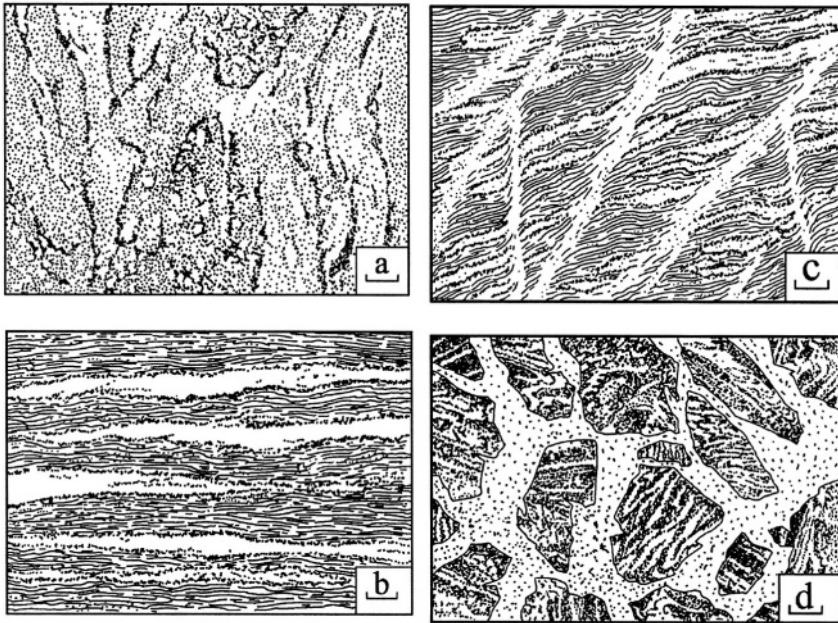


FIG. 69 — *Principal types of migmatite* (simplified after Mehnert, 1968).

a) Nebulitic migmatite: the leucosome is collected into small, poorly-developed pockets; beginning stages of anatexis; b) stromatite: neosome disposed in parallel layers; this distribution is either an extraction of anatectic liquid, or is perhaps inherited from the original metapelites: in the latter hypothesis the leucosomes represent original layers rich in granitic components which were largely melted with respect to adjacent refractory rocks; the structure bears witness to the original heterogeneity of the paleosome. c) diktyonite: the leucosome appears in layers parallel to the foliation and crosscutting veinlets show the mobility of the liquid phase. d) agmatite: blocks, both migmatitic and not, generally angular, are cemented in a leucosome which is not necessarily genetically related to the elements of the breccia (which do not necessarily represent their paleosome or melanosome). This last type of structure can result from hydraulic fracturing at the roof of migmatites. Scale 10 to 20 cm.

5.7.2 Stromatite

This consists of small-scale (several mm to several cm) alternating layers of neosome and mesosome. The limits between leucosome and mesosome are sometimes indistinct; in this case the migmatite also results from an *in situ* partial fusion of pre-existing layers of favourable composition (rich in granitic components). In contrast the limits are sometimes cross-cutting and discordant with respect to foliations older than the partial fusion; here the liquid demonstrates a certain mobility, and is collected into veinlets cutting the mesosome.

5.7.3 Diktyonite

This shows a complex interpenetration of the mesosome and the neosome (leucosome and melanosome) testifying to the genetic relationship between the two constituents. The segregation and mobility of the partial fusion liquid was induced by an anisotropic stress regime which is responsible for collecting the leucosome in anastomosing veinlets.

5.7.4 Agmatite or agmatitic migmatite

This is characterized by a breccia-like mesosome (paleosome?) impregnated by the leucosome. The genetic relations between the granitic liquid and the mesosome are not as evident as in the diktyonite, because of the general absence of well-constrained melanosome. The breccia-like character of this formation suggests hydraulic fracturing at the roof of the migmatite body, resulting from the accumulation of a sufficient quantity of granitic component to develop significant Archimedes buoyancy by density contrast. The agmatitic structure probably represents a transition between migmatite in the strictest sense, and a granitic pluton (“S” type from sediments or “C” type from continental crust, that is to say, by partial fusion of continental crust) escaped from their crustal sources.

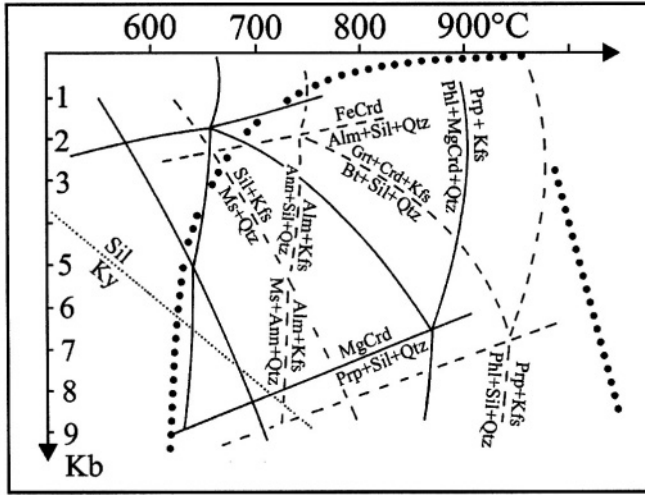
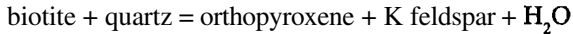


FIG. 70 — Role of the partial pressure of water on the appearance of the granulite facies.

The P-T diagram shows an offset toward lower temperatures as a function of the molar fraction of H₂O in the fluid phase of several dehydration reactions limiting the amphibolite and granulite facies. Dashed line: $P_{\text{H}_2\text{O}} = P_{\text{total}}$; Solid line: $P_{\text{H}_2\text{O}} = 0.4 P_{\text{total}}$ (after Vielzeuf, 1984); Bold dotted: granite solidus, dry and water saturated. Partial fusion of metapelites or else the CO₂ flux coming from the upper mantle or decarbonation reactions (Fig. 97), leading to a decrease in $X_{\text{H}_2\text{O}}$ in the fluid phase, favours the appearance of granulite assemblages at relatively low temperature.

5.8 Migmatites and the granulite facies

Migmatization commences at more or less elevated temperatures, depending on the presence of an interstitial fluid phase and as a function of the water content of this fluid phase (*cf.* Fig. 88). In all cases the interstitial water vapour, or that produced by fusion reaction, is preferentially dissolved in the granitic liquid (up to 10 weight % at 0.6 GPa). The interstitial fluid phase disappears from the melanosome or else it is considerably enriched in CO₂ in the domain of immiscibility between CO₂ and H₂O. The CO₂ is a species which is effectively much less soluble in magmas than in water. Under partial pressures of water which are weak to nil, the dehydration reactions which characterize the appearance of the granulite facies come into play at relatively low temperatures (700-750 °C; Fig. 70). These are the following reactions:



Therefore there is commonly a direct relation between migmatites and the appearance of granulite facies assemblages, or in a more general fashion, between partial fusion and granulitization.

In reality the conditions for the appearance of the granulite facies are linked to the low partial pressure of water in the fluid phase, whether this is caused by a decrease in the H_2O concentration or to an increase in XCO_2 . A carbonic flux coming from the upper mantle, accompanied (or not) by basic magmatism, is sometimes responsible for this compositional evolution of the fluid phase and the appearance of granulitic parageneses (Fig. 97). This role of CO_2 is shown by a comparison study of fluid inclusions in rocks of the amphibolite facies ($1 \geq \text{XH}_2\text{O} > 0.7$) with those from rocks of the granulite facies ($0.3 > \text{XH}_2\text{O} \geq 0.0$) following the concept popularized by Jacques Touret.

GEODYNAMIC INTERPRETATION OF METAMORPHIC GRADIENTS

Prograde and retrograde gradients allow interpretation of the “dynamothermal” history of metamorphic series, in other words the evolution of P-T conditions with time, as applied to materials of a specific geological unit. Pressure variations are directly and immediately (at a geologic time scale) related to load variation at depth; they become, therefore, direct measures of the burial (increasing P) or exhumation mechanism (uplift to the surface, decreasing P). Temperature variations are not as easily interpreted. Rocks are poor conductors and heat diffusion is extremely slow with respect to the displacement rates implied by orogenic phenomena. Geological units are therefore characterized by a strong thermal inertia and their displacements as a result of geodynamic processes, consequently, deform the isotherms which were developed in strictly conductive stable areas (Fig. 71). Heat production by radioactivity, the advection of magmas and hydrothermal fluids, as well as tectonic friction are equally capable of perturbing the thermal regime of a series during its metamorphism.

These diverse processes were analyzed in the first part of the text. Their modeling and the establishment of comparisons between prograde and retrograde gradients deduced from the assemblages of metamorphic series make it possible to analyze the evolution of geodynamic processes in relation with metamorphism with a certain precision. Two examples are proposed below.

5.9 Retrograde evolution and exhumation

Retrograde gradients are most commonly characterized by a significant decompression resulting from the uplift of units toward the surface. The form of these gradients is, however, variable, showing more or less well-developed loops toward high temperature. Numeric modeling shows (Fig. 72) the relation between the form of the gradient and the rate of vertical uplift of the units (the advection term v of the heat equations; *cf.* first part of text).

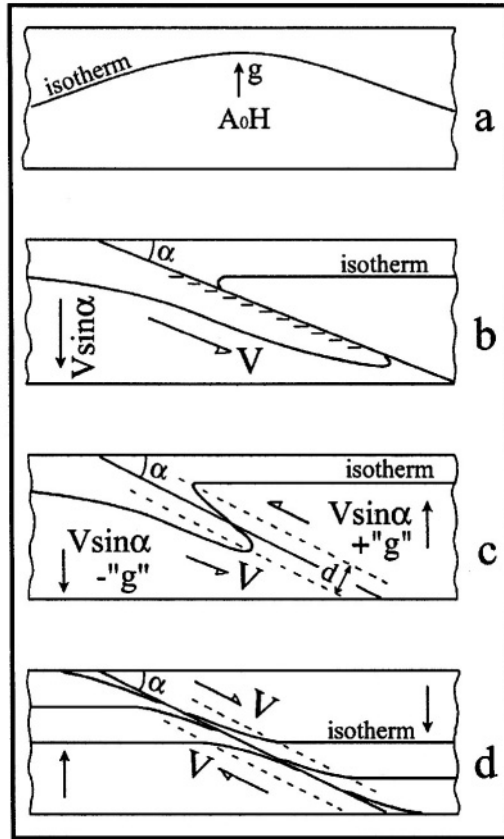


FIG. 71 — “Convective” heat transfers in a dynamic system: evolution $\partial T/\partial t$ and deformation of the isotherms.

- a) Erosion-isostatic re-equilibration: heat production A_0H is significant in a thickened continental crust. The vertical transport (g for gravitational equilibrium) is slow (several $1/10^6$ of mm per year), but enough to induce a bulge in the isotherms as a result of low values of thermal diffusivity κ of the rocks. The geothermal gradient is offset toward high temperatures (Fig. 72).
- b) Subduction: A_0H is negligible in oceanic crustal units. The vertical transport $V\sin\alpha$ is very rapid (3 to 4 cm per year); the isotherms are profoundly downwarped in the subduction slab. The geothermal gradient is offset toward low temperatures (Fig. 73). Mechanical heat production τV (hachured zone) ear the subduction surface is envisaged in some models (Fig. 73).
- c) Thrusting and underthrusting continental units: the underthrust slice is buried at a vertical speed ($V\sin\alpha - g$) which is much lower than in subduction; and the isotherms are weakly downwarped. The thrust slices rises at the speed ($V\sin\alpha + g$), a more rapid tectonic exhumation than mere isostatic re-equilibration, and at lower temperature. The zone between the two dashed lines is the domain where thermal re-equilibration by conduction occurs between the two slices, heat transfer in this zone obeys the formula of Carslaw and Jaeger (*cf.* above). Inverse gradients appear in this domain (Fig. 87). Mechanical heat production τV may take place at the plane of contact to produce “pseudotachylite”.
- d) Extension: the isotherms follow the movements of the uplifted and down-dropped segments; note their close spacing in the zone of conductive thermal re-equilibration, corresponding to high temperature gradients at the contacts of the rising segments (Figs. 92b and 93b). In these different cases the regional heat flow q_m is considered constant.

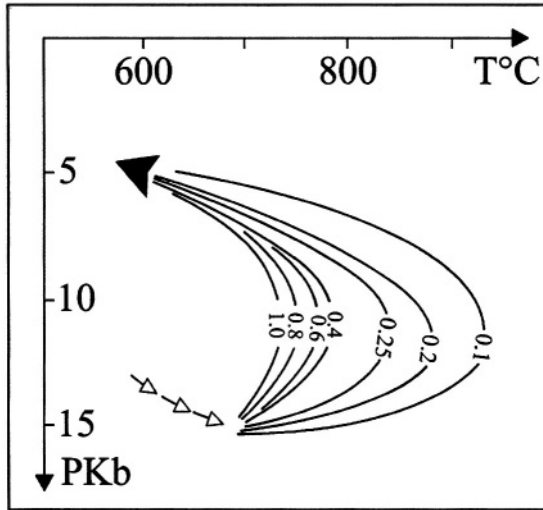


FIG. 72 — Form of the retrograde gradient and uplift rate of crustal units (after Mercier *et al.*, 1991).

The uplift rates are given in mm per year. The 0.25 to 0.4 mm per year curves limit, approximately, the conditions related to the effect of an isostatic re-equilibration only, following collision stages. Higher uplift rates imply the action of tectonic exhumation (Albarède, 1977). The curves were calculated for a constant heat production $A_0 = 0.5 \mu\text{W}/\text{m}^3$. White arrows : schematic prograde gradient.

5.9.1 Erosion and isostatic re-equilibration

The collision stages of orogenic evolution result in significant crustal thickening and the creation of elevated relief (*cf.* for example the Himalayan chain). Erosion of these high-relief areas is compensated by isostatic re-equilibration which results in uplift of the deep continental crust toward the surface. The rates of vertical uplift fall between 0.25 and 0.40 mm per year; the corresponding retrograde gradients are far from the prograde gradients in the P-T diagram, and pass through elevated temperatures (on the order of 800 °C; Fig. 72) located principally in the partial fusion domain of metapelites.

5.9.2 Tectonic exhumation

The stages of subduction and collision of orogens are characterized by significant decouplings and thrusting of tectonic units (*cf.* below). In this case the rate of vertical rise (deduced from the speed and inclination of the convergence) is generally high, on the order of cm per year. The retrograde gradients are therefore much less inflected toward high temperature than in the case of isostatic re-equilibration (Fig. 72), even if they too, break into the partial fusion domain.

Thus the characterization of the shape of the retrograde gradient in a metamorphic series brings significant insight into the orogenic stages (subduction, collision) to which they belong. Naturally the other factors likely to intervene in controlling the shape of this gradient must be taken into account; magmatic transfer into the post-collisional stage as well as the mechanical heat production at major tectonic contacts. Magmatic transfer toward the surface, from the upper mantle or the lower continental crust has the effect of

exaggerating the thermal loop toward high temperatures. Mechanical heat production may have a significant local effect (“pseudotachylites”) but its extent within the units remains limited by the effect of low thermal conductivity of natural rocks.

5.10 Prograde thermal evolution and burial

Apart from several particular cases of which examples will be given further on, the prograde gradients correspond almost exclusively to an increase in pressure conditions, in other words, burial of metamorphic units. The shape of the gradient in P-T space is largely controlled by the rate of vertical subsidence of the lithologic units.

$$v = V \sin \alpha$$

Where V is the rate of convergence and α the dip angle of the units. The more rapid the plunge, the higher the slope of the geothermal gradient in P-T space.

5.10.1 Subduction of oceanic crust: diversity of metamorphic facies

Subduction of the oceanic crust results in the rapid burial (several cm per year) of a several-kilometre-thick slab which follows the plunge of the oceanic lithosphere to depth. This results in the establishment of a low temperature prograde gradient related to a marked downwarp of the isotherms (*cf.* Fig. 6). However this gradient is not constant in all parts of the slab (Fig. 73a) for two reasons:

- 1) because of its thickness, the oceanic crust is subjected to more elevated pressures at its base than at its roof; the difference can exceed 2 kb;
- 2) the major shearing along the subduction plane situated on the roof of the oceanic crust, is the site of non-negligible mechanical heat production,

As a result of this situation, the distribution of metamorphic facies in subducted oceanic crust is not uniquely dependent on the subduction rate, but also to the position of the materials within the unit (Fig. 73b). Even though controversial, this idea should be taken into account when mapping and interpreting facies in these HP-LT domains.

5.10.2 Underthrusting of crustal units: plunge versus isostatic re-equilibration

At collision, the continental crust is involved in shortening. The crustal slices which result, develop separately on each side of the major shear zones.

- 1) upper thrust units which then undergo tectonic exhumation (Fig. 71),
- 2) lower units which are buried under the others (underthrusting).

Because of their low density ($\rho = 2.7$) with respect to oceanic crust ($\rho = 3.2$), the underthrust continental units do not follow the rapid subduction movement; their vertical downplunge is considerably lessened. Amongst other things, the superposition of two or more units creates an unstable “crustal thickening”. The evolution of this thick continental crust over time under the paired erosion-isostatic re-equilibration processes results in uplift toward the surface of the deep units, and the isotherm along with them.

This collision stage is therefore characterized by a complex thermal regime including a moderate downwarp of the isotherms in the underthrust units, counterbalanced by a generalized isostatic re-equilibration. The different stages of this evolution are illustrated in Figure 86.

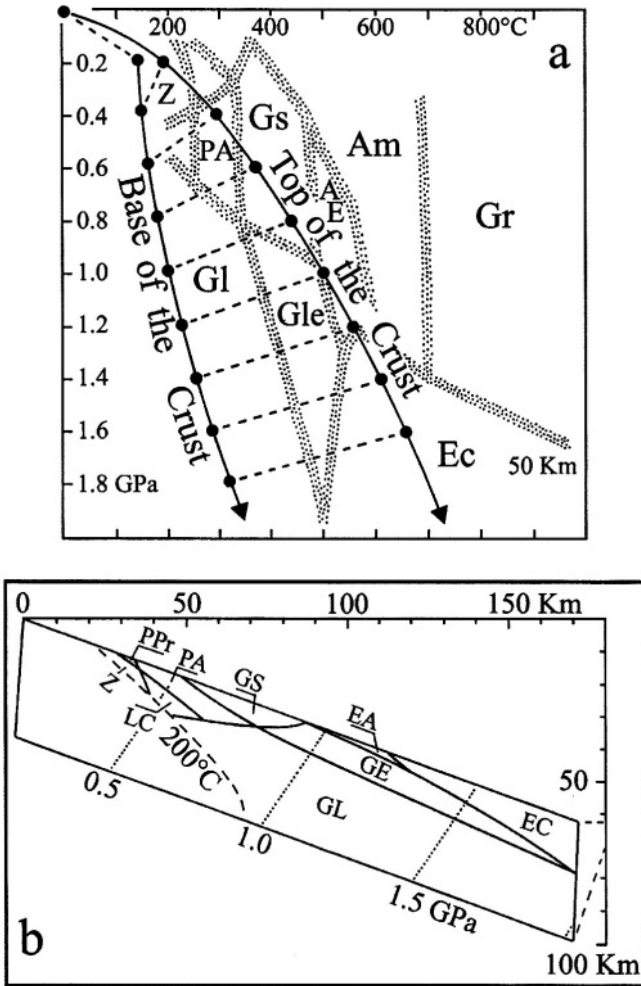


FIG. 73 — Prograde gradients and the diversity of metamorphic facies within subduction (after Peacock, 1993).

a) Prograde gradients and mechanical heat production: descending relatively cold oceanic lithosphere results in a downwarp of the isotherms (Figs. 6 and 71) and by establishing HP-LT gradients. The gradient corresponding to the top of the oceanic crust will, however, be significantly offset toward higher temperatures with respect to the prograde gradient at the base of the crust as a result of mechanical heat production associated with the shearing. Note that in this case an inverse gradient exists (dashed line) between the top and bottom of the oceanic crust. $Q_0 = 0.05 \text{ W/m}^2$; $\alpha = 20^\circ$; $\rho = 3000 \text{ kg/m}^3$; $K = 2.5 \text{ W/(m} \cdot \text{K)}$; $\kappa = 10^{-6} \text{ m}^2 \cdot \text{s}^{-1}$; $V = 10 \text{ cm per year}$; thickness of oceanic crust = 7 km; $\tau = 67 \text{ MPa}$. The production of radioactive heat is neglected.

b) Distribution of metamorphic facies in this segment of oceanic crust. The thickness of the oceanic crust is multiplied by five in the drawing in order to display the facies better.

Z: zeolite facies; PPr: prehnite-pumpellyite; PA: pumpellyite-actinolite; LC: lawsonite-chlorite; GL: glaucophane-lawsonite; GS: greenschist; GE: glaucophane-epidote; EA: epidote-amphibolite; EC: eclogite. Dotted lines: isobars in GPa.

5.11 Preferred sites for metamorphism

It may be deduced from the preceding discussion that metamorphism does not affect stable domains which are unperturbed thermally. The spatial distribution of isotherms at the lithospheric scale (Fig. 6) pinpoints sites characterized by anomalous gradients and/or intense tectonic deformation, one or other favourable for metamorphic recrystallization.

5.11.1 Extension domains

These show a closing up of the isotherms or a HT-LP gradient in other words. These characteristics are associated with lithospheric thinning, which results in a rise of high temperature convective mantle and the transfer of basic magma toward the surface.

5.11.2 Subduction zones

These correspond to deep downwarps in the isotherm pattern, related to the plunging lithosphere which is relatively cold. This downwarp results in the establishment of a HP-LT gradient in a context of intense penetrative deformation.

5.11.3 "Behind" subduction zones

These, like the extension domains, show a closing up of the isotherms and HT-LP gradients. This thermal regime is the result of two processes:

- 1) Lithospheric thinning behind subduction zones as a consequence of the dynamics of the convective mantle in this region (*cf.* Fig. 90);
- 2) Staged magmatic transfers: partial fusion of the hydrated upper mantle located over the subduction zone, and transfer of magma toward the base of the continental crust; partial fusion of the lower continental crust and transfer of granitoids toward the surface.

Specific cases of metamorphic development in these different sites are examined in the following pages, as well as examples corresponding to particular geodynamic situations.

HP-LT METAMORPHISM OR THE "FRANCISCAN" GRADIENT

The metamorphic series characterized by this type of gradient are mainly constituted of metabasites and are generally associated with present-day subduction zones, or fossil ones. This is the case of the Franciscan units of the type area in California which overlie the subduction zone along which the Pacific plate presently dips under the North American plate. This relationship between HP-LT metamorphism and subduction occurs as well in Japan (Sanbagawa belt) and New Caledonia (Ouega district) and in Cuba etc. In recent collision chains (Alps, Himalayas) or in older ones (the Hercynian and Caledonian chains) the HP-LT units represent former oceanic sutures between different continental domains. The units are often interpreted as the trace of old subduction zones; they are, however, sometimes related to *obduction* of oceanic floor on a continental margin during the early phases of collision.

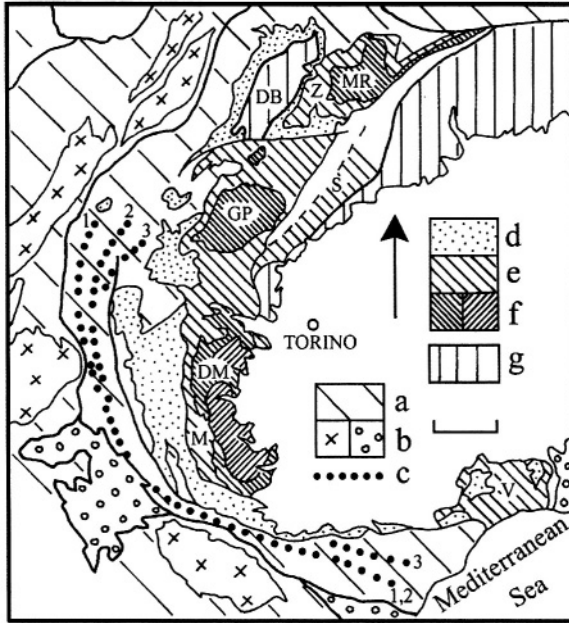
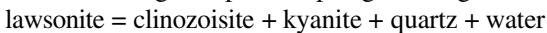
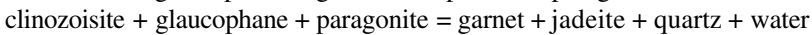
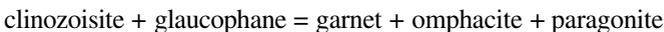


FIG. 74—*Distribution of metamorphic facies in the Western Alps* (after Deville *et al.*, 1992 and Goffé and Chopin, 1986).

a : European, Helvetic, Pennine and Briançonnais Alpine units; b : External crystalline massifs (crosses); and ultrabriançonnais nappes (circles); c₁ and c₂ : appearance of lawsonite and carpholite in Briançonnais metapelites; c₃ : disappearance of carpholite in these series; d : ophiolitic units recrystallized in the greenschist and glaucophane schist facies; e : ophiolitic and metapelitic units recrystallized in the eclogite facies (Z = Zermatt - Saas Fee unit; S = Sesia-Lanzo; M = Monviso; V = Voltri Group); f : Internal crystalline massifs recrystallized in the eclogite facies (MR = Mont Rose; GP = Gran Paradiso; DM = Dora Maira); hachured NE-SW : Extent of the coesite domain; g : Austro-Alpine units (DB = Dent Blanche nappe). Scale bar = 25 km.

5.12 Prograde HP-LT gradients and subduction: example of the Western Alps

It is generally difficult to characterize the prograde gradients in the HP-LT metamorphic series clearly; these series effectively underwent intense syn- to post-metamorphic deformation and they are cut up into numerous slices. Only some series still display a part of the prograde evolution. Thus, the Zermatt-Saas unit located below the Dent Blanche nappe, and the Tsate unit (Fig. 74) make it possible to examine the prograde evolution between 1.5 and 2.0 GPa and 500 and 600 °C (Fig 75). This evolution is characterized by the following succession of reactions observed in the metabasalts:



These reactions document the prograde passage from the glaucophane schist facies to the eclogite facies (*cf.* Fig. 31).

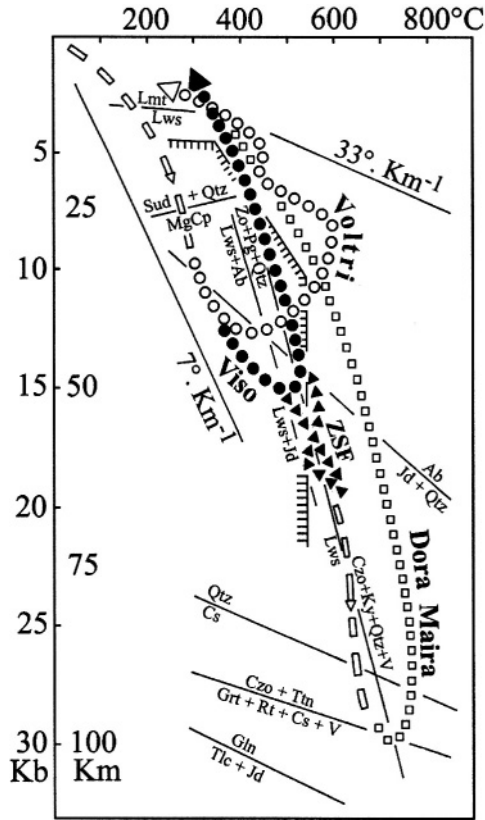


FIG. 75 — Prograde and retrograde metamorphic gradients in the Western Alps.

The shape of the prograde gradient (large dashes) is deduced from the geometry of the metamorphic units (Fig. 74, west to east succession prehnite-pumpellyite facies \Rightarrow glaucophane schist facies \Rightarrow eclogite facies). According to the units (ZSF = Zermatt - Saas Fee, black triangles; Monviso : black dots; Voltri Group : white circles) the prograde gradient culminates between 13 and 20 kb (35 to 60 km depth); the Dora Maira coesite-bearing units (white squares) are an exception, with peak pressures of 30 kb (close to 100 km depth). The retrograde gradients display trajectories very close to those of the prograde gradients; this suggests relatively rapid tectonic exhumation. The retrograde gradient of the Voltri Group describes a loop in the amphibolite facies and returns toward the glaucophane schist facies. This suggests a relatively slow exhumation which is probably polyphase. Lmt : laumontite; Lws : lawsonite; Sud : sudoite; Qtz : quartz; MgCp : Mg-carpholite; Ab : albite; Zo : zoisite; Pg : paragonite; Jd : jadeite; Cs : coesite; Czo : clinozoisite; Ky : kyanite; Grt : garnet; Rt : rutile; Tlc : talc; v : vapour; hachured line : stability limit of glaucophane. After the data of Barnicoat and Fry (1986), Lardeaux *et al.* (1987), Messina and Scambelluri (1991) and Chopin *et al.* (1991).

In a more general way the geographical distribution of the mineral facies in the internal Western Alps (between the external crystalline massifs and the Ivrea Zone, Fig. 74) give a simplified overall view of the succession of recrystallization in the metabasalt and metagabbro of the ophiolite series during Alpine metamorphism. It shows *grosso modo* an increase in metamorphic intensity from west to east along a HP-LT gradient characterized by the following succession of assemblages (Fig. 74):

prehnite + pumpellyite
 lawsonite + albite + chlorite + actinolite
 glaucophane + lawsonite \pm albite \pm omphacite + quartz
 omphacite + garnet + kyanite + quartz

This gradient, slightly concave toward high pressure at the start of the process (Fig. 75) in agreement with the numerical modeling, is interpreted as the result of rapid burial (several cm per year) along an east-dipping subduction zone (Fig. 76). The general form of this gradient is confirmed by the study of the metapelitic series associated with the metaophiolites. These show, in particular, the presence of a carpholite domain (Fig. 74) located between Briançonnais and the Piemont zone, which corresponds approximately to the transition between the lawsonite + actinolite and the glaucophane + lawsonite associations. The transition between glaucophane schist and eclogite facies occurs along a gradient which is not as steep (Fig. 75); this inflection foretells the retrograde process described later on.

The extreme conditions indicated by the Alpine metamorphic assemblages are on the order of 2 GPa and 600 °C in the metabasalts of the Zermatt-Saas zone; 1.5 GPa and 500 °C at Monviso located in the Piemont zone west of Dora Maira (Fig. 74). These conditions correspond to a burial between 50 and 70 km deep. Pressures on the order of 2.8 GPa (100 km depth and around 800 °C) were registered southeast of Dora Maira in special units which will be described later.

5.13 Retrograde gradients and exhumation of HP-LT units

5.13.1 Diversity of the retrograde evolution of HP-LT series

In a great number of cases the secondary parageneses which are more or less widely developed, are superimposed on high pressure prograde parageneses. They generally crystallized during heterogeneous deformation and left the earlier mineral association partly preserved. The deformation chronology makes it possible to develop a recrystallization chronology to control the temporal evolution of P-T conditions. All the observations show an important decrease in pressure conditions or an uplift of units toward the surface. This decompression results from their exhumation from a depth of 50 to 70 km where the HP-LT assemblages were acquired. This retrograde P-T-t trajectory has various forms depending on the various exhumation processes. The example of the Monviso metabasites, and those of the Voltri massif (Ligurian zone) are shown below (Fig. 75).

Monviso. The finite strain study shows three phases posterior to the development of the high pressure prograde parageneses (Fig. 77). This succession is characterized by four types of mineral assemblage, which differ in nature or in the composition of phases in equilibrium. The P-T conditions corresponding to these assemblages are shown in Figure 75. The retrograde gradient traced by this evolution corresponds to temperatures significantly higher than those of the prograde development, but still remain very low with respect to the pressure.

Voltri Group. As at Monviso, a heterogeneous deformation succession accompanied by recrystallization made it possible to trace the retrograde evolution of the iron-rich eclogitic metagabbros. This evolution passes through amphibolite facies conditions (600 °C, 0.8

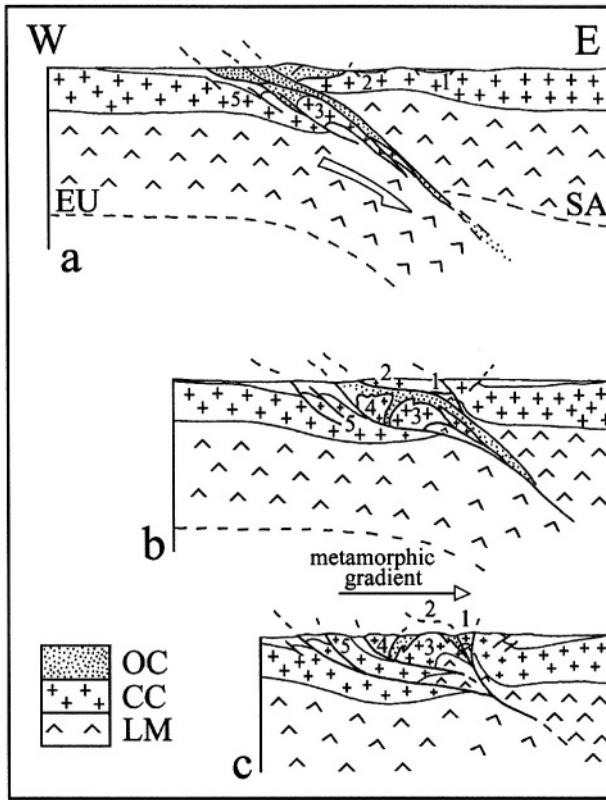


FIG. 76 — *Place of metamorphism in the Western Alpine Orogen* (after Malavielle *et al.* 1984).

Polyphase metamorphism is developed from the External Crystalline Massifs (5) up to the Sesia Zone (1); the prograde gradient (arrow *cf.* Fig. 74) of Upper Cretaceous age is directed from west to east. This metamorphism affects the Sesia crustal units and the base of the Dent Blanche nappe (2) in a heterogeneous manner, and it affects the crustal units of the Internal Crystalline Massifs profoundly (3) and the Briançonnais (4), as well as units derived from oceanic crust (OC : ophiolites and lustrous schists). This distribution agrees with subduction of the European Plate (EU) beneath the South Alpine (or 'Austro-Alpine' SA) Plate. The retrograde gradients of Eocene age affect all the units and correspond to exhumation mechanisms which operated during the collision stage. a) Closure of the Alpine ocean in the Upper Cretaceous; the European Margin underwent deep burial whose effects are seen in the coesite-bearing units of the Dora Maira Massif. b) Collision between the European and South Alpine lithospheres (Eocene-Oligocene). c) Present-day structure of the Alps. CC : continental crust; LM : upper lithospheric mantle.

GPa) and returns to the greenschist facies after a brief incursion into the glaucophane schist field (Fig.75). This incursion is partly because of the composition of the protolith, the stability field of Fe-glaucophane is extended toward high temperature with respect to that of Mg-glaucophane, but it has a probable geodynamic significance which will be discussed in the following paragraphs. The retrograde evolution of the Voltri Group metagabbros therefore differs significantly from that of the Viso eclogites, by a sharply marked loop

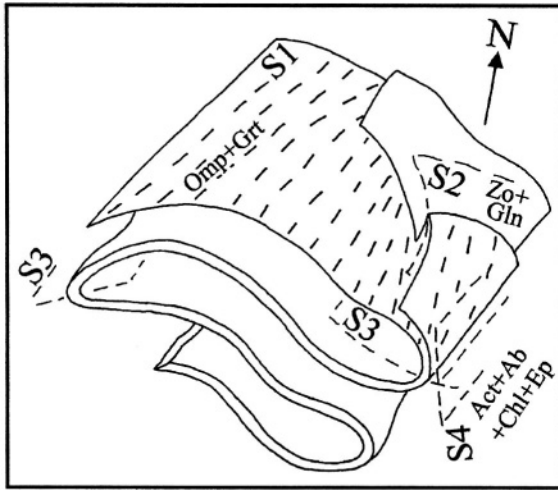


FIG. 77 — Schematic relations between deformation and recrystallization in the meta-ophiolite formations of the Lago Superiore at Monviso (after Lardeaux *et al.*, 1987).

Omp : omphacite; Grt : garnet; Zo : zoisite; Gln : glaucophane; Act : actinolite; Ab : albite; Chl: chlorite; Ep : epidote. S_1 to S_4 : succession of surfaces contemporaneous with the four established mineral assemblages. The assemblages contemporaneous with S_3 and S_4 are mineralogically identical (Act + Ab + Chl + Ep), but the actinolite related to S_3 is richer in Na than that related to S_4 , which indicates higher crystallization pressures.

toward relatively high temperatures.

5.13.2 Retrograde evolution and tectonic exhumation

The retrograde gradients observed in the HP-LT unit at Viso and the Voltri Group record an uplift of rocks toward the surface as well as a positive thermal re-equilibration with respect to the LT conditions of subduction. The tight trajectory (close to the inverse of the prograde gradient) at Monviso denotes a very rapid exhumation after establishment of the HP assemblages in an environment of low heat production (oceanic crust). In the Voltri Group the retrograde gradient crossed relatively high temperature domains which suggests a relatively slow uplift to the surface, allowing partial thermal equilibration under the effect of regional heat flow. In neither case a model of exhumation linked to erosion-isostatic re-equilibration processes could have provided a decompression rapid enough (several tens of mm per year, *cf.* Fig 72) to account for the shape of the retrograde gradients. The exhumation of these HP-LT units is certainly linked in large part to shortening tectonics which allow uplift rates of the same order of magnitude as the convergence: several mm to several cm per year. Several dynamic models are compatible with the shape of the retrograde gradient (Fig 76). In the particular case of the Voltri Group, the inflection of the retrograde gradient toward the lower temperature part of the glaucophane schist facies is also interpreted as a result of thrusting of this unit, upon a colder unit experiencing subduction.

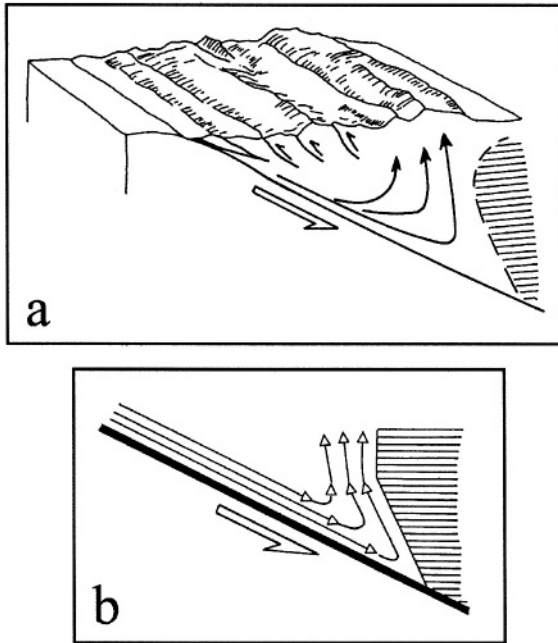


FIG. 78— *Model of tectonic exhumation of Franciscan units by flow along the lithospheric front* (After Cowan and Silling, 1978).

a) Diagram of an accretionary prism and its dynamic behaviour in contact with a wedge of rigid lithosphere. The trajectories of the different units, shown by the three arrows, are covered in the same time period; the exhumation of the unit farthest inside is more rapid than that of the external ones.

b) Analogue model of the process based on scale model experiments (length of model, one metre) : the white triangles show the position of particles on three separate flow lines at the same times t_1 , t_2 and t_3 , the burial and exhumation rate is greater when the unit is deeper. This model may be applied to the sediments of the accretionary prism, and to a variable thickness of part of the oceanic crust undergoing subduction.

5.14 HP-LT metamorphism and obduction

The ophiolitic Oman nappe in the Muscat region gives a particularly interesting example of this process (Fig. 79). This mechanism is characterized by a P-T evolution of the prograde and retrograde gradient opposite to that seen in the case of subduction. The earliest parageneses developed under conditions of a high temperature-low pressure gradient and evolved with time toward high pressure-low temperature assemblages. The decompression which accompanied the exhumation of the units took place under low temperature conditions (Fig. 80). This behaviour is related to the obduction of a segment of young oceanic lithosphere, which was thin, and at high temperature (about 1000 °C) onto the oceanic crust and then onto the Arabian continental margin at the start of the Upper Cretaceous (Fig. 81). The units located immediately under the thrust were brought to high temperatures at low pressures (several km of load) at the start of the process. The continuing shortening resulted in successive thrusts, piling up of units and collapse of the margin. The weight,

and in consequence the pressure, increased significantly, whereas the heat transported by the thrust was dissipated progressively by conduction and the temperature decreased as a result, whereas the pressure rose. The exhumation of metamorphic units, linked partly to the terminal phase of tangential tectonics and partly to the isostatic re-equilibration of the Arabian lithosphere during the erosion of the upper units of the chain, was therefore produced in a low temperature milieu.

This model was applied in the Briançonnais zone of the Alps, as well as certain portions of the Hercynian chain (Île de Groix), where it is, however, much more difficult to characterize.

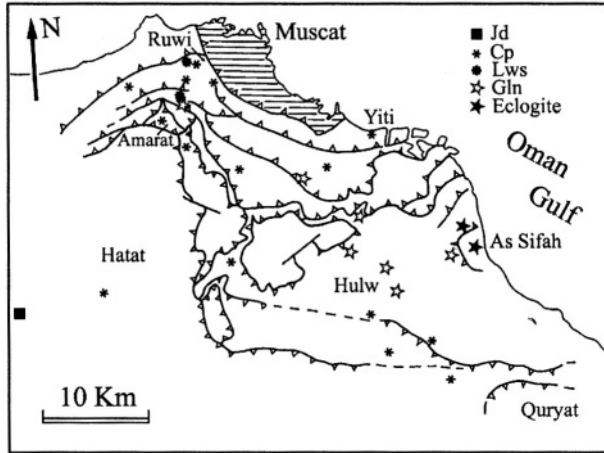


FIG. 79—*Mapping of imbricate tectonic units under the Muscat (Oman) ophiolitic nappe; simplified (after Goffé et al. 1988).*

A schematic cross section of this metapelitic and metabasaltic assemblage is given in Figure 81. Jd : jadeite; Cp : carpholite; Lws : lawsonite; Gl n : glaucophane; eclogite = omphacite + garnet. Hachured : Muscat ophiolitic nappe.

INTERMEDIATE PRESSURE METAMORPHISM: THE “DALRADIAN” GRADIENT

The metamorphic series exemplified by this type of gradient are associated with the collision phase of orogens. They are principally composed of metapelites and metagreywackes, although they may contain appreciable amounts of meta-igneous rocks, some metabasalts and metagabbros but mostly metagranitoids.

The Bas-Limousin metamorphic series (Fig. 64) is a good example of this type of gradient, in spite of the geological complexity of the region (Fig. 30). It is characterized particularly by the kyanite-staurolite association and by the prograde transition kyanite \Rightarrow sillimanite. The metabasalt assemblages in equilibrium with these conditions are those of the amphibolite facies: plagioclase + hornblende \pm garnet \pm clinopyroxene. The shape of the gradient, as deciphered from observations, is very close to that of an equilibrium conductive gradient. On this basis it is sometimes considered the “normal” gradient characterizing stable zones. This simplistic view is contrary to the dynamic character of the recrystallization, which is associated with major deformation.

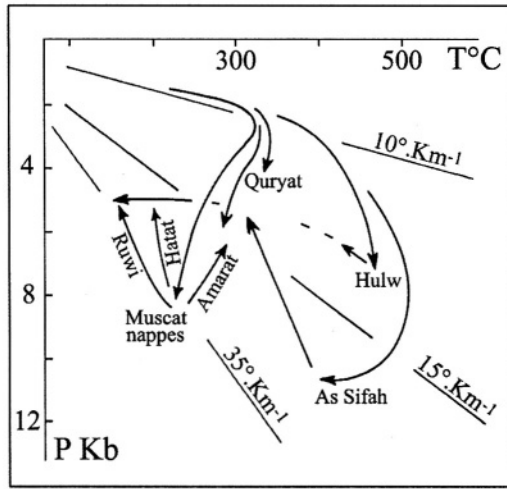


FIG. 80 — Prograde and retrograde evolution of continental units (metapelitic and metabasaltic) located below the Muscat (Oman) ophiolitic nappe; simplified (after Goffé et al. 1988).

The general form of the P-T-t evolution describes a loop which is inverse to that observed in the case of subduction: the earliest recrystallization is produced under a HT-LP gradient resulting from the thrusting of high temperature oceanic lithosphere; the progressive evolution of the gradient toward LT-HP conditions results from heat dissipation by conduction and the increase in the load.

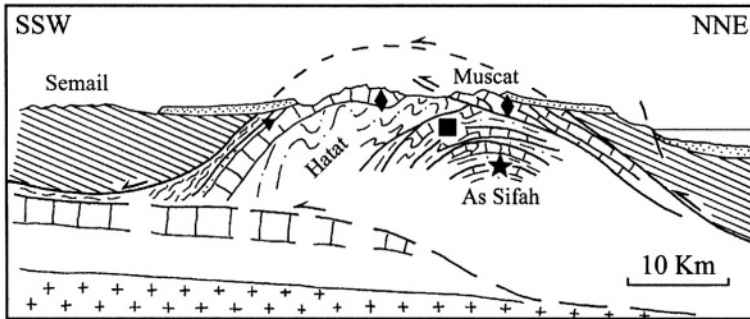


FIG. 81 — Schematic cross section of the continental units located under the Oman ophiolitic nappes (hachured, the Muscat nappe to the right the Semail to the left) (after Goffé et al. 1988).

The arrows indicate the thrust direction. Black triangle : very low grade metamorphic assemblages (kaolinite-chlorite); black diamonds : low grade assemblages (carpholite); black square: medium grade assemblages (chloritoid-chlorite); black star : low temperature eclogite; stipple pattern : Tertiary transgressive terrains; their position indicates that the uplift that affects the continental units is largely post-nappe, therefore post-metamorphic.

5.15 The prograde Dalradian gradient: burial slowdown

The Dalradian units are found in collision zones and are generally spatially associated with high pressure units (Fig. 67). They are recrystallized from former continental margin rocks. The shape change between the prograde Franciscan HP-LT and the Dalradian gradients results from the introduction of an increasing thickness of light density material ($\rho = 2.7$) from the continental wedge into the subduction zone (Fig. 82). Although the continental material comprises a small amount compared to the oceanic crust ($\rho > 3.0$) it may follow the oceanic lithosphere to great depth; up to 100 km in slices of the SE Dora Maira massif, which are characterized by pyrope + coesite parageneses (*cf.* below). The increasing thickness of the wedge dragged into subduction induces a slowing down, then a blockage of the burial process of the continental units. The downwarp of the isotherms, so pronounced in oceanic crust, under rapid subduction, is reduced here, accounting for the decrease in slope of the thermal gradient.

5.16 Underthrusting of continental units: migmatization and retrograde gradients

The slowdown and blocking of the crustal units of the continental wedge is not part of a general slowdown or blockage of the whole lithosphere, as the subduction engine is located in the convective upper mantle. The subcontinental lithosphere continues on its way to depth, whereas the crustal units are decoupled and pile up on one another (Fig. 82). This mechanism leads to crustal thickening typical of the collision stage. This pile-up of crustal nappes is the site of significant heat production (in contrast with that produced by the pile-up of oceanic units poor in radioactive elements).

From another point of view, two elements assist the uplift of these metamorphic units to the surface:

- 1) their displacement along abnormal inverse contacts developed by the collision;
- 2) the erosion of surface relief which results in isostatic re-equilibration (Figs. 71, 86).

It results in the following process:

- 1) a temperature increase resulting in partial fusion of metapelites and metagreywackes and the formation of migmatitic units;
- 2) a decompression resulting in the development of garnet + cordierite; cordierite + sillimanite; and cordierite + andalusite parageneses characterizing the evolution of P-T conditions along a retrograde gradient (Fig. 83).

5.17 Retrograde evolution of eclogitic metabasites: the initial HP-LT gradient

It was earlier noted that under high-grade conditions, metabasalts of the Dalradian series display hornblende + plagioclase (\pm clinopyroxene \pm garnet) assemblages in equilibrium with the parageneses of the associated metapelites. In a large number of localities, however, the metabasites still contain early assemblages belonging to the high pressure granulite or eclogite facies (Fig. 83):

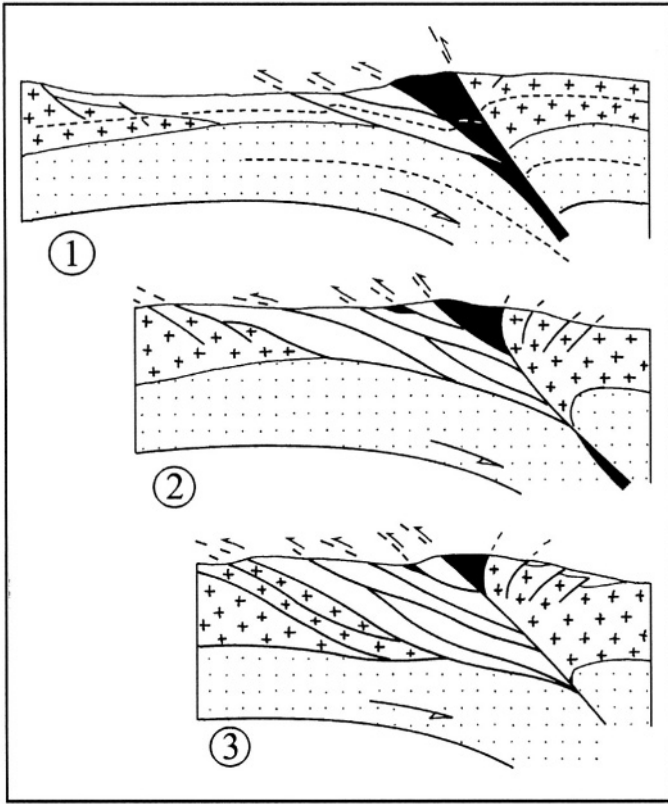


FIG 82 — Schematic diagram of the development of a prograde intermediate pressure gradient (Dalradian).

1) The continental wedge enters the subduction zone after the continental crust (black); less dense, it resists burial, decouples from the lithospheric upper mantle and is sliced and thrust upon the external zones. 2) The lithospheric mantle continues to subduct, and slices of the continental wedge pile up on one another (underthrusting). 3) Blocking of the burial starts thermal re-equilibration of the crustal slices under the effect of regional heat flow and radioactive heat. The highest units of the structure undergo the earliest burial and a principally tectonic exhumation which produces retrograde reactions. The dashed line represent the shape of the isotherms: note the weak downward of the isotherms in the continental wedge.

clinopyroxene + garnet + plagioclase + quartz
 omphacite + garnet ± kyanite ± quartz

These high pressure parageneses (up to 1.5 GPa 700-750 °C) are preserved in blocks dispersed by boudinage in the enclosing metapelites which are chiefly recrystallized under amphibolite facies conditions. This metastable preservation of high pressure assemblages in the metabasites indicates that the whole assemblage - metapelite included - were initially recrystallized under HP conditions. The diversity of the retrograde behaviour is caused by the heterogeneity of the post-eclogite deformation, the plastic metapelites were subject to penetrative deformation and totally recrystallized (or nearly totally, a few HP relics occur in certain rocks) under low pressure conditions. The much more rigid eclogitic metabasalts,

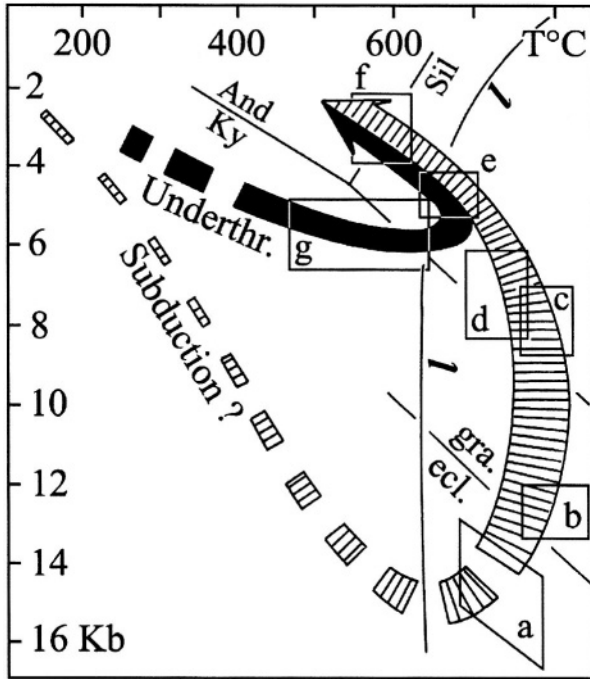


FIG. 83 — Prograde and retrograde evolution in Dalradian units from the French Massif Central.

Black arrow : P-T-t evolution at intermediate pressure, of "prograde" parautochthonous units : kyanite-sillimanite transition (g); partial fusion of metapelites (e); decompression (uplift towards surface) and cooling of units (f). Hatched arrow : P-T-t evolution of eclogitic and granulitic relics of the retrograde allochthonous units; intermittent path : supposed prograde evolution; peak of metamorphism in high temperature eclogite facies (a); retrograde evolution under high pressure granulite facies conditions (b) then intermediate pressure (c) and (d), and finally amphibolite facies (e) and (f); during this last stage the allochthonous retrograde units, at relatively high temperature, were thrust onto the colder prograde parautochthonous units; partial fusion of metapelite (migmatization) can take place at all stages between (a) and (e) if the P_{120} conditions remain high. underthr. : underthrusting of parautochthonous prograde units; ecl : eclogites; gra : granulites. l : partial melting of metapelites. Data of Burg *et al.* (1989) and Mercier *et al.* (1991).

weakly or undeformed in the core of the outcrops, only underwent inefficient isotropic recrystallization (no dislocation energy to minimize); this recrystallization left partly coronitic HP relics (*cf.* Fig 65) sometimes dispersed in a symplectic matrix. Nevertheless, a few petrologists believe that coexisting eclogites and amphibolite facies rocks indicate that local tectonic overpressures may play a role in metamorphic recrystallization.

5.18 Retrograde and prograde units

The study of Dalradian units at the scale of the Hercynian chain of the French Massif Central (Fig. 84) shows that these are in reality, two contrasting types:

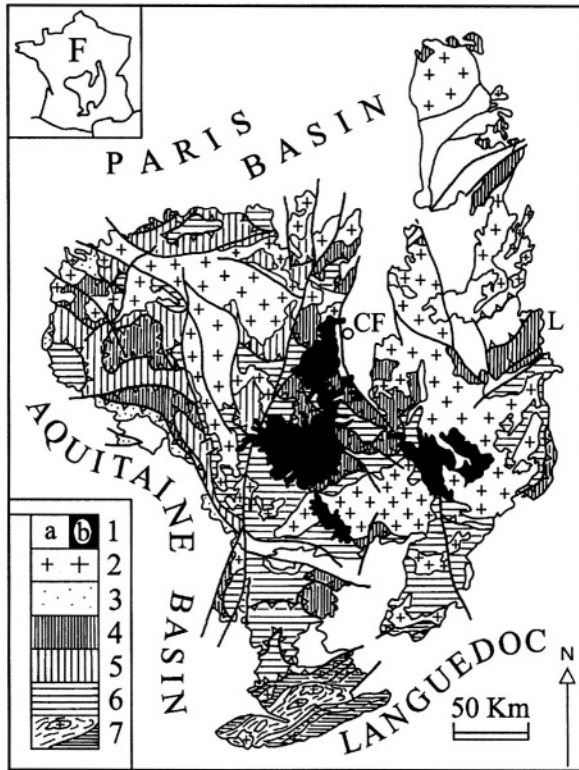


FIG 84 — Distribution of Variscan metamorphic units in the French Massif Central (after Matte, 1986; Ledru *et al.*, 1989 and Costa, 1992).

1a : post Visean sedimentary basins; 1b : Neogene and Quaternary volcanism; 2 : Variscan granitoids; 3 : low grade metamorphic allochthonous units; 4 : upper (allochthonous) metamorphic units including eclogite units (retrograde units); 5 : intermediate prograde parautochthonous metamorphic units (in the western Massif Central) with dispersed relic ophiolitic units; 6 : lower allochthonous and parautochthonous metamorphic units (prograde units); 7 : Montagne Noire migmatitic core complex and associated HT-LP units. F : France; CF : Clermont Ferrand; L : Lyon.

- 1) certain among these effectively contain relics of high pressure assemblages witnessing an initial recrystallization under subduction conditions;
- 2) other units do not display these characteristics, but show a typical prograde Dalradian gradient.

These two types of units, respectively *retrograde* and *prograde* do not occur in the same structural situation in the edifice, the first are largely thrust over the second type. This structural arrangement well illustrates the mechanism of underthrusting described above (Fig. 71): the retrograde units containing elements of oceanic crust or protocrust were first buried by subduction, or under conditions close to those of subduction; the gravity blocking of these units at depth was followed by the underthrusting at low speed, of the prograde units: Finally the polyphase retrograde units were exhumed and largely thrust over the prograde units (Figs. 83, 84, 85).

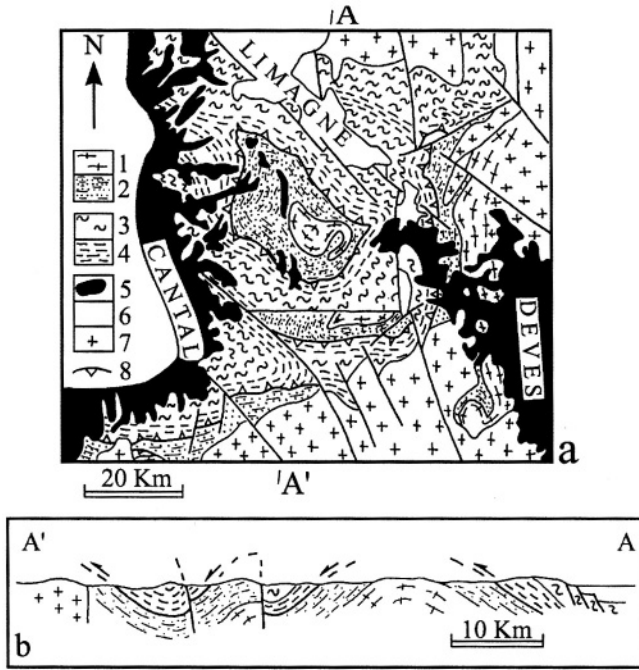


FIG. 85 — *Geometric relations between the allochthonous (retrograde) unit and the parautochthonous or autochthonous (prograde) unit south of Brioude in the French Massif Central (after Burg and Matte, 1978).*

Allochthonous unit (3 : migmatites; 4 : "leptyno-amphibolitic" series) largely thrust over the underlying unit (1 : orthogneiss; 2 : sillimanite metapelites) with a displacement greater than 50 km. 5 : Neogene and Quaternary volcanic rocks; 6 : Oligocene sedimentary basins; 7 : Variscan granitoids; 8 : thrust.

5.19 Underthrusting and inverse metamorphism

The underthrusting mechanism, as it was presented above and in Figure 71, results in the superposition of retrograde units on prograde ones. At the time of thrusting the retrograde units were at higher temperatures than the prograde units undergoing burial immediately below them. The retrograde units thus played the role of a pressing iron over the prograde units. Numerical modeling of the isotherms, taking into consideration both the effect of thrusting, the isostatic-erosion re-equilibration processes and radioactive heat production shows the size of the offset in temperature between the overthrust and underthrust units (Fig. 86). The model shows that an inverse metamorphic gradient will be established in the lower units near the abnormal contact.

This type of inverse gradient is observed in the Himalayan chain where it has been studied in detail (Fig. 87). It was also exposed in various sections of the Hercynian chain in the French Massif Central, linked to the major abnormal contacts which separate prograde and retrograde units in these "inverse metamorphic series". In the Lot Valley, for example, the metapelites at the top of the prograde unit contain relatively high grade sillimanite +

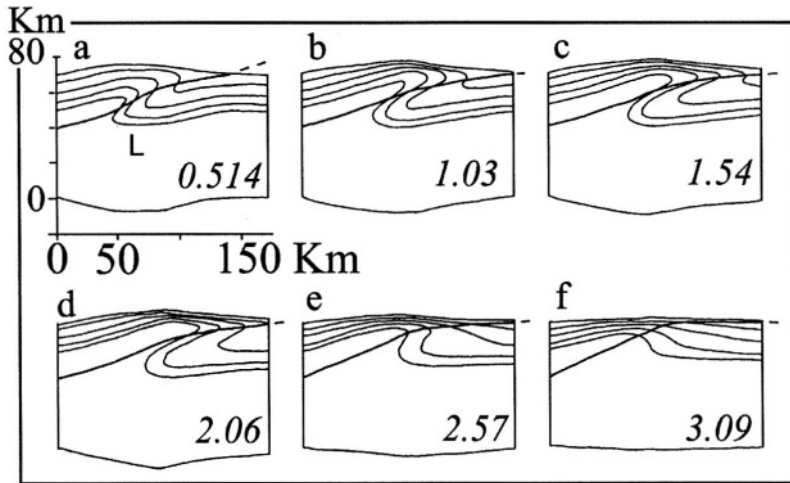


FIG. 86 — Deformation of isotherms in the continental crust under the joint effects of a thrust and isostatic re-equilibration. Numerical model (after Germann and Neugebauer, 1990). The model takes into account the entire lithosphere with a 30 km thick continental crust. The isotherms (lines) correspond approximately to 200, 350, 500 and 600 °C. Depths are designated from the compensation zone (0 km). L = lithospheric upper mantle. Stages a to d correlate with the effective activity of the thrust ($V : 10\text{cm/year}$; $\alpha : 20^\circ$); in e and f, only isostatic re-equilibration is occurring. The age of each stage is given in Ma. The inverse gradient, most apparent during thrusting (exaggerated by the high value of V chosen for the model) is re-sorbed at the end of the shortening.

almandine assemblages, whereas the assemblages located deeper in the edifice correlate to lower temperatures (staurolite + sillimanite and then staurolite + kyanite). Based on structural considerations, this relative placement is not considered to be the result of a structural reversal of the series, but as a manifestation of an inverse metamorphic gradient such as defined above.

LOW PRESSURE METAMORPHISM OR THE “ABUKUMA” GRADIENT

This type of gradient was defined by Miyashiro in the Abukuma and Ryoke belts of Japan. It is characterized by relatively high temperatures for relatively low pressure, and, significantly, by the andalusite \Rightarrow sillimanite transition in metapelites. This gradient, therefore, corresponds to a geologic domain where the heat flow is high (Fig. 6).

- 1) island arcs and back-arcs, sites of significant magmatic transfer from the upper mantle,
- 2) belts in collision stages, characterized by crustal overthrusting, strong radioactive heat production and slow uplift by isostatic-erosion re-equilibration, and
- 3) extensional zones: mid-ocean ridges and rifts.

Each of these domains have these particular characteristics, which are examined below.

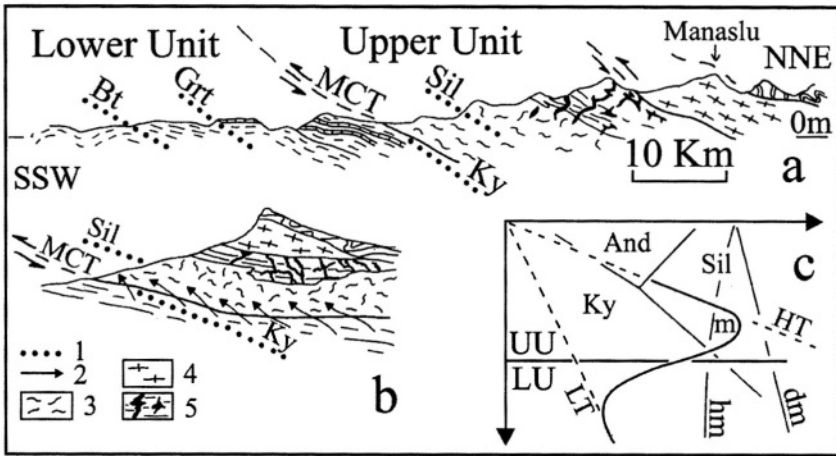


FIG. 87 — Inverse metamorphic gradient in the Himalayan Chain.

a) General cross section (after Le Fort, 1986). The lower unit ("Midlands" = LU) dips beneath the upper unit ("Tibetan Slab" = UU). The thrust zone (MCT throughout = "main central thrust") is characterized by an inverse metamorphic gradient interpreted by the distribution of the isograds (1; Bt = biotite; Grt = garnet; Ky = kyanite; Sil = sillimanite). The base of the Tibetan Slab is migmatitic (3); veins (5) from this zone fed the Manaslu Granite (4).

b) Interpretation of the relation between MCT and migmatization of the "Tibetan Slab" (Le Fort *et al.*, 1987). The prograde metamorphism of "Midlands" liberated a water-rich fluid which percolated into the formations at the base of the "Tibetan Slab" (2), inducing partial fusion at relatively low temperature (*cf.* Fig. 88).

c) The inverse gradient in a P-T diagram. The upper unit, brought up tectonically from the deeper zones of a thickened continental crust brought a significant quantity of heat (HT gradient); it thrusts over the colder lower part of the surface units (LT gradient); the base of the UU is cooled at the contact whereas the LU is heated by conduction (*cf.* Fig. 71c); the inverse gradient corresponds to the transition between the HT and LT gradients. The frictional heat production τV is not taken into account in this model. The UU follows a loop in the domain of partial fusion for hydrated metapelites and metagreywackes (m). dm and hm : dry and hydrous melting

5.20 Behind subduction zones and paired metamorphic belts

The classic example of this is the Ryoke-Abukuma belt in Japan (Fig. 89). In the Ryoke belt three principal zones of metamorphism were defined from the assemblages in metapelites:

- 1) chlorite + biotite + muscovite zone
- 2) biotite + andalusite zone
- 3) sillimanite zone

The absence of staurolite, the presence of cordierite and the coexistence of andalusite and microcline (indicating the start of the reaction of the muscovite + quartz association taking place in the andalusite stability field) in zone (2) corresponds to very low crystallization pressures ($P < 0.3$ GPa) comparable to those for assemblages in contact metamorphic aureoles. No migmatites are described from these metapelites, however the belt is intruded by significant granitoid masses resulting from fusion of the continental crust in deeper zones. The Abukuma belt itself has similar characteristics.

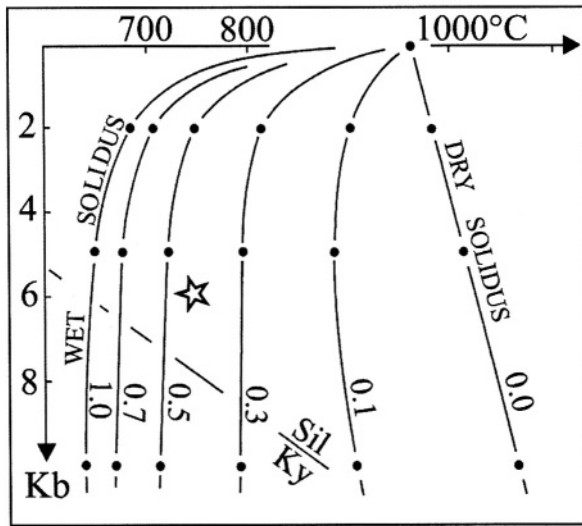


FIG. 88 — Influence of P_{H_2O} on the granite fusion curve (after Ebadi and Johannes, 1991). The curves, graduated in X_{H_2O} , are constructed from experimental data at 2, 5 and 10 kb (black points). The “hydrated” solidus corresponds to $P_{H_2O} = P_{total}$; the “dry” solidus to the absence of water in the fluid phase. A granitic or metapelitic (star) composition, initially located in the solid field for a low water pressure (for example $X_{H_2O} < 0.5$) melts under the same P-T conditions by a sharp increase of the molar fraction X_{H_2O} in the fluid phase. Sil = sillimanite; ky = kyanite.

5.20.1 Subduction and high temperature

The close structural association between the low pressure metamorphic belt (Ryoke-Abukuma) and the high pressure chain (Sanbagawa; Fig 89) located to the south toward the Pacific Ocean margin led Miyashiro to the concept of paired belts related directly to subduction. The Sangabawa belt, which comprises assemblages of prehnite-pumpellyite, glaucophane and jadeite-lawsonite, corresponds, therefore, to the subduction belt, whose assemblages later evolved under epidote-amphibolite facies conditions. It represents elements of the Pacific oceanic crust and accretionary prism, accreted to the Japanese microcontinent, metamorphosed (in the Jurassic or Lower Cretaceous) along a Franciscan gradient and later exhumed by mechanisms discussed previously.

The subduction of oceanic lithosphere corresponding to the formation of the Sangabawa Chain drags down hydrated materials (serpentines particularly) which liberate significant quantities of water in recrystallizing at depth. The infiltration of this water-rich phase into the peridotites of the upper mantle wedge, located above the subduction zone, provokes partial fusion (Fig. 90). Basaltic magmas (ancestors of the andesitic series) were thus produced and migrate to the surface. A convective heat transfer results from this magmatic transfer causing a coalescing of the isotherms behind the subduction zone. The heat transfer to the surface may be caused by successive relays, pooling of mantle-derived basaltic magma at the base of the continental crust (underplating or infracrustal storage) provokes partial fusion of metapelites, metagreywackes and metagranitoids. Then the rise of granitic liquids to upper crustal levels generates the high temperature gradients of the Ryoke and Abukuma belts (Fig. 90).

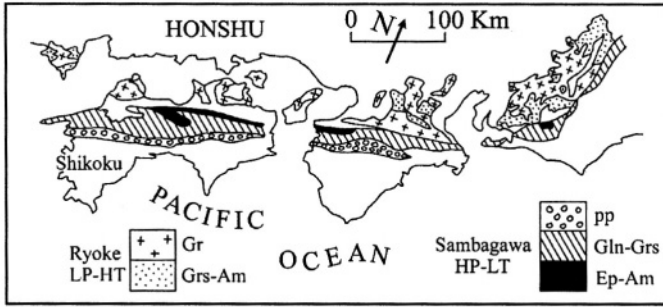


FIG 89— *Example of paired metamorphic belts in the Japanese Archipelago* (after Miyashiro, 1973).

Geometric relations between Franciscan metamorphic units (HP-LT Sambagawa Belt) and the HT-LP Ryoke-Abukuma Belt. gr : granitoids; Grs : greenschist facies; Am : amphibolite facies; pp : prehnite-pumpellyite facies; Gln : glaucophane schist facies; Ep-Am : epidote amphibolite facies. The Sambagawa Belt corresponds to a segment of the accretionary prism and the oceanic crust of the Pacific Ocean which was thrust under the Japanese microcontinent in the Cretaceous. The Ryoke-Abukuma Belt correspond to a strong thermal anomaly of the same age, located behind the subduction zone that operated at that period.

5.20.2 A problem of chronology

The above interpretation of the low pressure-high temperature gradients was very popular, and gave rise to the description of a large number of paired systems around the world, particularly in the Circum-Pacific domain. Most of these systems have since been given different interpretations as a result of precise absolute age dating which show that the high and low pressure paired belts are not the same age and cannot possibly result from the same period of subduction. The contrasting metamorphic series which crop out in the region of Vannes and Île de Groix (Morbihan) were also considered a good example of the double metamorphic belt of the Circum-Pacific type of Eohercynian age (420-375 Ma). The HP-LT belt is represented in the model by glaucophane, garnet, jadeitic pyroxene and locally lawsonite schists on Île de Groix and constitute a more-or-less continuous assemblage extending for 100 km to outcrops of the same type in the Bois de Cené in Vendée (Fig. 91). The LP-HT belt is represented by gneiss and migmatite located to the north (Cornouailles anticline). Actually the gneiss contains primary assemblages of relatively high pressure (kyanite + garnet + K feldspar + biotite + quartz) which evolved with time to LP-HT assemblages (sillimanite + cordierite + K feldspar + biotite + quartz). The migmatization is contemporaneous with this evolution to low pressure which resembles more the retrograde behaviour of the Dalradian series than the evolution of the Ryoke-Abukuma series. This model of paired belts in Mid-Brittany is no longer considered pertinent. In a general way the model does not appear clear for any point in the world, with the possible exception of Japan.

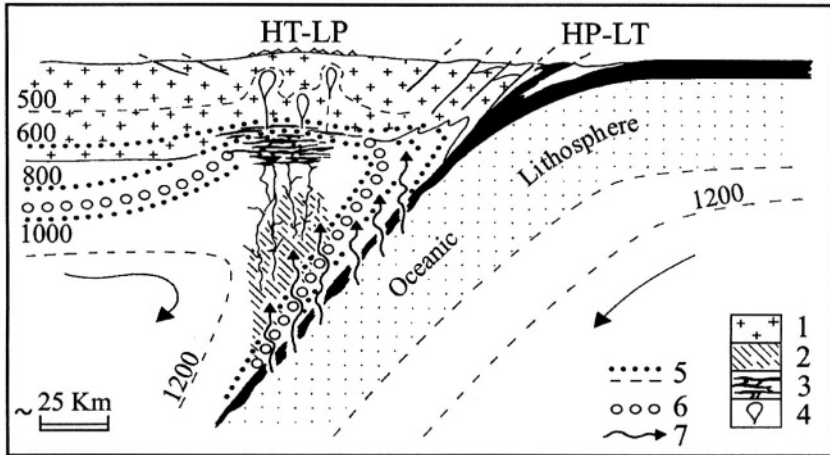


FIG. 90 — Formation mechanism for paired metamorphic belts in relation to subduction.

The descent of oceanic lithosphere along a subduction zone results in HP-LT metamorphism of the accretionary prism and oceanic crust. Part of the oceanic crust, together with the serpentinized upper lithospheric mantle is recrystallized at depth (50 to 120 km) freeing water. This then percolates through the subcontinental upper mantle provoking hydrated partial fusion. Basaltic liquids propagate upward to the base of the continental crust inducing a rise in the isotherms and HT-LP metamorphism in the crustal units, whose eventual fusion is the source of granitoids which propagate the thermal anomaly toward the surface. HP-LT : Franciscan gradient; HT-LP: Abukuma gradient; 1 : continental crust; 2 : region of extraction of basaltic magmas in the subcontinental mantle; 3 : accumulation of basaltic magmas at the base of the continental crust (underplating); 4 : granitoid diapirs; 5 : isotherms; 6 : solidus of hydrated peridotites; 7 : water infiltration from the oceanic lithosphere. Model after Tarney (1991).

5.21 Collision, crustal thickening and metamorphic core complexes

5.21.1 The Hercynian Chain of Western Europe

HT-LP gradients appear more commonly associated to late phases of orogeny than to subduction. This is notably the case in the Western European Hercynian Chain whose youngest metamorphic series are characterized by Abukuma-type gradients. Their chronological and structural position does not allow them to be interpreted from a behind-subduction model described above. These HT-LP gradients in fact develop much later in the orogenic evolution (around 320-300 Ma) during the period corresponding to the final stages of collision (Fig. 82).

5.21.2 Retrograde migmatitic domes and prograde metapelites:

Example of the Agly and Montagne Noire Massifs

Two Hercynian Massifs, among others, carry a certain amount of information useful for the comprehension of HT-LP gradients. These are the Agly Massif in the Eastern Pyrenees (Fig. 93) and the Montagne Noire in the South of the Massif Central (Fig. 92). In these two cases an orthogneissic *migmatitic core* is enveloped in a more-or-less continuous formation of allochthonous metapelitic rocks of probable Lower Paleozoic age. The metapelitic units display an increasing metamorphic grade in proximity to the metamorphic core complex. The isograds of this prograde gradient are arranged in a concentric fashion around

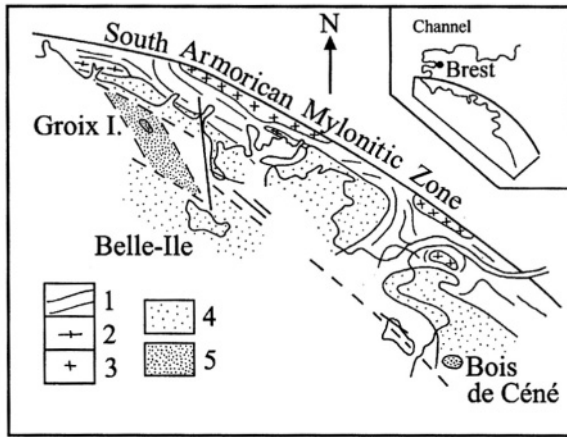


FIG. 91 — *Variscan paired belts in the Armorican Massif?*

This idea (Peucat et al., 1978), now generally abandoned, was based on the structural relations between:

- a) LP-HT units of the “Cornouailles anticline” on the one hand (1 : gneiss and migmatite; 2: orthogneiss; 3 : granitoids)
- b) HP-LT units of the Île de Groix and Bois de Céné on the other hand (5 : glaucophane schist and associated formations). 4 : weakly metamorphosed formations.

the structures. The succession of isograds appears to relate to the following mineral reactions ($A'KF$ qtz plus water in excess):

- 1) chlorite + microcline = biotite + muscovite
- 2) muscovite + chlorite = cordierite + biotite
- 3) cordierite + muscovite = andalusite + biotite
- 4) andalusite = sillimanite
- 5) muscovite = sillimanite + potassium feldspar
- 6) sillimanite + biotite = cordierite + garnet + potassium feldspar

The partial fusion of the metapelites intervenes at the level of reaction (6), quartzo-feldspathic garnet leucosomes are associated with biotite-cordierite-sillimanite and plagioclase melanosomes. This took place in the sillimanite stability field at temperatures above the destabilization of the muscovite-quartz assemblage (for P_{H_2O} close to P_{solid}). The prograde gradient of these metapelites thus peaked at around 700°C and 0.3GPa, in other words at pressures slightly above those of the Ryoike-Abukuma gradient. This is further attested to by the sporadic occurrence of staurolite, which, in the Montagne Noire, can be mapped as a partial isograd (Fig. 92).

The migmatitic core complexes are essentially composed of anatectic orthogneiss (Somail Series of the Montagne Noire, Belesta and Caramany gneisses in the Agly Massif) amongst which mafic intrusions (tholeiitic and/or calc-alkaline affinities) were emplaced, and syntectonic and syn-metamorphic granitoids. The Agly Massif is characterized by the Ansignan charnockite, an orthopyroxene granitoid which constitutes a sill (or laccolith) more than a kilometre thick in the Caramany gneiss. These charnockites are closely associated with large masses of granoblastic norite and gabbro. The principal mineral associations observed in the migmatitic core complexes are the following:

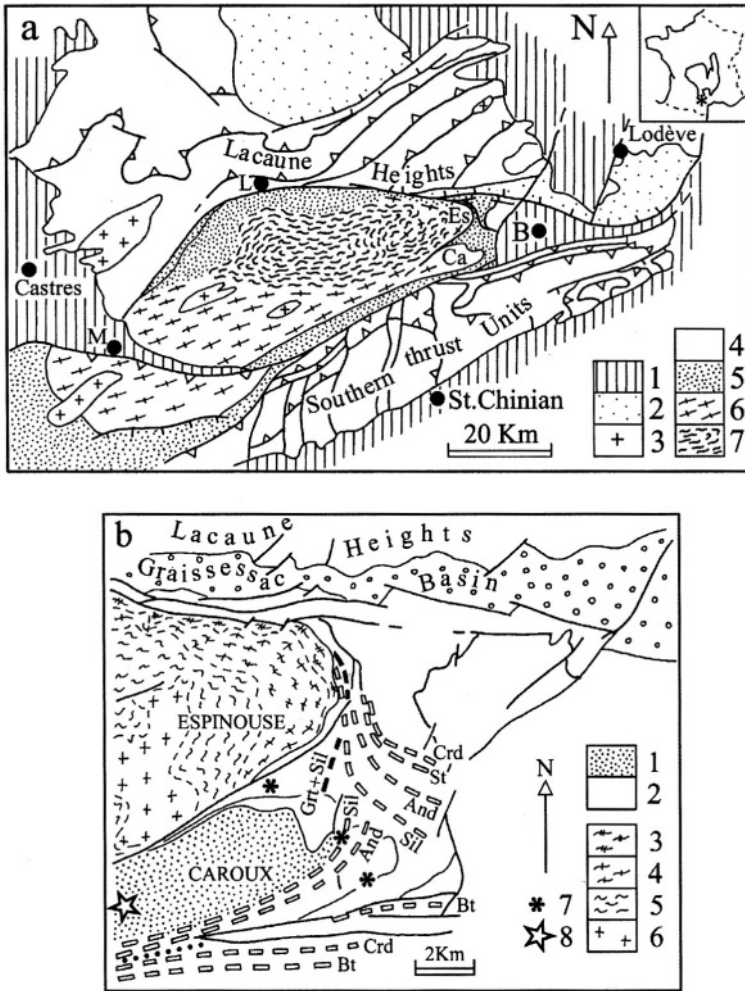


FIG. 92 — Example of a metamorphic core complex: Montagne Noire Massif (French Massif Central).

a) Structure of the Montagne Noire. 1 : Post-Hercynian terrains; 2 : Stephano-Permian basins; 3 : Variscan granitoids; 4 : Lower Paleozoic metapelitic terrains; 5 : metapelitic gneiss; 6 : orthogneiss; 7 : strongly migmatized zone. L : Lacaune; M : Mazamet; B : Bédarioux; Ca : Caroux Massif; Es : Espinouze Dome. After Demange, 1985.

b) Distribution of metamorphic isograds in the east of the "axial zone" after Demange (1985) and Van Den Driessche and Brun (1992). These isograds describe a HT-LP gradient which wraps around the migmatitic core (cf. Fig. 94). 1 : Caroux orthogneiss; 2 : metamorphic Paleozoic rocks. Migmatitic domain - 3 : "leucocratic" gneiss; 4 : migmatitic gneisses (stromatites); 5 : migmatites; 6 : anatectic granite; 7 : relics of kyanite in the LP assemblage; 8 : eclogite relics. Dashed black line : discontinuous isograd of the appearance of staurolite.

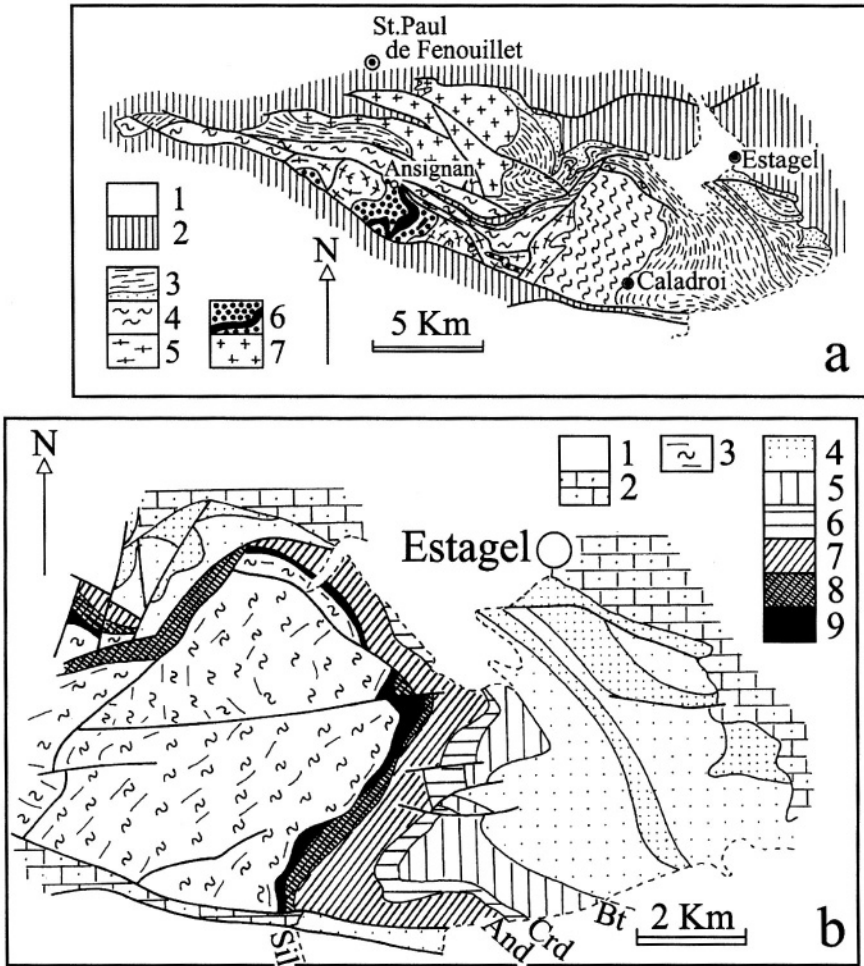


FIG. 93 — Example of a metamorphic core complex: the internal zone of the Agly Massif (Eastern Pyrenees) (after Fonteilles, 1970).

The location of this massif in the Pyrenees may be seen in Figure 110.

a) Structure of the Agly Massif. 1 : Quaternary; 2 : Secondary terrains; 3 : quartzo-pelitic Paleozoic terrain, variably metamorphosed (dashed lines metapelite; stippled Silurian quartzite); 4 : Belesta migmatitic gneiss; 5 : Caramany migmatitic gneiss; 6 : Ansignan charnockite and associated mafic rocks (black); 7 : Saint Arnac granite.

b) Distribution of isograds in the eastern part of the massif. 1 : Quaternary; 2 : Secondary terrains; 3 : Belesta and Caramany migmatitic gneiss; 4 : chlorite zone; 5 : biotite zone; 6 : cordierite zone; 7 : andalusite + biotite zone, 8 : sillimanite-muscovite zone, 9 : sillimanite + liquid zone (anatexis isograd).

grt + sil + crd + bt + Kfs + pl + qtz
 grt + crd + pl + sil + qtz
 opx + Kfs ± bt + pl + qtz
 opx + grt + Kfs ± bt + pl + qtz
 opx + cpx + pl + qtz
 cpx + pl + qtz

The first of these assemblages is widespread in the Agly as in the Montagne Noire; it is a multivariant association (“kinzigite”) which makes it possible to evaluate the temperature and pressure of formation, based on the grt-bt and grt-crd equilibria. The opx-cpx and opx-Kfs-bt equilibria also allow determination of temperature whereas opx-grt cpx-pl-qtz and grt-pl-sil give barometric data. Using this array, it was shown, in the Montagne Noire as in the Agly, that the crystallization conditions of the anatectic cores occurred at relatively elevated temperatures (750 to 850 °C) and at pressures significantly higher (0.5GPa for the Montagne Noire; 0.6GPa in the Agly) to those which were deduced for the enclosing metapelite assemblages. The P-T conditions described for the migmatites do not fall on the prolongation of the prograde gradient of the metapelitic series (Fig. 94). In addition, in the Montagne Noire, relic parageneses of kyanite as well as omphacite and garnet (low pressure eclogite, 1GPa) were described within certain of the paragneisses.

Thus the barometric history of the migmatitic cores appears to have been more complex than that of the enclosing metapelites, it is characterized, in particular, by an evolution at high or medium pressure which is not manifested in the surrounding series. If the metamorphism registered by the metapelites agrees well with the definition of a LP-HT gradient, the evolution of the migmatite is closer to that of Dalradian units characterized by a retrograde high temperature evolution. Figure 94 shows the P-T-t paths deduced for the three principal lithologic entities for the Agly as for the Montagne Noire. The metapelites recrystallized along a prograde LP-HT gradient characteristic of a region of high heat flow; the orthogneissic migmatites show a retrograde evolution of the Dalradian type with an inflection toward high temperatures documented by advanced partial fusion. The syn- or late metabasites underwent isobaric cooling around 0.6 GPa or about 25 km depth. These data suggest the following general interpretation.

5.21.2.1 Metamorphic core complexes: early Dalradian evolution and gravitational disequilibrium. The retrograde gradient shown by the orthogneissic migmatites is the result of a mechanism of underthrusting of crustal units, comparable in type to that proposed to interpret the Dalradian series. The deviation toward high temperatures which results in extensive migmatization is linked to two principal reasons:

- 1) slowing of the ascension of units to the surface; tectonic shortening was limited, non-existent or even negative (see below) at this stage of the orogeny. The dominant uplift control was a relatively slow (several tenths of mm per year) erosion-isostatic re-equilibration. Thermal re-equilibration by conduction and heat production were therefore important at depth.
- 2) Injection of mafic rocks from the upper mantle constituted a convective heat transfer. In the case of the Agly the spatial relation between metabasites and charnockites show that the former are probably linked to the origin of the latter, which resulted in the near-total fusion of the Caramany gneiss.

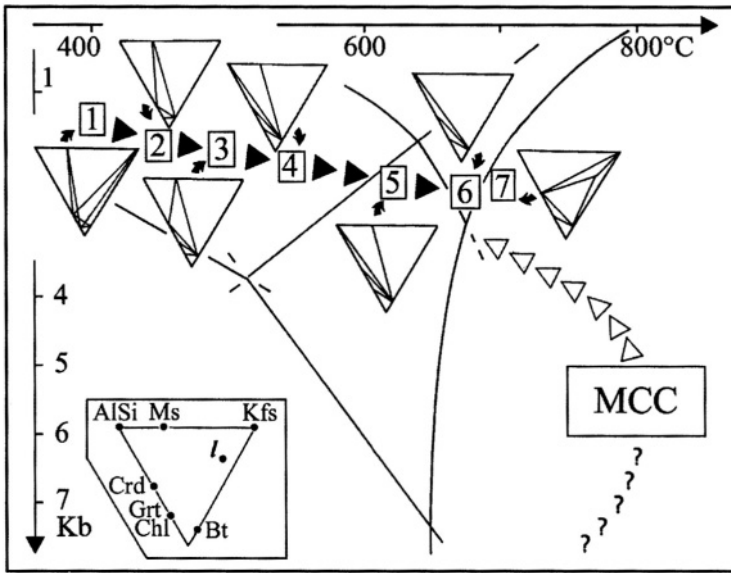


FIG. 94 — Prograde and retrograde gradients associated with the Agly and Montagne Noire metamorphic core complexes (based on data from Andrieux, 1984; Demange, 1985; Fonteilles, 1970; Van Den Driessche and Brun, 1991, 1992; Vielzeuf, 1984).

The prograde gradient (black arrows) is drawn from seven steps (1-7) which characterize the metapelitic envelope of the Agly Massif (Fig. 93). The gentle slope of this gradient is demonstrated, in particular, by the instability of the quartz-muscovite association at temperatures below that of the partial fusion of pelite (steps 6 and 7). The stability conditions of the assemblages of the migmatitic core complexes (MCC) are not in continuity with the prograde gradient. The retrograde evolution which affects these units (white arrows) converge approximately on the peak steps of the prograde gradient. In the case of the Montagne Noire, the kyanite and eclogite relics indicate early high pressure crystallization stages. The metamorphic core complexes, therefore, followed a P-T evolution distinct from that of their metapelitic envelopes. A plastic rise of the cores with respect to their wall rocks along extensional breaks is deduced. This hypothesis accounts for the apparent very high temperature gradient (*cf.* Fig 71d). Als: andalusite or sillimanite; Ms: muscovite; Kfs: potassium feldspar; Crd: cordierite; Grt: garnet; Chl: chlorite; Bt: biotite; *l*: granitic liquid.

5.21.2.2 The metapelites: overlying wall rocks of rising metamorphic cores. The prograde gradient of the metapelitic units is linked to the abnormally high regional heat flow centred on the anatectic domes. These last, therefore, probably played the role of carrier in the heat transfer, from the relatively deep domain of the thickened continental crust (50 km or more in the stability field of kyanite and the eclogites of the Montagne Noire) up to the near-surface zone (about 10 km depth). This hypothesis is justified by the convergence of the prograde gradients of the metapelites and the retrograde gradients of the migmatitic orthogneiss (Fig. 94).

5.21.3 Migmatitic metamorphic cores and post-collisional extension

In summary, the evolution of the LP-HT metamorphic series such as the Montagne Noire

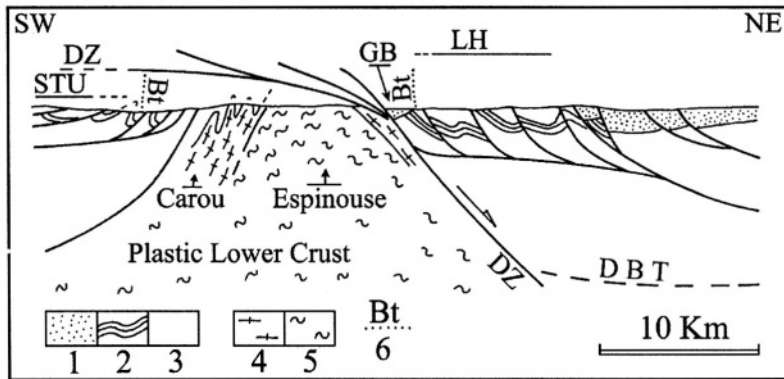


FIG 95 — *Synmetamorphic structural relations between metamorphic core complexes and the metapelitic envelope in the Montagne Noire Massif (after Van Den Driessche and Brun 1991, 1992).*

The “axial zone” of the Montagne Noire (Caroux and Espinouse domes) welled up in response to gravity from the migmatitic lower continental crust during an extensional phase marked by activity along a major normal fault (DZ: detachment zone). The intrusion of retrograde migmatite units into allochthonous metapelitic units (LH: Lacaune Heights; STU: Southern Thrust Units) established a prograde LP-HT metamorphic gradient (Bt: biotite isograd) in the latter units. The units in the axial zone underwent a complex high pressure evolution before migmatization (cf. Fig 94).

1: Post-metamorphic Carboniferous basins (GB = Graissessac Basin); 2: prograde metapelitic units; 3: upper continental crust; 4: weakly or non-migmatitic orthogneiss; 5: migmatite; 6: biotite isograd; DBT: present day ductile-brittle transition. Recent work (Mattaueer *et al.*, 1996) sheds serious doubt on the above cross section and its interpretation.

and Agly is linked to the following succession of events which are part of the orogenic evolution of the Hercynian Chain;

- 1) Underthrusting of crustal units at the final stage of collision according to mechanisms described above;
- 2) slow isostatic uplift and heat accumulation (by radioactive breakdown and by magmatic injection from the mantle), variably important partial fusion and development of a ductile, low density, lower crust;
- 3) accelerated uplift, toward the surface, of this lower crust in the post-collisional phase with the formation of localized metamorphic domes. These domes deform and pierce the overlying sedimentary series and/or syncollisional thrusts;
- 4) establishment of a LP-HT gradient around the domes.

Structural observations in the Montagne Noire (Fig. 95) agree with this model, according to certain authors. The prograde gradient of the metapelitic rocks would effectively be developed, at least in part, in an extensional regime, thus underlining the synmetamorphic ascension of the dome with respect to its wall rocks. Identical observations were made in other regions of the Hercynian Chain, for example Mont Pilat. In the Agly Massif, in contrast, extension followed the development of high temperature assemblages in the metamorphic envelope, and is even post-Hercynian. This extension regime was not a local consequence of the rise of anatectic domes, but was a general process at this stage of the orogeny. It not only affected the continental crust at the post-collisional stage, but

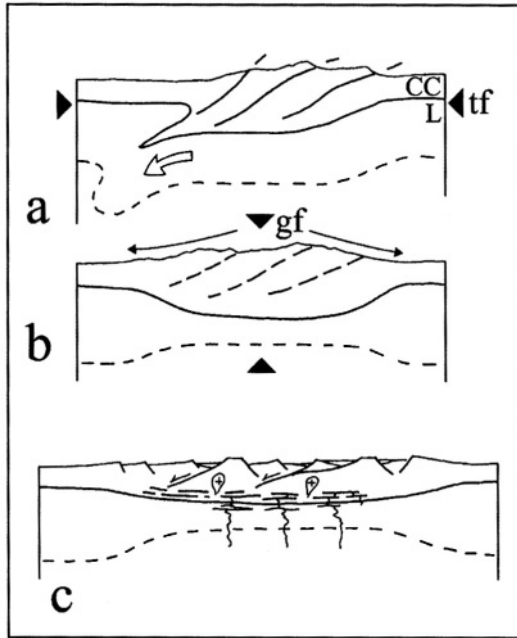


FIG. 96— Post-collision lithosphere extension (after Malavielle *et al.*, 1990).

The diagram is based on the Hercynian evolution of the French Massif Central. The stage of collision (a) is characterized by crustal thickening resulting from the convergence (tf = tectonic forces). Erosion of high relief (arrows) results in isostatic rebound induced by gravitational forces (gf), which results in lithospheric thinning (b). Decompression of the upper mantle results in partial fusion and emplacement of tholeiitic magmatic rocks at the base of the continental crust (underplating) which contributes to the rise in temperature in this domain. (c) A partial fusion of the lower crust, leads to the association of metapelitic granulites (restites of partial fusion) and metabasites (magmatic intrusions which cooled isobarically). The granitoids resulting from this partial fusion migrate toward the surface, agents of an upward convective heat transfer. This model agrees with the late character of the development of certain granulites ("Type II" in the terminology of Pin and Vielzeuf, 1983) in orogens (Fig. 97).

also the lithosphere, as is indicated by the mafic intrusions associated with these LP-HT structures (Fig. 96).

From the point of view of metamorphism, this late extension phase would have two important consequences.

5.21.3.1 Underplating (infracrustal storage) and isobaric cooling. The basic magma produced during lithospheric thinning will accumulate at the base of the continental crust, around 40 km depth; these accumulations would constitute an infracrustal storage or underplating responsible for the "layered" character of the lower continental crust such as appears on seismic surveys. The retrograde evolution of these intrusions is characterized by an "isobaric cooling" as the magmatic crystallization of the intrusion (cpx + opx + pl ± ol ± amphibole) at depth is followed by solid state reactions charting a progressive cooling at constant pressure. An example of this process is given further on (Fig. 106).

5.21.3.2 Final annealing and late medium pressure granulites. The emplacement of basic magmas liberated a significant quantity of heat at the base of the lower crust, as a result provoking or accentuating partial fusion and migmatization. The progression of the migmatitic cores and type “C” plutons (of crustal origin), toward the surface, thus operated an effective heat transfer toward the upper continental crust, as was shown above. The residues of this partial fusion and the associated basic intrusions recrystallized in place at high temperature and medium pressure (about 8 kb) under conditions of low water and high CO₂ concentrations in the fluid phase. The shear stress contemporaneous to this crystallization being low, these rocks are constituted of granulitic units commonly characterized by granoblastic textures with a coarse grain size as a result of the importance of post-dynamic annealing. These granulites, produced late in the evolution of the orogeny, have different characteristics from the early granulites associated with eclogites, which are developed immediately after subduction at the onset of the retrograde evolution (Fig 83). The late granulites of the Hercynian Chain, dated around 300 Ma are known from the Ivrean Zone where they constitute the base of the Austro-Alpine continental crust (Fig. 97). They have also been identified as enclaves in certain Neogene volcanic structures of the French Massif Central (Maar de Bournac, Haut-Loire for example).

5.22 Metamorphism in extension zones:

Recrystallization of the oceanic crust near oceanic ridges

The domains located near active oceanic ridges are characterized by high heat flow and by a tensional deformation regime. In effect, if the basalts of the oceanic crust are rapidly cooled after emplacement, the deeper layers, notably the gabbroic layer, remain at high temperature several tens of kilometres from the ridge (Fig. 98). Oceanic extension results in normal faults in the brittle domain (basalts and sheeted dykes) and by ductile shears in the hotter units (gabbros). Sea water circulates in a convective manner in these faults, it infiltrates to depths of around 6 km, from where the permeability of the material becomes negligible, reaching temperatures over 350 °C. It exchanges cations with the rock, saturates in solutes and returns to the oceanic reservoir via “black smokers”, high temperature thermal springs observed near ocean ridges.

This convective circulation process results in recrystallization in an open system within the principal units of the oceanic crust: dykes and flows of layer 2 are crosscut by hydrothermal veins (generally epidote and quartz); gabbros of layer 3 are the site of heterogeneous low pressure recrystallization ($P < 0.2$ GPa) in the zeolite, greenschist and epidote amphibolite facies.

5.23 Sea water convection and low pressure recrystallization near ocean ridges

Mineralogical petrological and geochemical observations, both in the ocean and in the ophiolite series (probable fragments of oceanic crust involved in orogens) lead to a general scheme of convective sea water circulation and the low pressure transformations which are associated in different units of the oceanic crust (Fig. 98). This convective domain is divided into three zones: *recharge*, *reaction* and *discharge*.

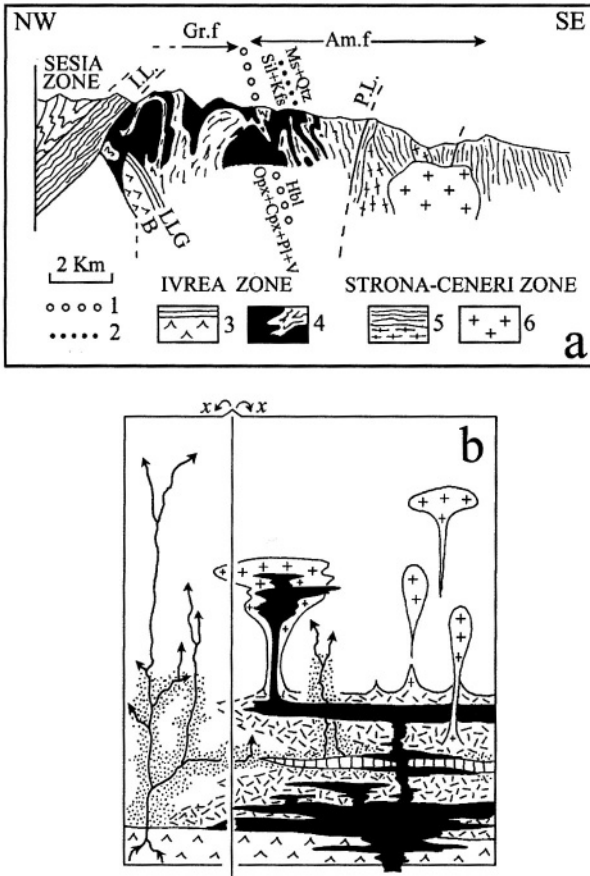


FIG. 97 — Medium pressure granulites from the base of the crust.

a) Granulite at the base of the Austro-Alpine continental crust: structure of the Ivrea Zone (after Zingg *et al.*, 1990 and Pin, 1990). 1 : transition from granulite to amphibolite facies; 2 : muscovite isograd; **Ivrea Zone** - 3 : basal complex, Balmuccia mantle peridotites (B); lower layered group (LLG); granoblastic gabbros and pyroxenite emplaced around 600 Ma. 4 : in black, Late Hercynian (300-280 Ma) basic complex composed of gabbro, pyroxenite and anorthosite (Cpx + Opx + Pl) in the granulite facies (Gr.f), and diorite (Hbl + Pl) in the amphibolite facies (Am.f); lines : restitic metapelites, these are stromalites (Grt + Sil + Pl + Kfs + Qtz) in the granulite facies and "kinzigites" (Grt + Bt ± Crd + Pl + Kfs + Qtz) in the amphibolite facies. **Strona-Ceneri Zone** - 5 : orthogneiss (elongate crosses), gneiss and schist (lines); 6 : late Hercynian granitoids. IL Insubrian Line; PL Pogallo Line. The intrusion of the late Hercynian basic complex provoked partial fusion in the metapelite at the base of the continental crust. The granitic liquids then migrated toward the upper crust. The association of granoblastic metabasites (after isobaric cooling and annealing) and metapelite restites constituted the post-Hercynian granulitic lower crust in the domain of low water fugacity (*cf.* Fig. 97b).

(Continued on facing page)

5.23.1 *The recharge zone*

This corresponds to the alimentation of the convective system by sea water infiltration into the fractured pillow lavas and into the much less permeable deeper units, the sheeted dykes and gabbros. The break in the porosity at the transition between the flows and dykes is also marked by a significant jump in the temperature related precisely to the effect that convective cooling is slower in low permeability zones. A series of water-rock exchanges and recrystallization takes place in this zone;

1) The upper low temperature layer (in the lava flows up to about 150 °C) is characterized by oxidation of olivine, the fixing of alkali ions (K, Li, Rb, Cs) in the clay minerals (smectite, celadonite) and by $K \leftrightarrow Ca$ exchanges between solutions and plagioclase. This last mineral is partly or totally transformed into low temperature potassium feldspar (adularia) and the infiltrating solution is enriched in Ca^{++} . These transformations are little different from those which characterize the surface alteration of lava flows on the ocean bottom, and cannot be considered relevant to metamorphism.

2) The deeper domains at high temperature (250 to 350 °C) corresponding principally to the sheeted dykes, are characterized by the fixing of Mg in chlorite, $Na \leftrightarrow Ca$ exchanges between solids and solutions resulting in the replacement of plagioclase by albite, whereas actinolite and epidote crystallize at the expense of olivine and augite. The olivine may sometimes be converted to talc. High Ca concentration in the solution results in the precipitation of calcic zeolites and anhydrite ($CaSO_4$) in this domain. The assemblage albite + epidote + actinolite + chlorite corresponds to the LP-LT greenschist facies (*cf.* Fig 34) and must be considered metamorphic, but this recrystallization is heterogeneous, principally localized near percolation zones, leaving panels or fragments of intact or weakly altered rocks away from the fluid circulation passages.

5.23.2 *The reaction zone*

This is situated at the base of the sheeted dykes, or even within the gabbros. It corresponds to the domain of interaction between the fluids (charged with mineral salts) and rocks of low permeability, still at high temperatures. These are over 400 °C and could rise to 600 or 700 °C in the immediate proximity of the magmatic reservoir. These high temperatures allow plastic deformation of basaltic and, above all, gabbroic protoliths under tensional stress, and the development of relatively high temperature parageneses of calcic plagi-

(FIG. 97 facing page)

b) Diagram illustrating the different models of late granulitization in the lower continental crust (after Clemens, 1990): injection of basic magmas (in black) from the upper mantle (inverse v pattern) in the metagranitic and metapelitic lower crust: partial fusion of metapelites resulting from this heat transfer; the anatectic granitic liquids absorb the water from the system and migrate toward the surface, leaving behind granulitic restites (dashed pattern) at depth. The addition of heat also induces decarbonation reactions in the marbles (brick pattern) releasing a CO_2 flux (arrows). The water concentration in the fluid phase decreases and the stability field of the hydrated phases is reduced. Granulite assemblages develop in the CO_2 percolation network (dot pattern). A CO_2 flux could also come directly from the mantle and have the same effect; it is, in principle, possible to distinguish the two types of flux by the study of $\delta^{13}C$, the carbon isotopic ratios being different in the mantle from those carbonates of sedimentary origin. From a certain level of the continental crust the fracture network is permeable enough to allow water vapour circulation, and the stability field of the hydrated phases is extended, and granulitic assemblages are no longer possible. This type of granulitic lower crust crops out directly as a result of major tectonic breaks (Ivrea Zone *cf.* Fig. 97a); it is also sampled at depth and brought to the surface by explosive alkaline volcanism. xenoliths (x).

remains trapped in fissures and fractures in the gabbro at the base of the dykes, leading to the precipitation of a network of quartz and amphibole bearing hydrothermal veins.

5.23.3 *The discharge zone*

This corresponds to the percolation zone of the vapour phase which escapes from the reaction zone. The descriptions below are essentially drawn from observations made on ophiolite series.

The discharge occurs in two different ways depending on the intensity of deformation:

1) It can be “focused” if fracturing opens a relatively easy path to the surface; this is generally the case at the axes of ridges and paleoridges, the fluids, impoverished in Mg and enriched in Ca (characteristic of smokers) leach the “sheeted dyke” unit, extracting metals and sulphur, leaving a typical assemblage of “epidosites” composed of quartz, epidote and sphene. These rocks are made up of hydrothermal veins or anastomosing veins over hundreds of metres thick, parallel to the basalt dykes (themselves hydrothermally altered and recrystallized in the greenschist facies: actinolite + chlorite + albite + titanite) and at the paleoridge axis. As the fluids rise toward the surface, the hydrothermal assemblage is modified and the association quartz + epidote grades into quartz + sulphide veins (pyrite, chalcopyrite, sphalerite), and in certain cases into sulphide masses (Fig. 98).

2) The discharge is “diffuse” when the rising fluids are not channeled by a fracture network. The fluids are dispersed, therefore, in a large volume of rock and mix progressively with sea water (mixing attested to by the evolution of $^{18}\text{O}/^{16}\text{O}$ ratios, see below) before reaching the crust-ocean interface. The basalt dykes and flows are altered in a heterogeneous manner by associations of chlorite + albite + titanite + sulphides and are cut by quartz-rich veins.

In this model of convective circulation, described above, the water infiltrated at the ocean-ocean crust interface plays a major role. In reality, a small but real participation of fluids of magmatic origin, that is to say, mantle origin, contributes to the global circulation budget: ^3H , CO_2 , Cl , SO_4 , and H_2O are liberated by degassing of basaltic magmas, as attested to notably by the values of isotopic ratios of carbon, sulphur, oxygen and hydrogen. The volumes concerned are relatively small with respect to the circulation of waters derived from the oceanic reservoir, which plays a major role in the recrystallization.

5.23.4 *Sea floor metamorphism in the Atlantic:*

Gorringe Bank and the Mid-Cayman Rise

The Gorringe Bank, located off Portugal, displays a good example of sea floor metamorphism of the layer 3 gabbros. These gabbros crop out because of a tectonic break along the Azores-Gibraltar line allowing erosion of the upper levels of the crust. They were sampled by submersible in 1984 and 1996. Most of the gabbros are isotropically recrystallized (50-80% secondary phases) under static conditions, or during deformation which established only a slight foliation. In the latter case the granoblastic, porphyroclastic textures result from a high temperature recrystallization under anisotropic stress followed by annealing. Mylonitic textures are linked to recrystallization at lower temperatures. The metamorphic evolution is principally characterized by hydration of the primary ferromagnesian phases; olivine is replaced by talc and actinolite assemblages and clinopyroxene by actinolite and hornblende. The plagioclase evolved toward a more albitic composition, especially along

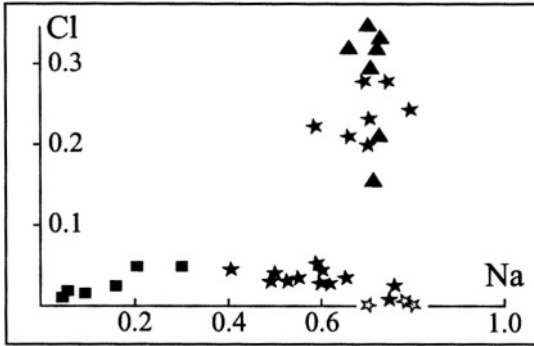


FIG. 99 — Amphibole composition in gabbros of the Gorrige Bank in the Na versus Cl diagram (after Mével, 1988).

white stars : uncontaminated magmatic amphiboles; black stars and triangles : amphibole recrystallized at high temperature in undeformed gabbro and along hydrothermal veins; black squares : actinolite recrystallized at low temperature.

hydrothermal veins (as a result of Ca-Na exchange between solid and solution).

5.23.4.1 Contamination by sea water. The role of hydrothermal solutions fed by the convective circulation of sea water results, in particular, in a global addition of sodium and chlorine in the recrystallized assemblages. A mass balance calculation shows that to account for the Na concentration in the secondary assemblages, at least 57 g of sea water is necessary to alter 100 g of fresh gabbro. The evolution of Cl concentrations in amphibole during metamorphism shows the importance of this outside contribution as well (Fig. 99). The coexistence of different types of gabbro, non-metamorphic, granoblastic and mylonitic in the same place, as well as the heterogeneous recrystallization of all these types is attributed to a close liaison between the deformation and fluid percolation (Fig. 100).

5.23.4.2 Stable isotopes: contamination tracers. The geochemistry of stable isotopes, in particular those of hydrogen and oxygen, allow evaluation of the contribution of sea water during recrystallization of the oceanic crust. The light weight of the hydrogen (^1H and ^2D) and oxygen (^{16}O , ^{17}O , ^{18}O) isotopes and the very large mass ratio (proportionally) between the different isotopes of these elements result in isotopic fractionating by various geologic processes. The D/H and $^{18}\text{O}/^{16}\text{O}$ ratios are quite variable, for example, in different types of rocks as a function of their origin and the characteristics of their evolution. This variability is measured by a mass spectrometer and is expressed in $\delta\text{‰}$ by comparison with a definite value of average ocean water SMOW (standard mean ocean water).

Thus for oxygen:

$$\delta \text{O}\text{‰} = \frac{(^{18}\text{O}/^{16}\text{O})_{\text{sample}} - (^{18}\text{O}/^{16}\text{O})_{\text{SMOW}}}{(^{18}\text{O}/^{16}\text{O})_{\text{SMOW}}} \cdot 10^3$$

By definition the values of $\delta^{18}\text{O}$ and δD are zero for sea water whereas they are on the

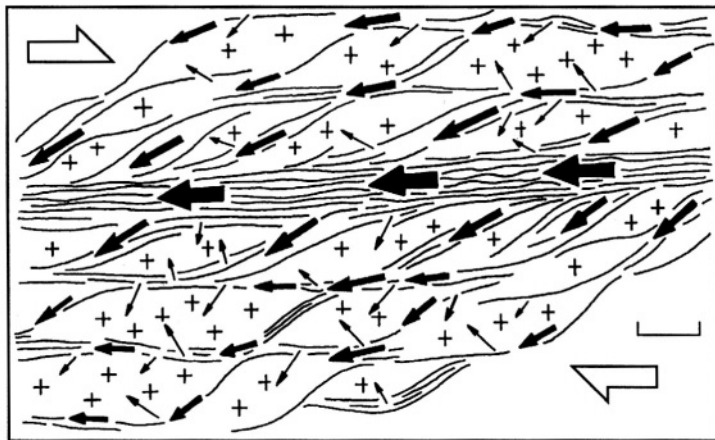


FIG. 100— *Deformation of gabbros of the oceanic crust and percolation of fluid phase in a shear zone (after Mével, 1988).*

The black arrows represent the importance of hydrothermal flow schematically, according to their dimensions. The weakly uncontaminated gabbro (cross pattern) forms blocks surrounded by the schistosity. (Scale : 10 cm to 1 m),

order of 6‰ - 8‰ respectively for the hydrated phase in isotopic equilibrium with an uncontaminated basalt. It is, therefore, in principle easy to characterize the degree of contamination of a basalt by sea water or of a rock derived from a basalt, by measuring the values of δ .

Thus the gabbros of the Mid-Cayman Rise, in the Caribbean, contain secondary amphiboles characterized by low values of $\delta^{18}\text{O}$, and high values of $\delta^{2}\text{D}$; these minerals crystallized in the presence of a fluid rich in sea water (Fig. 101) during the high temperature alteration of the gabbros.

5.23.5 An example of sea floor metamorphism in the Alpine Chain: the Chenaillet Massif

During the Alpine collision, certain units of the Tethyan oceanic crust were thrust onto the European continent by obduction (Fig. 76). These still show local traces of sea floor metamorphism which preceded the effects of Alpine deformation and metamorphism. This is the case of the Chenaillet unit of the Piemont zone (Fig 102). The typical ophiolitic formations (serpentine, gabbro, pillow lavas) were partly recrystallized during the Alpine Orogeny under prehnite-pumpellyite or greenschist facies conditions. However the gabbros, still displaying their magmatic layering, have undergone a high temperature extension deformation (Fig. 103); a foliation is shown by secondary brown amphibole developed at the expense of augite; it is cut, with knife-sharp contacts, by the dolerite dykes of the ophiolite series. The deformation and high temperature metamorphic parageneses predate, therefore, the end of the magmatic episode forming the ophiolite series (Lower Jurassic), and *a fortiori* the Alpine tectonism and metamorphism. It is therefore a sea floor metamorphism developed near an active ridge.

It is important to record the occurrence of these events in the ophiolitic series, in order

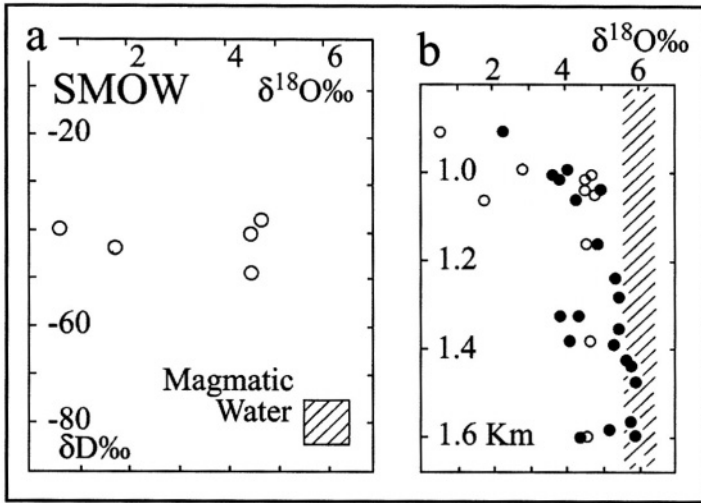


FIG. 101 — *Isotopic composition of amphibole (empty circles) and plagioclase (black circles) of the Mid-Cayman Rise (Caribbean Sea) (after Ito and Clayton 1983).*

a) $\delta^{18}\text{O}$ vs. $\delta^2\text{D}$ diagram : the amphiboles which plot away from the field of water dissolved in magmatic liquid from the upper mantle (hachured field) approach the theoretical composition of "SMOW".

b) variation of $\delta^{18}\text{O}$ of amphibole and plagioclase as a function of depth below the surface of the oceanic crust. The offset with regard to mantellic values (hachured zone, $\delta^{18}\text{O} = 6$) diminishes at depth. This is attributed to the decrease in permeability in rocks of the oceanic crust as a function of depth, hand-in-hand with less well developed fracturing.

to distinguish their effects from those of further metamorphism at subduction, obduction and collision stages. This is only possible when the later transformations were discrete. The example of Chamrousse ophiolite (Isère) in this regard is quite remarkable; emplaced during a Cambro-Ordovician extensional phase (496 Ma), this series passed through two important orogenies (Hercynian and Alpine), but nevertheless still shows the deformation and recrystallization acquired during the ocean floor event.

5.24 Metamorphism in extension zones: rifts

5.24.1 Continental rifts: zones of high heat flow

Continental rifts are the surface expression of zones of lithospheric and crustal thinning in a continental extension system. This thinning results in boudinage of the brittle lithosphere and by the emplacement of relatively low density material ($\rho = 3.1$) at the base of the thinned crust. Seismic waves travel at relatively low velocities ($V_p = \text{km}\cdot\text{sec}^{-1}$) through this material. According to interpretations, this "abnormal mantle" results from a tumescence of the plastic asthenosphere, or to the emplacement of basic magmas in the stretched and fractured lithosphere. Either of these hypotheses can result in a heat transfer toward the surface, and in consequence, a high thermal gradient.

The Rhine Graben, between the Vosges and the Black Forest is thus characterized by

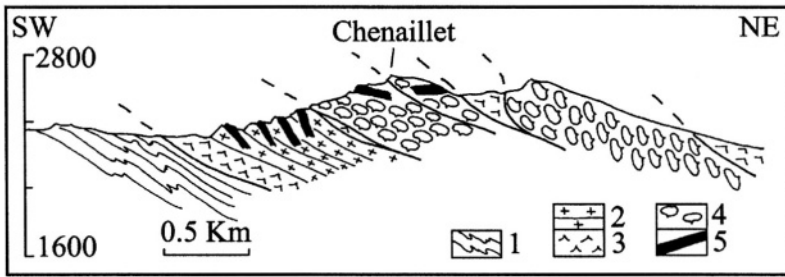


FIG. 102 — Cross section of the ophiolite series of the Chenaillet Massif (Montgenèvre-Piemont Zone, Franco-Italian Alps (after Steen *et al.*, 1980).

The ophiolites comprise several slices which thrust over a sedimentary series (1); gabbros (2) and pillow lavas (4) are cut by dolerite dykes (5) of the sheeted complex. These dykes were emplaced after the deformation and recrystallization which affected the gabbros (*cf.* Fig. 103). These events are therefore contemporaneous with the genesis of the ophiolitic series in an extension zone. The imprint of the Alpine metamorphism is weak or non-existent. (3) serpentines.



FIG. 103 — Sea floor metamorphism in the Chenaillet gabbros (after Steen *et al.*, 1980).

The gabbro at the right of the figure displays a porphyroclastic texture typical of "flaser gabbros". They recrystallized in a heterogeneous fashion at high temperatures (600-700 °C) into a brown hornblende-plagioclase assemblage. This deformation and recrystallization under an extensional regime took place before the emplacement of the dolerite dyke (on the left) of the dyke swarm. (diameter of coin : 24 mm).

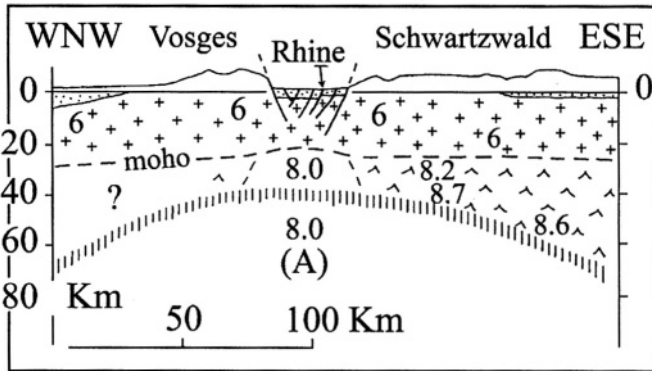


FIG. 104 — Cross section of the lithosphere below the Rhine Graben (simplified from Glahn *et al.*, 1991).

This structure is based on seismic wave speed (bold numbers : V_p km.sec⁻¹) under the whole of the Vosges-Black Forest region. The topographic profile is drawn with a strong vertical exaggeration above altitude 0m. Stipple pattern : sediments of the Rhine Graben and Paris Basin ($V_p \leq 4$ km.sec⁻¹). The granitic continental crust ($5.9 \leq V_p \leq 6.4$) is slightly thinned near the graben. The Moho is situated between 20 and 25 km depth. The upper lithospheric mantle ($V_p = 8.2$ to 8.7) is clearly identified in the east. The bottom of the Rhine Graben appears to rest on an “abnormal” mantle ($V_p = 8$ km.sec⁻¹) a possible relic of an old (Oligo-Miocene) incompletely cooled, asthenosphere bulge. This structure accounts for the positive thermal anomaly noted in the Rhine Graben (Fig. 105). The asthenosphere-lithosphere boundary determined by surface waves (A = asthenosphere) is not in agreement with the tomography presented above.

an abnormal mantle located at shallow depth (Fig. 104) and by a high heat flow which locally rises to 120 mW.m^{-2} . The temperature measured in geothermal bore holes during drilling surpassed 150°C at 2000 m depth (Fig. 105). The high gradient which results in these measurements does not, however, result from a conductive gradient because it is in large part related to water convection in the fissure system of the rocks traversed. It indicates, nevertheless, that this structure, which was in extension to the end of the Oligocene or start of the Miocene, still displays a remarkable thermal anomaly.

5.24.2 Metamorphism and crustal thinning:

Example of the Madagascar granulites

In the south of Madagascar, the continental crust formed during the Pan-African Orogeny (560 - 565 Ma) consists of three high grade metamorphic series (Fig. 106) of which the aluminous parageneses have a strongly refractory character (depleted in the geochemical sense of the term). These units are associated with a gabbroic and an anorthositic complex emplaced during metamorphism. The temperatures calculated from mineral assemblages are high in the three series: 750 to 800°C and even to 850°C in certain formations of the “Androyen”. The peak pressures of the prograde gradient are, in contrast, variable from one to another.

The “Vohibory” Formation is of Dalradian type: sapphirine and corundum amphibolites, serendibite and clintonite pyroxenites crystallized under pressures greater than 1 GPa. The garnet and sillimanite leptynites of the *Ampanihy Formation* crystallized around 0.7 GPa, and the *Androyen Formations* crystallized around 0.5 GPa (Fig. 106). This diversity of

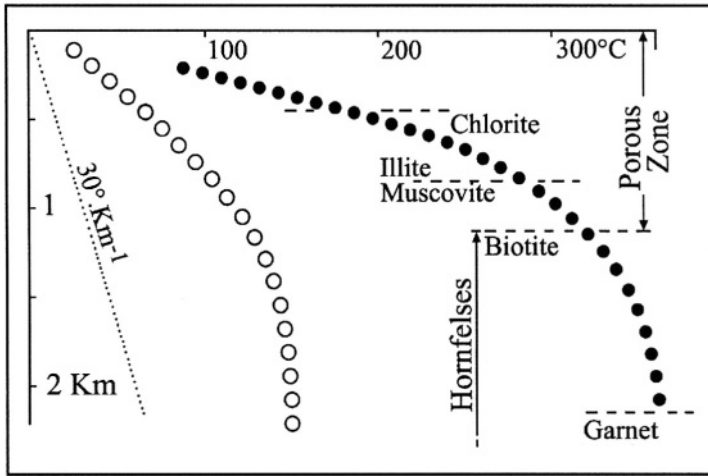


FIG. 105 — *Thermal gradients in extension zones.*

a) Salton Sea (black circles; data of McDowell and Elders, 1983). The slope of the gradient is gentle for the first 1000 metres, and steepens at depth into the low permeability “hornfels” zone. The heat transfer in hornfels is essentially conductive, whereas in the “porous” zone it results from water convection in a porous medium. The principal isograds are indicated along the gradient.

b) Rhine Graben HDR (“Hot dry rocks”) project of Soultz-sous-Forêts (white circles; after Schellschmidt and Schultz, 1990, and personal communications from Socomine). The slope of the gradient is comparable to the Salton Sea gradient. The low slope of the gradient corresponds to a highly permeable zone (sedimentary cover and fractured granite) site of water convection in a porous medium. Because of the age of this structure and of much less pronounced lithospheric thinning (compare Figure 104 and 108), the temperatures measured at 2000 metres are much lower than those of the Salton Sea.

gradients in a relatively restricted region is interpreted as the result of lithospheric and crustal thinning (Fig. 106) associated with the emplacement of the gabbroic and anorthositic complex. The assemblages of the intrusions evolved by isobaric cooling, notably with the appearance of garnet + quartz assemblages at the expense of the primary igneous parageneses of orthopyroxene and plagioclase. The individual crystallization conditions of each of the series is a result of the initial position of each of the units with respect to the structure in extension (Fig. 106). Later compression and shortening have led to the present-day structure.

A certain similarity must be noted between this model of pre-orogenic extension and the late- to post-orogenic extension model envisaged for the case of the Montagne Noire above. In the two examples, the emplacement of mafic rocks derived from the upper mantle at the base of the crust was responsible for the advanced partial fusion of the metapelites and metagranites. Only the outside addition of heat will allow crustal formations to attain temperatures sufficiently high enough to produce anatectic liquids capable of migrating *en masse* to the surface in the form of granite plutons. In the particular case of Madagascar, the advanced extraction of partial fusion liquids induced the formation of very refractory aluminous units (fusion residues) displaying unusual mineral assemblages.

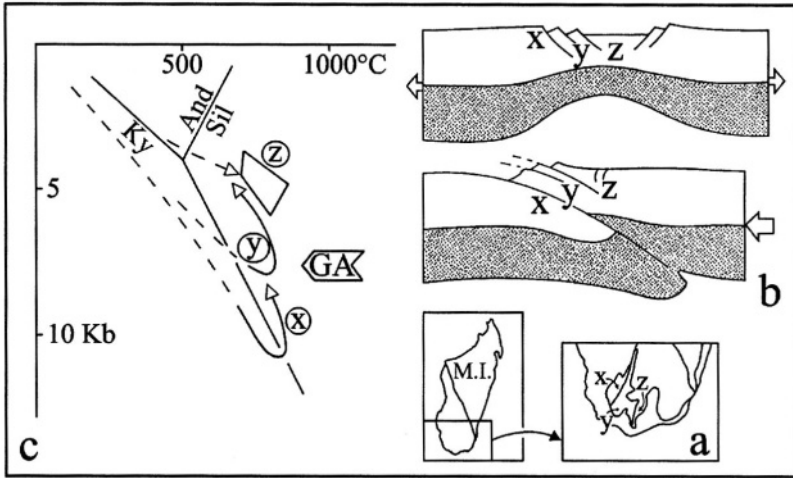


FIG. 106 — *Metamorphism in extension zones: evolution of the metamorphic series of the south of Madagascar (after Nicollet, 1990).*

a) Location of the units in the south of Madagascar : (x) Vohibory unit; (y) Ampanihy unit; (z) Androyen Formations; b) simplified geometrical relations between the units at the extension stage contemporaneous with the emplacement of the gabbro and anorthosite suite, and after collision; (c) P-T-t path for the three different units. GA isobaric cooling of the gabbroic anorthositic complex.

5.24.3 Active metamorphism in the Salton Trough: lithospheric thinning in a transform zone

The Salton Trough, located in the northern prolongation of the Gulf of California, results in the present-day subsidence of a basin in extension, in relation to the San Andreas Fault (Fig. 107). In this type of pull-apart basin (or rhombochasm), the rate of lithospheric thinning is significant, much more so than in grabens affected by a simple lateral extension. In the case of the Salton Sea and the Imperial Valley, the low density “abnormal mantle” is very close to the surface at less than 10 km depth (Fig. 108). The geothermal characteristics of this depression are well known because they are intensively exploited. The heat flow rises to 2400 mW.m^{-2} locally (Fig. 109) and the temperature is above $360 \text{ }^\circ\text{C}$ at 2200 m depth, that is to say, for a fluid pressure of the order of 0.02 GPa (Fig. 105). As in the case of the Rhine Graben, it is not strictly a conductive gradient, but rather a thermal structure related to convective circulation of high temperature fluids in materials of high porosity and permeability, all at least in the upper part of the structure.

The basin-fill materials are shales and sandstones as well as recent or present-day volcanic rocks. These have undergone, or are presently undergoing recrystallization in an open system. The mineral reactions take place in relation to high temperature brines which percolate through the assemblages (*cf.* as the convective circulation of sea water near oceanic ridges described above). The principal stages of this recrystallization as a function of temperature are (Fig. 105):

- 1) the appearance of epidote (600m; $243 \text{ }^\circ\text{C}$)
- 2) the appearance of biotite (1135m; $325 \text{ }^\circ\text{C}$)

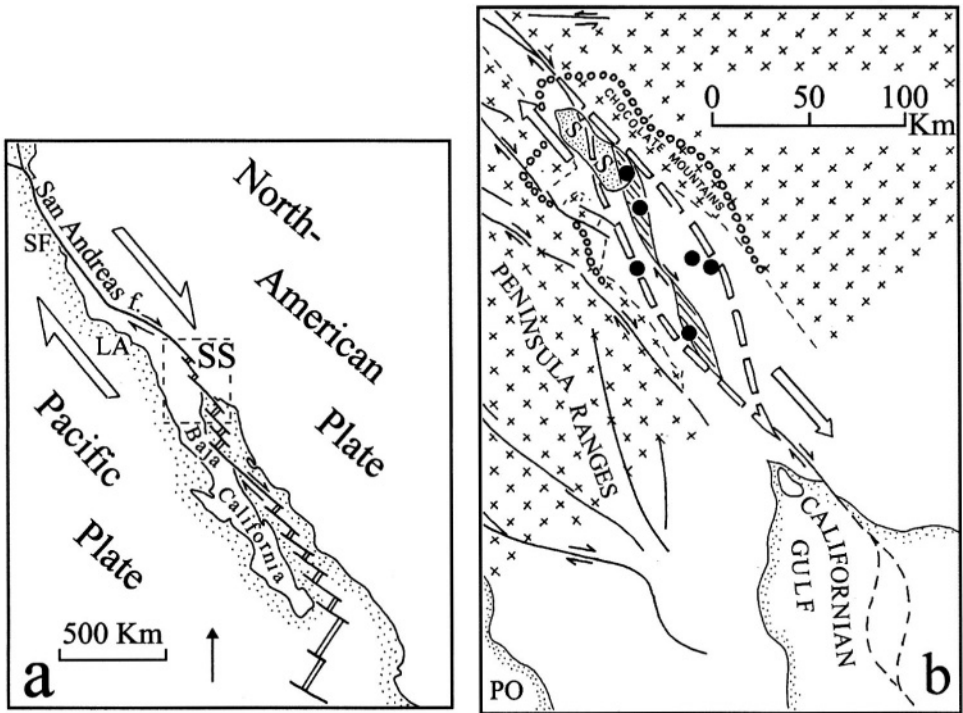


FIG. 107 — *The Salton Trough (California) : zone of lithospheric thinning and transtension* (after Lachenbruch *et al.*, 1985).

a) Structural setting of the Salton Sea (box SS). The dextral offset of the San Andreas induces formation of transtensional basins ("pull-aparts" or "rhombochasms") related to a very high rate of lithospheric thinning (*cf.* Fig. 108). Farther to the southeast in the Gulf of California this strike-slip movement is accommodated by transform faults in the oceanic domain. The Salton Trough is, in effect, a pre-oceanic stage.

b) Dynamic and thermal context of the Salton Trough. Crosses : thick continental crust. The broad dashed lines delineate a lozenge-shaped domain corresponding to the almost complete stretching of the continental crust (*cf.* Fig 108). The hachured lozenge-shaped domains are the site of intense seismic activity. The open circles delineate the zone in which the heat flow is above 100mW.m^{-2} , a thermal anomaly resulting from the lithospheric thinning. SS : Salton Sea; PO : Pacific Ocean; black circles : principal industrial thermal fields.

- 3) the disappearance of potassium feldspar, and the appearance of andradite garnet (2120m; $360\text{ }^{\circ}\text{C}$)

This high-temperature, near surface recrystallization indicates the presence of a geothermal tumescence at a greater depth which induces a local tightening of the isotherms as a result of lithospheric thinning. This hypothesis is all the more plausible because, to the south the thinned structure of the Salton Trough passes directly into the oceanic domain of the Gulf of California. This type of thermal configuration - very narrow localized high temperature zones - is sometime identified in older metamorphic domains and may be interpreted in the same manner.

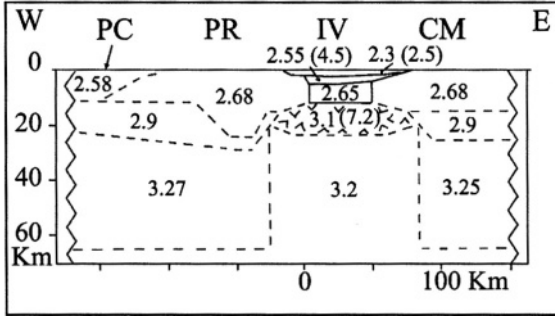


FIG. 108 — Gravimetric cross section in the region of the Salton Trough and the Imperial Valley (after Lachenbruch *et al.*, 1985).

The figures indicate the rock densities calculated from seismic velocities. In brackets : velocity of P waves. CM : Chocolate Mountains; IV : Imperial Valley; PR : Peninsular Ranges; CP : Pacific coast. The trough is filled with sediments ($\rho = 2.3$ to 2.55) which lie on a thinned continental crust ($\rho = 2.65$) or on a "type 3 crust" in the sense of Nicolas (1985); a low velocity "abnormal mantle" ($\rho = 3.1$) representing, according to the interpretation, an asthenospheric bulge ($\rho = 3.2$) or else gabbroic masses injected between the mantle and the crust (crustal underplating). The whole of this structure corresponds to lithospheric thinning in a very narrow domain, related to transtensional tectonics. This thinning (and the magmatism which results) is the cause of the thermal anomaly observed in the trough, and results from the rise of the low density asthenospheric mantle toward the surface surrounded by rigid upper lithospheric mantle ($\rho = 3.25$ to 3.27).

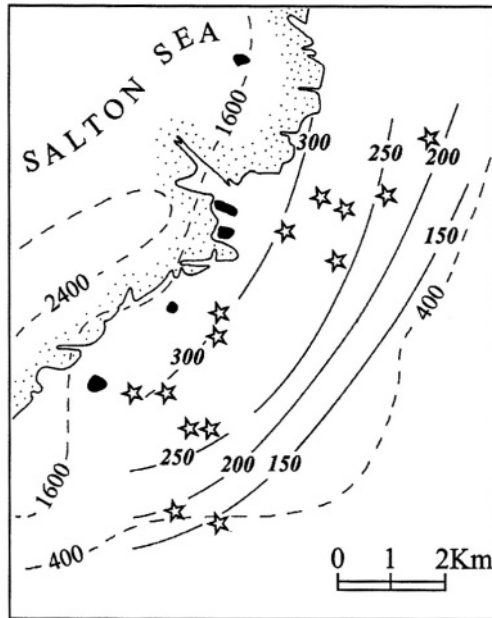


FIG. 109 — Configuration of the thermal anomaly of the Salton Trough (after McDowell and Elders, 1983).

Solid curves : temperatures in $^{\circ}\text{C}$ at 914 m depth (3000 feet); dashed : lines of equal heat flow intensity in mW per m^2 ; Black surfaces : rhyolitic intrusions resulting from crustal fusion at depth at temperature around 700°C .

*5.24.4 Lithospheric thinning and crustal shearing:
Metamorphism of the North Pyrenean Zone*

The North Pyrenean Zone is characterized by a HT-LP Cretaceous metamorphism located in small, discontinuous basins all along the north limit of the Pyrenees. This metamorphism is quite unusual, with similar characteristics to those just described for the Salton Trough.

5.24.4.1 North Pyrenean Zone; Cretaceous lithospheric thinning corridor. The North Pyrenean Zone (NPZ) is a narrow unit (0-5 km wide, identified over 300 km, and bounded on the south by the North Pyrenean fault (NPF) and to the north by the North Pyrenean Frontal Thrust (NPFT) (Fig. 110). It shows many distinctive characteristics.

5.24.4.2 The orogenic formations. During the Upper Albian, the NPZ was the deposition site of a thick turbidite series (up to 3 to 4000 m thick), in narrow discontinuous basins. This sedimentation showed evidence of strong bottom instability at this period related to extension tectonics marked by rotated blocks affecting the reef facies of the Upper Jurassic and Lower Cretaceous.

5.24.4.3 Alkaline magmatism. Dykes and flows of silica-undersaturated alkaline rocks were emplaced in the NPZ at the onset of the Upper Cretaceous. These rocks are unknown in other parts of the Pyrenees, and although they represent a very small volume, they are characteristic of a “continental rift” type of magmatism.

5.24.4.4 Tectonic slices from a deep source. At the end of the Cretaceous and in the Eocene, during the compressive mountain-building episodes of the Pyrenean Chain, slices of granulites and peridotites were emplaced tectonically in the NPZ. Their presence indicates that the deep Hercynian continental crust and the lithospheric upper mantle were very close to the surface before the shortening. Locally, mantle peridotites probably constituted the floor of certain flysch basins.

All of these characteristics indicate that from the end of the Lower Cretaceous to the start of the Upper Cretaceous, (Upper Albian to Lower Cenomanian) the future NPZ was a zone of rapid subsidence in extension related to a significant lithospheric thinning because locally it gets to the stage of a crustal shear. The width of the zone at this time did not exceed several tens of kilometres, and it is not possible, under these conditions, to expect, as in the case of a simple graben, a rate of extension sufficient to bring the upper mantle near to the surface; only the development of “pull-apart” basins along a strike-slip break will permit such drastic thinning. The NPZ thus could have functioned as a transform fault, comparable to the San Andreas, during the Upper Albian-Cenomanian. In the model, the flysch basins with thinned or sheared floors, were like a series of Salton Seas along the tectonic break (Figs 111 and 113).

Two significant arguments support this point of view:

- 1) the kinematics of the European and Iberian plates at this time, which display effective sinistral movement between Spain and France, accommodating the opening of the Atlantic and the Bay of Biscay, along the future NPZ (Fig. 111).

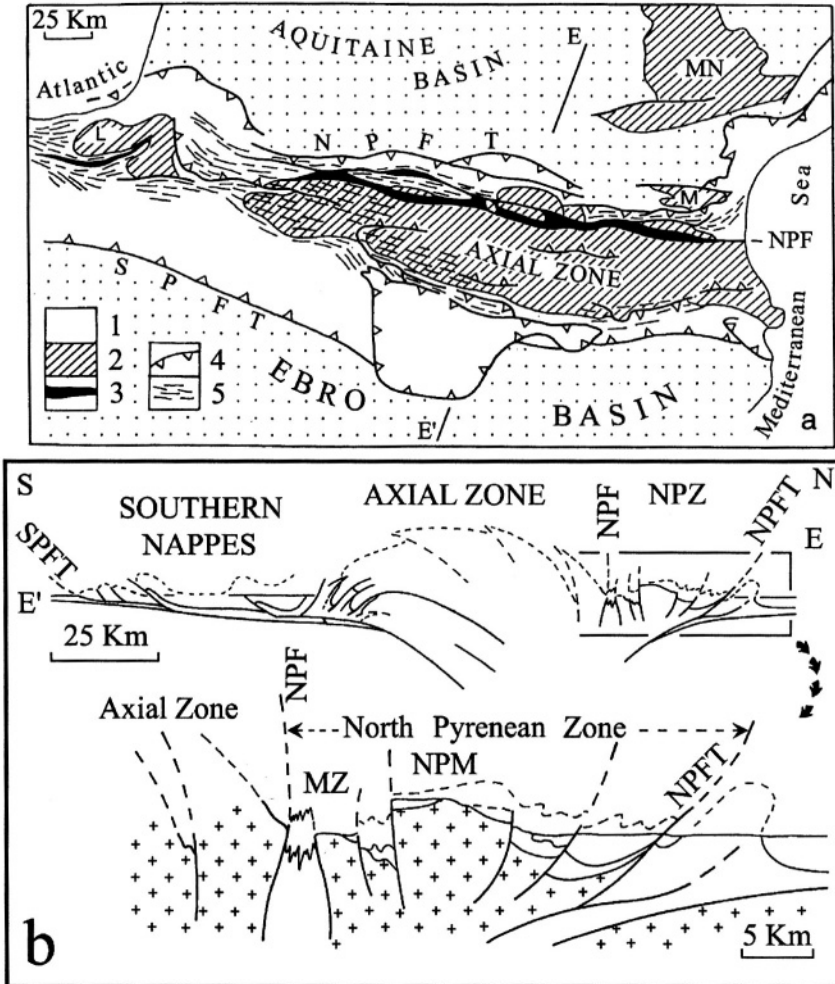


FIG. 110 — The North Pyrenean Zone (NPZ) in the Pyrenees (after Choukroune *et al.*, 1989).

a) Structural plan. The NPZ is squeezed between the North Pyrenean Fault (NPF) and the North Pyrenean Frontal Thrust (NPFT). 1: folded Secondary terrains; 2: Hercynian Massifs (axial zone; L: Labourd; MN: Montagne Noire; M: Mouthoumet); The Hercynian Massifs within the NPZ are the North Pyrenean Massifs (NPM; Castillon, Trois Seigneurs, Arize, and Agly, the easternmost); 3: metamorphic zone; 4: principal thrusts; 5: Cretaceous schistosity. EE' section line of figure 110b.

b) Cross section along EE': above, generalized section; below, detailed cross section of the NPZ; crosses: Hercynian basement; North Pyrenean Massifs (NPM) to the north of the NPZ; MZ: metamorphic zone, limited in this section to the domain located between the NPF and the North Pyrenean Massifs. The limit of schistosity development oversteps the metamorphic front to the north (*cf.* Fig 112).

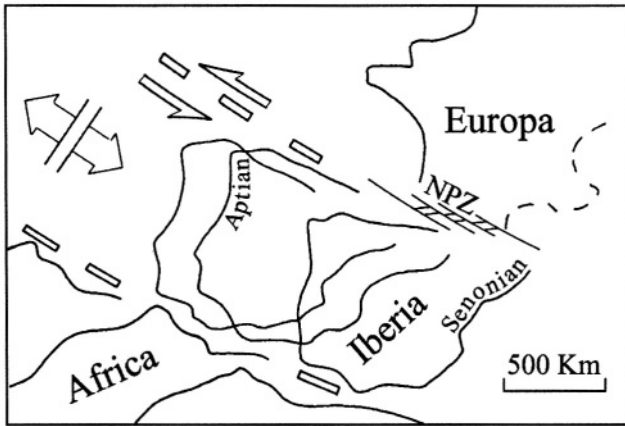


FIG 111 — Place of the future North Pyrenean Zone (NPZ) in the kinematic framework of the opening of the North Atlantic (after Choukroune and Mattauer, 1978; Patriat *et al.*, 1982; and Kornprobst and Vielzeuf, 1984).

The sinistral displacement of Iberia with respect to Europe during the Upper Cretaceous results in the development of a transform zone in a continental domain, and by the formation of secondary lozenge-shaped basins (pull-aparts) in the zones with a high degree of continental and lithospheric thinning. These basins were *ipso facto* the site of significant thermal anomalies.

- 2) the deformation style of the NPZ, the subvertical syn-metamorphic schistositities developed in the Cenomanian, and related intrafolial folds with steeply plunging axes near the NPF (Fig. 112) underlines the sinistral strike-slip character of the deformation.

5.24.4.5 Low pressure metamorphism of the NPZ. The “Pyrenean” metamorphism affects the whole of the secondary series (Triassic to Upper Albian) of the subsidiary basins. K/Ar, $^{39}\text{Ar}/^{40}\text{Ar}$, and Rb/Sr dates indicate that the recrystallization took place between 98 and 87 Ma. From the structural point of view, these metamorphic parageneses preceded, or were contemporaneous with, the principal phase of deformation (D_1) associated with a flow cleavage (S_1). The later deformations (D_2 and D_3) affect the metamorphic assemblages and are only accompanied by minor recrystallization. The pre-kinematic parageneses (**pre- D_1**) give ages between 97 and 91 Ma and the synkinematic parageneses were dated between 95 and 87 Ma. These data indicate that the metamorphism was active when the Upper Albian pelites were just deposited, a situation comparable to that observed at present in the Salton Trough. Amongst other things the spread of the radioactive dates, much greater than their analytic errors, shows that the tectonometamorphic events were not synchronous along the length of the NPZ.

The metamorphic rocks of the NPZ are classed in three lithologic families; carbonate and calcaro-pelitic rocks which are represented by different types of marble, and polytic rocks which occur as dark, finely granoblastic hornfels. The polytic facies display five characteristic mineral assemblages.

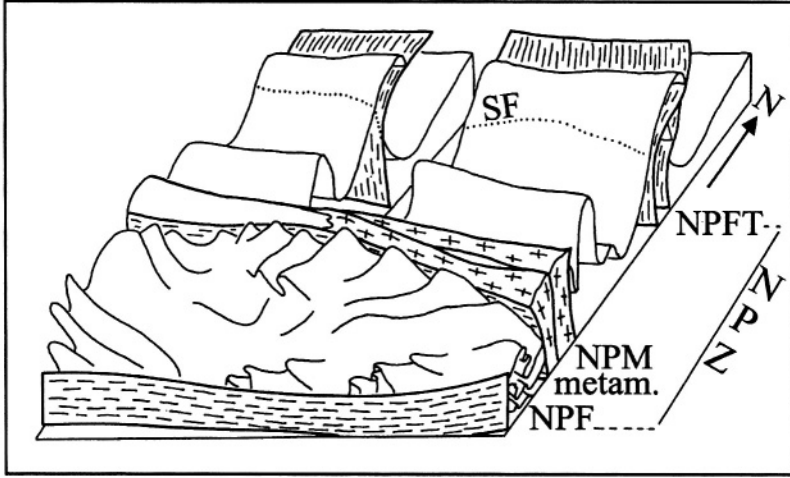


FIG. 112 — Schematic diagram of the deformation style in the NPZ (after Choukroune and Mattauer, 1978).

The unmetamorphosed or weakly metamorphosed domain between the NPM and the NPFT is characterized by flattening and isoclinal folds overturned to the north. The schistosity front (SF) is located in this zone; the metamorphic domain (metam), between the NPM and the NPFT is characterized by complex deformation; the sinistral strike-slip component is marked by drag folds with vertical axes.

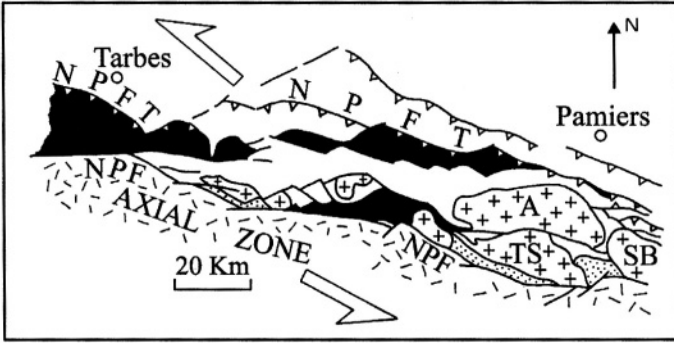


FIG. 113 — Opening of pull-aparts of the North Pyrenean Basin along a sinistral transform fault (after Debros, 1987).

The lozenge shape of the Albo-Cenomanian black flysch of the NPZ is a result of the action of a divergent sinistral strike-slip fault movement. In white : Secondary and Tertiary Basins; in black : Albo-Cenomanian flysch; crosses : North Pyrenean Massifs (A : Arize; TS : Trois Seigneurs; S : Saint Barthélémy), dashes : axial zone; stipple : metamorphic zone.

- 1) bt + ms + chl + ab + qtz
- 2) bt + ms + chl + Kfs + qtz
- 3) bt + ms + crd + Kfs + qtz
- 4) bt + crd + and + Kfs + qtz
- 5) bt + crd + sill + Kfs + qtz

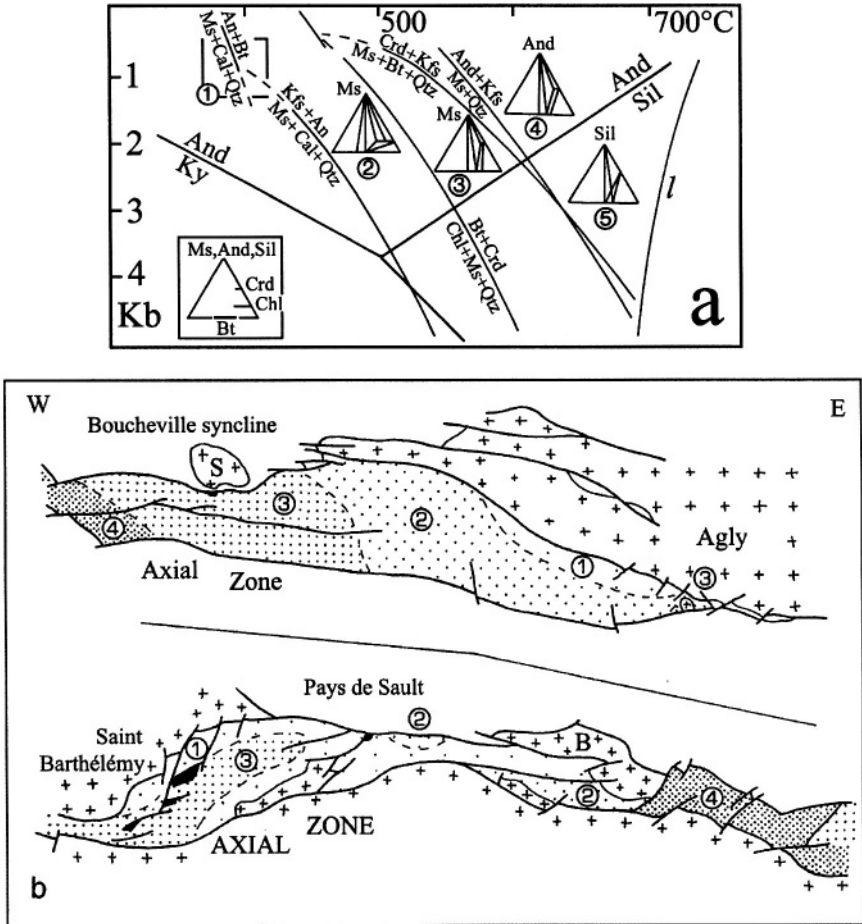


FIG. 114 — *Metamorphic conditions in the North Pyrenean Zone.*

a) The principal mineral assemblages of pelitic rocks in the KFMASH system (after Goldberg and Leyreloup, 1990); the numbers of the subsfacies are used in the text, ms : muscovite; and : andalusite; sil : sillimanite; crd : cordierite; chl : chlorite; bt : biotite; qtz : quartz; cal : calcite; an : anorthite; Kfs : potassium feldspar; l : partial fusion of pelites. Note the low slope of the gradient and the fact that the conditions do not enter into the anatectic domain.

b) Approximate mapping of metamorphic conditions based on pelitic and carbonate assemblages in two segments of the North Pyrenean metamorphic zone. The four metamorphic zones (2 to 5) correspond to conditions of subsfacies 2 to 5 described in Figure 114a. After Goldberg and Leyreloup, (1990) and the data of Ravier (1959) and Bernus-Maury (1984). S : Salvezines Massif; B : Bessède de Sault Massif. Continuous black : outcrops of mantle peridotites. Note the apparent independence of the isograds with respect to the tectonic structures.

These parageneses indicate temperatures between 400 and 650 °C for pressures below 0.3 GPa (Fig 114a), thus a gradient with a very low slope.

The assemblages of carbonate and calcareo-pelitic rocks vary as a function of temperature and fluid-phase CO₂ concentration. The principal stages in the evolution are marked by:

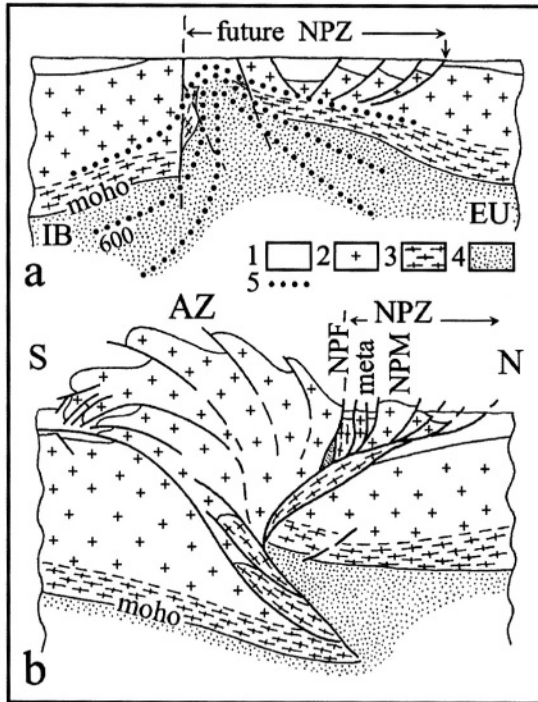


FIG. 115 — Interpretation of the HT-LP metamorphism of the North Pyrenean Zone.

a) “Transtension” in the Upper Cretaceous. The sinistral displacement of Iberia (IB) with respect to Europe (EU) provoked the formation of a series of lozenge-shaped basins (“pull-aparts”) aligned along the break (cf. Fig. 111 and 113). Each of these basins corresponds to significant crustal and lithospheric thinning, as in the case of the Salton Sea. The granulitic lower crust and the upper mantle itself constitute the base of certain basins directly. The thermal anomalies related to these asthenospheric bulges brought the 600 °C isotherm up to the base of the Upper Albian flysch deposits. A slight amount of upper mantle fusion resulted in the emplacement of undersaturated basic magmas in the NPZ. 1 : sediments of Secondary age; 2 : upper continental crust; 3 : lower granulitic crust; 4 : upper mantle; 5 : isotherms. This diagram is a synthesis of the interpretations of Ravier (1959), Azambre and Ravier (1978), Albarède and Michard-Vitrac (1978), Kornprobst *et al.* (1981), Vielzeuf and Kornprobst (1984), Kornprobst and Vielzeuf (1984), Nicolas (1985), Boillot *et al.* (1988), Goldberg and Leyreloup (1990) and Roure and Choukroune (1992).

b) Present structure in the Pyrenees, based on ECORS data (Roure and Choukroune, 1992). Note the structural coherence of the association of the HT-LP metamorphism and the slices of granulite and mantellic peridotite in the NPZ.

- 1) The appearance of tremolite-actinolite, then diopside in the carbonate rocks.
- 2) The appearance of actinolite, garnet, then salite in the calcaro-pelitic rocks.

Scapolite is also present sporadically in these rocks, with Na concentrations proportional to Cl suggesting an evaporitic origin for the protoliths, or sea water circulating during metamorphism. The objective determination of crystallization conditions for these assemblages is delicate; a tentative map of metamorphic zones taking into account partial pressures of CO₂ has been attempted, however (Fig. 114b).

Based on all the available data, there does not appear to be either a clear thermal

gradient observed in the field, or any relationship between calculated temperatures on one side or the extension or depth of the basin on the other (Fig 114b). For this reason it is thought that the heat propagation in the NPZ at the time of metamorphism was essentially produced from superficial discontinuous sources favoured by a convective fluid system which percolated along a fracture network of varying density. The presence of late (syn D₃) prehnite and zeolite veins gives an image of this situation and recalls the schemes elaborated for the Salton Sea.

5.24.4.6 *The NPZ metamorphism and sinistral intracontinental “transform” movement.*

It is clear that the NPZ is associated with a certain number of remarkable characteristics:

- 1) Recrystallization contemporaneous to, or slightly after, sedimentation of the metamorphosed terrains (Upper Albian),
- 2) Temporal imbrication of static and synkinematic recrystallization, at the scale of the NPZ,
- 3) Absence of a regional thermal gradient and very low recrystallization pressures,
- 4) Association of metamorphism to the near-surface emplacement of lithologic units from the deep continental crust (granulites) and the upper lithospheric mantle (peridotites), and
- 5) Metamorphism contemporaneous with discrete alkaline magmatism.

The NPZ allows elaboration of a dynamic model which is close, in its early phases, to that proposed for the Salton Trough and its geothermal field. Extension in transtension is responsible for locally pronounced lithospheric thinning, individualization of rapidly subsiding basins, the site of exceptionally high heat flows. The different basins of the NPZ, opened in a non-synchronous fashion between 98 and 91 Ma, have experienced non-synchronous shortening between 95 and 87 Ma in relation to sinistral shearing. Effectively, in each of the basins, taken individually, the first recrystallization is pre-kinematic, but it is not possible, at the scale of the whole NPZ, to single out clearly an extension phase followed by a compression phase. The basins and their basements were deformed and emplaced in their present position during the final stages of collision between Iberia and Europe (terminal Cretaceous-Eocene: Fig. 115).

The interpretation of the NPZ and of the LP-HT metamorphism that affects the secondary terrains is presented schematically in Figure 115a: an extension in transtension resulted in boudinage of the lithosphere, and the gravitational rise of the high-temperature, ductile upper mantle. The Eocene shortening of the system led to the extrusion, toward the surface, of elements of the lithospheric mantle located below the subsiding basins, and a structure comparable to that which is exposed in the NPZ (Fig. 115b).

It is interesting to note that the tectonometamorphic events recorded in the Upper Cretaceous in the NPZ fit the global dynamics of the entire Alpine Chain. In effect, the transform movement related to the opening of the North Atlantic which resulted in the slip of Iberia along the NPZ, had a corollary in the closing of the Tethyan ocean basin of the Ligurian Zone. The LP-HT metamorphism of the NPZ is chronologically and dynamically associated to the HP-LT metamorphism of the Internal Zone of the Alps, which resulted from the subduction or obduction of oceanic crust and marginal units.

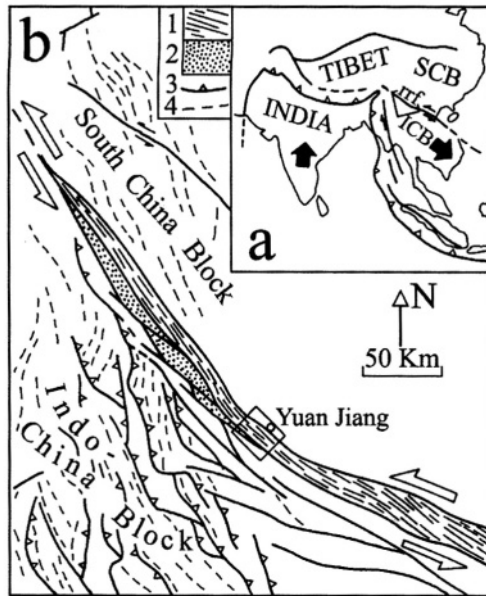


FIG. 116— *The sinistral strike-slip displacement of the Red River fault and the Ailao Shan shear Zone (after Tapponnier et al., 1990)*

a) Location of the Red River fault (rrf) in the kinematic model of Southeast Asia. ICB : Indo-China block; SCB : South China Block. The square locates Figure 116b.

b) The sinistral Ailao Shan shear zone in the context of post-Cretaceous tectonics of Yunnan Province. 1 : high temperature Ailao Shan unit; 2 : weakly metamorphosed schistose series; 3 : thrusts; 4 : axial traces of anticlines. The square gives the location of Figure 117.

5.25 The role of friction:

HT-LP gradients and continental shear zones

Mechanical heat production by friction along a tectonic contact is sometimes considered an important factor in the establishment of HT-LP metamorphic gradients. The Red River fault zone or Ailao Shan-Red River shear zone in Southeast Asia is a particularly representative case of this idea. This shear zone is a gigantic sinistral strike-slip fault which accommodated the eastward displacement of Indo-China as a result of the Indo-Eurasian collision (Fig 116). A high-temperature low-pressure metamorphism is associated with this break, both structurally and chronologically.

- 1) The synkinematic high temperature parageneses are controlled by a horizontal stretching lineation parallel to the shear plane,
- 2) Veins of late-kinematic leucogranite injected in these formations were dated 23 ± 0.2 Ma by U-Pb on monazite.

5.25.1 High temperature gneiss

The Ailao Shan gneiss forms in a corridor parallel to the strike-slip fault, within weakly to unmetamorphosed formations. It is essentially a partly migmatized metapelitic complex, and includes amphibolites, “skarnoids” (hedenbergite-grossularite-carbonate pyroxenites)

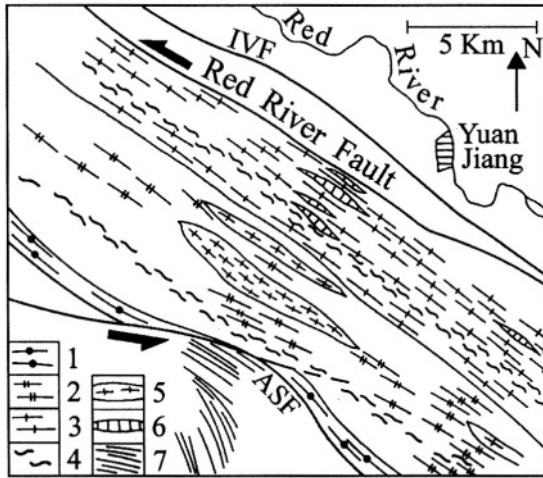
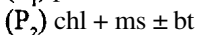
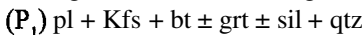


FIG. 117 — *Simplified geological map of a segment of the Ailao Shan shear zone (after Leloup and Kienast, 1993).*

The high temperature metamorphic domain (Ailao Shan gneiss; 1 : garnet gneiss; 2 : andalusite-sillimanite gneiss; 3 : sillimanite gneiss; 4 : migmatite; 5 : granitoid intrusions; 6 : marble) forms a corridor through non-metamorphosed to weakly metamorphosed formations (7 : greenschists). This corridor was subjected to sinistral shear during metamorphism (black arrows). The faults (Red River normal strike-slip fault and IVF, intermediate valley fault) are still active, but have a dextral sense of movement. ASF : Ailao Shan Fault.

and marbles. The entire mass was injected by leucogranitic bodies (Fig. 117). The metapelites contain high temperature (P_1) as well as retrograde (P_2) assemblages which were developed in a heterogeneous fashion during the exhumation of the units.



The crystallization conditions deduced for these assemblages (from $\text{grt} + \text{bt}$; $\text{sil} + \text{pl} + \text{qtz}$; $\text{bt} + \text{ms} + \text{chl}$ equilibria) are 4.5 ± 1.5 kb and 710 ± 70 °C for P_1 and on the order of 4 kb at 500 °C for P_2 (Fig. 118). These conditions reflect a strongly perturbed gradient along the shear zone (45 °C per km, approximately).

5.25.2 Shearing and high temperature

The studied region has not undergone significant crustal thickening, the high temperatures expressed by the Ailao Shan gneiss are not, therefore, inherited from an earlier equilibrium at the base of the thickened crust as in the case of the Montagne Noire. This fact, as well as the synchronism between granitoid emplacement, migmatization and strike-slip movement indicate a probable link between shearing and heat production. This hypothesis leads, nevertheless, to a paradox already pointed out; heat production by friction results in a reduction of viscosity to the materials affected by shear, which then can deform much more easily and rapidly. The shear stress τ decreases and the heat production $V\tau$ is strongly reduced. It appears therefore improbable that friction along a tectonic break could lead to great increases in temperature - with respect to the regional gradient - in the formations affected by the break. A numeric model is proposed in Figure 119, which shows clearly

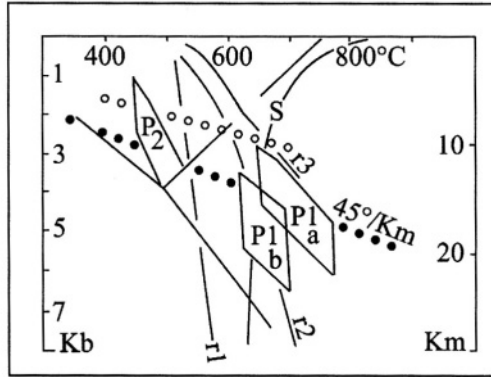


FIG. 118 — *Crystallization conditions in the Ailao Shan gneiss* (after Leloup and Kienast, 1993).

P₁a and P₁b : primary metapelite assemblages. P₂ : retrograde assemblages; black dotted line : supposed prograde gradient; white dotted line : prograde HT-LP gradient of the Agly and Montagne Noire metapelites; S : solidus of hydrous granite; r₁ : Chl + Ms = St + Bt + Qtz; r₂ : St + Kfs = Grt + Bt + Sil; r₃ : Bt + Sil = Grt + Crd + Kfs.

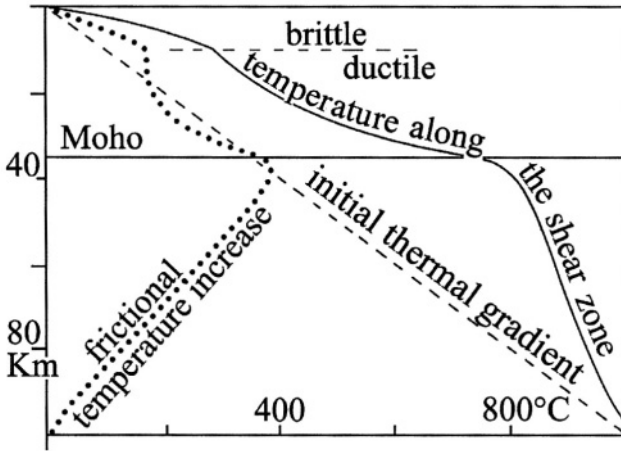


FIG. 119 — *Model of the temperature profile of the Ailao Shan shear zone. Numerical simulation* (after Leloup and Kienast, 1993).

The continental crust is represented by a layer of granite 35 km thick; the upper lithospheric mantle is represented by a dunite layer 65 km thick. The lateral displacement is 3.3 cm per year, the shear stress τ depends on the temperature and the brittle-ductile nature of the milieu. At 20 km depth the model indicates a temperature on the order of 400 °C, clearly below that calculated (700 °C) from the assemblages. The mechanical heat production along the shear zone is therefore insufficient to explain the Ailao Shan gneiss without invoking vertical heat transfer from the lower crust.

that the temperature profile around the shear does not rise, for a given depth, to the values drawn from the study of mineral assemblages.

5.25.3 *Frictional heat and vertical transfer*

A major fault such as the Red River fault, affects, without doubt, the whole thickness of the lithosphere. The rigid lithospheric mantle is therefore probably the site of a large frictional heat production along the fault (Fig. 119). This heat, partly transferred by conduction toward the base of the ductile continental crust, causes partial fusion. The granitoids thus produced and transported toward the surface of the break, are the carriers of vertical heat transfer, which account for the elevated temperature at shallow depths observed in the gneiss and migmatite.

Thus only the frictional heat production mechanism is not enough to explain the HT-LP gradient of the Red River zone completely, but it nevertheless is a determining factor in the establishment of this gradient.

METAMORPHISM UNDER EXTREME CONDITIONS

In all the cases examined above, the metamorphic units were buried to depths which, even in the case of subduction, did not exceed 70 km, for a load pressure of the order of 2 GPa. There are, however, cases which show that segments of the continental crust, or more generally the crust or oceanic lithosphere, attained much greater depths before arriving back to the surface by various exhumation mechanisms. These units contain assemblages characterized by very high pressure mineral species, such as coesite (SiO_2), or even diamond.

5.26 **Coesite-bearing crustal units: example of the Dora Maira massif**

In the example of Dalradian metamorphism at intermediate pressure, it was noted that the insertion of a continental wedge into the subduction zone results in decoupling of the low density crustal units which do not accompany the lithospheric mantle down the subduction zone (Fig. 82). The Dora Maira massif in the western Alps (Fig. 74) shows that this behaviour is not always the case.

5.26.1 *Dora Maira Massif: European continental margin*

The Dora Maura Massif is one of the principal internal crystalline massifs in the Alps. Its middle part contains, from bottom to top, the following units in superposition (Fig. 120):

- 1) the unit called "Pinerolo" constituted of detrital Carboniferous terrains,
- 2) a composite unit called "polymetamorphic" containing Hercynian granitoids (300 Ma) injected in an older metamorphic series, and
- 3) a unit called "Upper Paleozoic" composed of Permo-Carboniferous and Permo-Triassic terrains injected by acid rocks and associated with slices of polymetamorphic material comparable to those of the unit with the same name.

All these terrains contain metabasaltic intercalations. Taking into account their age, their nature and their structural situation, it is conceded that these units constitute all or part of the eastern continental margin of Europe before the Alpine collision (Fig. 76).

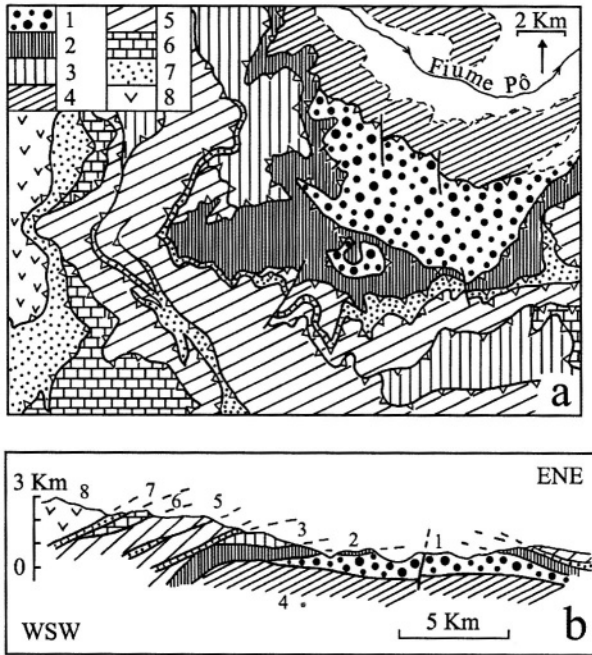


FIG. 120 — *Structural distribution of the continental units of the Dora Maira Massif (simplified from Chopin et al., 1991).*

- a) Map of the units. For the location of the Dora Maira Massif see Figure 74. Polymetamorphic group : coesite unit (1); cold eclogite unit (2); upper metapelitic units (3). Lower Pinerolo unit (4); Upper Paleozoic unit (5); lustrous schists (6 and 7); Monviso ophiolite (8).
- b) Schematic cross section. Same legend and in (a).

5.26.2 The coesite-bearing unit: VHP prograde gradient

The materials of the units enumerated above were metamorphosed during the Alpine Orogeny. Uniformly affected by a late regional foliation parallel to the lithology and to tectonic contacts, they were mostly recrystallized under greenschist facies conditions. There are, however, in each of the units, relic high pressure assemblages from before the development of this schistosity.

5.26.2.1 *Pinerolo Unit.* The crystallization conditions did not go beyond those of the epidote-blueschist facies (8-10 kb; 500 °C).

5.26.2.2 *Polymetamorphic Unit.* Two imbricate slices, very different from the point of view of peak metamorphic conditions, have been distinguished in this unit.

- 1) the lower “coesite-bearing” unit is characterized by the following relic assemblages, respectively, in the metapelites and metabasalts
 phengite + talc + kyanite + pyrope + jadeite ± coesite ± quartz
 omphacite + garnet + kyanite + phengite + rutile ± coesite ± quartz

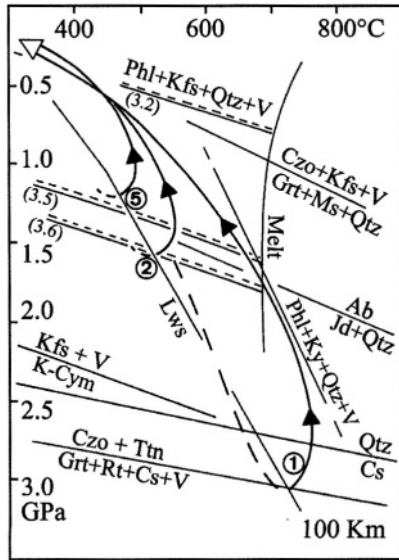


FIG. 121 — *P-T-t* paths of the continental metapelitic units of the Dora Maira Massif (after Chopin *et al.*, 1991).

Coesite (1) and cold eclogite (2) units of the polymetamorphic group; Upper Paleozoic units (5). The numbers are located on the structural cross section of Figure 120. The HP-LT gradients are identical to those characterizing the Franciscan units of oceanic cycles (*cf.* Fig. 75). Phl : phlogopite; Kfs : potassium feldspar; Qtz : quartz; Czo : clinozoisite; Grt : garnet; Ms : muscovite; Ab : albite; Jd : jadeite; Lws : lawsonite; Ky : kyanite; Cs : coesite; Ttn : titanite; Rt : rutile; V : vapour. The numbers in brackets indicate the number of atoms of Si in the structural formula of the phengite in equilibrium with Kfs, Qtz and V.

The pyrope garnet contains up to 98% of the magnesium molecule $Mg_3Al_2Si_3O_{12}$. The coesite is generally recrystallized to quartz (which, however, displays a very particular crystal habit); it persists sometimes in inclusions in garnet or kyanite. The onset of polymorphic transformation into quartz is accompanied by a large volume change in the inclusion and by the development of radial fractures in the host mineral (Fig. 122). Peak crystallization conditions of this “coesite-bearing” unit are estimated at 30 kb for 700 to 750 °C (Fig. 121).

- 2) The upper unit with “cold eclogites” show assemblages of:
- kyanite + chlorite + chloritoid + quartz
 - chloritoid + garnet + talc + quartz
 - paragonite + omphacite + garnet + quartz

The SiO_2 phase is always quartz and never shows the crystal habit noted in the coesite-bearing rocks. Peak metamorphic conditions evaluated for these assemblages are 15 kb and 550 °C (Fig. 121).

5.26.2.3 Upper Paleozoic Unit. This contains glaucophane and kyanite bearing assemblages corresponding to pressures of 10 to 12 kb at around 550 °C (Fig. 121).



FIG. 122—Polymorphic transformation coesite \Rightarrow quartz in the polymetamorphic unit of the Dora Maira Massif (from a photograph in Chopin *et al.*, 1984). The coesite (Cs) which survives in inclusions in garnet is partly transformed into quartz (Qtz). The positive change in molar volume which results from this transformation bursts the garnet host creating a network of radial fractures around the inclusion. Scale is 100 μm .

5.26.3 Dora Maira: a continental margin subducted to great depth

Clearly the diverse continental units of the southern portion of the Dora Maira Massif display mineral assemblages which result from burial along a HP-LT metamorphic gradient typical of subduction gradients generally observed in units derived from oceanic lithosphere. One of the units implicated in this subduction even recrystallized under the particularly severe conditions of the “coesite-eclogite facies” demonstrating the possibility of burial of crustal units to very great depths (about 100 km). It is undoubtedly not an isolated case, because coesite-eclogites are known from several other occurrences (in the Norwegian Caledonides or North China, for example) some of which even involve the formation of diamond.

The form of the retrograde gradients deduced for the recrystallization of the high pressure assemblages (Fig. 121) suggests rapid tectonic exhumation, probably related to the first stages of collision, rather than a late isostatic re-equilibration.

5.27 Diamond-bearing crustal units

The presence of diamond, the high-pressure form of carbon (cf Fig. 123) in metamorphic rocks of the continental crust was noted for the first time in the Kokchetav massif (Republic of Kazakhstan). This metamorphic unit, of Proterozoic age, belongs to the Caledonian Ural-Mongolia chain, a major collisional zone of the Asiatic continent.

The diamonds, in idiomorphic cubo-octahedral crystals, are seen in inclusions (10-20 μm) in zircons and garnets in pyroxenites, gneiss and schist, occurring in elongate lenses within a plagioclase-rich gneiss. The diamond is partly replaced by graphite and, curiously, closely associated with biotite. Based on a number of morphological arguments, a pre-metamorphic, detrital origin is rejected. As well, the relatively light carbon isotope ratios (*cf.* below) favour a crustal, rather than mantellic, origin for the carbon (although this isotopic argumentation is controversial at present). The growth of diamond in the crustal

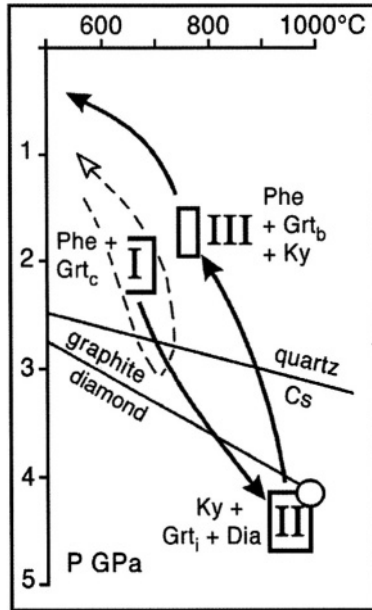
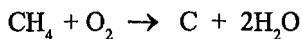


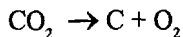
FIG. 123 —Crystallization conditions of diamond-bearing crustal units (modified after Massonne, 1999).

The peak metamorphic conditions culminated around 4 GPa and 1000°C for diamond units in Kokchetav (circle; after Sobolev and Shatsky, 1990) and for the Erzgebirge (phase II). The P-T-t path of the Erzgebirge (I, II, III) is traced by mineral assemblages and the composition of successive garnet growth zones (c core; i intermediate; b border). The absence of coesite relics is notable, both at Kochetav and the Erzgebirge (the presence of quartz pseudomorphs of coesite is described by Schmädacke 1991, but questioned by Massonne, 1992). For comparison, the P-T-t path of the crustal units of the Dora Maira is added to the figure (dashed lines).

rocks is attributed to two original processes of prograde carbon crystallization from a hydrocarbon-bearing fluid; 1) at increasing pressure the solubility of C decreases in the fluid phase and carbon (graphite or diamond, depending on the pressure) precipitates from solution; 2) the oxidation of a methane-rich fluid results in precipitation of graphite or diamond depending on the value of P or fO_2 .



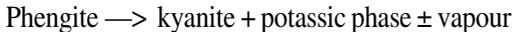
Carbon may also have precipitated from a CO_2 -rich fluid phase, according to the reaction:



The crystallization conditions of the diamond-bearing units was evaluated at 4GPa and 1000°C (Fig. 123).

After the diamonds were described from Kokchetav, a series of analogous discoveries were made, for example in China (Dabie Shan) and Norway (western gneiss region), but the most remarkable locality, without question, is that of the “gneiss and eclogite (GEU) unit” of the Erzgebirge in Saxony (Germany). The careful study of this unit, in effect, allows the characterization of the prograde and retrograde evolution of diamond-bearing rocks in a detailed manner.

These units are Variscan ortho- and paragneiss containing elongate lenses of garnet peridotite and eclogite, an association totally comparable to the Hercynian retrograde units of the French Massif Central (*cf.* Fig. 83). The parageneses of the gneiss consist of potassic white mica (phengite) and quartz matrix in which relatively large (1–4 mm) garnets are dispersed. These garnets have the particularity of being chemically zoned; the core and periphery of the crystals are relatively rich in Ca, whereas the intermediate zone is less calcic and more magnesian. The striking feature is that the idiomorphic diamond inclusions (1 to 25 μm), and their graphite pseudomorphs, occur exclusively in the intermediate zone of the garnet (as well as in zircon crystals). This intermediate zone also contains inclusions which could have been derived from kyanite, associated with a potassic phase as yet unidentified, whereas the core and the periphery of the garnet contains only phengite inclusions. Based on these observations (in particular the Si^{4+} concentration of the phengite: *cf.* Appendix III) three metamorphic phases are distinguished (Fig. 123); 1) a first phase (characterized by the garnet cores and their inclusions) formed at crystallization conditions around 700°C and 2.0 GPa, comparable to the subduction gradient which affected the coesite-bearing units of the Dora Maira; 2) a second phase (intermediate garnet zone) corresponding to a “dramatic” pressure increase which attained at least 4 Gpa, at a temperature of 1000°C; 3) a third, retrograde, phase (fine-grained matrix and the outer zone of the garnet) resulting from a re-equilibration between 1.5 and 2.0 GPa at about 750°C. The passage from phase I to phase II is probably marked by the destabilization of phengite following the reaction:



The phengite reappears during phase III in equilibrium with kyanite. Curiously no relic of coesite was clearly identified although the garnet contains quartz inclusions.

The prograde and retrograde gradients have trajectories which are close in P-T space, which suggests rapid exhumation of the high pressure units after their burial. In effect, such crustal materials relatively rich in radioactive elements, and held for a long time at depth, would have been characterized by a significant heat accumulation resulting in a marked loop toward high temperature on the retrograde path. The geodynamic mechanisms associated with deep subduction of crustal material are not yet clearly explained.

5.28 Mantle eclogites: recycled oceanic lithosphere?

The development of high pressure and low temperature facies (lawsonite and glaucophane schists, eclogites), in metabasites of the Franciscan Series, illustrates well the evolution of the oceanic crust and formations of the accretionary prism at the start of subduction (up to 50 or 60 km depth, in general). It must be realized that only a small portion of the oceanic lithosphere is exhumed tectonically or obducted on the continental margin. The lithospheric mantle involved in subduction flows to depth in the upper mantle dragging along with it a considerable part of the oceanic crust (Fig. 90). It is interesting to speculate as to what becomes of these units.

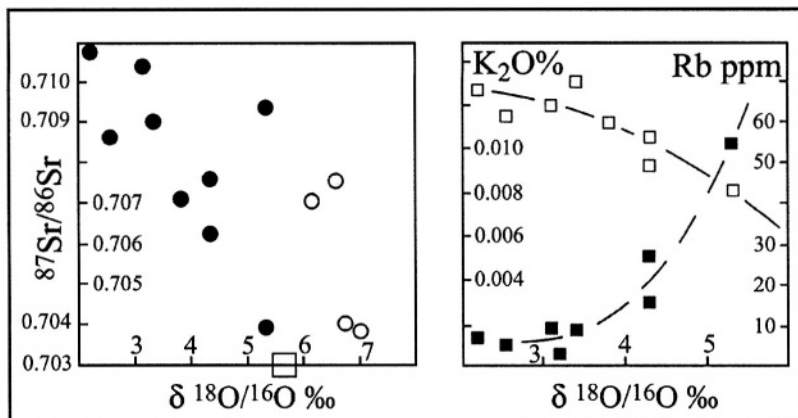


FIG. 124 — *Pre-eclogitization of the hydrothermal alteration in the garnet pyroxenites of "Roberts Victor" Mine* (after MacGregor and Manton, 1986).

a) Co-variation of $\delta^{18}\text{O}$ vs. $^{87}\text{Sr}/^{86}\text{Sr}$. The mantle values (5.7‰ and 0.708) are represented by empty square. A population of pyroxenites (type II, black circles) shows a linear variation toward low values of $\delta^{18}\text{O}$: this is the behaviour of hydrothermally altered basalts of the oceanic crust. Another population (type I, open circles) shows, in contrast, $\delta^{18}\text{O}$ values above mantle values, the habitual behaviour of gabbros.

b) Co-variation of Rb (ppm; scale at right) and K_2O (weight %; scale at left, values calculated from the mode and composition of clinopyroxenes and garnets) as a function of $\delta^{18}\text{O}$ for type II pyroxenites; the decrease in value of $\delta^{18}\text{O}$ is accompanied by a leaching of Rb and an enrichment in K_2O , the habitual behaviour of basalts in the oceanic crust.

5.28.1 Mafic enclaves in kimberlites and alkali basalts: evidence of ocean engulfed in the mantle?

The explosive nature of the emplacement of kimberlites and certain alkali basalts (maars and diatremes) allows fragments of their deep source to be brought to surface in the form of xenoliths. These fragments are principally composed of peridotite, but large quantities of garnet pyroxenite or eclogite occur in certain occurrences.

5.28.1.1 *Eclogites of the upper mantle: High pressure fractional crystallization of basaltic liquid.* The garnet pyroxenites from the upper mantle are commonly considered to be the result of fractionation of clinopyroxene and garnet, high pressure primary phases, at the liquidus of basaltic magmas, produced by partial fusion of mantle peridotites. In this hypothesis of "eclogitic fractionation" garnet pyroxenites are igneous cumulates which evolved into a granoblastic texture by annealing. To emphasize their origin, considered non-metamorphic, these eclogite are often called "griquaites".

Garnet pyroxenites of "Roberts Victor" and the Colorado Plateau: Sea water contamination! Diverse populations of garnet pyroxenites show petrological and geochemical characteristics which refute the hypothesis of direct crystallization from a basaltic liquid at depth.

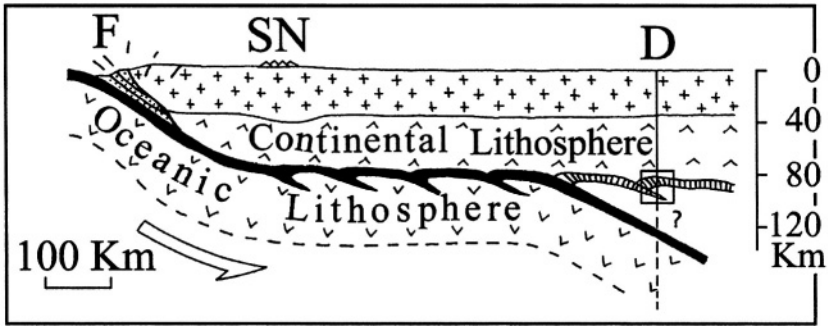


FIG. 125 — *Eclogites from the Pacific oceanic crust in the diatremes of the Colorado Plateau* (modified from Helmstaedt and Schultze, 1988).

The diatremes (D) contain xenoliths derived from an oceanic crust crystallized under Franciscan gradient conditions and stored around 80 km depth below the Colorado Plateau (inset square). These enclaves must be fragments of the oceanic crust of the Pacific Ocean subducted below the North American Plate. During the sampling, however, 25 or 30 Ma ago, the diatremes were located about 900 km from the continental margin. It is therefore necessary to imagine “creep” of the subducted lithosphere below the continental lithosphere by tectonic imbrication, in order to justify the presence of eclogite immediately below the diatremes. This mechanism is not clearly understood, but is supported by geochemical arguments (Livacarrì and Perry, 1993) who show that the oceanic lithosphere is immediately below the continental lithosphere up to 750 km from the margin. It is not supported by the seismic tomography models presently available. F : Franciscan units of the Coastal Ranges; SN : calc-alkaline magmatism of the Sierra Nevada.

The Roberts Victor Mine, South Africa Kimberlites from this locality contain a large quantity of garnet pyroxenites, with slightly deformed granoblastic assemblages of the two minerals. These rocks have interesting geochemical characteristics: the isotopic ratios of strontium and oxygen are very variable, and, in a general way, are very far removed from mantle values (Fig. 124). Amongst other things, these ratios may be correlated with characteristics of certain mobile elements such as K and Rb. This behaviour is interpreted as proof that this population of enclaves comes from an ancient oceanic crust, contaminated by hydrothermal circulation at the ocean-lithosphere interface (Fig. 98). This oceanic crust was subducted in the Archean, during which time the basalts and gabbros were altered and converted to eclogites. They constitute a layer of unknown dimension at the base of the lithospheric mantle in South Africa (at around 180 km depth).

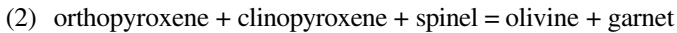
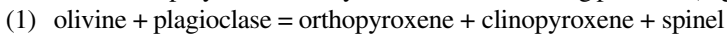
The Colorado Plateau. A large number of localities in the Colorado Plateau (Western USA) have explosive volcanic structures (diatremes) which resemble kimberlite pipes. These breccia diatremes contain diverse types of high pressure xenoliths; omphacite eclogites, jadeite clinopyroxenites, lawsonite and chlorite eclogites. These rocks crystallized at low temperature (550 to 700 °C) at pressures on the order of 25 kb. These are the conditions of a prograde subduction gradient (Fig. 73 and 75). The persistence of lawsonite in certain assemblages clearly necessitates this type of HP-LT gradient (Fig. 75). Amongst other things, the chemical composition of the rocks indicates that, as in the case of the Roberts Victor xenoliths, they were variably altered by hydrothermal solutions before undergoing

HP-LT metamorphism. This enclave population is considered to be the result of recrystallization of the oceanic crust of the Pacific ocean along the subduction which is still in operation on the west coast of the North American continent and which was responsible for the Franciscan Series *sensu stricto*. This idea is acceptable for geometric reasons, only in the hypothesis of slicing up of the lithosphere into tectonic imbrications, allowing it to creep under the North American continent. In fact, at the moment of their emplacement, 30 Ma ago, these diatremes were located 900 km from the continental margin (Fig 125). This model thus envisages the formation of a layer of metamorphic oceanic crust at the lithosphere-asthenosphere interface under the North American Plate.

5.28.2 Convective circulation of the oceanic lithosphere

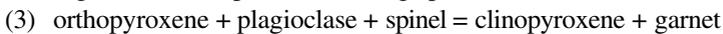
The enclaves in alkali basalts and kimberlites yield valuable information on the storage of fragments of older oceanic crust at certain levels of the upper mantle. The ultramafic mantle massifs emplaced at plate limits during orogenies (“orogenic peridotites”) bring, for their part, dynamic arguments significant to the comprehension of recycling processes of the oceanic lithosphere in the upper mantle.

5.28.2.1 Barometry and thermometry of the upper mantle. The lithosphere is essentially composed of peridotites (about 95%), gabbros and pyroxenites. The peridotites contain magnesium-rich parageneses composed of three principal minerals: olivine (70%), orthopyroxene (20%) and clinopyroxene (5%). The following minerals may be added to these: plagioclase, spinel and garnet. Even though present in only small quantities, these aluminous minerals have an important barometric significance because the following mineral reactions come into play successively as a function of rising pressure (Fig. 126).



These reactions result in the development of mineral assemblages for which the density increases as a function of depth: plagioclase, spinel or garnet peridotites.

The pyroxenites associated with the peridotites are olivine-poor or olivine-absent. Their assemblages commonly include plagioclase, spinel or garnet. The following reaction signals the change from a low pressure to a high pressure association.



The minerals of the peridotites and pyroxenites are not pure phases but complex solid solutions. The distribution of certain elements, notably iron and magnesium, within the solid solutions allows utilization of divariant equilibria, which are fairly good geothermometers or geothermobarometers (olivine-spinel, orthopyroxene-clinopyroxene, orthopyroxene-garnet, clinopyroxene-garnet). From all of these reactions and the mineral assemblages that they concern, the barometry and thermometry of the upper mantle are well-controlled up to a hundred kilometre depth. The mantle phases which crystallize at very high pressures are generally not preserved at surface, with the notable exception of diamond.

5.28.2.2 Orogenic peridotite: low temperature prograde and high temperature retrograde massifs.. The petrological study of ultramafic massifs of mantle origin show there are two broad categories.

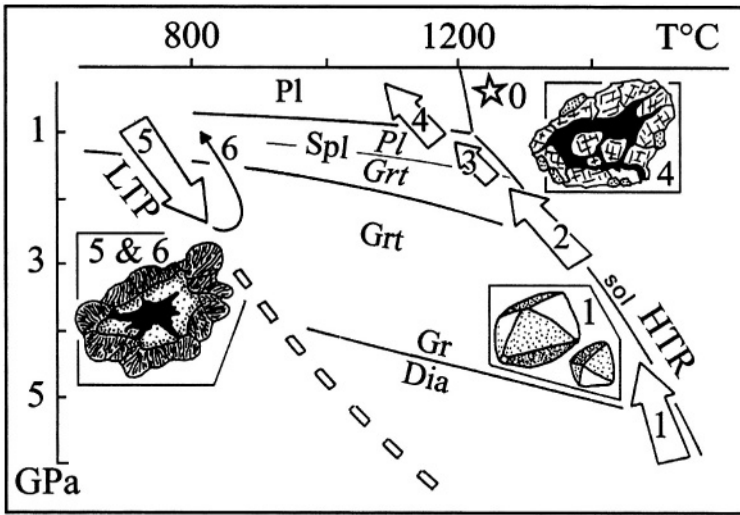


FIG. 126 — “HT retrograde” or “LT prograde” behaviour of ultramafic massifs: convective circulation of the oceanic lithosphere (after Kornprobst, 1992).

At high temperature: solid-state rise of ductile upper mantle in extension zones (HT retrograde massifs : HTR), the example of the Betic-Rifian massifs; 1 : diamond-graphite transition (Dia-Gr); the inset shows graphite pseudomorphs of diamond; 2 : garnet peridotite \Rightarrow spinel peridotite transition (Grt-Spl); 3 : garnet pyroxenite \Rightarrow plagioclase pyroxenite transition (Grt-Pl); 4 : spinel peridotite \Rightarrow plagioclase peridotite (Spl-Pl); the inset shows residual chromiferous spinel after retrograde plagioclase and olivine crystallization.

At low temperature: slab of oceanic lithosphere being subducted (LT prograde massifs : LTP); 5 : spinel peridotite \Rightarrow garnet peridotite transition; the inset shows residual chromiferous spinel after crystallization of prograde garnet; 6 : complex coronitic reactions ($\text{Opx} + \text{Cpx} + \text{Spl} \pm \text{Ol} \pm \text{Pl} \pm \text{amphibole}$) linked to tectono-isostatic decompression. The star indicates stage 0 of the evolution of certain corundum eclogites of the Beni-Bousera massif, having crystallized initially at low pressure as gabbros. These rocks apparently followed a prograde LTP trajectory before being exhumed taking the HTR retrograde path. sol : “dry” solidus of upper mantle peridotites.

Low temperature prograde massifs. These are observed in numerous orogens, generally associated with low temperature and high pressure units and their relics. They represent fragments of oceanic lithosphere which initially went down a subduction zone. The reactions observed in these peridotites are simply those of a rise in pressure.

spinel peridotite \Rightarrow garnet peridotite

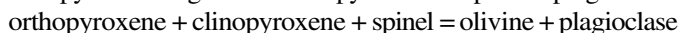
The geometric relation between residual spinel and neofomed garnet show clearly the prograde play of the reaction. Basic intercalations in the peridotites (former gabbros?) are now garnet pyroxenites or eclogites. The P-T crystallization conditions are comparable to those of high temperature eclogites of the Franciscan or Dalradian series (Fig. 83).

The subduction of these ultramafic units, however, failed, and they were brought back up to the surface by tectono-isostatic mechanisms. The garnet destabilized and complex spinel-plagioclase coronites developed at grain boundaries, recording the successive operation of reactions (1), (2) and (3) in the sense of lowering pressure. These prograde

massifs nevertheless show the petrographic expression of the reintroduction of oceanic lithospheric mantle into the convective system of the upper mantle, in agreement with seismic tomography.

High temperature retrograde massifs. These were emplaced in extension zones; and a high degree of lithospheric and crustal thinning allowed the deep domains of the subcontinental lithosphere or asthenosphere to rise toward the surface (*cf.* Fig. 108 and 115). The Zabargad Massif (Red Sea) as well as the abyssal Galician Margin Massif (Spain) are still in the same structural situation in which they were emplaced. Other massifs : Lherz (NPZ), Lanzo (internal zone of the Alps) Ronda and Beni Bousera (Betico-Rifean Chain), for example, have undergone post-extension compression (Fig. 115) and thrusts, which, however, left the mineralogical and structural characteristics acquired by the massifs during their early emplacement almost intact.

The example of the Betico-Rifean ultramafic massifs (Ronda and Beni Bousera) is particularly characteristic. The peridotites and pyroxenites have undergone the following reactions in a heterogeneous fashion:



Also certain garnet pyroxenites of the Beni Bousera Massif contain "pseudomorphs" of diamond converted to graphite. Taken together, these two massifs show the effects of decompression close to 50 kb, or in other words a rise from depths of over 150 km.

The temperature calculated from opx-cpx and ol-spl equilibria in the peridotites is around 900 °C. Temperatures deduced from the cpx-grt equilibrium in certain pyroxenites are much higher - around 1300 °C. Are these realistic temperatures? Two arguments favour a positive response to the question.

- 1) The dynamic behaviour of these massifs, as well as the structures and textures of the rocks suggest a plastic deformation during emplacement requiring high temperatures (> 1000 °C).
- 2) The massifs developed a contact metamorphism in their wall rocks during emplacement. The temperatures attained in the metapelites were on the order of 800 °C. By accepting the conditions defined above (infinite wall rocks with respect to the intrusion) and considering the massifs as sheets, it is possible to calculate:

$$T_0 = 2T_c - \tau$$

For τ , initial temperature of the wall rocks between 100 and 400 °C, the emplacement temperatures are between 1500 and 1200 °C. If the massifs are considered spheres (a shape closer to the diapiric model), even higher emplacement temperatures are obtained.

All of the observations suggest that the massifs are emplaced at higher temperature than their present surroundings from a depth of at least 150 km (Fig. 126).

Contamination of high temperature retrograde massifs: convective circulation in the oceanic lithosphere. The emplacement conditions of the retrograde massifs emphasize an origin from relatively deep within the upper mantle and a rising P-T-t path during their recent history. Certain high pressure and high temperature assemblages of these massifs show geochemical characteristics, however, emphasizing their close affinities to oceanic

lithosphere, contaminated or not, by hydrothermal solutions of surface origin.

Considering, as before, the massifs of the Betico-Rifean chain, the following points may be emphasized:

- 1) The peridotite assemblages crystallized under conditions of low oxygen fugacity ($\Delta QFM = 0$ to -2) a characteristic typical of the oceanic lithosphere with respect to the continental lithosphere.
- 2) Certain garnet-corundum pyroxenites display geochemical characteristics (high Sr concentrations, low heavy rare earth concentrations, europium anomalies) typical of plagioclase-bearing rock; they are former gabbros, originally crystallized at low pressure.
- 3) Numerous garnet pyroxenites have Sr and Pb isotopic ratios as well as $\delta^{18}O$ which are very different from typical mantle values, and agree with a crustal or oceanic contamination before the crystallization of the high pressure assemblages.
- 4) The diamonds converted to graphite have carbon isotope ratios close to the organic components of sediment ($-25 < \delta^{13}C < 15$, the mantle value is in the neighbourhood of -7).

These observations suggest that the high temperature retrograde massifs represent segments of the oceanic lithosphere recycled in the upper mantle. These units would rise to the surface thanks to extension tectonics after a stay of variable length in the upper mantle, probably at the base of the lithosphere. In this hypothesis the low temperature prograde massifs illustrate the descending branch of the mantle convection, whereas the HT retrograde massifs envisage the rising branch (Fig. 126)

5.28.3 *The upper mantle: marble cake or plum pudding?*

The preceding observations show that the slab of oceanic lithospheric mantle descending along a subduction zone, drags along a significant part of the oceanic crust, as well as diverse contaminants from the continental crust or of supergene origin collected at the sediment-lithosphere or sea water-lithosphere interface. The convective upper mantle (asthenosphere) is the receptacle of these altered units, which are metamorphosed at high pressures and temperatures during their travels. These units are stretched, boudinaged and mechanically dispersed in their environment. The image of the asthenospheric upper mantle is that of a "marble cake" or "plum pudding" (Fig. 127), including the heterogeneities brought by the recycled lithospheric elements which constitute the stretched layers or dispersed masses gradually mixed in a more or less intimate manner with their environment during the advance of the convective displacement. These heterogeneities are identified in the partial fusion products of the upper mantle which come to the surface; continental and oceanic basalts.

In this hypothesis the associated garnet pyroxenites of the upper mantle result, in large part, from the eclogitization of basic rocks (variably altered basalts and gabbros) from the oceanic lithosphere. In this perspective the upper mantle is the most important metamorphic unit of the earth.

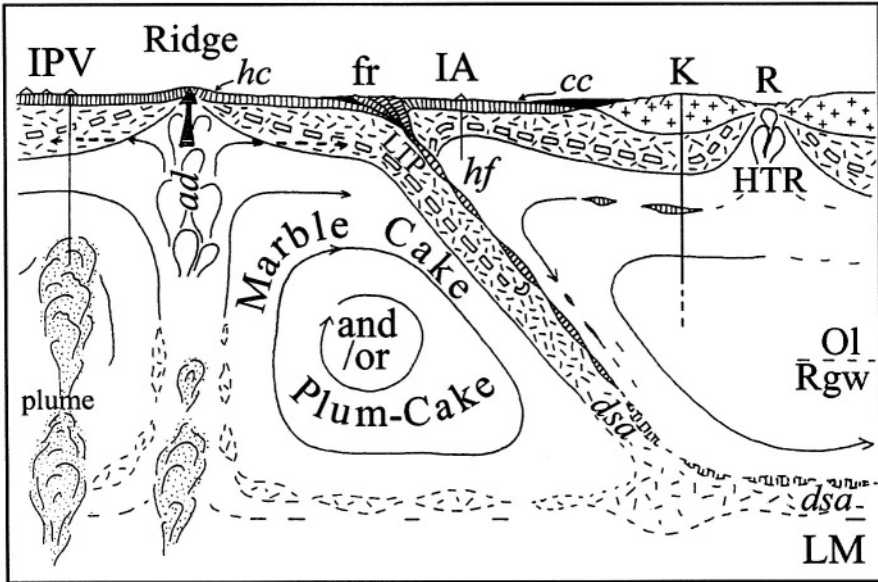


FIG. 127 — *Convective circulation of the oceanic lithosphere : genesis of upper mantle eclogites and contamination of the asthenosphere* (after Kornprobst, 1992, based on the concept of Allègre and Turcotte, 1986).

The oceanic lithosphere is carried down into the upper mantle by subduction: it re-equilibrates progressively, both thermally and rheologically with the asthenosphere. The eclogitized oceanic crust consists of a garnet-bearing layer (including "majorite" garnets, high pressure transformation of pyroxenes) near 600 km depth. This layer will be progressively stretched and dispersed by the convective movement. The upper mantle will then be composed of more-or-less continuous layers of former oceanic lithosphere inserted in the asthenosphere (marble cake model) or of lithospheric patches dispersed within the asthenosphere (plum-cake model). This mechanism introduces geochemical heterogeneities of supergene origin into the upper mantle. These are detected in the composition of basalts derived by partial fusion of contaminated and uncontaminated peridotites. Other heterogeneities come, however, from the lower mantle (LM) and the outer core via mantle plumes (pan). Hachured : oceanic crust; dashed : upper lithospheric mantle; crosses : continental crust; thick dashed lines : isotherms; Ol-Rgw : olivine-ringwoodite transition (high pressure cubic form of olivine); IA : island arc; R : rifting; K : kimberlites; HTR : high temperature retrograde ultramafic massifs; fr : Franciscan units; hc : hydrothermal contamination; cc : sedimentary crustal contamination (in black); hf : hydrous fusion of the mantle; dsa : deep seismic activity.

This page intentionally left blank

**CHARACTERISTIC MINERAL ASSEMBLAGES
OF THE PRINCIPAL METAMORPHIC FACIES**

(Modified after Yardley, 1989)

	Metabasalts	Metapelites
<i>Very low grade</i>		
Zeolite facies	heterogeneous recrystallization	interstratified shales
Z	laumontite, analcime, heulandite, wairakite	
<i>Low pressure</i>		
prehnite-actinolite facies PrA	albite + prehnite + actinolite + chlorite	
albite-epidote hornfels	albite + epidote + actinolite + chlorite	muscovite + biotite ± chlorite
AE	actinolite + oligoclase	
hornblende hornfels	hornblende + plagioclase ± diopside	biotite + muscovite + cordierite + chlorite
HH		biotite + muscovite + andalusite
		muscovite + andalusite + cordierite
Pyroxene hornfels	clinopyroxene + orthopyroxene + plagioclase	cordierite + andalusite + K feldspar
PH	± olivine ± hornblende	
Sanidinite facies	orthopyroxene + cordierite + quartz	mullite + quartz
S	orthopyroxene + sillimanite + quartz	corundum + magnetite + anorthite + glass
<i>Low temperature</i>		
Prehnite-pumpellyite facies	prehnite + pumpellyite ± chlorite ± albite	illite/muscovite + chlorite + albite + quartz
PPr	± epidote	
PA	pumpellyite + actinolite	
LC	lawsonite + albite + chlorite	
Glaucofane schist facies	glaucofane + lawsonite	phengite + carpholite + chlorite + quartz
GL		phengite + chlorite + chloritoid + kyanite + quartz
		phengite + kyanite + chloritoid + talc + quartz
GE	glaucofane + zoisite + paragonite + quartz	phengite + chloritoid + garnet + talc + quartz

Capital letters refer to Figure 31

	Metabasalts	Metapelites
<i>High Temperature and High Pressure</i>		
Greenschist facies GS	albite + epidote + chlorite + actinolite ± stilpnomelane albite + epidote + actinolite ± chlorite ± garnet	chlorite + muscovite + albite ± microcline chlorite + muscovite + biotite + albite chlorite + muscovite + chloritoid + paragonite muscovite + biotite + albite ± chlorite ± garnet
Amphibolite facies AE A	hornblende + epidote + Ca plagioclase hornblende + plagioclase + garnet hornblende + plagioclase + diopside	staurolite + ky or sil + biotite ± muscovite crd or grt + ky or sil + biotite ± muscovite crd or grt + ky or sil + biotite ± K feldspar
Eclogite facies E	omphacite + garnet	talc + kyanite + garnet coesite
Granulite facies LPG IPG HPG	orthopyroxene + plagioclase garnet + clinopyroxene + quartz	cordierite + sillimanite + K feldspar garnet + sillimanite + K feldspar garnet + kyanite + K feldspar

Capital letters refer to Figure 31

This page intentionally left blank

**GRAPHICAL REPRESENTATION
OF ROCK AND MINERAL COMPOSITIONS
ON TRIANGULAR DIAGRAMS**

ACF - A'KF diagrams

A detailed description of the calculation method is given in Winkler's (1967) text and in Bucher and Frey, 1994. Only summary methods of diagram construction are given here. The compositions are in molar percent; quartz and water are "in excess" (always present as specific phases).

For the ACF triangle one can write

$$(A) = (Al_2O_3 + Fe_2O_3) - (Na_2O + K_2O)$$

$$(C) = CaO - 3.3 P_2O_5$$

$$(F) = FeO + MgO + MnO$$

(A) represents principally the alumina in the system; neither sodium nor potassium is represented in the diagram; (A) is therefore corrected for the presence of albite and potassium feldspar, (1 Na₂O or 1 K₂O for 1 Al₂O₃). (A) is also corrected for the quantities of muscovite and biotite present (cf. Winkler, 1967) because these minerals, which contain significant quantities of Al₂O₃, are not represented in the ACF diagram. (C) is corrected for the presence of apatite (3.3 CaO for 1 P₂O₅). (F) is corrected for amounts of biotite present in the rock, because that mineral, which contains significant proportions of iron and magnesium, is not represented in the diagram. To calculate:

$$A = \frac{(A) \cdot 100}{(A) + (C) + (F)} \quad C = \frac{(C) \cdot 100}{(A) + (C) + (F)} \quad F = \frac{(F) \cdot 100}{(A) + (C) + (F)}$$

With

$$A + C + F = 100$$

For A'KF, in the same way

$$(A') = (Al_2O_3 + Fe_2O_3) - (Na_2O + K_2O + CaO)$$

$$(K) = K_2O$$

$$(F) = FeO + MgO + MnO$$

(A) is corrected for the presence of anorthite (1 CaO for 1 Al₂O₃) not represented in the diagram. Although the biotite, muscovite and potassium feldspar are all represented, the K₂O correction remains. This device enlarges the field of rocks rich in micas and potassium feldspar. (F) should be corrected for the presence of clinopyroxenes and amphiboles, minerals not represented in the diagram.

$$A' = \frac{(A') \cdot 100}{(A') + (K) + (F)} \quad K = \frac{(K) \cdot 100}{(A') + (K) + (F)} \quad F = \frac{(F) \cdot 100}{(A') + (K) + (F)}$$

With $A' + K + F = 100$

The mineral representation is based on their structural formulae:

muscovite: $K[Si_3AlO_{10}]Al_2(OH)_2$; $A' = 1.5 - 0.5$; $K = 0.5$; $F = 0$

$$A' = (1/1.5) \cdot 100 = 66$$

$$K = (0.5/1.5) \cdot 100 = 33$$

$$F = 0$$

Rock compositions are generally given in weight percentage. In order to represent these in ACF - A'KF diagrams, they must be recalculated into molar percentage by dividing the weight by the molecular weight. Examples of three compositions are given in Table A1.

Table A1. Calculation of the ACF, A'KF and AFM coordinates for a gneiss (G) a metapelite (P) and a metagranite (MG).

	Weight percent			Mol mass	Number of mols x 1000		
	G	P	MG		G	P	MG
SiO ₂	60.50	59.85	70.65	60	1008	998	1177
Al ₂ O ₃	16.80	18.26	14.60	102	165	179	143
K ₂ O	3.35	4.23	4.22	94	36	45	45
Na ₂ O	2.45	1.70	3.71	62	39	27	60
CaO	4.68	1.09	1.80	56	84	19	32
FeO	5.25	5.89	2.73	72	73	82	38
MnO	0.42	0.45	0.12	71	6	6	2
MgO	4.55	5.22	0.78	40	114	130	20
TiO ₂	0.94	1.46	0.27	80	12	18	3
P ₂ O ₅	0.40	0.36	0.25	142	3	3	2
H ₂ O	0.95	1.45	0.50				
Total	99.49	99.96	99.63				

	A	C	F	A'	K	F	A	(F)	M
G	25	21	54	3	15	82	-0.61		0.59
P	32	3	65	25	13	62	0.09		0.60
MG	31	21	48	6	41	54	-1.76		0.33

AFM Diagrams

This scheme has the advantage of distinguishing between Fe and Mg; and makes it possible to display parageneses bearing three collinear phases on the AF join of the ACF - A'KF diagram.

This is a *projection* onto the AFM plane of compositions located within the Al_2O_3 - FeO - MgO - K_2O tetrahedron (in moles) from a point represented by muscovite (Fig. A1). Muscovite is therefore in excess in these assemblages as well as quartz and water. Neither CaO nor Na_2O are taken into consideration. The compositions are corrected for quantities of plagioclase and white sodic mica (paragonite) present in the rocks under consideration.

All the compositions located in the volume Ms - A - F - M are projected within the triangle AFM or on the FM join. The compositions located in the volume Ms -F - M- $0.25\text{K}_2\text{O}$ are projected outside the triangle below the F-M join. This concerns biotite and rocks rich in biotite. The compositions for which $\text{K}_2\text{O} > 0.25$ project to infinity, this applies to potassium feldspar and rocks rich in potassium feldspar. The AFM diagram is therefore very useful for metapelites, and much less so, in general, for the gneisses.

The rocks and minerals are defined within the diagram by a system of coordinates, A and M, for which:

$$A = \frac{(\text{Al}_2\text{O}_3 - 3\text{K}_2\text{O})}{(\text{Al}_2\text{O}_3 - 3\text{K}_2\text{O}) + \text{MgO} + \text{FeO}} \quad \text{and} \quad M = \frac{\text{MgO}}{\text{MgO} + \text{FeO}}$$

The calculation of A takes into account the fact that muscovite is in excess; the A value is calculated *after* correction for quantities of Al_2O_3 related to CaO and Na_2O in plagioclase.

A variation of the AFM diagram is used for higher grades of metamorphic pelites and gneiss (amphibolite and granulite facies) above the stability field of muscovite. The compositions are no longer projected from a point representative of muscovite, but from that of orthoclase. The A and M coordinates of the composition are calculated in the following fashion (after corrections for Al_2O_3 for the presence of plagioclase):

$$A = \frac{(\text{Al}_2\text{O}_3 - \text{K}_2\text{O})}{(\text{Al}_2\text{O}_3 - \text{K}_2\text{O}) + \text{MgO} + \text{FeO}} \quad \text{and} \quad M = \frac{\text{XMgO}}{\text{XMgO} + \text{XFeO}}$$

In this configuration most rocks appear within the AFM triangle (there are no negative values of A) because, with the exception of granites or hyperalkaline syenites, there are no rock compositions in the Or - F - M - K_2O volume.

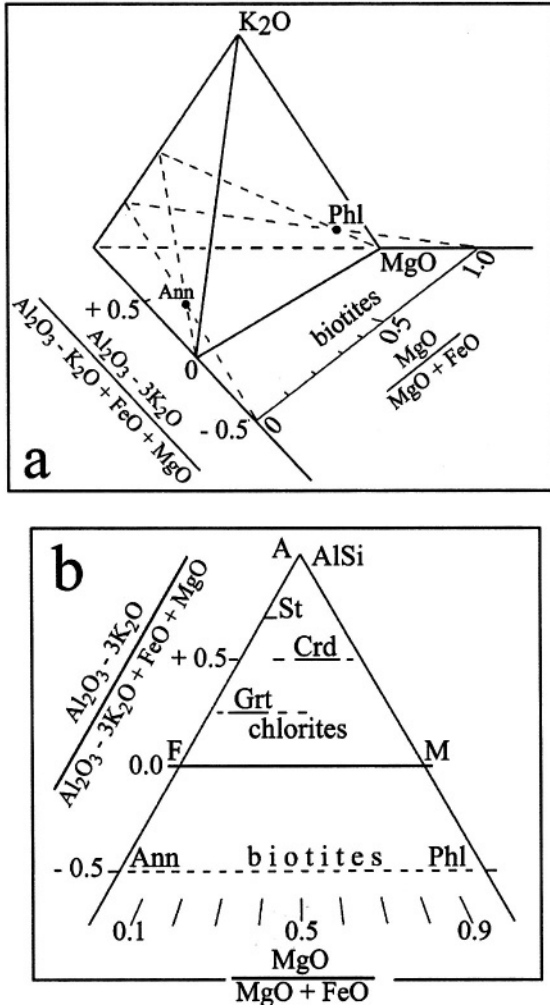


FIG. A1 — Construction of the AFM diagram.

The compositions located in the tetrahedron $Al_2O_3 - FeO - MgO - K_2O$ are projected from the muscovite pole (Ms) when the mineral is present. Biotites of the annite (Ann) -phlogopite (Phl) series are projected onto the basal plane, outside the tetrahedron on a segment whose coordinate is $A = -0.5$. In fact most natural biotites contain eastonite in solid solution, that is with aluminum in six-fold coordination, and project between the $A = -0.5$ segment and the F-M join. In the absence of muscovite (higher degrees of metamorphism) the projection pole is potassium feldspar (Kfs) if this mineral is present. The biotites of the annite-phlogopite series are then projected on the F-M join.

a) method of projection. b) AFM diagram, muscovite, quartz and water are in excess. Standard mineral symbols. Potassium feldspar and rocks rich in potassium feldspar are projected to infinity.

EXAMPLES OF GEOTHERMOMETERS AND GEOBAROMETERS

Three examples among the most popular geothermobarometers are given below. For more details the reader is advised to consult articles in "Thermométrie et barométrie géologique" a symposium of la Société française de minéralogie et cristallographie (M. Lagache ed.); an exhaustive compendium of geothermobarometers applied to metagranitoids may also be found in the work of Le Goff (1989). Recently Spear (1993) has developed a method for a complete analysis of metamorphic rocks.

The orthopyroxene-clinopyroxene thermometer

(Wood and Banno, 1973; Wells 1977)

When an orthopyroxene and a clinopyroxene are in equilibrium (in a pyroxenite or a peridotite) it may be written:

$$a_{\text{enstatite}}^{\text{cpx}} = K \cdot a_{\text{enstatite}}^{\text{opx}} \quad \text{and} \quad K = \frac{a_{\text{en}}^{\text{cpx}}}{a_{\text{en}}^{\text{opx}}}$$

Where $a_{\text{enstatite}}^{\text{px}}$ is the activity of $\text{Mg}_2\text{Si}_2\text{O}_6$ in the orthopyroxene and in the clinopyroxene and K is the equilibrium constant. A model of the activity of enstatite, $\text{Mg}_2\text{Si}_2\text{O}_6$, in clinopyroxene and orthopyroxene is based on the structure of these minerals which contains three principal sites for cations: two categories of octahedral sites M_1 and M_2 and a tetrahedral site T

M_2 accepts the largest cations Ca, Na as well as Fe and Mg

M_1 accepts small cations, Fe, Mg, Al, Cr, Ti

T accepts Si principally, as well as a limited quantity of Al

The activity of enstatite in a pyroxene is defined by the product of Mg concentration in the M_1 and M_2 sites:

$$a_{\text{en}}^{\text{px}} = X_{\text{Mg}}^{M_1} \cdot X_{\text{Mg}}^{M_2}$$

Where
$$\left(X_{M_1}^{M_1} \right) = \left(\frac{\text{Mg}}{\text{Mg} + \text{Fe} + \text{Al} + \text{Cr} + \text{Ti}} \right) M_1$$

and
$$\left(X_{M_2}^{M_2} \right) = \left(\frac{\text{Mg}}{\text{Mg} + \text{Fe} + \text{Ca} + \text{Na}} \right) M_2$$

Simplifying on the basis of a pyroxene formula containing 6 oxygens:

$$a_{\text{en}}^{\text{px}} = \left(\frac{\text{Mg}}{\text{Mg} + \text{Fe}} \right)^2 \cdot (1 - \text{Al} - \text{Cr} - \text{Ti})_{\text{M1}} \cdot (1 - \text{Ca} - \text{Na})_{\text{M2}}$$

In order to use this expression Al_{M1} must be taken into consideration and not the total Al in the formula. An acceptable solution may be found using the relation:

$$\text{Al}_{\text{M1}} = \Sigma \text{Al} - (2 - \text{Si})$$

because the number of tetrahedral sites occupied by Si or Al is 2 in a formula of six oxygens.

The empirical expression furnished by Wood and Banno (1973) is the following:

$$\ln K = -\frac{10202}{T} + 5.35 \quad \text{where } T \text{ is in } ^\circ\text{K}$$

However, $\ln K$ is not only a function of $1/T$ but also of the concentration of iron in the system. The expression proposed by Wells (1977) gives more realistic temperatures.

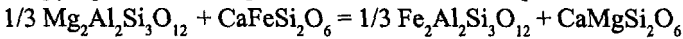
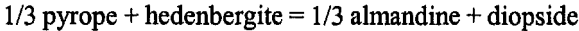
$$T^\circ\text{C} = \left(\frac{7341}{3.355 + [2.44(X_{\text{Fe}}^{\text{opx}})] - \ln K} \right) - 273$$

where

$$(X_{\text{Fe}}^{\text{opx}}) = \left(\frac{\text{Fe}}{\text{Fe} + \text{Mg}} \right)_{\text{opx}}$$

The clinopyroxene - garnet thermometer (Ellis and Green, 1979)

The equilibrium which is considered concerns the exchange of iron and magnesium between clinopyroxene and garnet.



The equilibrium constant is expressed by the following function:

$$K = \frac{\left(a_{\text{alm}}^{\text{grt}} \right)^{\frac{1}{3}} \cdot a_{\text{di}}^{\text{cpx}}}{\left(a_{\text{prp}}^{\text{grt}} \right)^{\frac{1}{3}} \cdot a_{\text{hd}}^{\text{cpx}}}$$

These phases are considered to be ideal solid solutions and the activities are equivalent to concentrations :

$$K = K_D = \frac{(\text{Fe} / \text{Mg})_{\text{grt}}}{(\text{Fe} / \text{Mg})_{\text{cpx}}}$$

$\ln K_D$ is a function of $1/T$, but also the concentration of Ca in garnet

$$X_{\text{Ca}}^{\text{grt}} = \frac{\text{Ca}}{\text{Ca} + \text{Mg} + \text{Fe}}$$

Experimental data allow calculation of the empirical expression:

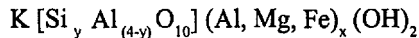
$$T^{\circ} \text{C} = \frac{(3104 X_{\text{Ca}}^{\text{grt}} + 3030 + 10.86 \text{Pkb})}{\ln K_D + 1.9034} - 273$$

This equation overestimates the temperature significantly when $X_{\text{Ca}}^{\text{grt}}$ is above 0.15 (Chrifi *et al.*, 1998).

The Si⁴⁺ in phengite barometer

(Velde, 1967; Massonne and Schreyer, 1987)

In metamorphic metapelitic rocks containing biotite, potassium feldspar and quartz, white mica does not generally have the composition of pure muscovite $\text{K}[\text{Si}_3\text{AlO}_{10}]\text{Al}_2(\text{OH})_2$. It corresponds, in most cases to a solid solution along the muscovite-celadonite $\text{K}[\text{Si}_4\text{O}_{10}]\text{Al}(\text{Mg}, \text{Fe}(\text{OH})_2)$ join. In reality this solid solution is not complete, and the natural compositions of potassic white mica evolve near the muscovite and the phengite end members (Fig A2b). This evolution is characterized by a substitution of Al for Si in the tetrahedral sites and Fe and Mg for Al in the octahedral sites such that electrostatic equilibrium is maintained. The general formula of these white micas is the following :



where: $\text{Mg} + \text{Fe} = x + 3y - 9$ and $\text{Al}^6 = 9 - x - 2y$
and $3 < y < 4$

The most notable effect of this substitution is the diminution of \bar{V} of the white mica as a function of the occupation of tetrahedral sites by Si. The composition of potassic white mica in equilibrium with potassium feldspar, biotite and quartz for $P_{\text{H}_2\text{O}} = P_{\text{total}}$ constitutes, therefore, an excellent geobarometer which is presented in graphic form in Figure

A2a. It must be noted that numerous authors use this barometer outside the strict limits of its definition (equilibrium with Kfs, biotite and quartz); the pressure is therefore underestimated.

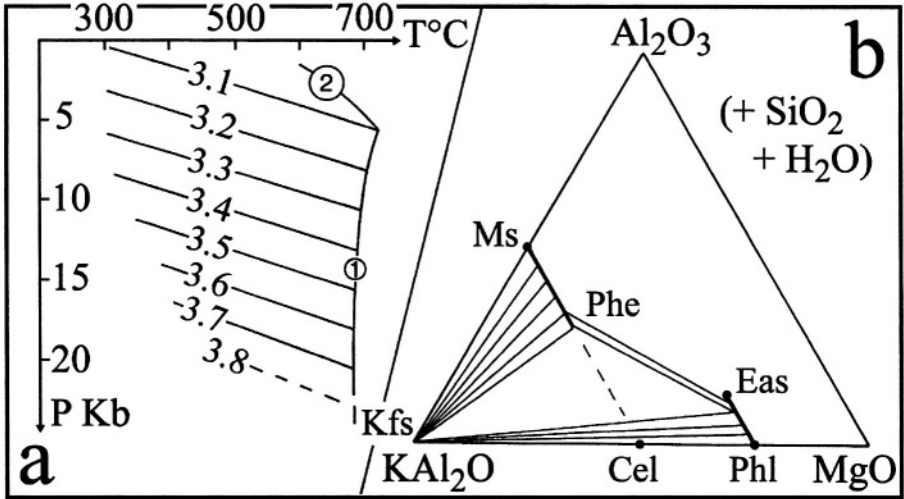


FIG. A2 — *Composition of phengite in a magnesian system as a function of P and T* (after Massonne and Schreyer, 1987)

a) Isopleths of tetrahedral site occupation in potassic white micas by Si⁴⁺: number of Si per structural formula $K[\text{Si}_y\text{Al}_{(4-y)}\text{O}_{10}](\text{Al}, \text{Mg})_x(\text{OH})_2$ (1) melting of the assemblage phengite + phlogopite + potassium feldspar + quartz + water; (2) equilibrium: Ms + Phl + Qtz = Crd + Kfs + vapour.

b) System $\text{Al}_2\text{O}_3 - \text{MgO} - \text{KAlO}_2 (+\text{SiO}_2 + \text{H}_2\text{O})$.

The data of Figure A2a are only usable for assemblages of phengite + potassium feldspar + phlogopite + quartz + water for $P_{\text{H}_2\text{O}} = P_{\text{total}}$.

STRUCTURAL FORMULAE OF MINERALS

CITED IN THIS TEXT

Mineral	Structural Formula	Comments
Actinolite	$\text{Ca}_2(\text{Mg, Fe})_5[\text{Si}_8\text{O}_{22}](\text{OH})_2$	monoclinic amphibole
Albite	$\text{Na}[\text{Si}_3\text{AlO}_8]$	sodic end-member of plagioclase
Almandine	$\text{Ca}_3\text{Al}_2\text{Si}_3\text{O}_{12}$	ferrous end-member of garnet
Analcime	$\text{NaAlSi}_2\text{O}_6 \cdot \text{H}_2\text{O}$	zeolite group
Andalusite	Al_2SiO_5	LT-LP polymorph
Annite	$\text{K}[\text{Si}_3\text{AlO}_{10}]\text{Fe}_3(\text{OH})_2$	ferrous end-member of biotite
Anorthite	$\text{Ca}[\text{Si}_2\text{Al}_2\text{O}_8]$	calcic end-member of plagioclase
Aragonite	CaCO_3	HP polymorph
Biotite	$\text{K}[\text{Si}_{(3-x)}\text{Al}_x\text{O}_{10}](\text{Mg, Fe, Al})_{2-3}(\text{OH})_2$	solid solution annite-phlogopite \pm eastonite
Calcite	CaCO_3	LP polymorph
Carpholite	$(\text{Mg, Fe})\text{Al}_2\text{Si}_2\text{O}_6(\text{OH})_4$	Mg carpholite -Fe carpholite solid solution
Celadonite	$\text{K}_2\text{Al}_2(\text{Fe, Mg})_2\text{Si}_6\text{O}_{20}(\text{OH})_4$	clay mineral group
Chlorite	$(\text{Mg, Fe, Al})_6(\text{Si, Al})_4\text{O}_{10}(\text{OH})_8$	complex solid solutions
Chloritoid	$(\text{Fe, Mg})_2\text{Al}_4\text{Si}_2\text{O}_{10}(\text{OH})_4$	generally ferrous except in HP-LT assemblages
Clinopyroxene	$(\text{M2})(\text{M1})\text{Z}_2\text{O}_6$	complex solid solution M2 = Ca, Na, Mg, Fe, Mn ; M1 = Mg, Fe, Mn, Al, Cr, Ti ; Z = Si, Al
Clinzoisite	$\text{CaAl}_3\text{Si}_3\text{O}_{12}(\text{OH})$	monoclinic aluminous end-member of the epidote group

Mineral	Structural Formula	Comments
Coesite	SiO_2	HP polymorph
Cordierite	$(\text{Mg, Fe})_2\text{Al}_4\text{Si}_5\text{O}_{18}\cdot n\text{H}_2\text{O}$	n between 0.5 and 1.0
Corundum	Al_2O_3	ruby (red) or sapphire (blue)
Cummingtonite	$\text{Mg}_7\text{Si}_8\text{O}_{22}(\text{OH})_2$	monoclinic amphibole, magnesian end-member of the cummingtonite-grünerite series
Diamond	C	HP polymorph
Diopside	$\text{CaMgSi}_2\text{O}_6$	magnesian end-member of clinopyroxenes
Dolomite	$\text{CaMg}(\text{CO}_3)_2$	
Epidote	$\text{Ca}(\text{Fe}^{3+})_3\text{Si}_3\text{O}_{12}(\text{OH})$	ferric end-member of epidote group
Fayalite	Fe_2SiO_4	ferrous end-member of olivine series
Garnet	$\text{X}_3\text{Y}_2\text{Si}_3\text{O}_{12}$	complex solid solutions ; X = Ca, Mg, Fe, Mn; Y = Al, Fe^{3+} , Cr
Glaucophane	$\text{Na}_2(\text{Fe, Mg})_3\text{Al}_2\text{Si}_8\text{O}_{22}(\text{OH})_2$	monoclinic HP-LT amphibole
Graphite	C	LP polymorph
Grossularite	$\text{Ca}_3\text{Al}_2\text{Si}_3\text{O}_{12}$	calcic end-member of aluminous garnets
Hedenbergite	$\text{CaFeSi}_2\text{O}_6$	ferrous end-member of clinopyroxenes
Heulandite	$(\text{Ca, Na}_2)\text{Al}_2\text{Si}_7\text{O}_{18}\cdot 6\text{H}_2\text{O}$	zeolite group
Hornblende	$\text{Na}_{0-1}\text{Ca}_2(\text{Mg, Fe, Fe}^{3+}, \text{Al})_5\text{Al}_{2-1}\text{Si}_{6-7}\text{O}_{22}(\text{OH})_2$	monoclinic amphibole
Illite	$\text{K}_{1-5}\text{Al}_{3-5.5}\text{Si}_{7-6.5}\text{O}_{20}(\text{OH})_4$	clay mineral group
Jadeite	$\text{NaAlSi}_2\text{O}_6$	sodic end-member of clinopyroxenes, HP-LT
K feldspar	$\text{K}[\text{Si}_3\text{AlO}_8]$	orthoclase or microcline according to the symmetry

Mineral	Structural Formula	Comments
Kaolinite	$\text{Al}_4\text{Si}_4\text{O}_{10}(\text{OH})_8$	clay mineral group
Kyanite	Al_2SiO_5	HP-LT polymorph
Laumontite	$\text{CaAl}_2\text{Si}_4\text{O}_{12} \cdot 4\text{H}_2\text{O}$	
Lawsonite	$\text{CaAl}_2\text{Si}_2\text{O}_7(\text{OH})_2 \cdot \text{H}_2\text{O}$	HP-LT
Microcline	$\text{K}[\text{Si}_3\text{AlO}_8]$	triclinic K feldspar
Mullite	$\text{Si}_2\text{Al}_6\text{O}_{13}$	HT-LP
Muscovite	$\text{K}[\text{Si}_3\text{AlO}_{10}]\text{Al}_2(\text{OH})_2$	dioctahedral potassic white mica
Omphacite	$(\text{Ca}, \text{Na})(\text{Mg}, \text{Fe}, \text{Al})\text{Si}_2\text{O}_6$	solid solution jadeite-diopside-hedenbergite
Paragonite	$\text{Na}[\text{Si}_3\text{AlO}_{10}]\text{Al}_2(\text{OH})_2$	dioctahedral sodic white mica
Phengite	$\text{K}[\text{Si}_{(3+y)}\text{Al}_{(1-y)}](\text{Al}, \text{Fe}, \text{Mg})_{2-3}(\text{OH})_2$	
Phlogopite	$\text{K}[\text{Si}_3\text{AlO}_{10}]\text{Mg}_3(\text{OH})_2$	magnesian end-member of biotite
Plagioclase	$(\text{Na}, \text{Ca})[\text{Si}_{3-2}\text{Al}_{1-2}\text{O}_8]$	albite-anorthite solid solution
Prehnite	$\text{Ca}_4\text{Al}_2\text{Si}_3\text{O}_{10}(\text{OH})_2$	
Pumpellyite	$\text{Ca}_2(\text{Mg}, \text{Fe})(\text{Al}, \text{Fe}^{3+})_5\text{Si}_6\text{O}_{23}(\text{OH})_3 \cdot 2\text{H}_2\text{O}$	
Pyrope	$\text{Mg}_3\text{Al}_2\text{Si}_3\text{O}_{12}$	magnesian end-member of aluminous garnets
Pyrophyllite	$\text{Al}_4\text{Si}_8\text{O}_{20}(\text{OH})_4$	
Quartz	SiO_2	α and β polymorphs
Rutile	TiO_2	
Scheelite	CaWO_4	
Sillimanite	Al_2SiO_5	HT-LP polymorph
Spessartine	$\text{Mn}_3\text{Al}_2\text{Si}_3\text{O}_{12}$	manganiferous end-member of aluminous garnets
Sphene	$\text{CaTiSiO}_4(\text{O}, \text{OH})$	also called titanite
Spinel	$(\text{Mg}, \text{Fe})(\text{Al}, \text{Cr}, \text{Fe}^{3+})_2\text{O}_4$	complex solid solutions
Staurolite	$(\text{Fe}, \text{Mg})_4\text{Al}_{18}\text{Si}_{7.5}\text{O}_{44}(\text{OH})_2$	generally ferrous except for HP-LT assemblages

Mineral	Structural Formula	Comments
Stilpnomelane	$(K, Ca)_{0-1.4}(Fe, Mg, Al)_{5.9-8.2}Si_8O_{20}(OH)_4(O, OH, H_2O)_{3.8-8.5}$	LT
Sudoite	$Mg_2Al_3[Si_3AlO_{10}](OH)_8$	chlorite group
Talc	$Mg_3Si_4O_{10}(OH)_2$	
Titanite	$CaTiSiO_4(O, OH)$	also called sphene
Vesuvianite	$Ca_{10}(Mg, Fe)_2Al_4Si_9O_{34}(OH, F)_4$	also known as idocrase, HT-LP
Wairakite	$CaAl_2Si_4O_{12} \cdot 2H_2O$	zeolite group
Wollastonite	$CaSiO_3$	HT, low PCO_2
Zeolite		Very low T and P
Zoisite	$CaAl_3Si_3O_{12}(OH)$	orthorhombic aluminous epidote

MINERAL ABBREVIATIONS

The mineral abbreviations suggested by Kretz (1983) have been adopted for this manual, as they are widely accepted for use in metamorphic petrology.

Acmite : Acm	Ca clinoamphibole : Cam	Fassaite : Fst
Actinolite : Act	Ca clinopyroxene : Cpx	Fayalite : Fa
Aegerine : Agr	Cancrinite : Ccn	Ferroactinolite : Fac
Akermanite : Ak	Carpholite : Cp	FerrocapholNNNNite : Fcp
Albite : Ab	Cassiterite : Cst	Ferroedenite : Fed
Allanite : Aln	Celadonite : Cel	Ferropargasite : Fpa
Almandine : Alm	Celestite : Cls	Ferrosilite : Fs
Aluminosilicate : Als	Chabazite : Cbz	Ferrotschermakite : Fts
Amphibole : Am	Chlorite : Chl	Fluorite : Flt
Analcite : Anl	Chloritoid : Cld	Forsterite : Fo
Anatase : Ant	Chondrodite : Chn	
Andalusite : And	Chromite : Chr	Galena : Gn
Andradite : Adr	Chrysocolla : Ccl	Garnet : Grt
Anhydrite : Anh	Chrysotile : Ctl	Gedrite : Ged
Ankerite : Ank	Clinoenstatite : Cen	Gehlenite : Gh
Annite : Ann	Clinoferrosilite : Cfs	Gibbsite : Gbs
Anthophyllite : Ath	Clinohumite : Chu	Glaucophanes : Gln
Antigorite : Atg	Clinzoisite : Czo	Glauconite : Glt
Apatite : Ap	Coesite : Cs	Goethite : Gt
Apophyllite : Apo	Cordierite : Crd	Graphite : Gr
Aragonite : Arg	Corundum : Crn	Grossular : Grs
Arfvedsonite : Arf	Cristobalite : Crs	Grunerite : Gru
Arsenopyrite : Apy	Cummingtonite : Cum	Gypsum : Gp
Augite : Aug		
Axinite : Ax	Diamond : Dia	Halite : Hl
	Diaspore : Dsp	Hastingsite : Hs
Barite : Brt	Digenite : Dg	Häuyne : Hyn
Beryl : Brl	Diopside : Di	Hedenbergite : Hd
Biotite : Bt	Dolomite : Dol	Hematite : Hem
Boehmite : Bhm	Dravite : Drv	Hercynite : Hc
Bornite : Bn		Heulandite : Hul
Brucite : Brc	Eckermannite : Eck	Hornblende : Hbl
Brookite : Brk	Edenite : Ed	Humite : Hu
Bustamite : Bst	Elbaite : Elb	
Calcite : Cal	Enstatite : En	Idocrase/Vesuvianite : Ves
Chalcocite : Cc	Epidote : Ep	Illite : Ill
Chalcopyrite : Ccp		Ilmenite : Ilm

Jadeite : Jd	Olivine : Ol	Sericite : Ser
Johannsenite : Jh	Omphacite : Omp	Siderite : Sd
	Orthoamphibole : Oam	Sillimanite : Sil
Kaersutite : Krs	Orthopyroxene : Opx	Sodalite : Sdl
Kalsilite : Kls	Orthoclase : Or	Spessartine : Sps
Kaolinite : Kln	Osumilite : Osm	Sphalerite : Sp
Kataphorite :Ktp		Sphene : Ttn
Kornerupine : Krn	Paragonite : Pg	Spinel : Spl
Kyanite : Ky	Pargasite : Prg	Spodumene : Spd
	Pectolite : Pec	Staurolite : St
Laumontite : Lmt	Pentlandite : Pn	Stilbite : Stb
Lawsonite : Lws	Periclase : Per	Stilpnomelane : Stp
Lepidolite : Lpd	Perovskite : Prv	Strontianite : Str
Leucite : Lct	Pigeonite : Pgt	Sudoite : Sud
Limonite : Lm	Phengite : Phe	
Lizardite : Lz	Phlogopite : Phl	Talc : Tlc
Loellingite : Lo	Plagioclase : Pl	Thomsonite : Tmp
	Potassium feldspar : Kfs	Titanite : Ttn
Maghemite : Mgh	Prehnite : Prh	Topaz : Toz
Magnesiocarpholite : Mcp	Protoenstatite : Pen	Tourmaline : Tur
Magnesiokataphorite : Mkt	Pumpellyite : Pmp	Tridymite : Trd
Magnesioriebeckite : Mrb	Pyrite : Py	Troilite : Tro
Magnesite : Mgs	Pyrophyllite : Prl	Tschermakite : Ts
Magnetite Mgt	Pyrope : Prp	
Margarite : Mrg	Pyrrhotite : Po	Ulvöspinel; : Usp
Melilite : Mel		
Molybdenite : Mo	Quartz : Qtz	Vermiculite : Vrm
Monazite : Mnz		Vesuvianite : Ves
Monticellite : Mtc	Riebeckite : Rbk	
Montmorillonite : Mnt	Rhodochrosite : Rds	Wairakite : Wa
Mullite : Mul	Rhodonite : Rdn	Witherite : Wth
Muscovite : Ms	Rutile : Rt	Wollastonite : Wo
	Sanidine : Sa	Wüstite : Wus
Natrolite : Ntr	Sapphirine : Spr	
Nepheline : Ne	Scapolite : Scp	Zircon : Zrn
Norbergite : Nrb	Schorl : Srl	Zoisite : Zo
Nosean : Nsn		

BIBLIOGRAPHY

- Allègre, C.-J. (1983) L'écume de la Terre. *Le temps des Sciences*, Fayard .
- Bard, J.P. (1980) Microtextures des roches magmatiques et métamorphiques. Masson, Paris, 192p.
- Bucher, K. and Frey, M., (1994) - Petrogenesis of metamorphic rocks. Springer-Verlag, 318 pp.
- Bayly, B. (1968) Introduction to Petrology. Prentice-Hall Inc., Englewood Cliffs, N.J. 371 p.
- Debelmas, J. and Mascle, G. (1991) Les grandes structures géologiques. *Enseigt. Sci. Terre*, Masson, 300p.
- Foucault, A. and Raoult, J.F. (1980) Dictionnaire de Géologie. Masson, Paris.
- Fyfe, W.S., Price, N.J. and Thompson, A.B. (1978) Fluids in the Earth's crust. *Devlp. Geochemistry 1*, Elsevier, 383p.
- Goguel, J. (1975) La Géothermie, Doin, 171p.
- Greenwood, H.J. (ed) (1977) Application of thermodynamics to petrology and ore deposits. *Short Course handbook*. Mineral. Ass. Canada, 231p.
- Grolier, J., Fernandez, A., Hucher, M. and Riss J. (1991) Les propriétés physiques des roches. Théories et modèles. Masson, Paris. 462p.
- Helgeson, H.C., Delany, J.M., Nesbitt, H.W. and Bird, D.K. (1978) Summary and critique of the thermodynamic properties of rock-forming minerals. *Amer. J. Sci.*, **278-A**, 1-229.
- Liboutry, L. (1998) Géophysique et Géologie. *Enseigt Sci Terre*. Masson, Paris, 462p.
- Mattauer, M. (1973) Les déformations des matériaux de l'écorce terrestre. Hermann, Paris, 493p.
- Miyashiro, A. (1973) Metamorphism and metamorphic belts. George, Allen & Unwin éd., London, 492p.
- Miyashiro, A. (1994)
- Nicolas, A. (1988) Principes de tectonique. Masson, Paris, 2nd ed, 223p.
- Nicolas, A. (1989) Structures of ophiolites and dynamics of oceanic lithosphere. Kluwer Academic Pub, 367p.
- Powell, R. (1978) Equilibrium thermodynamics in Petrology; an introduction. Harper & Row, 284p.
- Robie, R.A., Hemingway, B.S. and Fisher, J.R. (1978) Thermodynamic properties of Minerals and related substances at 298.15 K. and 1 bar (10^5 Pascals) pressure and at higher temperatures. *Geol. Surv. Bull.*, **1452**, 456p.
- Spear, F.S. and Peacock, S.M. (1989) Metamorphic Pressure-Temperature-Time paths. *Amer. Geophys. Union, Short course in Geology*, **7**, 102 p.
- Spear, F.S. (1993)
- Vernon, R.H. (1976) Metamorphic processes. George Allen & Unwin, 247p.
- Vidal, Ph. (1994) La géochimie. Dunod, 190p.
- Winkler, H.G.F. (1967) Petrogenesis of metamorphic rocks. Springer-Verlag, **2nd** ed.
- Wood, B.J. and Fraser, D.G. (1977) Elementary thermodynamics for geologists. Oxford Univ. Press, 303p.
- Yardley, B.W.D. (1989) An introduction to metamorphic petrology. Longman Earth Sci. Series, 248p.
- Zen, E.A. (1966) Construction of pressure-temperature diagrams for multi-component systems after the method of Schreinemakers - a geometric approach. *U.S. Geol. Surv. Bull.*, **1225**, 56 p.

This page intentionally left blank

REFERENCES CITED

- Albarède, F. (1976) Thermal models of post-tectonic decompression as exemplified by the Haut-Allier granulites (Massif Central, France). *Bull. Soc. Géol Fr.*, **7**, XVIII, 4, 1023-1031.
- Albarède, F. and Michard-Vitrac, A. (1978) Age and significance of the North-Pyrenean metamorphism. *Earth Planet. Sci. Lett.*, **40**, 327-332.
- Allègre, C.J. and Turcotte, D.L. (1986) Implications of a two-component marble-cake mantle. *Nature*, **323**, 123-127.
- Alt, (1994) Subseafloor processes in mid-ocean ridge hydrothermal systems. *Geophys. Monographs*, 91, AGU, Washington, 85-114
- Azambre, B. and Ravier, J. (1978) Les écaillés de gneiss du faciès granulite du Port de Saleix et de la région de Lherz (Ariège). Nouveaux témoins du socle profond des Pyrénées. *Bull. Soc. Géol. Fr.*, **XX**, 3,221-228.
- Andrieux, P. (1982) La charnockite d'Ansignan: mise en place et évolution paragéométrique. Unpub thesis, Univ. Clermont Ferrand, 109pp.
- Barnicoat, A.C. and Fry, N. (1986) High-pressure metamorphism of the Zermat-Saas ophiolite zone, Switzerland. *J. Geol. Soc. London*, **143**, 607-618.
- Berman, R.G. 1988 Internally-consistent thermodynamic data for minerals in the system $\text{Na}_2\text{O}-\text{K}_2\text{O}-\text{CaO}-\text{MgO}-\text{FeO}-\text{Fe}_2\text{O}_3-\text{Al}_2\text{O}_3-\text{SiO}_2-\text{TiO}_2-\text{H}_2\text{O}-\text{CO}_2$. *J. Petrology*, **29**, 445-522.
- Bernus-Maury, C. (1984) Etude des paragenèses caractéristiques du métamorphisme mésozoïque dans la partie orientale des Pyrénées. Unpub thesis, Paris.
- Boillot, G, Girardeau, J. and Kornprobst, J. (1988) Rifting of the Galicia Margin : crustal thinning and emplacement of mantle rocks on the seafloor. In : G. Boillot et E.L. Winterer eds, *Proc. ODP, Sci. Results.*, **103**, 741-756.
- Brun, J.-P. and Pons, J. (1981) Strain patterns of pluton emplacement in crust undergoing non-coaxial deformation, Sierra Morena, southern Spain. *J. Struct. Geol.*, **3**, 219-230.
- Burg, J.-P., Delor, C.P., Leyreloup, A.F. and Romney, F. (1989) Inverted metamorphic zonation and Variscan thrust tectonics in the Rouergue area (Massif Central, France): P-T-t record from mineral to regional scale. In: J.S. Daly, R.A. Cliff and B.W.D. Yardley eds.; *Evolution of metamorphic belts. Geol. Soc. Spec. Pub.* n°**43**, Blackwell Scientific Pub., 423-439.
- Burg, J.P. and Matte, Ph. (1978) Across section through the French Massif Central and the scope of its Variscan geodynamic evolution. *Z. dt. Geol. Ges.*, **129**, 429-460.
- Burnham, C.W., Holloway, J.R. and Davis, N.F. (1969) Thermodynamic properties of water to 1000°C and 10000 bars. *Geol. Soc. Amer. Spec. Pap.* 132.
- Cathelineau, M., Boiron, M.C., Essaraj, S., Dubessy, J., Lespinasse, M. and Poty, B. (1993) Fluid pressure variations in relation to multistage deformation and uplift : a fluid inclusion study of Au quartz veins. *Eur. J. Mineral.*, **5**, 107-121.
- Chopin, C. (1984) Coesite and pure pyrope in high-grade blueschists of the western Alps : a first record and some consequences. *Contrib. Mineral. Petrol.*, **86**, 107-118.
- Chopin, C., Henry, C. and Michard, A. (1991) Geology and petrology of the coesite-bearing terrain, Dora Maira massif, Western Alps. *Eur. J. Mineral.*, **3**, 263-291.
- Choukroune, P., Roure, F., Pinet, B. and l'équipe ECORS-Pyrénées (1989) Main results of the ECORS Pyrenees profile. *Tectonophysics*, **173**, 411-423.

- Choukroune, P. and Mattauer, M. (1978) Tectonique des plaques et Pyrénées : sur le fonctionnement de la faille transformante nord-pyrénéenne ; comparaisons avec des modèles actuels. *Bull. Soc. géol. Fr.*, (7), XX, 5, 689-700.
- Clark, S.P.Jr. and Ringwood, A.E. (1964) Density distribution and constitution of the mantle. *Reviews of Geophysics*, **2**, 1, 35-88.
- Clemens, J.D. (1990) The granulite-granite connexion. In : *Granulites and crustal evolution*, D. Vielzeuf and Ph. Vidal eds., NATO ASI Series, 25-36.
- Costa, S. (1991-1992) East-west diachronism of the collisional stage in the French Massif Central: implications for the European Variscan Orogen. *Geodinamica Acta*, **5**, 1-2, 51-68.
- Cowan, D.A. and Silling, R.M. (1978) A dynamic scaled model of accretion at trenches and its implication for the tectonic evolution of subduction complexes. *J. Geophys. Res.*, **83**, 5389-5396.
- Debroas, E.-J. (1987) Modèle de bassin triangulaire à l'intersection de décrochements divergents pour le fossé albo-cénomaniens de la Ballongue (Zone Nord-Pyrénéenne, France). *Bull. Soc. géol. Fr.*, (8), III, 5, 887-898.
- Demange, M. (1985) The eclogite-facies rocks of the Montagne Noire, France. *Chem. Geol.*, **50**, 173-188.
- Deville, E., Fudral, S., Lagabrielle, Y., Marthaler, M. and Sartori, M. (1992) From oceanic closure to continental collision: a synthesis of the «Schistes lustrés» metamorphic complex of the western Alps. *Geol. Soc. Amer. Bull.*, **104**, 127-139.
- Dubuisson, G., Hirn, A., Girardeau, J., Mercier, J.-C.C. and Veinante, J.-L. (1988) Multiple Variscan nappes in Limousin, western Massif Central, France : geophysical constraints to the geological model and geodynamic implications. *Tectonophysics*, **147**, 19-31.
- Ebadi, A. and Johannes, W. (1991) Beginning of melting and composition of first melts in the system Qz-Ab-Or-H₂O-CO₂. *Contrib. Mineral. Petrol.*, **106**, 286-295.
- Ellis D.J. and Green, D.H. (1979) An experimental study of the effect of Ca upon garnet-clinopyroxene Fe-Mg exchange equilibria. *Contrib. Mineral. Petrol.*, **71**, 13-22.
- Eugster, H.P. (1970) Thermal and ionic equilibria among muscovite, K-feldspar and aluminosilicate assemblages. *Fortsch. Miner.*, **47**, 106-123.
- Ferry, J.M. and Spear, F.S. (1978) Experimental calibration of the partitioning of Fe and Mg between biotite and garnet. *Contrib. Mineral. Petrol.*, **66**, 113-117.
- Floc'h, J.P. (1983) Le socle métamorphique du Limousin central : une traversée de la branche ligérienne de l'orogène varisque de l'Aquitaine à la zone broyée d'Argentat. Unpub. thesis, Limoges, 445 pp + annexes.
- Floc'h, J.P., Grolier, J., Guillot, P.L. and Santallier, D. (1978) Données récentes sur la géologie du Bas-Limousin. *102ème Congrès Soc. Sav.*, Limoges, Sci., fasc. II, 147-158.
- Flood, R.H. and Vernon, R.H. (1978) The Cooma granodiorite, Australia: an example of in situ crustal anatexis ? *Geology*, **6**, 81-84.
- Fonteilles, M. (1970) Géologie des terrains métamorphiques et granitiques du massif hercynien de l'Agly (Pyrénées orientales). *Bull. BRGM*, (2), IV, 21-72.
- Fonteilles, M., Soler, P., Demange, M., Derre, C., Krier-Schellen, A.D., Verkaeren, J., Guy, B., and Zahm, A. (1989) The scheelite skarn deposit of Salau (Ariège, France). *Economic Geol.* **84**, 1172-1209.
- Frizon, de Lamotte, D. (1985) La structure du Rif oriental (Maroc). Thèse inédite, Paris 6, 433 pp.
- Fry, N and Fyfe, W.S. (1969) Eclogites and water pressure. *Contrib. Mineral. Petrol.*, **24**, 1.
- Furlong, K.P., Hanson, R.B. and Bowers, J.R. (1991) Modeling thermal regimes, In : « Contact Metamorphism », D.M. Kerrick ed., *Reviews in Mineralogy*, **26**, 437-505.

- Fyfe, W.S. and Henley, R.W. (1973) Some thoughts on chemical transport processes, with particular reference to gold. *Mineral. Sci. Enginer.*, **5**, 295-303.
- Gavrilenko, O.P. and Gueguen, Y. (1989) Percolation in the crust. *Terra Nova*, **1**, 63-68.
- Germann, D. and Neugebauer, H.J. (1990) Thermal history of overthrust tectonics under erosional and isostatic conditions in two-dimensional numerical models. In : *Crustal dynamics pathways and records*, Geol. Verein. and Konink. Ned. Geol. Mijnb. Genoots. joint ann. Meeting, S7/3, Blackwell Sci. Pub.
- Glahn, A., Granet, M. and le groupe Télésismique du Graben du Rhin (1993) Southern Rhine Graben : small-wavelength tomographic study and implications for the dynamic evolution of the graben. *Geophys. J. Int.*, **113**, 399-418.
- Goffe, B. and Chopin, C. (1986) High-pressure metamorphism in the western Alps: zoneography of metapelites, chronology and consequences. *Schweiz. Min. Petr. Mitt.*, **66**, 41-52.
- Goffe, B., Michard, A., Kienast, J.R. and Le Mer, O. (1988) A case of obduction-related high-pressure, low-temperature metamorphism in upper crustal nappes, Arabian continental margin, Oman: P-T paths and kinematic interpretation. *Tectonophysics*, **151**, 363-386.
- Goldberg, J.M. and Leyreloup, A. (1990) High temperature-low pressure Cretaceous metamorphism related to crustal thinning (Eastern North Pyrenean Zone, France). *Contrib. Mineral. Petrol.*, **104**, 194-207.
- Gratier, J.P. (1993) Le fluage des roches par dissolution-cristallisation sous contrainte, dans la croûte supérieure. *Bull. Soc. géol. Fr.*, **164**, 2, 267-287.
- Guitard, G. (1970) Le métamorphisme progressif et les gneiss oeilés du massif du Canigou (Pyrénées Orientales). *Mém. BRGM*, 63.
- Helmstaedt, H. and Schultze, D.J. (1988) Eclogite-facies ultramafic xenoliths from Colorado Plateau diatremes breccias. In : D.C. Smith, ed. *Eclogites and eclogite-facies rocks*, Dev. Petrol. Series **12**, Elsevier Pub., 387-450.
- Holdaway, M.J. (1971) Stability of andalusite and the aluminium silicate phase diagram. *Am. J. Sci.*, **271**, 97-131.
- Ito, E. and Clayton, R.N. (1983) Submarine metamorphism of gabbros from the Mid-Cayman Rise: an oxygen isotopic study. *Geochim. Cosmochim. Acta*, **47**, 535-546.
- Jaeger, J.C. (1964) Thermal effects of intrusions. *Reviews in Geophys.*, **2**, 443-466.
- Joanny, V. (1991) La précipitation discontinue « omphacite - clinopyroxène+plagioclase » : contribution à l'étude de l'évolution thermique des éclogites. Unpub. thesis, Université Claude Bernard, Lyon.
- Johannes, W. (1988) What controls partial melting in migmatites ? *J. Metamorphic geol.*, **6**, 461-465.
- Kornprobst, J. (1974) Contribution à l'étude pétrographique et structurale de la zone interne du Rif, Maroc septentrional. *Notes Mém. Serv. géol. Maroc*, 251.
- Kornprobst, J. (1992) La convection dans le manteau supérieur. *Coll. Nat. APBG*, Clermont Fd., **2**, 1-10.
- Kornprobst, J., Bard, J.P., Briand, B., Cantagrel, J.M., Guitard, G., Kienast, J.R., Lasnier, B., Le Corre, C. and Santallier D. (1981) Le métamorphisme en France. in: *Evolution géologique de la France*, A. Autran and J. Dercourt (éds.), 26^e Congr. géol. int., coll C7, mém. BRGM, Fr., n°**107**, 161-189.
- Kornprobst, J. and Vielzeuf, D. (1984) Transcurrent crustal thinning: a mechanism for the uplift of deep continental crust/upper mantle associations. In : *Kimberlites II : The mantle and crust-mantle relationships*, J. Kornprobst ed., Dev. Petrol. Series **11B**, Elsevier Pub., 347-359.
- Kretz, R. (1961) Some applications of thermodynamics to coexisting minerals of variable composition; examples of orthopyroxene-clinopyroxene and orthopyroxene-garnet. *J. Geology*, **69**, 4, 361-387.
- Kubler, B., (1984) Les indicateurs des transformations physiques et chimiques dans la diagenèse. Température et calorimétrie. In : Thermométrie et barométrie géologiques, M. Lagache ed., *Soc. Fr. Minéral. Cristallog*, **2**, 489-596.

- Lachenbruch, A.H., Sass, J.H. and Galanis, S.P.Jr. (1985) Heat flow in Southernmost California and the origin of the Salton Trough. *J. Geophys. Res.*, **90**, 6709-6736.
- Lardeaux, J.M., Nisio, P. and Boudeulle, M. (1987) Deformational and metamorphic history at the Lago Superiore area of the Monviso ophiolitic complex (Italian western Alps): a record of subduction-collision cycle? *Ophioliti*, **12** (3), 479-502.
- Lardeaux, J.M. and Spalla, M.I. (1991) From granulites to eclogites in the Sesia Zone (Italian Western Alps) : a record of the opening and closure of the Piedmont Ocean. *J. Metam. Geol.*, **9**, 35-59.
- Lardeaux, J.M. and Spalla, M.I. (1990) Tectonic significance of P-T-t paths in metamorphic rocks : examples from ancient and modern orogenic belts. *Mem. Soc. Geol. It.* **45**, 51 -69.
- Laverne, C., Vanko, D.A., Tartarotti, P and Alt, J.C. (1994) Chemistry and geothermometry of secondary minerals from the deep sheeted dyke complex, DsDP/ODP hole 504B. In: Dick, H.I. B., Erzinger, J., Stokking L. et al. Proc. ODP, Sci. Results, 140, Coll. St. Texas.
- Ledru, P., Lardeaux, J.M., Santallier, D., Autran, A., Quenardel, J.M., Floc'h, J.P., Lerouge, G., Maillet, N., Marchand, J. and Ploquin, A. (1989) Où sont les nappes dans le Massif Central français ? *Bull. Soc. Géol. Fr.*, (8)V, 3, 605-618.
- Le Goff, E. (1989) Conditions pression-température de la déformation dans les orthogneiss. Unpub. thesis, Université de Nantes, 304 pp.
- Le Fort, P. (1986) Metamorphism and magmatism during the Himalayan collision. In : Collision Tectonics, M.P. Cowards & A.C. Rieds eds., *Geol. Soc. spec. Pub.*, **19**, 159-172.
- Le Fort, P., Cuney, M., Deniel, C., France-Lanord, C., Sheppard, S.M.F., Upreti, B.N. and Vidal, P. (1987) Crustal generation of the Himalayan leucogranites. *Tectonophysics*, **134**, 39-57.
- Leloup, Ph.H. and Kienast, J.R. (1993) High-temperature metamorphism in a major strike-slip shear zone : the Ailao Shan-Red River, People's Republic of China. *Earth Planet. Sci. Lett.*, **118**, 213-234.
- Livaccari, R.F. and Perry, F.V. (1993) Isotopic evidence for preservation of cordilleran lithospheric mantle during the Sevier-Laramide orogeny, western United States. *Geology* (Boulder), **21**, 719-722.
- MacGregor, I.D. and Manton, W.I. (1986) Roberts Victor eclogites : ancient oceanic crust. *J. Geophys. Res.*, **91**, 14063-14079.
- Malavieille, J., Lacassin, R. and Mattauer, M. (1984) Signification tectonique des linéations d'allongement dans les Alpes occidentales. *Bull. Soc. Géol. Fr.*, 895-906.
- Malavieille, J., Guihot, P., Costa, S., Lardeaux, J.M. and Gardien, V. (1990) Collapse of the thickened Variscan crust in the French Massif Central : Mont Pilat extensional shear zone and St. Etienne late Carboniferous basin. *Tectonophysics*, **177**, 139-149.
- Massonne, H.J., 1992. Thermochemical determination of water activities relevant to eclogite rocks. In : Kharaka Y.K. & Maest A.S. eds., Water-rock interaction, Proc. 7th Int. Symp. Park City, Utah, U.S.A., **2**, 1523-1526.
- Massonne, H. J., 1999. A new occurrence of microdiamonds in quartzofeldspathic rocks of the Saxonian Erzgebirge, Germany, and their metamorphic evolution. Proc. Int. Kimb. Conf. **7**, **2**, 533-539.
- Massonne, H.J. and Schreyer, W. (1987) Phengite geobarometry based on the limiting assemblage with K-feldspar, phlogopite, and quartz. *Contrib. Mineral. Petrol.*, **96**, 212-224.
- Mattauer, M., Laurent, P.H., and Matte P. (1996) Plissement Hercynien synschisteux post nappe et étirement subhorizontal dans le versant sud de la Montagne Noire (sud du Massif Central, France) CR. Acad. Sci. Paris, 322, II, 309-315.
- Matte, Ph. (1986) Tectonics and plate tectonics model for the Variscan belt of Europe. *Tectonophysics*, **126**, 329-374.
- Mc Dowell, S.D. and Elders, W.A. (1983) Allogenic layer silicate minerals in borehole Elmore 1, Salton Sea Geothermal field, California. *Amer. Mineral.*, **68**, 1146-1159.

- Mehnert, K.R. (1968) Migmatites and the origin of granitic rocks. Elsevier., 393 pp.
- Mercier, L., Lardeaux, J.M. and Davy, Ph. (1991) On the tectonic significance of retrograde P,T,t paths in eclogites of the French Massif Central. *Tectonics*, **10**, 1, 131-140.
- Messiga, B. and Scambelluri, M. (1991) Retrograde P-T-t path for the Voltri Massif eclogites (Ligurian Alps, Italy): some tectonic implications. *J. Metam. Geol.*, **9**, 1, 93-109.
- Mevel, C. (1988) Metamorphism in oceanic layer 3, Gorrington Bank, Eastern Atlantic. *Contrib. Mineral. Petrol.*, **100**, 496-509.
- Miyashiro, A. (1961) Evolution of metamorphic belts. *J. Petrology*, **2**, 277-311.
- Muffler, L.J.P. and White, D.E. (1969) Active metamorphism of Upper Cenozoic sediments in the Salton Sea geothermal field and the Salton Trough, Southeastern California. *Geol. Soc. Amer. Bull.*, **80**, 157-182.
- Nehlig, P. (1993) Interactions between magma chambers and hydrothermal systems: oceanic and ophiolitic constraints. *J. Geophys. Res.* **98**, 19621-19633.
- Nicolas, A. (1985) Novel type of crust produced during continental rifting. *Nature*, **315**, 112-115.
- Nicollet, C. (1990) Crustal evolution of the granulites of Madagascar. In : *Granulites and crustal evolution*, D. Vielzeuf and Ph. Vidal eds., NATO ASI Series, 291-310.
- Oxburg, E.R. (1980) Heat flow and magma genesis. In : *Physics of magmatic processes*, R.B. Hargraves ed., Princeton Univ. Press, Ch. 5, 161-199.
- Paterson, S.R., Vernon, R.H. and Fowler, T.K.Jr. (1991) Aureole Tectonics. In : « Contact Metamorphism », D.M. Kerrick ed., *Reviews in Mineralogy*, **26**, 673-722.
- Patriat, P., Segoufin, J., Schlich, R., Goslin J., Auzende, J.M., Benzart, P., Bonnin, J. and Olivet, J.L. (1982) Les mouvements relatifs de l'Inde, de l'Afrique et de l'Eurasie. *Bull. Soc. Géol. Fr.*, **7**, **24**, 2, 363-373.
- Pattison, D.R.M. and Harte, B. (1988) Evolution of structurally contrasting anatectic migmatites in the 3-kbar Ballachulish aureole, Scotland. *J. metamorphic Geol.*, **6**, 475-494.
- Pattison, D.R.M. and Tracy, R.J. (1991) Phase equilibria and thermobarometry of metapelites. In : « Contact Metamorphism », D.M. Kerrick ed., *Reviews in Mineralogy*, **26**, 105-206.
- Peacock, S.M. (1993) The importance of blueschists - eclogite dehydration reactions in subducting oceanic crust. *Geol. Soc. Amer. Bull.*, **105**, 684-694.
- Pecher, A. (1984) Chronologie et rééquilibrage des inclusions fluides : quelques limites à leur utilisation en microthermométrie. In : Thermométrie et barométrie géologiques, M. Lagache ed., *Soc. Fr. Minéral. Cristallog.*, **2**, 463-485.
- Peucat, J.J., Le Metour, J. and Audren, C. (1978) Arguments géochronologiques en faveur de l'existence d'une double ceinture métamorphique d'âge siluro-dévonien en Bretagne méridionale. *Bull. Soc. géol. Fr.*, (7) **20**, 2, 163-167.
- Pin, C. (1990) Evolution of the lower crust in the Ivrea Zone : a model based on isotopic and geochemical data. In : *Granulites and crustal evolution*, D. Vielzeuf and Ph. Vidal, eds., NATO ASI Series, 87-110.
- Pin, C. and Vielzeuf, D. (1983) Granulites and related rocks in Variscan median Europe : a dualistic interpretation. *Tectonophysics*, **93**, 47-74.
- Pognante, U. (1991) Petrological constraints on the eclogite- and blueschist-facies metamorphism, and P-T-t paths in the western Alps. *J. Metam. Geol.*, **9**, 1, 5-17.
- Ravier, J. (1959) Le métamorphisme des terrains secondaires des Pyrénées. *Mém. Soc. Géol. Fr.*, **XXXVIII**, 86.
- Roure, F. and Choukroune, P. (1992) Apport des données sismiques ECORS à la géologie pyrénéenne : structure crustale et évolution des Pyrénées. In : *Proyecto Hispano-Frances ECORS-Pyreneos*, C. Hernandez Lucendo ed., Madrid, 63-79.

- Rubie, D.C. (1984) A thermal-tectonic model for high pressure metamorphism and deformation in the Sesia Zone, Western Alps. *J. Geol.*, **92**, 21-36.
- Schmädicke, E., (1991) Quartz pseudomorphs after coesite in eclogites from the Saxonian Erzgebirge. *Eur. J. Mineralogy*, **3**, 231-238.
- Schellschmidt, R. and Schultz, R.É. (1991) Hydrogeothermic studies in the hot dry rock project at Soultz-sous-Forêts. *Geothermal Sci. & Tech.*, **3** (1-4), 217-238.
- Sobolev, N.V., Shatsky, V.S., 1990. Diamond inclusions in garnets from metamorphic rocks : a new environment for diamond formation. *Nature*, **343**, 742-745.
- Steen, D., Vuagnat, M. and Wagner, J.J. (1980) Early deformations in Montgenèvre gabbros. In : C.J. Allègre and J. Aubouin eds., *Coll. Int. CNRS, «Associations mafiques-ultramafiques dans les orogènes»*, n°**272**, 97-103.
- Tapponnier, P., Lacassin, R., Leloup, H., Schärer, U., Zhong, Dalai, Wu, Haiwei, Liu, Xiaohan, Ji, Shaocheng, Zhang, Liangshen and Zhong, Jiayou. (1990) The Ailao Shan-Red River metamorphic belt : Tertiary left lateral shear between Sundaland and South China. *Nature*, **343**, 431-437.
- Tamey, J., Pickening, K., Knipe, R. and Dewey, J. (1991) Preface. In : J. Tamey, K. Pickening, R. Knipe and J. Dewey eds, *The behaviour and influence of fluids in subduction zones. Royal Soc London*, v-xi.
- Thompson, A.B. (1976) Mineral reactions in pelitic rocks : I. Prediction of P-T-X (Fe-Mg) phase relations. *Am. J. Sci.*, **276**, 401-424.
- Turcotte, D.L. and Schubert, G. (1982) *Geodynamics*. John Wiley & Sons.
- Van Den Driessche, J. and Brun, J.-P. (1991-1992) Tectonic evolution of the Montagne Noire (French Massif Central): a model of extensional gneiss dome. *Geodinamica Acta*, **5**, 1-2,85-99.
- Velde, B. (1967) Si⁴⁺ content of natural phengites. *Contrib. Mineral. Petrol.*, **14**, 250-258.
- Vielzeuf D. (1984) Relations de phases dans le faciès granulite et implications géodynamiques. L'exemple des granulites des Pyrénées. Unpub. thesis, Université de Clermont II.
- Vielzeuf, D. (1982) Considérations sur les limites de stabilité de la Fe- et Mg-trémolite. *Comptes Rendus Acad. Sci. Paris*, **295**, 375-380.
- Vielzeuf, D. and Boivin, P. (1984) An algorithm for the construction of petrogenetic grids : application to some equilibria in granulitic paragneisses. *Am. J. Sci.*, **284**, 760-791.
- Vielzeuf, D. and Holloway, J.R. (1988) Experimental determination of the fluid-absent melting relations in the pelitic system. Consequences for crustal differentiation. *Contr. Mineral. Petrol*, **98**, 257-276.
- Vielzeuf, D. and Kornprobst, J. (1984) Crustal splitting and the emplacement of the Pyrenean lherzolites and granulites. *Earth Planet. Sci. Lett.*, **67**, 87-96.
- Weisbrod, A. (1984) Utilisation des inclusions fluides en géothermobarométrie. In : Thermométrie et barométrie géologiques; M. Lagache ed., *Soc. Fr. Minéral. Cristallog.*, **2**, 415-459.
- Wells, P.R.A (1977) Pyroxene thermometry in simple and complex systems. *Contrib. Mineral. Petrol.*, **62**, 129-139.
- Winkler, H.G.F. (1970) Abolition of metamorphic facies. *Fortschr. Mineral.*, **47**, 84-105.
- Wood, B.J. and Banno, S. (1973) Garnet-orthopyroxene and orthopyroxene-clinopyroxene relationships in simple and complex systems. *Contrib. Mineral. Petrol.*, **42**, 109-124.
- Zingg, A., Handy, M.R., Hunziker, J.C. and Schmid, S.M. (1990) Tectonometamorphic history of the Ivrea Zone and its relationship to the crustal evolution of the Southern Alps. *Tectonophysics*, **182**, 169-192.

Index

A

A'KF 50, 68, 72, 183
Abukuma 104, 106, 129, 130
ACF 50, 53, 183
ACF-A'KF 52, 53, 183
activity 30, 77
advection 110
advective 10
AFM 52, 72, 185
Agly 105, 133, 134, 137, 139
agmatite 107
Ailao Shan 162, 163
Alps 115, 117, 175
aluminosilicate 14, 17
amphibolite 45
anatexis 49, 108, 136
anchimetamorphism 3
annealing 13, 33, 94 141
augen gneiss 45
aureole 89, 94, 95, 97

B

Ballachulish 90
behind subduction 115
Beni Bousera 175
binary system 18
Bois de Cené 132
Briançonnais 118
burial 101, 110, 113, 168

C

Canigou 105
Chamrousse 148
charnockite 137

chemical potential 29, 96
Chenaillet 147, 149
coesite 165, 166, 167
collinearity 64, 71
collision 12, 112, 113, 133,139
conduction 9, 137
conductivity 113
convection 10, 176
convective heat transfer 131
coronitization 44
crystallinity 3

D

Dalradian 103, 105, 106, 122,
124, 126,132, 137, 150, 174
decarbonation 27, 96, 109
degenerate 64
Dent Blanche 116
diagenesis 3, 21
diamond 168, 169, 176
diffusion 90, 96, 98, 110
diktyonite 107, 108
dislocation energy 13, 34
divariant
57, 59, 60, 65, 68, 71, 73, 78
Dora Maira 118, 124, 165, 168, 170

E

eclogite 45,117, 120, 125, 170
entropy 15, 16, 27, 65, 66
equilibrium curve slope 17
Erzgebirge 169
exhumation
103, 110, 120, 121, 168, 170
extension 111, 115,139, 148,161

F

fluid phase 22, 25, 26,
27, 35, 74, 95, 100, 109, 110, 141
fluid pressure 24
foliation 36
fracture cleavage 36
Franciscan
103, 106, 115, 124, 131, 170, 174
free energy
13, 15, 19, 33, 35, 47, 72, 73
French Massif Central 128, 141, 170
friction 162, 163
fugacity 25, 26

G

geothermal gradient 8, 11, 111, 113
geothermobarometer 78, 173
geothermobarometry 78, 80
geothermometer 73, 79, 173
Gorringe Bank 145
granoblastic 42, 43
granulite 141, 161

H

heat flow 8
heat production
8, 11, 120, 124, 137, 163
hornfels 44, 45, 95

I

Île de Groix 132
illite 3
independent constituent 57, 59, 71
intrusion 89, 91, 92, 94, 96, 98, 140
invariant 58, 63, 65, 69, 70, 71
inverse metamorphism 128
isochore 82
isograd 47, 101, 133
isopleth 73
isostatic re-equilibration 112, 168
isotherm 11, 113, 124, 131

K

kinzigite 137
kinzigitic 78
Kokchetav 168, 169

L

Lanzo 175
lepidoblastic 44
leucosome 106, 108
Lherz 175
Limousin 122
lineation 37
lithospheric mantle 176
lithospheric thinning 140, 115, 155, 161
lithostatic pressure 4

M

Madagascar 150, 151
Manaslu 130
marble 46
marble cake 176
Massif Central 104, 126
melanosome 106, 107, 108, 109
mesosome 106, 108
metamorphic core complex 133
metamorphic facies 48, 54, 101
metapelite
44, 106, 122, 125, 129, 134, 138
metasomatic 13, 29, 99
metasomatism 13, 100
metastable extension 61, 64, 70
Mid-Cayman Rise 146, 147
mid-ocean ridge 129
migmatite 23, 57, 106, 110, 132, 137
migmatitic core complex 134
migmatization 106, 109, 141
molar volume 63
Montagne Noire
105, 133, 134, 137, 138, 139, 151
Monviso 118
Muscat 121

N

nematoblastic 44
 neoblast 33, 43
 neosome 106, 108
 North Pyrenean Zone 105, 155, 159, 160

O

obduction 115, 121
 oceanic crust
 8, 113, 120, 124, 127, 144, 173
 Oman 121
 orthogneiss 44, 138

P

P-T-t path 13, 42, 175
 paired metamorphic belts 130
 paleosome 106, 107
 paragenesis 40
 paragneiss 44, 137
 partial fusion 106, 107,
 108, 110, 112, 115, 134, 137, 141, 151, 165
 partial pressure 25, 28, 109, 110
 percolation 100
 peridotite 8, 176
 petrogenetic grid 69
 phase diagram 61
 phase rule 57
 Piemontais zone 103
 plum pudding 176
 polymetamorphism 40
 polymorphic change 13
 polyphase 41
 Polyphase metamorphism 40
 porphyroblast 40
 porphyroblastic 44
 porphyroclast 33, 38, 40, 43
 post-kinematic 102
 post-tectonic phase 40
 prekinematic 38
 prograde
 102, 110, 120, 122, 124, 127, 128
 prograde gradient 112, 113, 116, 150
 protolith 33, 34, 44, 106, 119

pseudotachylite 113
 pull-apart 155
 pyroxenite 45

R

Red River 162, 165
 retrograde
 103, 110, 112, 118, 120, 124, 127, 128, 137
 Rhine Graben 150, 152
 rifts 129, 148
 Ronda 175
 Ryoike 104, 129, 130

S

Salau 99
 Salton Sea 152
 Sanbagawa 115, 131, 132
 schistosity 36, 38
 skarn 96, 99, 100
 skarnoid 162
 slaty cleavage 36
 solid solution 67, 75, 77
 solvus 72, 74
 stable isotope 146
 stromatolite 107, 108
 subduction 11, 112, 113,
 115, 120, 121, 124, 127, 131, 132, 141, 168,
 170, 174, 176
 subduction zone 12, 118
 subfacies 54, 56
 subgrain 33, 38
 synkinematic 102
 syntectonic 40
 syntectonic recrystallization 13

T

tectonic overpressure 5
 temperature 6
 ternary system 20
 texture 33, 42, 43
 thermal conductivity 8, 92
 thrusting 112
 topochemical 13, 57
 Tsate 116

typomorphic 49

U

underplating 11, 131, 140

underthrusting 113, 124, 128

univariant 58, 60, 63, 71

upper mantle 8, 10, 176

V

variance 57

Viso 120

Voltri 118, 119, 120

X

xenolith 172

Z

Zabargad 175

Zermatt-Saas 116, 118